UNIVERSITY OF NAPLES FEDERICO II

Department of Civil, Architectural and Environmental Engineering

PH.D. PROGRAMME IN
HYDRAULIC SYSTEMS, TRANSPORTATION AND
URBAN DEVELOPMENT ENGINEERING

COORDINATOR PROF. ELVIRA PETRONCELLI
XXVIII CYCLE

ILARIA DEL VITA

PH.D. THESIS

Hydraulic response of submerged breakwaters in Reef Ball modules

TUTORS: PROF. MARIO CALABRESE, PROF. MARIANO BUCCINO
CO-TUTOR: PROF. GIUSEPPE DEL GIUDICE

2016

To my father Bruno,
my mother Ornella and
my sister Giorgia

ABSTRACT

Worldwide coasts are globally threatened by the effects of shore erosion, with increasing consequences from both a social and economic point of view. In recent decades the use of environmentally friendly artificial submerged barriers have been receiving an increasing interest from the research, due to a high biological compatibility associated to shore protection.

Among them, Reef Ball^{TM} (RB) represents one of the most commonly used environmentally friendly modules. The latter was originally employed for biological enhancement, and more recently for the shoreline stabilization of high valued sites. To this specific aim, RBs modules can be arranged in rows, according to different configurations, to realize submerged breakwaters even of significant width.

However, in spite of the clear environmental benefit deriving from the adoption of similar structures, their application is still affected by large uncertainties in the estimation of the hydraulic characteristics of the wave-barrier interaction. In particular, very limited studies exist providing equations for the prediction of the effectiveness of Reef ball structures, generally focused on very peculiar and uncommon configurations.

In order to produce a systematic characterization of the hydraulic properties of these breakwaters, and overcome the abovementioned limitations, a wide experimental campaign consisting in 1,440 tests has been conducted with irregular waves in the flume of the Department of Civil, Architectural and Environmental Engineering (DICEA) of the University of Naples "Federico II". In these tests a wide range of submergences, wave attacks and configurations was investigated, in order to analyse the behaviour or RB barriers under breaking and non-breaking waves. To the Author's knowledge, this represents the widest experimental investigation on this specific type of submerged barrier.

The most relevant aspects related to the wave-barrier interaction have been addressed, namely the wave breaking , the rate of energy dissipation, the wave set-up and the variation in the wave spectrum.

In particular, predictive equations have been proposed for the estimation of the transmission coefficients defined both in terms of wave heights and periods. More specifically, the comparison between the *DICEA* data and literature equations allowed to develop a new conceptual approach for the assessment of the rate of energy dissipation of RB barriers.
Furthermore, the analyses performed allowed a better comprehension of the overall hydraulic behaviour of these structures, especially for what concerns breaking occurrence and typological characterization, and RB barrier's influence on nearshore circulation.

Keywords: Wave Transmission, Wave Set-up, Wave breaking, Submerged Breakwaters, Reef Ball, Physical Modelling.

ACKNOWLEDGMENTS

I express my sincere gratitude to my Tutors, Prof. Mario Calabrese, for the opportunity he gave me to join his group and for having initiated me into research, and Prof. Mariano Buccino, for his technical advice, his patience, and the thoughtful support of my work. His competence and devotion to research have been, and will be in the future, an example for me.

A great acknowledgment is due to the Co-Tutor, Prof. Giuseppe Del Giudice, for his availability, openness and for the suggestions provided.

I wish to acknowledge also Todd Barber, Mariano Buogo and Sara Cirelli, from Reef Ball Foundation, for the information provided about Reef Ball modules.

I would like to thank all the colleagues at the University of Naples, for their time and friendship. I particularly wish to thank: Daniela Salerno, Alessandro Capobianco, Francesco Pugliese, Vittorio Pasquino, Roberta Padulano, Giuseppe Ascione, Oreste Fecarotta and Francesco Morlando.

A great, warm and loving thank goes to Fabio, for having been beside me throughout these years. Your love, continuous support and care have made this goal possible.

My deepest gratitude goes to my family, my father Bruno, my mother Ornella, my sister Giorgia, to whom I dedicate all the work done in these years. Their unconditional love and their patience made me stronger and more determined.

TABLE OF CONTENTS

LIST OF TABLES

LIST OF FIGURES

LIST OF SYMBOLS

A_0	[-]	scale factor of the model of Armono;
A_1	[m^2]	area of the surface roller in the vertical plane;
A_{rect}	[m^2]	area of rectangle inscribing RB configurations.
A_{RB}	[m^2]	base area of one RB module.
A_t	[m^2]	cross-section area of the breakwater;
B	[m]	crest width of the breakwater;
B_0	[m]	wave peakedness parameter;
B_{bR}	[m]	crest width of Reef Ball structures;
B_{eq}	[m]	equivalent rectangular crest width;
B_m	[m]	berm crest width;
B_t	[m]	nominal crown width of Reef Ball structures;
B_t^*	[m]	effective crown width of Reef Ball structures;
c	[ms^{-1}]	phase speed;
C_v	[-]	discharge coefficient;
d	[m]	water depth;
d_I	[m]	still water depth offshore the barrier;
d_{II}	[m]	still water depth inshore the barrier;
d_b	[m]	still water depth at incipient breaking;
d_{gI}	[m]	still water depth offshore entrance of gap between breakwaters;
D_{n50}	[m]	nominal rock diameter, $D_{n50}=(M_{50}/\rho_r)^{1/3}$;
D_R	[m]	base diameter of Reef Ball;
d_{sI}	[m]	still water depth at offshore of the barrier;
d_{sII}	[m]	still water depth at inshore of the barrier;
E	[Wm^{-2}]	wave energy;
F	[m]	freeboard. i.e. the difference between the height of structure and the water depth;
f	[$m^{1/3}s^{-1}$]	friction parameter of Glaukler-Strickler's formula;
f'	[-]	friction factor;

f_0	[-]	drag coefficient for close modules with no-breaking waves;
G	[-]	geometrical quantities related to equivalent water thickness over breakwater;
g	[ms^{-2}]	gravity acceleration;
G', G_1, G_2	[-]	dissipation factors;
G_R	[-]	dissipation factor of RB modules in CA for bermed layout;
$\overline{H}$	[m]	average wave height;
H_0	[m]	deep water wave height;
H_I	[m]	offshore wave height at the toe of the structure;
H_{II}	[m]	onshore wave height at the toe of the structure;
H_b	[m]	wave height at incipient wave breaking;
H_b^{cr}	[m]	wave height at incipient wave breaking on the crown of a breakwater;
H_{en}	[m]	energetically equivalent wave height;
$H_{en,i}$	[m]	energetically equivalent incident wave height;
H_i	[m]	incident wave height;
h_m	[m]	height of berm;
H_{m0}	[m]	spectral wave height;
$H_{m0,i}$	[m]	incident significant spectral wave height;
$H_{m0,t}$	[m]	transmitted significant spectral wave height;
H_R	[m]	reflected wave height;
h_R	[m]	height of Reef Ball;
H_{rms}	[m]	energetically equivalent wave height, $H_{rms}=8\sqrt{m_0}$);
h_s	[m]	height of structure;
h_{se}	[m]	equivalent height of Reef Ball structure;
H_{si}	[m]	incident significant wave height;
H_{st}	[m]	transmitted significant wave height;
H_μ	[m]	mean wave height, $H_\mu=\sqrt{2\pi m_0}$;
k_I	[m^{-1}]	wave number offshore the barrier;
k_{II}	[m^{-1}]	wave number inshore the barrier;

K_R	[-]	reflection coefficient;
K_T	[-]	transmission coefficient;
$K_{T,calc}$	[-]	calculated transmission coefficient;
$K_{T,meas}$	[-]	measured transmission coefficient;
$K_{t,over}$	[-]	partial transmission coefficient over the breakwater;
$K_{t,\ thru}$	[-]	partial transmission coefficient through the breakwater;
$K^{s}_{t,0}$, $K^{nt,0}$	[-]	transmission coefficients for triangular breakwaters;
L	[m]	wave length;
L_0	[m]	deep water wave length;
L_{0p}	[m]	deep water wave length calculated in function of T_p;
L_b	[m]	wave length at incipient breaking;
L_{bs}	[m]	distance between the breaking point and onshore toe of structure;
L_g	[m]	mean length of gaps between breakwaters;
L_i	[m]	incident wave length;
L_{ip}	[m]	incident wave length calculated in function of T_p;
L_s	[m]	mean length of breakwater;
m	[-]	bottom slope;
m_0	[m^2]	zero order spectral moment;
M_{50}	[Kg]	50% value of rock mass distribution curve;
$m_{0,i}$	[m^2]	incident zero order spectral moment;
$m_{0,T}$	[m^2]	transmitted zero order spectral moment;
n	[-]	number of Reef Ball rows at the top of the structure;
q_{in}	[m^2s^{-1}]	incoming flux per unit of length;
q_{over}	[m^2s^{-1}]	outgoing flux over breakwater per unit of length;
$q_{through}$	[m^2s^{-1}]	outgoing flux through breakwater per unit of length;
R_c	[m]	submergence of the structure, $R_c = d-h_s$;

R_{ce}	[m]	equivalent submergence of Reef Ball structure, $R_c = d\text{-}h_{se}$;
R_{cm}	[m]	submergence of the Reef Ball mound, $R_{cm} = d\text{-}h_m$;
R_{su}	[m]	significant wave run up;
R_u	[m]	wave run up;
S_w	[-]	slope of the energy grade line;
s_0	[-]	deep water wave steepness, $s_0 = H_i/L_0$;
s_{0p}	[-]	deep water wave steepness, $s_{0p} = H_{si}/L_{0p}$;
T	[s]	wave period;
T_{pi}	[s]	incident peak wave period;
T_{pT}	[s]	transmitted peak wave period;
Ub	[ms^{-1}]	bottom velocity;
u_{gI}	[ms^{-1}]	rip current velocity offshore breakwaters;
U_R	[-]	Ursell's number;
w_s	[m]	width of structure at sea bottom;
x_I	[m]	distance between the shoreline and the offshore toe of the breakwater;
x_{II}	[m]	distance between the shoreline and the inshore toe of the breakwater;
x_b	[m]	distance between breaking point and seaward edge of structure;
α_{in}	[-]	inshore breakwater slope;
α_{off}	[-]	offshore breakwater slope;
γf	[-]	roughness factor for wave overtopping;
δ	[m]	total wave set up;
δ'	[m]	difference between the water level shoreward and seaward the breakwater;
δ_{1DH}	[m]	wave set up for continuous breakwater;
δ_{BT}	[Wm^{-2}]	energy dissipation per unit area;
δ_c	[m]	mass flux contribution to set up;
δ_{mf}	[m]	breaking momentum flux contribution to set up;
δ_{ns}	[m]	wave set-up without RB barriers;
δ_s	[m]	wave set-up inducted by RB barriers;

η	[-]	ratio between the transmitted wave height and the wave height at landward edge of the crest;
λ	[-]	friction factor;
ν	[-]	dissipation factor;
ν_{φ}	[-]	arrangement dissipation factor;
ν_{br}	[-]	breaking factor;
ξ	[-]	Iribarren parameter $\xi = tg\alpha_{off}/s_0^{0.5}$;
ξ_p	[-]	Iribarren parameter $\xi_p = tg\alpha_{off}/s_{0p}^{0.5}$);
$\prod$	[-]	transmission coefficient for structures with $R_c = 0$.
ρ_r	[kgm^{-3}]	rock density;
ρ_w	[kgm^{-3}]	water density;
τ_b	[$kgm^{-1}s^{-2}$]	unitary shear stress at bottom;
υ	[-]	transmission factor for through-passing;
Φ	[-]	dissipation factor for breaking waves;
φ	[-]	configuration density;
φ_p	[-]	thickness coefficient;

LIST OF ABBREVIATIONS

B	Bermed Reef Ball layout;
BS	Bottom Seated Reef Ball layout;
CA	Conceptual Approach;
DICEA	Dipartimento di Ingegneria Civile Edile ed Ambientale (Department of Civil, Architectural, Hydraulic and Environmental Engineering);
ERDC/CHL	Engineering Research and Development Centre Coastal and Hydraulics Laboratory;
QUCERL	Queen's University Coastal Engineering Research Laboratory;
RB	Reef Ball;

Chapter 1 – INTRODUCTION

World's total coasts extend for about 1,635,000 km and are characterized by an ample variety of geomorphological features, weather regimes and biomes (Burke et al., 2001). Whatever coasts' characteristics, their ecological, economic and social importance is beyond dispute. In fact, coastal ecosystems provide a complex of goods and services which are indispensable for the human life. Furthermore, they sustain biodiversity and offer a greatly valued habitat, as well as areas for recreation and tourism (van der Meulen et al., 2004). These services are estimated at some 25,780 $x10^9$ US Dollars per year (Martinez et al., 2007), which roughly correspond to 77% of global ecosystem-services value (Costanza et al, 1997). On a global scale, coastal ecosystems are threatened by the rapidly-growing concentrations of people and socio-economic activities (Bijlsma et al., 1996), and nowadays 28% of them results to be altered by human activities (Figure 1.1).

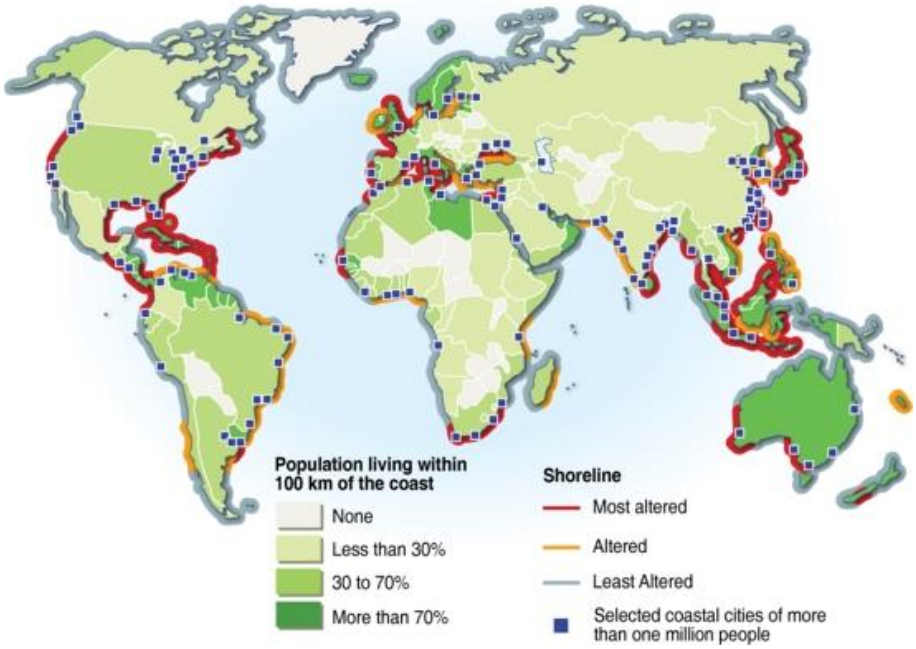

Figure 1.1. Coastal population and shoreline degradation (UNEP, 2002).

It has been estimated that the average population density in coastal areas is now twice as high as the global average (UNEP 2005). Worldwide, about 60% of the world's population live in the coastal zone (Nicholls et al., 2007) and more than 100 million people live in areas no more than 1 m above sea level (Douglas and Peltier 2002).

Coastal erosion is among the most common and important phenomena affecting world's coasts. In fact, over 70% of the World's beaches experiences coastal erosion (Dar and Dar, 2009) and the total coastal area, including houses and buildings, currently being lost in Europe is estimated to be about 15 km2 per year (Van Rijn, 2011).

From one hand, Coastal erosion is a natural, long-term, process able to pose serious threats to life and property (Rangel-Butrago and Anfuso, 2009). Suffice to say, the annual property loss in the US due to coastal erosion is estimated in 500 million US Dollars, and about 150 million US Dollars are spent every year by the US Government in erosion control measures (NOAA, 2013).

On the other hand, coastal erosion is a process which can be triggered or exacerbated by anthropic actions, such as:

- coastal development and land reclamation, which can change the alongshore sediment transportation;
- modification of river catchments, which can modify the sediment delivery to the coast;
- global climate change, which is expected to worsen the exposure of coasts, due to rising sea levels, increased erosion and salinity and degradation of wetlands (IPCC, 2007).

The engineering solution most widely employed in the practical applications for the mitigation of beach erosion is the use of submerged detached breakwaters, often in conjunction with beach nourishment. Traditional submerged breakwaters are rubble-mound structures stretched along the coast for several kilometres and characterized by a crown height under the mean sea water level (m.s.w.l.), that favours the water exchange at the back of the structures. The main purpose of these structures is to force the wave breaking and cause the turbulent dissipation of wave energy.

In many countries of the world, Italy, Spain and Japan among them, submerged breakwaters are considered the sole structural measure for shore erosion control

that is consistent with a policy of protection of the natural and historical beauties of coastal areas. For this reason, their structural, hydraulic and environmental responses have been intensively investigated in the recent decades. The EU-funded project DELOS (Lamberti, 2005, Burcharth et al., 2007) is among the most fruitful research efforts.

In spite of their undoubted advantages, conventional submerged breakwaters generally require the quarrying of a large amount of rocky material; in addition to the expense, especially when the structures are long and wide, quarrying inflicts noticeable harm to the environment, and for this reason, it is often forbidden or extremely difficult to achieve.

The use of prefabricated concrete modular elements can represent an alternate to traditional rubble-mound structures, thanks to relatively low costs, durability, manageability and standardization of the construction process. Similar artificial reefs can efficiently reproduce most of the characteristics of natural reefs (Jensen, 1998). In fact, they were initially used for purposes such as fish production, in Japan, recreational diving, in the USA, prevention of trawling, in Europe (Baine, 2001) or for the protection of areas with a particularly high environmental and landscape value (Calabrese et al., 2011). In these cases great attention should be paid on the chemical characteristic of the concrete, because of its potential interaction with the coastal ecosystem.

The use of environmentally friendly concrete units may represent a suitable trade-off between, shore erosion control and environmental compatibility. In fact, in addition to reducing the volume of rock to be employed, these units are able to interact with marine life, favouring a number of recreational activities, such as surfing, snorkelling and fishing. This may ultimately increase the appeal of the beach, generating economic benefits. Nevertheless, in the face of the advantages above, larger uncertainties in the prediction of the response of the beach in the protected area exist for these structures (Dean et al., 1997).

In this study, one of the most popular environmentally friendly units for submerged breakwaters, the Reef Ball^{TM} (Barber, 2001), has been analysed. These modules were originally designed for biological enhancements, due to their peculiar shape and high biocompatibility, which render them particularly suitable for use in delicate and fragile ecosystems, such as coral reefs. Their use was later expanded to shoreline stabilization and interventions were done in

highly-valuable beaches, although limited studies exist in the literature providing readily available design equations and reliable predictions of their overall behavior. In fact, the main studies dedicated to Reef Ball structures are those by Armono (2003) and Ward (2011), who mainly focused on the assessment of wave transmission for structures arranged according to peculiar configurations.

The present study intends to fill this gap in the literature, on the basis of the results of an extensive experimental campaign performed at the Department of Civil, Architectural and Environmental Engineering (*Dipartimento di Ingegneria Civile, Edile ed Ambientale, DICEA*) of the University of Naples Federico II, Italy. This campaign was designed to investigate the main features of submerged breakwaters made of Reef Balls, namely wave breaking, transmission, set-up and spectral variations. To the Author's knowledge, the *DICEA* campaign represents the widest investigation performed to date on these specific structures.

1.1 Objectives of the Study

The general objective of this thesis is to contribute to the understanding of the physical behaviour of submerged barriers made of Reef Ball modules and provide predictive models for the estimation of main hydraulic parameters. To achieve this, the results of the *DICEA* experimental campaign have been analysed and compared to previous literature experiences.

More specifically, this thesis intends to:

- characterize the occurrence and typology of wave breaking at Reef Ball barriers, as a fundamental step in the comprehension of the energy dissipation phenomena;
- overcome the lack in reliable predictive tools for the design of Reef Ball Barriers, through the definition of predictive equations for the transmission coefficients. In fact, this is the main parameter measuring wave attenuation and allowing to assess the level of protection ensured by a submerged breakwater;
- investigate the presence and amount of the wave set-up, i.e. the variation of the mean water level induced by the presence of the barrier, in order

to obtain indications about the influence of RBs on the nearshore currents;

- Provide predictive equations for the spectral variations, to further characterize wave-barrier interaction in the case of Reef Ball modules.

1.2 Organization of the thesis

This thesis presents the analysis of the behaviour of Reef Ball submerged breakwaters on the basis of the results of the *DICEA* experimental campaign.
The thesis is divided into twelve Chapters and structured in three main parts, described below.
The first part provides a general description of Reef Ball modules (Chapter 2) and presents main projects in which Reef Balls were employed, mainly for shore protection purposes (Chapter 3).
The second part is dedicated to the review of existing studies and to analyses based on literature data. More specifically, previous studies on traditional breakwaters (Chapter 4) and Reef Ball breakwaters (Chapter 5) are firstly presented. Subsequently, the assessment of the transmission coefficient of Reef Ball barriers, based on previous literature data, is presented (Chapter 6).
The third part of the work is completely devoted to the *DICEA* experimental campaign. After a description of the experimental setup and a presentation of the analysis carried out (Chapter 7), the results of the *DICEA* campaign are analysed and critically discussed, separately for what concerns the wave breaking (Chapter 8), wave transmission (Chapter 9), wave set-up (Chapter 10) and spectral variations (Chapter 11). The thesis concludes with a summary of the most important outcomings deriving from the analysis of the *DICEA* campaign and final remarks (Chapter 12).

Chapter 2 – REEF BALL™ MODULES

2.1 General characteristics and properties

Reef Balls (RBs; Barber, 2001) are hollow hemispherical-shaped artificial units (Figure 2.1), originally designed for biological enhancement and coral reef restoration and subsequently employed for shore erosion control.

Reef Balls are characterized by a central cavity, a complex system of lateral holes, peculiar surface textures and a neutral pH. These peculiarities allow modules to recreate a suitable habitat for benthic and pelagic species and make them suitable to be used in areas with a fragile ecosystem, as the one typical of coral reefs.

In particular, the central cavity represents a possible repair for fishes from predators. Furthermore, the system of lateral holes, which may vary in number and diameter, determines turbulences that attract fishes following the current. Their particular superficial textures exhibit a roughness that favours the colonization of modules by fouling and non-fouling communities (Armono, 2003).

RBs are made of concrete with a pH of about 8.3, close to that of the sea. This allows to insert RB modules in the marine environment minimizing potential negative impacts and fostering the development of the existing ecosystem.

In order to provide a rapid colonization of RB units, it is possible to implant oysters (Figure 2.2a) or other types of filter-feeding communities on RB's lateral surface, through the use of epoxy glue. In case RB modules are employed for coral reef restoration, corals can be implanted on their surface. For this aim, star-shaped supports made of sand and resin can be attached on modules via stainless steel screws (Figure 2.2b). Otherwise, it is possible to allocate corals in appropriate grooves, realized beforehand (Figure 2.3).

To date a number of different types of RB units are commercially available, characterized by different size, weight and hole pattern, as reported in Table 2.1.

Figure 2.1. Example of Reef Ball units (www.reefball.org).

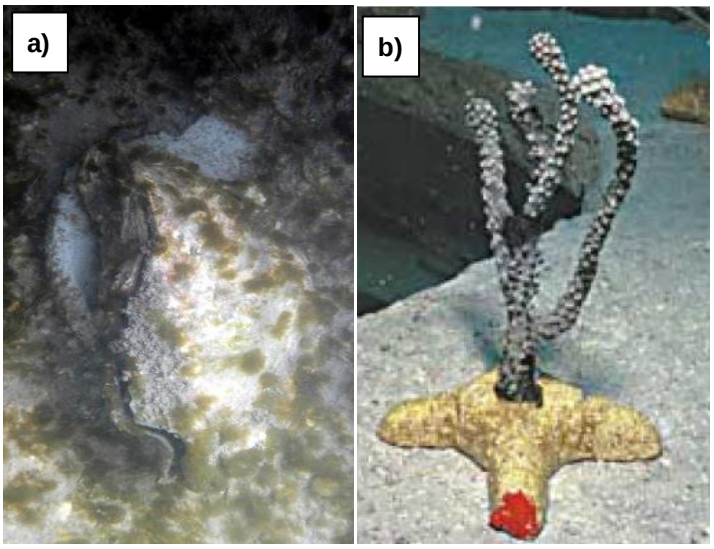

Figure 2.2. a) Ostrea Edulys applied through epoxy glue on a Reef Ball, 20 days after the installation of the module in Venice, Italy, in 2012 (courtesy of Reef Ball Italia); b) coral implanted on a Reef Ball module through star-shaped supports in Dominica, Caribbean Island, in 2000 (Whitford, 2001).

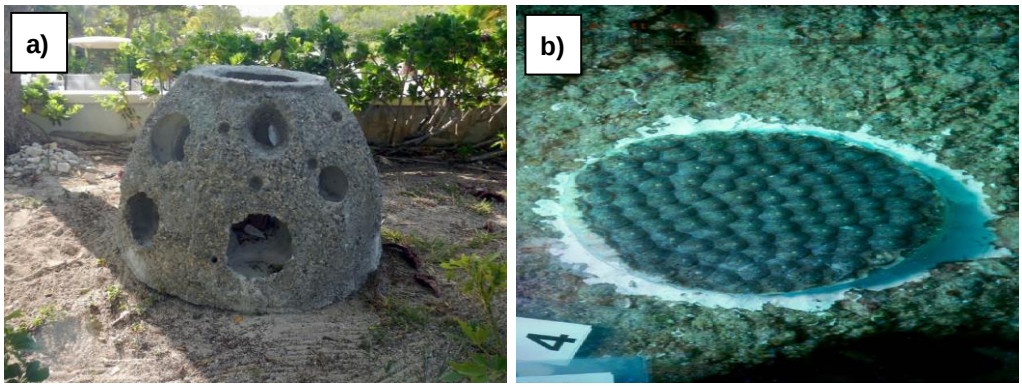

Figure 2.3. a) RB module with grooves (small holes) realized on their surface for coral settlement (www.ioseaturtles.org); b) Coral transplanted in groove. (Reef Ball Foundation, 2008).

Unit Types	Base Diam. (m)	Height (m)	Weight (Kg)	Concrete Volume (m^3)	# of holes
Goliath Ball	1.83	1.52	1800-2700	1.0	25-40
Super Ball	1.83	1.37	1800-2700	1.0	22-34
Ultra Ball	1.83	1.31	1600-2000	0.7	22-34
Reef Ball	1.83	1.22	1350-1900	0.6	22-34
Pallet Ball	1.22	0.9	700-1000	0.25	17-24
Bay Ball	0.9	0.61	170-340	0.08	11-16
Mini-Bay Ball	0.76	0.53	70-90	less than 0.04	8-12
Lo-Pro Ball	0.61	0.46	35-60	less than 0.02	6-10
Oyster Ball	0.46	0.30	15-20	less than 0.01	6-8

Table 2.1. Reef Balls characteristics (www.reefball.org).

All the above-mentioned characteristics motivated a first application of RB modules for purely rehabilitation purposes. Subsequently, their use was expanded to shore erosion control. In fact, submerged breakwaters, even of significant width, can be realized through RB modules (Figure 2.4). To this aim, units with significant heights (Table 2.1) are generally employed, arranged according to different layouts. Conversely, smaller modules are usually employed in aquaculture and for coral transplanting and propagations.

Figure 2.4. Example of Reef Ball submerged breakwater (www.reefball.org).

2.2 Construction process

Reef Balls are made of concrete and additives, providing to the mixture a rapid pouring and allowing the installation of modules within 24÷48 hours from the cast. These additives also reduce the mixture pH to a value very close to that one of sea.

The peculiar shape is obtained by casting concrete into a fiberglass assembled mold (Figure 2.5a) with a system of buoys. The central buoy (Figure 2.5b) is usually a polyform-type one, which is resistant to high pressure and temperature, whereas smaller buoys (Figure 2.6a) are used to realize holes on the lateral surface. As shown in Figure 2.6b, the concrete mixture is poured through the central hole on the top of the mold. After hardening, the central buoy can be deflated and removed or it can be left in place, to facilitate the floating and positioning of the module. Subsequently, RBs are washed to provide an adequate roughness to the surface and to further reduce the pH (Sherman et al, 2002; Harris, 2007a).

Modules are generally located to their final position though the use of cranes and barges (Figure 2.7). Alternatively, they can be equipped with lift bags (Figure 2.8a) and moved to their final destination by floating. In case the modules are directly realized on site, the most economical solution is to move them without deflating the central buoy (Figure 2.8b).

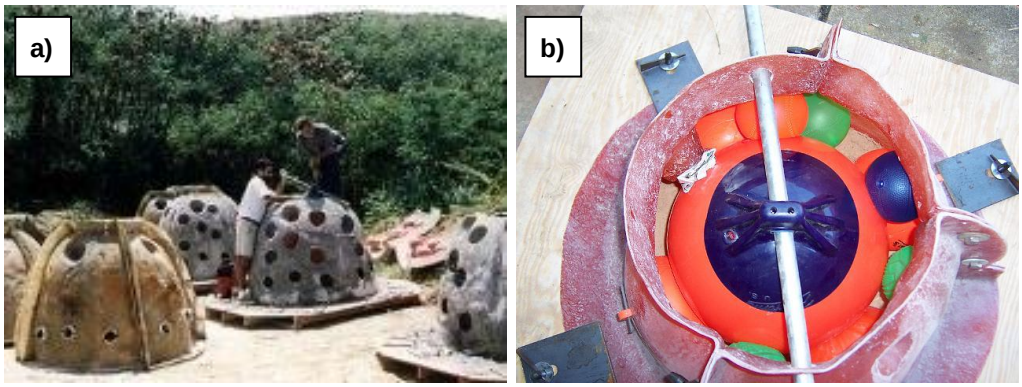

Figure 2.5. a) Construction of RBs in Puerto Rico. On the bottom-left corner a mold can be observed (www.coralations.com); b) Mold and central buoy used in the construction of RB, Maryland Reef Ball Project (www. reefball.org).

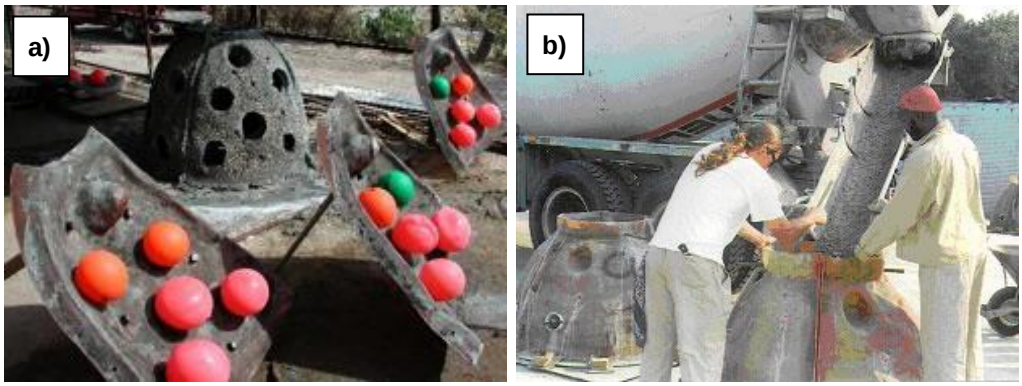

Figure 2.6. a) Inner part of a mold with the system of buoys used to create lateral holes (Harris, 2007a); b) Concrete pouring at the top of a mold (www.nj.gov).

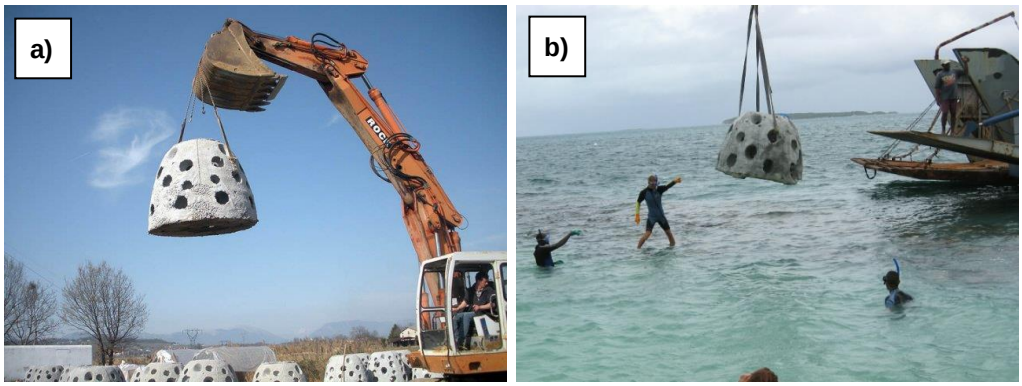

Figure 2.7. Transportation of modules to their final location through the use of cranes (panel a) or barges (panel b) (www.reefballitalia.it; www.reefball.com).

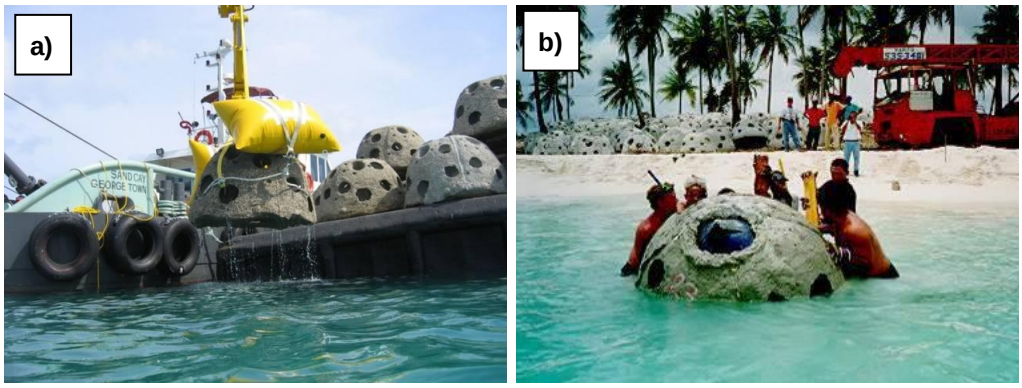

Figure 2.8. a) Example of lift bag (Arnouil, 2008); b) Arrangement of Reef Ball with inflated central buoy (Harris, 2007a).

In case the design requires modules higher than Goliath Ball-type (Table 2.1) it is possible to increase the height of each module by placing it on the crest of a traditional mound, or using Goliath Booster Ring[1]. The latter is a concrete base in which a Goliath Ball can be placed (Figure 2.9). The characteristics of the ring are listed in Table 2.2.

Figure 2.9. Goliath Booster Ring (Harris, 2009).

Base Diam. (m)	Height m)	Weight (Kg)	Concrete. Volume (m^3)	# of holes
2	1	1816-2727	1.19	15-25

Table 2.2. Goliath Booster Ring characteristics.

[1] Goliath Booster Ring were firstly employed for a submerged breakwater in Malaysia

2.3 Anchoring systems

The stability of modules is definitely one of the most important conditions to verify, both in case of a submerged breakwater for shore erosion control and of biological enhancement interventions. This is particularly important for coral planting, due to their high value.
In order to avoid the occurrence of instability phenomena, different types of anchors can be used, depending on the bottom and on the displacement that it is necessary to limit. In particular, sliding generally occurs when Reef Balls are disposed on a rocky bottom and arranged with a low submergence or in areas with high energy rates. Conversely, in the presence of a sandy bottom, settlement phenomena may often take place.
The largest stabilizing contribution to the overall equilibrium of the module is provided by its weight, that can be increased employing so-called "heavy modules", i.e. units characterized by a high weight in their bottom third.
Main anchor types which can be used for RBs are:

- cone anchors;
- spike anchors;
- battered piles;
- friction piles;
- mattresses.

The first two types (Figure 2.10) are generally used to prevent the occurrence sliding phenomena.
Cone anchors (Figure 2.10a) are suitable in the case of soft bottoms and consist of four cones cast monolithically with the Reef Ball. Hollow cones (Figure 2.11) are a special type of cone anchors which can be used when it is necessary to preserve sea grass under the base of modules. This can be particularly important for both the biological preservation of the area and preventing/limiting module sliding and sinking, due to subsoil enhancement produced by roots.

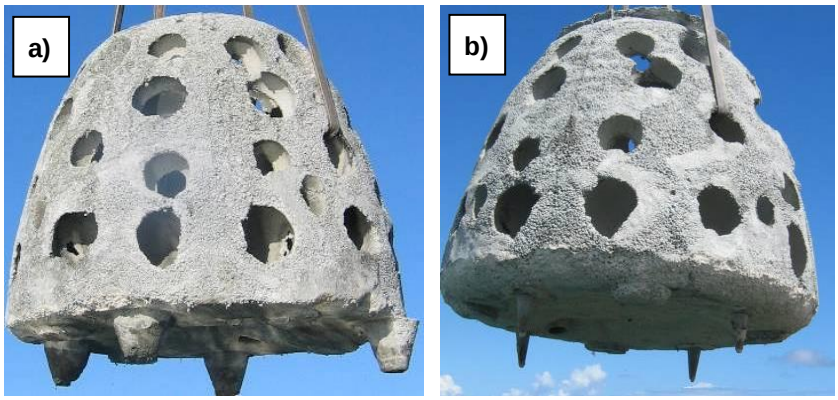

Figure 2.10. a). Anchoring cones; b) Anchoring spikes (Reef Ball Foundation, 2008).

Figure 2.11. Hallow anchoring cones (Reef Ball Foundation, 2008).

Spikes anchors (Figure 2.10b) are tapered pre-cast concrete anchors, reinforced by five fibreglass rebar each. The size of the spikes is designed after pressure tests and calibrated to penetrate inside the rocky bottom.

Battered piles (Figure 2.12) are generally used in order to limit both the horizontal and vertical displacements. This anchor system consists of three or four piles driven, either hydraulically or by means of compressed air, through the Reef Ball's lateral holes, up to the pre-drilled bottom. Each pile, characterized by a maximum length of 2.4 m and a diameter of 10 cm, is reinforced by a maximum of three fibreglass rebar and equipped with a 1 cm thick PVC pipe, allowing the pile to be jetted into the bottom.

Another type of anchoring is provided by the friction piles. These piles are similar to the previous ones, but characterized by a larger diameters, to increase the surface in contact with the subsoil and, therefore, the friction resistance.
In order to control the development of settlements, it is also possible to distribute the RB weight on a larger surface and reduce the pressure applied at bottom through the use of adequate concrete mattresses (Figure 2.13).
These are generally realized during the construction of Reef Balls by means of dedicated formworks.

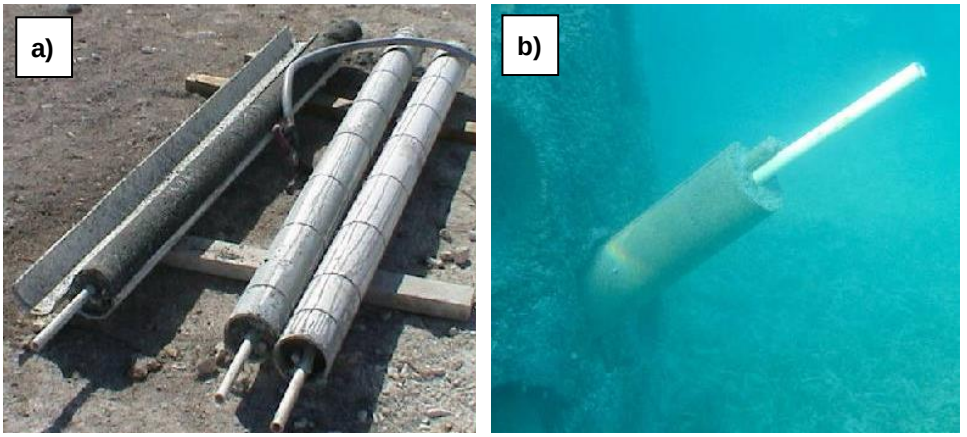

Figure 2.12. Battered piles (Reef Ball Foundation, 2008).

Figure 2.13. Concrete mattress (Reef Ball Foundation, 2008).

Besides, different mattresses at the base of RBs can be connected each other by means of steel bars, to realize a so-called articulated mattress (Figure 2.14). This allows to distribute the weight of the structure on larger areas and to significantly increase the overall stability of the modules.
Another type of mattress can be realized by the use of Armorflex modules (ARMORTEC™). These are prefabricated permeable elements which can be connected each other by means of longitudinal cables laid down in dedicated holes (Figure 2.15). These modules allow the free growth of the vegetation and are generally employed for revetments. Nevertheless, they can be employed as a base for Reef Ball modules providing a contribution in limiting their settlement and sinking. Furthermore, this type of mattress could play a role in sediment transport by trapping the sand in the central holes.

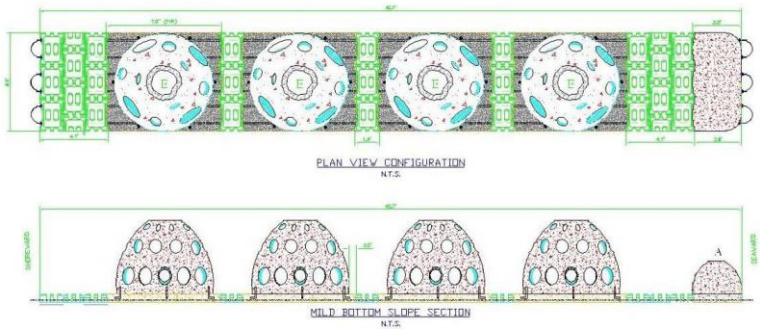

Figure 2.14. Articulated mattress. (Harris, 2007a).

Figure 2.15. Armorflex mattress (Ward, 2011).

Chapter 3 – REEF BALL PROJECTS

To date, Reef Balls have been employed in approximately 7,600 projects throughout the World. In 80% of the cases the main objective of the intervention was biological enhancement and reef ecosystem restoration, the remaining part was aimed at shore erosion control too.
In the following, the most relevant projects providing indications regarding the effectiveness of the intervention and the increase in the beach after the installation of RBs are presented. Although very limited information was available regarding the meteorological and marine conditions as well as design assumptions, it is believed these can provide useful insights about the feasibility of interventions aimed at finding the best trade-off between the need for coastal protection and biological enhancement.

3.1 Gran Dominicus Resort and Iberostar Hotel, Carribbean Coast, Dominican Republic

The first documented project, firstly realized for shoreline stabilization and secondly for environmental enhancement and recreation, is that of the Gran Dominicus Resort (Figure 3.1), in southern Caribbean, Dominican Republic.
In order to contrast the phenomenon of coastal erosion, a segmented submerged breakwater made of RB units and a beach nourishment were realized offshore the Grand Dominicus Resort, in August 1998 (Harris, 2001).
400 Reef Ball and 50 Ultra Ball modules (Table 2.1) were arranged to form 3 structures, each composed of 3 rows. The total length of the breakwater was about 250 m and the submergence was variable between 0.3 m and 0.8 m. The m.s.w.l was ranging between 1.6 to 2.0 m.
A comparison between the beach profiles observed at 6 and 32 months since the end of the project resulted in an average increment of the protected beach of about 12 m (35 m^3/m of sand volume) and a stable shoreline was observed for the adjacent beaches (Harris, 2001). The three sections monitored over time,

namely the "west gap", the "east gap" and the "phase 2" profile lines, are depicted in Figure 3.2.

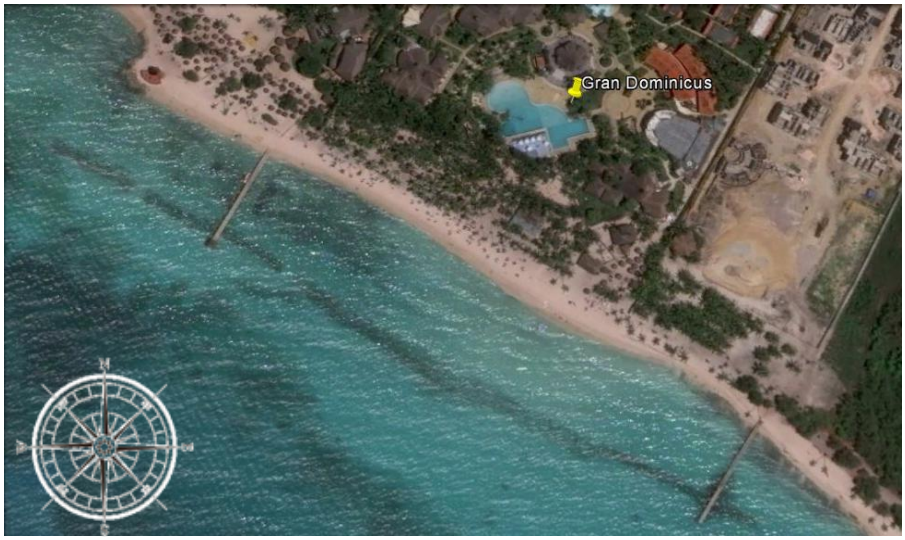

Figure 3.1. Satellite view of the Gran Dominicus Resort (Google Earth, 05/19/2014, 18°20'33.63"N - 68°49'15.27''O, elev. 0 m, alt.436 m).

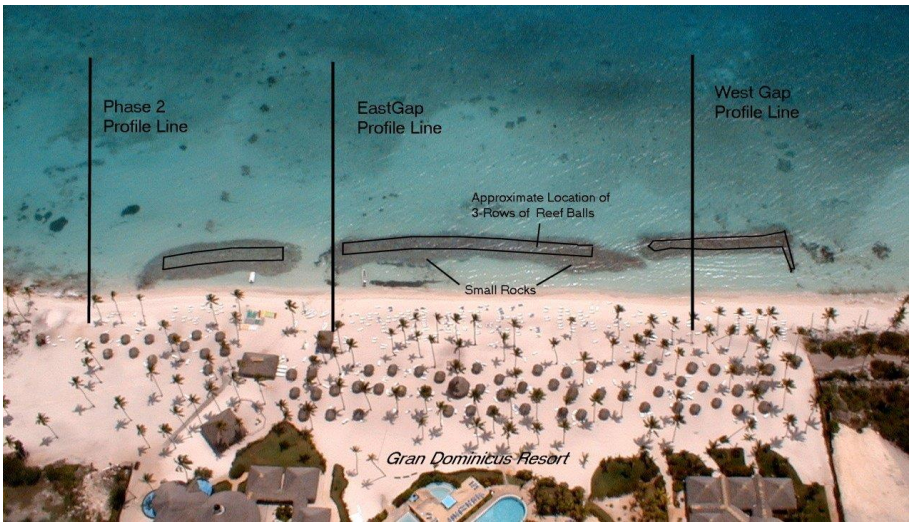

Figure 3.2. Profile lines of the beach of Grand Dominicus Resort. (Harris, 2001).

Reportedly, shoreline increments of 13 m and 10 m were respectively observed for the "west gap" (Figure 3.3) and for the "east gap" profile lines (Figure 3.4). At "phase 2" section the beach profile resulted to be stable (Figure 3.5). Worth noting, this monitoring was performed by comparing the beach profiles in two different seasonal periods, in which different beach behaviours are generally expected (April 2001 and February 1999). In fact it is well-known the cross-shore sediment transport is deeply influenced by seasonal phenomena.

In 1998, the breakwater was interested by the direct hit of the Hurricane George (Category 3) and by the large waves produced by the Hurricane Mitch (Category 5). A survey conducted after these events revealed that no modules were displaced or damaged (Harris, 2007a).

In September 2001, 278 Ultra Balls (Table 2.1) were placed to realize an additional segmented breakwater for the protection of the Iberostar Hotel, adjacent to the Grand Dominucs Resort (Figure 3.6). 9 months after the end of the construction a survey of both projects was conducted. This resulted in a slightly increment of the beaches and no adverse impacts were observed for the adjacent ones (Harris, 2002).

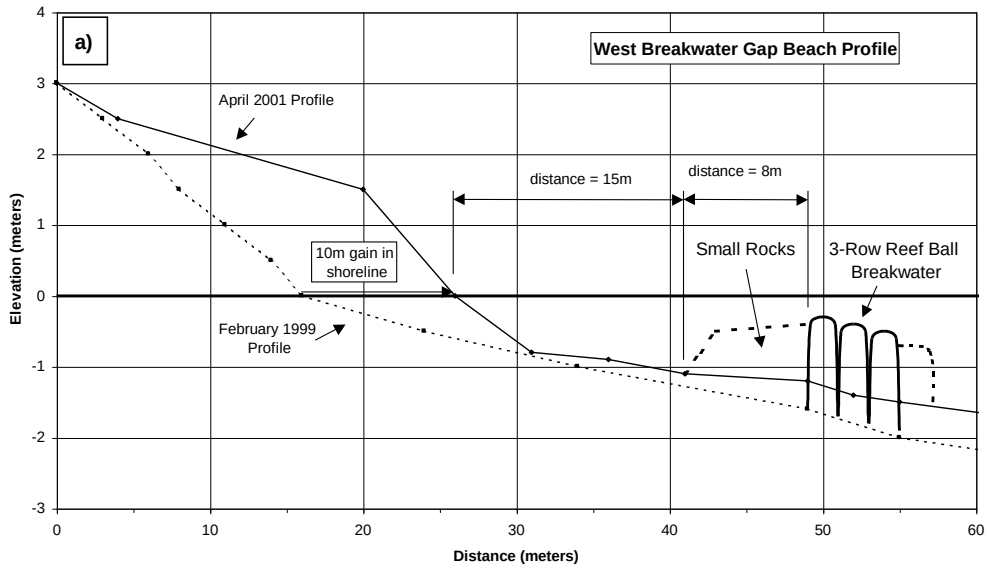

Figure 3.3. Shoreline changes for the "west gap" profile (Harris, 2001).

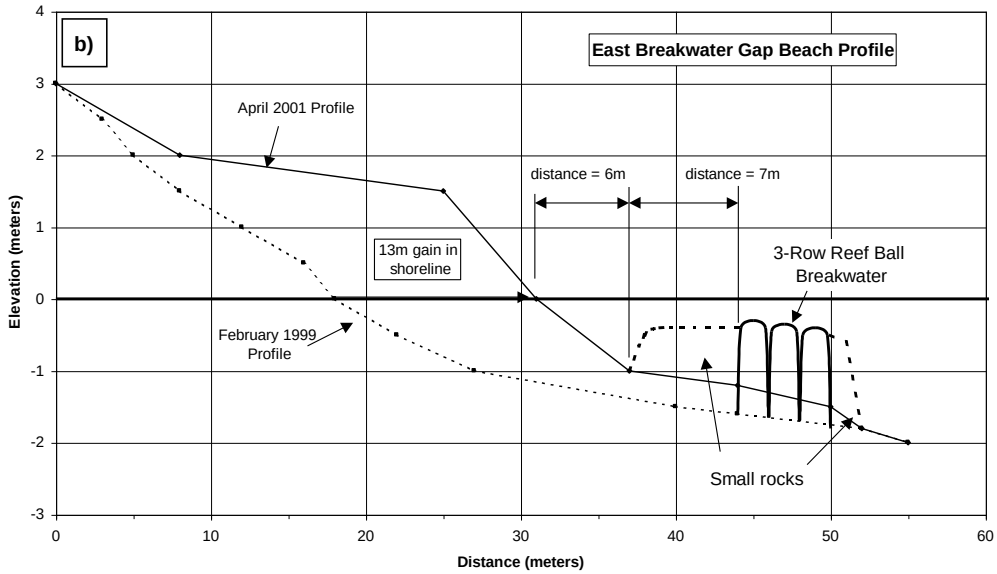

Figure 3.4. Shoreline changes fort the "east gap" profile (Harris, 2001).

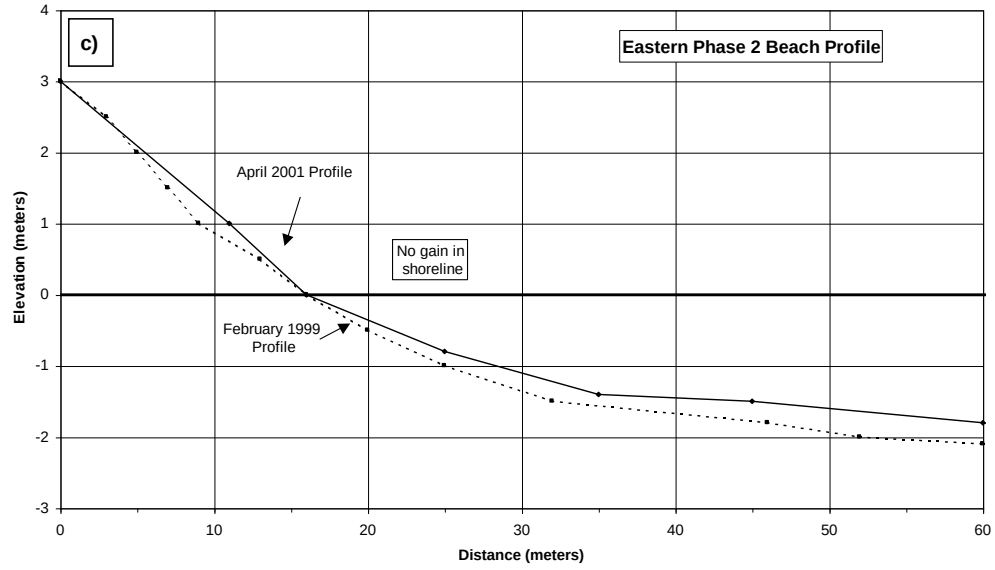

Figure 3.5. Shoreline changes fort the "phase 2" profile (Harris, 2001).

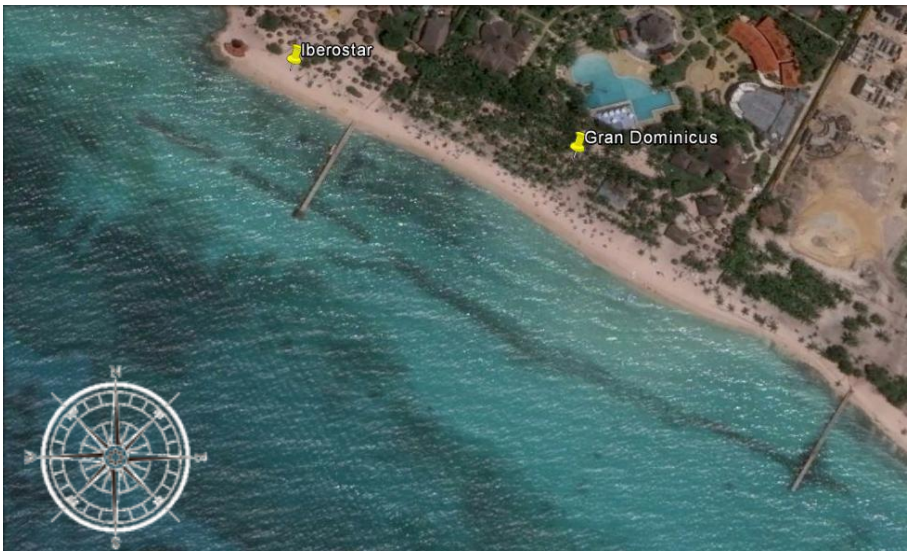

Figure 3.6. View of Iberostar (Google Earth, 05/19/2014, 18°20’32.75”N – 68°49’15.31”O, elev. 0 m, alt. 693 m).

3.2 Marriott beach Hotel, Cayman Island.

The project of a Reef Ball breakwater at Marriott Beach Resort was aimed at producing the shoreline stabilization and favouring an equilibrate growth of flora and fauna, thus increasing the general appeal of the beach.

The Resort, located in the southern part of Seven Mile Beach, Cayman Island, was affected by a significant erosion phenomenon due to the alongshore sediment transport, directed from south to north (Figure 3.7).

Figure 3.8 shows the alonghshore beach profile evolution from April 1994 to November 2002. In these years the beach retreated up to the perimetral seawall of the hotel structure. In particular a 30.5 m erosion was registered from 1997 to 2002 (Harris, 2003).

In 2002, a segmented submerged breakwater made with 5 rows of Ultra Ball units (Table 2.1) was set up shoreward a natural reef (Figure 3.9), about 49 m far from the beach. A gap between the two structures was left approximately in the central part of the natural reef, where the latter achieved minimum submergence values of about 0.30 to 0.61 m below the mean sea water level.

The two RB breakwaters were, respectively, 43.9 m and 29.26 m long, 7.62 m and 9.14 m wide, with a submergence of 0.10 and 0.55 m.

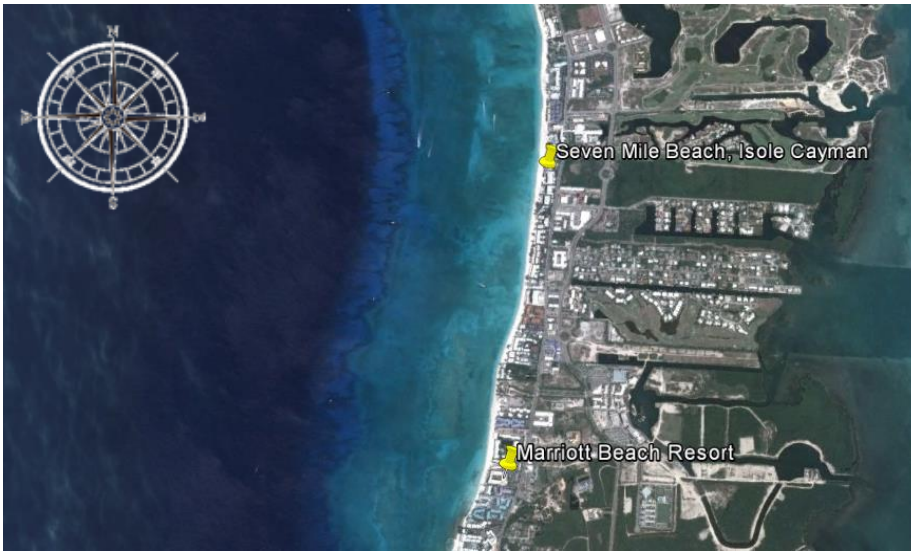

Figure 3.7. Satellite view of Marriott Beach Resort (Google Earth, 03/11/2014, 19°19’05.05”N – 81°22’51.58”O, elev. 5 m, alt.651 m).

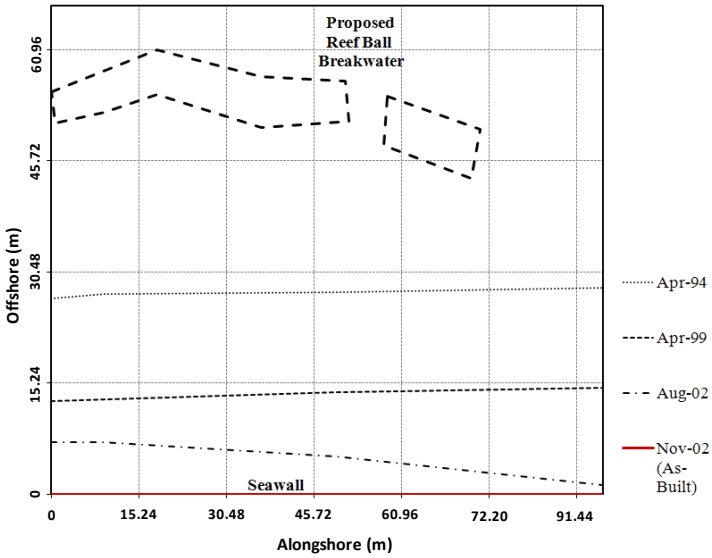

Figure 3.8. Marriot beach profiles in the period 1994-2002. (Adapted from Arnouil, 2008).

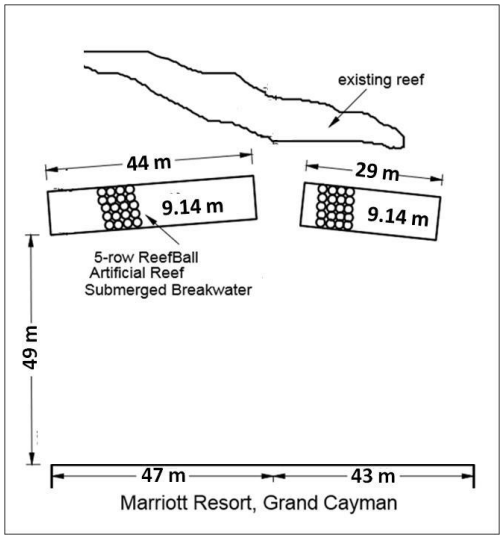

Figure 3.9. Graphic representation of the RB breakwater at Marriot Beach Resort. (Adapted from Harris, 2003).

In order to avoid sliding, each module was anchored by 5 fiberglass rebar (see section 2.3), driven through the lateral holes of the module to reach the rocky bottom. In addition, several types of corals were implanted on RB surfaces (Figure 3.10) to promote the ecotourism and encourage recreational activities such as snorkeling and diving.

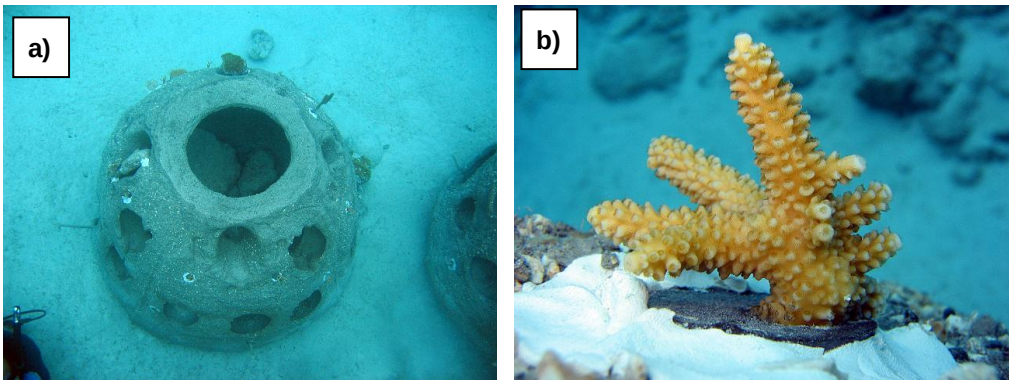

Figure 3.10. Coral on Reef Ball at Marriott Beach.(www.reefball.org).

In order to investigate the response of the beach, several surveys were conducted after the end of the project. As shown in Figures from 3.11 to 3.13,

an initial average increment of the shore line of 14.5 m was observed from November 2002 to February 2003 (Harris, 2003).

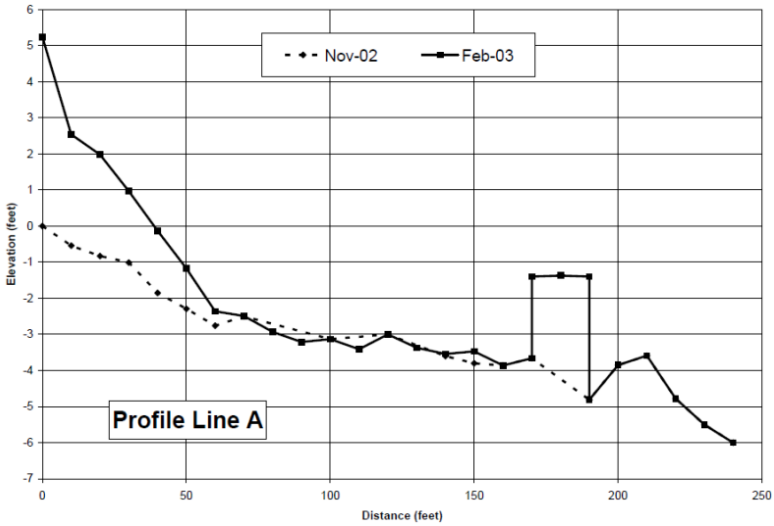

Figure 3.11. Comparison between the cross shore beach profile between November 2002 and February 2003 at Southern end of RB breakwaters (Harris, 2003).

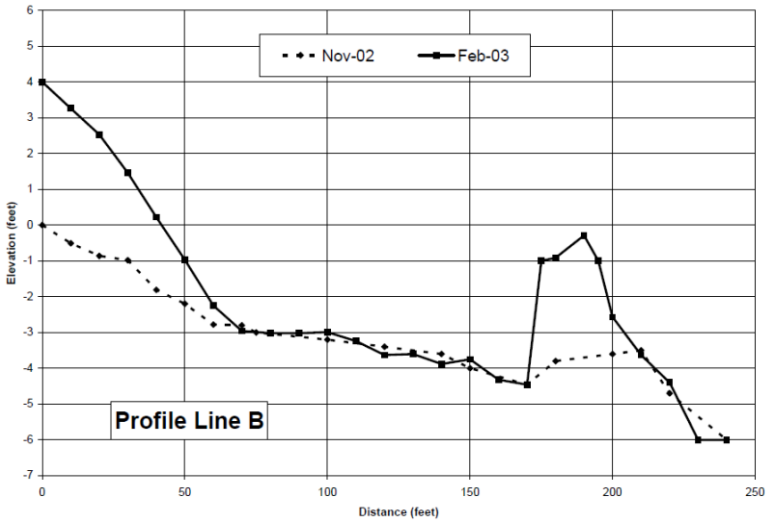

Figure 3.12. Comparison between the cross shore beach profile between November 2002 and February 2003 at 9 m North of Southern end of RB breakwaters (Harris, 2003).

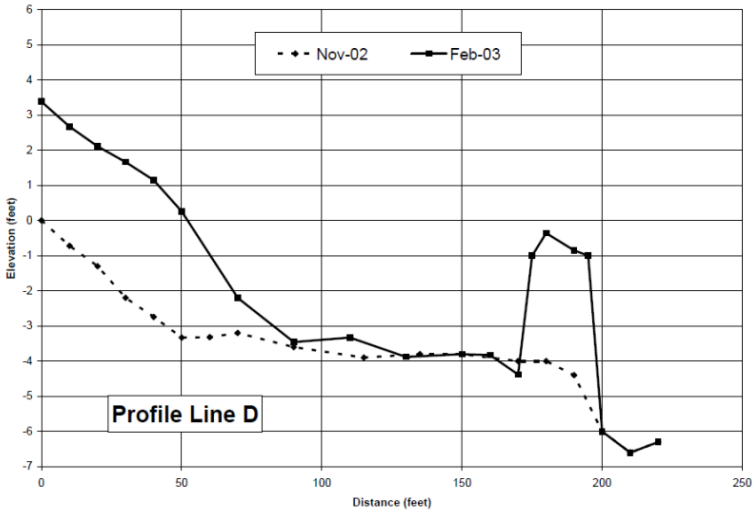

Figure 3.13. Comparison between the cross shore beach profile between November 2002 and February 2003 at 40 m North of Southern end of RB breakwaters (Harris, 2003).

Subsequently, after the hurricane season and the tropical storms of 2003, the beach reached a width of about 5.8 m, while a complete retreatment of adjacent beaches was observed (Harris, 2003).

After Charley (category 1/2), Ivan (category 5) and Emily (category 4/5) Hurricanes, in 2004 and 2005, the state of the units was verified, resulting to be stable and undamaged (Harris, 2009).

In order to increase the protection of the beach from SW waves, in November 2005 the existing breakwaters, made of 200 modules, was extended with 32 additional units (Figure 3.14). Ultimately 232 modules, at a cost of US$ 1,000 per Reef Ball installed (Harris, 2007b), were placed for the protection of the Marriott Beach.

Furthermore, approximately 15 m^3/m of beach nourishment were placed along 3 km in the southern Seven Mile Beach area, including the Marriott Beach (Harris, 2007a).

An extensive monitoring of the beach profile between November 2002 and June 2008 was performed by Arnouil, 2008. Results are shown in Figure 3.15 from which an overall increment of the beach from 0 - 9.14 m to 7.62 - 21.3 m can be observed.

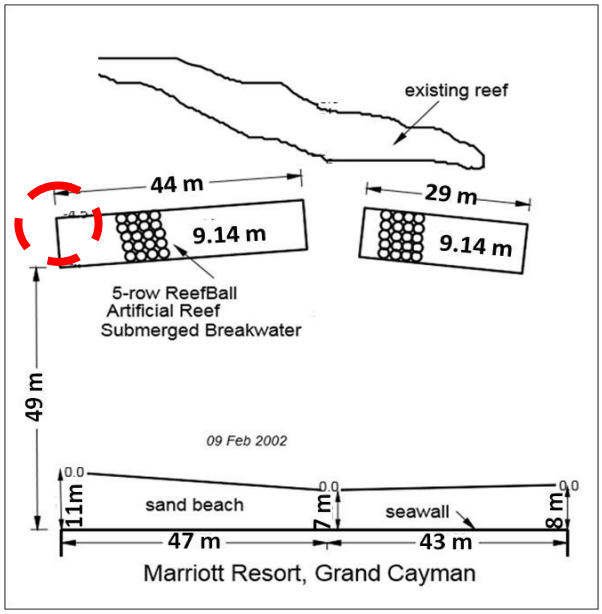

Figure 3.14. Original scheme of Reef Ball submerged breakwaters. The red circle identifies the area of the subsequent expansion of the structures. (Adapted from Harris, 2003).

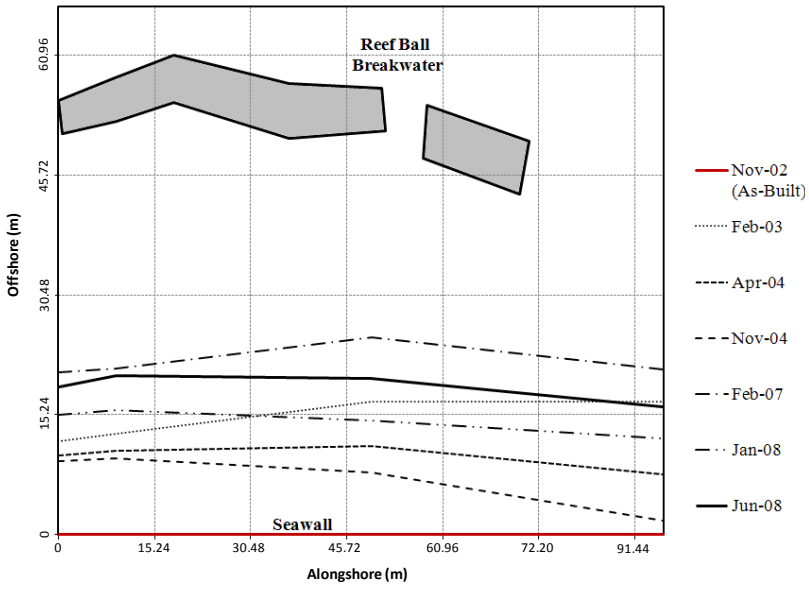

Figure 3.15. Beach lines after the installation of Reef Ball Breakwaters at Grand Cayman Marriott Hotel during the period 2003-2008. (Adapted from Arnouil, 2008).

The first biological monitoring was conducted in February 2003 (three months after the end of the project) and a significant growth of marine species was found. Some photographic documents of the biological enhancement produced in the period 2006-2008 are shown in Figure 3.16.

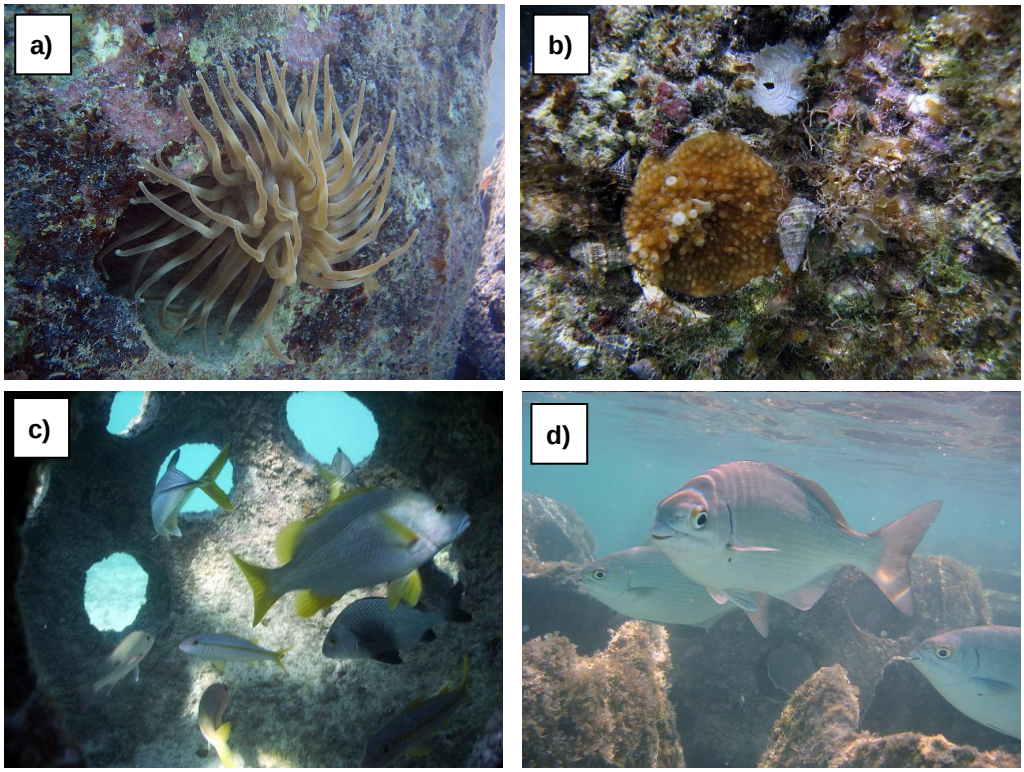

Figure 3.16. a)Encrusting Gorgonia; b) Finger Coral and hermit crabs; c) several fishes including Yellowstail Snapper, Black Margate and Schoolmaster; d) some fishes belonging to the family of Snappers. (www.reefball.com).

3.3 Maiden Island, Antigua project

The Maiden Island, Antigua was a "bio-engineering" project aimed at the realization of an artificial fringing reef[2] (Figure 3.17).

[2] Coral reefs are generally classified in: fringing reefs, barrier reefs and atolls. The first one is the most common type of coral reef, characterized by the absence of a backreef (lagoon). This peculiarity makes them the most vulnerable to pollutants which can't be properly diluted. Less diffused then the previous, barrier reefs are generally located in

The main goals of this project were, on the one hand, to recreate the natural reef destroyed by the 1995 Hurricane Luis (category 4) and, on the other hand, foster the ecotourism and protect the beach nourishment.

Figure 3.17. Satellite view of Maiden Island, about 0.5 MN off the coast of Antigua (Google Earth 1/2/2015, 17°07'34.52"N-61°44'55.51"O, elev.11 km, alt. 15.49 km).

In this project 1,200 RB modules (Table 2.1) were employed, placed at depths ranging between 1 and 2 m., For large part of the structure, the modules were arranged in 5 rows and different snorkelling and diving paths were realized (Figure 3.18).

Modules were anchored by means of 4 different systems, namely fiberglass rebar, cones, spikes and battered concrete piles with fibreglass rebar (see Section 2.3).

About 5,000 new corals were placed on the surface of Reef Balls, as well as 17.4 tons of adults corals, taken from Antigua Island where environmental conditions were compromising their life.

the Atlantic Ocean. In this case, the coral reef is linear and detached from shoreline by a wide backreef. Atolls are circular coral reefs characterized by a large lagoon. They are mostly spread in the Pacific Ocean.

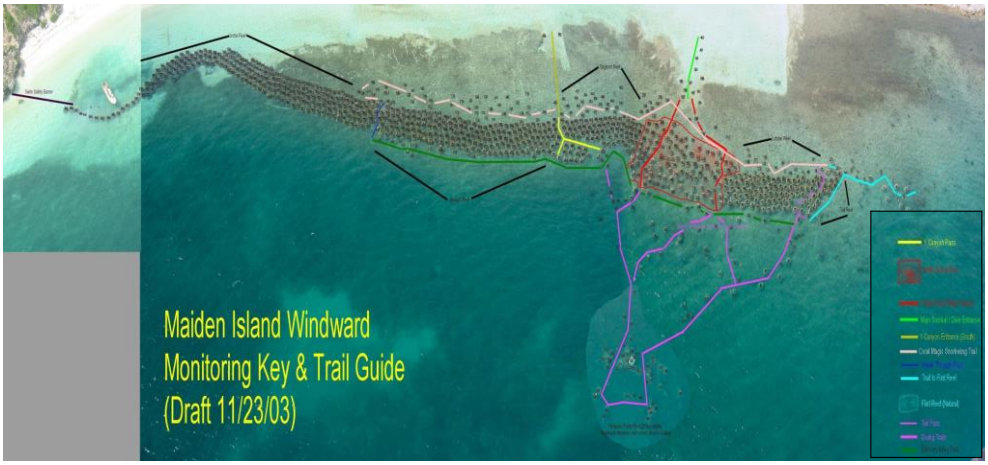

Figure 3.18. Plan view of Maiden Island submerged breakwater (www.reefball.org).

In order to avoid the expansion of algae and favour the growth of corals, 500 sea urchins (*Echinometra lucunter*) were inserted into grooves realized *ad-hoc* on Reef Ball surface (Figure 3.19).

According to the indications provided by the Nova Southeastern University FL,USA (www.reefball.com), a number of modules were filled for one-third of their height with stones to reproduce the typical habitat of juveniles. Moreover, some units were equipped with meshes to attract young lobsters.

Several pinnacles were built for spawning protection in the area offshore the barrier (represented by violet lines in Figure 3.18). The layout of these structures was expressly designed so that juveniles could be transported by currents to the back of the reef, finding protection from predators.

Throughout the structure, corridors were provided to allow fish migration from shallow to deep water.

One peculiar aspect of this project is the installation of Reef Balls lifted from the bottom through the use of dedicated supports (Figure 3.20). This way it was possible to preserve the seagrass representing the habitat for the conch *Strombus gigas*. Worth noting, the preservation of seagrass also produces important consequences from an engineering point of view, because roots are able to limit the sinking of modules and generally allow to avoid the use of geotextiles.

Figure 3.19. Sea Urchin into Reef Ball lateral groove (www.reefball.com).

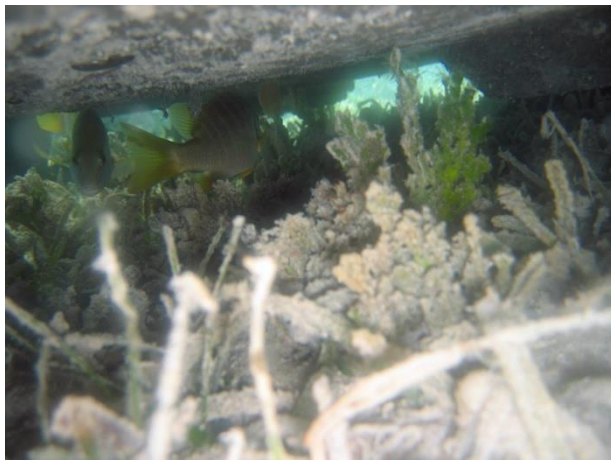

Figure 3.20. Marine life under the base of a lifted Reef Ball (www.reefball.com).

The environmental response to the installation of the fringing reef was monitored in 2010. The results showed a general increase in the number and type of marine species in the area, in particular several spawns of *Lutjanus grisou*, 73 different species of fishes, 71 of invertebrates, 30 of corals and 26 of algae (Figure 3.21).

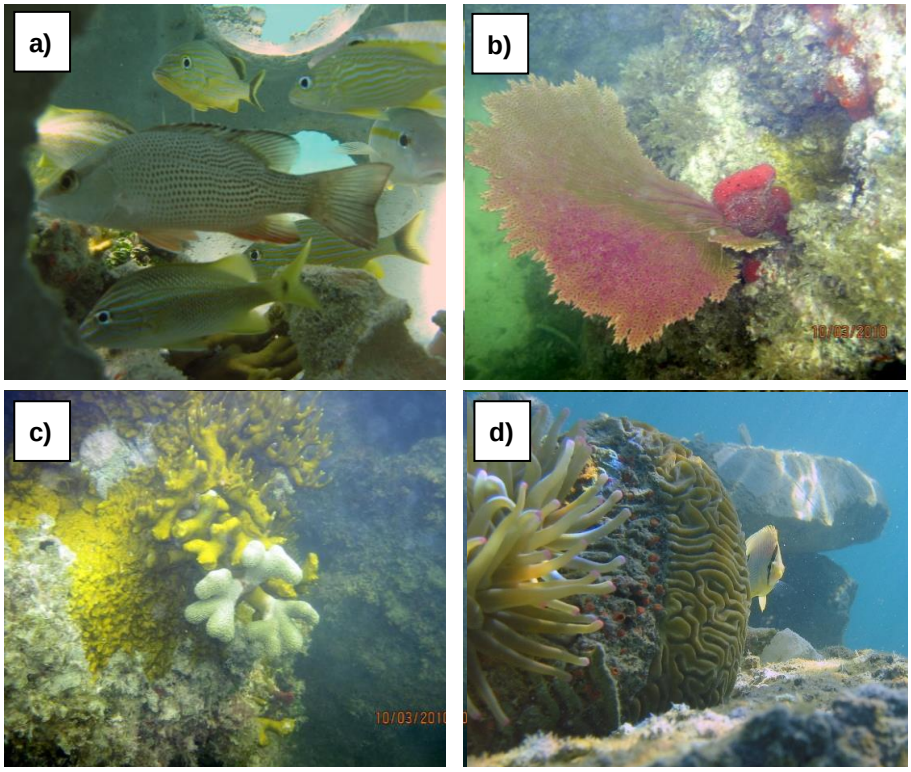

Figure 3.21. Colonization of Reef Ball surface 7 years after the end of the project: a) numbers of fish including French Grunt, Tomtate and Sailors choice; b) Gorgonia; c) Branching fire coral and the Finger coral; d) Several marine organism including Spotfin Butterflay Graved Brain coral and an Anemone. (www.reefball.com).

3.4 Venice lagoon, Italy, project

At the time being, the only significant RB project realized in Italy is that of the Venice lagoon. This project was completed in March 2012 for the morphological and environmental recovery of the area of the channel of Bastia, close to the Lake of Ripola and to the access to the Venice lagoon (Figure 3.22).

Figure 3.22. Satellite view of the Lake of Ripola and surrounding area (Google Earth 3/28/2015; 45°20'24.99"N – 12°23'00.29"E, elev. -11 m, alt. 70.45 km).

This intervention was required because the intensification of currents directed to the lagoon and the deepening of its accesses, performed on behalf of the MOSE project, produced an erosion of the "Barene" and "Velme" [3] areas. To contrast the loss of sediments, a 3 Km long submerged levee was realized, made of gravelly material, confined through geogrid. This barrier was realized at a distance of 500 m from the mouth of the port. In order to allow a certain degree of water exchange, a 200 m long permeable submerged barrier was realized through artificial modules, 93 of which were Reef Balls (Figure 3.23).
In particular, Goliath Ball-type modules (Table 2.1) were arranged in 3 rows, with a distance between units of 1 m. Units were placed on a gravel confined mattress, characterized by a height of 1 m and by a crest width of 8 m. The total height of the structures (including Goliath Ball and mattress) was about of 2.40 m with a submergence of 0.20 m. The main characteristics of the Reef Ball structure are shown in Figure 3.24.

[3] The venetian word "Barene" indicates the vegetated areas of a lagoon, while "Velme" describes the submerged areas emerging only during low tide periods.

Figure 3.23. Satellite view of the Reef Ball barrier in the Venice lagoon, Italy (Google Earth 3/28/2015; 45°20'19.14"N – 12°13'54.43"E, elev. 0 m, alt. 599 m).

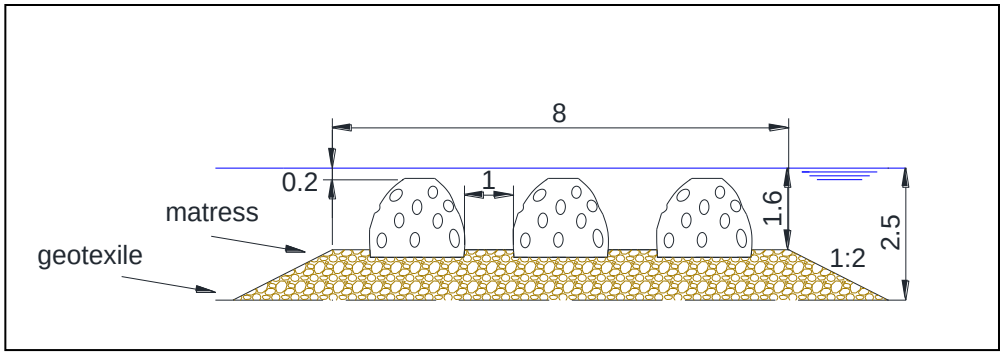

Figure 3.24. Cross-section of the Reef Ball structure of the Venice lagoon, Italy project (measures in meters).

To favour an environmental enhancement, about 10 *Ostrea edulis* were implanted on surface of each unit. The biological response was monitored over time and already 20 days after the end of the project the colonization of Reef Balls by different types of sea species was observed, such as *sponges brotozoan*, *green algae* and *brown algae*, *hermit crabs* and *snails* (Figure 3.25). In Figure 3.26 the presence of marine organisms in September 2013 is also shown.

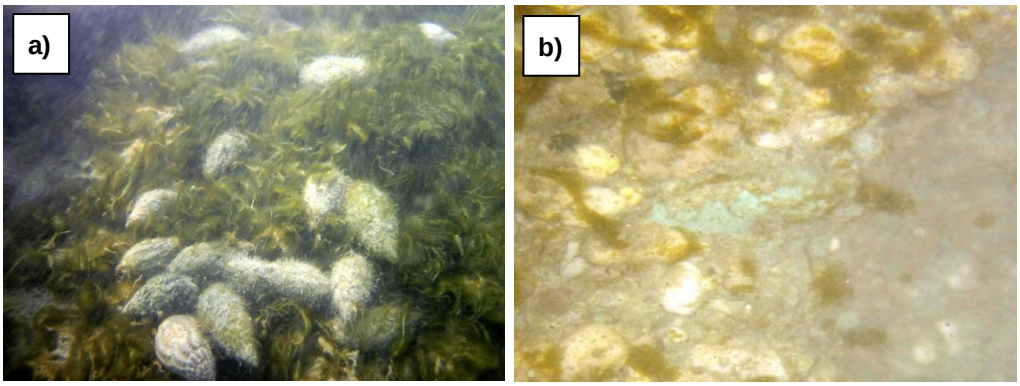

Figure 3.25. Reef Ball surface in May 2012. a) Green algae and hermit crabs; b) Sponges Brotozoan (www.reefballitalia.it).

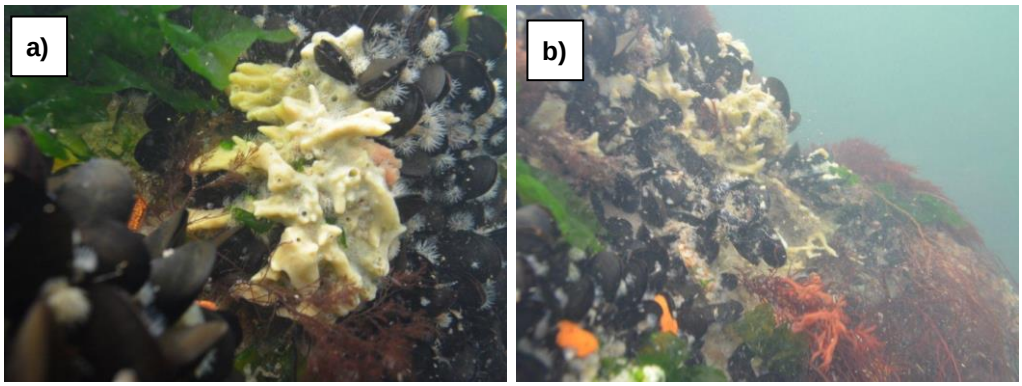

Figure 3.26. Reef Ball colonization in September 2013 by bivalve molluscs (oysters), calcareous red algae and Porifera sponges. (www.reefballitalia.it).

Chapter 4 – STATE OF THE ART ON SUBMERGED AND LOW-CRESTED TRADITIONAL BREAKWATERS

4.1 Wave-breaking occurrence and macro-features

The wave breaking is one of the most important turbulent energy dissipation processes influencing coastal dynamics. It is defined as the transformation of the particle motion form the irrotational to the rotational state, generating vortices and turbulences (Basco, 1985). This phenomenon plays a central role not only in the reduction of the wave height, but also in the wave set up/set-down and in the creation of nearshore currents, which are an important factor in the sediment transportation.

This local and non-stationary phenomenon typically occurs in the open sea, or during the wave propagation from deep to shallow water. In the former case, waves lose their stability originating the so called “whitecap”; in the latter case the breaking occurs when either a steepness limit or a depth limit are reached. Apart from its natural occurrence, wave breaking, is often induced by coastal defence structures, as a main mechanism for the energy dissipation.

Although several studies have been carried out to define suitable wave breaking criteria for natural beaches (Stokes, 1847, 1880; Miche, 1944; Battjes and Janssen, 1978; Goda,1970; Kamphius, 1991) or induced by structures (Dean et al. 1997; Ranasighe and Turner, 2006, Calabrese et al., 2008a), no studies have been performed to date in order to investigate whether the presence of RB structures is able to induce the wave breaking and to assess its typology. These aspects will be investigated in Section Chapter 8.

In the following, a review of the state of art concerning the occurrence, classification and wave breaking criteria for natural beaches and in presence of submerged traditional structures is reported.

4.1.1. Wave breaking phenomenon in natural beaches

4.1.1.1. Occurrence of wave breaking for flat or gentle sloped natural beaches

The first studies conducted for gentle sloped bottoms (slopes in the range of 1:100÷1:50) are those proposed by Stokes in 1847 and 1880. In these studies, focused on regular waves, the incipient breaking was defined as the condition in which the horizontal component of the wave velocity at the crest equals or exceeds the wave propagation celerity.

According to these studies, the wave breaking can be expressed by two different breaker indices: the s_0 index, identifying the achievement of a limit of wave steepness, defined as the ratio between the incident wave height, H_i, and the deep wave length, L_0; and the H_i/d index, addressing the exceedance of a given incident wave height, with respect to the water depth, d. The former index is typical of a deep water breaking criteria, while the latter is most commonly used in shallow water.

Starting from the previous studies, several Authors focused on the identification and definition of an incipient wave breaking condition, mainly through experimental tests.

A shallow water breaking criteria was proposed by McCowan (1894) in the case of solitary waves shoaling, on a quasi-horizontal bottom (1:100). The Author defined that the wave breaking occurred when the wave height at the condition of incipient breaking equals 0.78 the water depth (Eq. 4.1).

$$\frac{H_b}{d_b} = 0.78 \tag{4.1}$$

It is worth noting that in the previous Equation, and elsewhere in this Thesis, the *b* subscript refers to the incipient wave breaking condition.

The aforementioned limit was subsequently increased by Southgate (1995) to a value of 0.83, while 0.55 was proposed by Le Mehauté (Allsop, 1998).

In 1944, Miche proposed a semi-theoretical breaking criterion for periodic waves, expressed by the following general Equation:

$$\frac{H_b}{L_b} = 0.142 tanh\left(\frac{2\pi d_b}{L_b}\right) \tag{4.2}$$

By applying the Equation above in deep water, the Author retrieved a deep water breaker index of 0.88, similar to that observed by Southgate (1995).
Subsequently, Danel (1952) modified the previous wave breaking criteria proposing a coefficient equal to 0.12 instead of 0.142. This variation returned a breaker index equal to 0.75, more similar to that proposed by McCowan (1894) than to the others.

4.1.1.2. Occurrence of wave breaking for sloped natural beaches

The most widely employed criterion for identifying the wave breaking for sloped natural beaches and for the design of structures is that proposed by Weggel in 1972 (Allosop et al., 1998). Analysing regular waves, the Author developed the following shallow water breaking criterion:

$$\frac{H_b}{d_b} = \frac{a}{\left(1 + b\frac{d_b}{gT^2}\right)} \tag{4.3}$$

where the wave breaking condition is assumed as a function of the wave period, *T*, of the water depth at the incipient breaking, d_b, and of the seabed slope, *m*, by means of the *a* and *b* coefficients, reported below.

$$a = 1.56/(1 + \exp(-19.5m)) \tag{4.4}$$

$$b = 43.75(1 - \exp(-19m) \tag{4.5}$$

In the previous Equations, *a* and *b* decrease as the slope bottom decreases, until they reach constant values. These are, respectively, zero and 0.78 in the case of an horizontal bottom. By substituting these values into Equation (4.3), the

model provides a breaker index value of 0.78, i.e. the same proposed by McCowan (1894).
Subsequently, Goda (1974) proposed an alternate criterion after the analyses of the experimental data obtained by several researchers (Iversen, 1951; Mitsuyasu, 1962 and Goda, 1964), summarized in Equation (4.6). As it is possible to observe, the breaker index increases as m and H_b/L_0 terms do.

$$\frac{H_b}{L_0} = 0.17\left\{1 - exp\left[-1.5\frac{\pi d_b}{L_0}\left(1 + 15m^{4/3}\right)\right]\right\} \tag{4.6}$$

In the same years, Battjes (1974) observed that the wave breaking phenomenon is able to directly and indirectly influence the main hydraulic properties of wave shoaling (e.g. phase difference across the surfzone, run-up, set-up, reflection), and that these are governed, to some extent, by the so-called "surf-similarity" parameter, ξ. The latter, also known as "Iribarren parameter", is defined as the ratio between the slope of the bottom, and the root square of the wave steepness (Eq. 4.7).

$$\xi = \frac{m}{s_0^{0.5}} \tag{4.7}$$

The study also showed that the surf-similarity parameter can be used to estimate the wave breaking limit and to classify the typology of breaking from a macroscopic point of view (Galvin, 1968).
Similar considerations were done by Iribarren and Nogales (1949), who identified the condition of incipient breaking for values of ξ approximately equal to 2.3.
Subsequently, the formula by Miche (1944) was modified by Battjes and Jansen in 1978 and by Ostendorf and Madsen in 1979.
The former suggested to include the ratio between the breaker index (H_i/d) and 0.88 in Equation (4.2); furthermore, the breaker index was considered as an adjustable parameter, whose best fit was found at 0.8 (Eq. 4.8).

$$\frac{H_b}{L_b} = 0.142 \tanh\left(0.91 \frac{2\pi d_b}{L_b}\right) \tag{4.8}$$

Ostendorf and Madsen (1979) proposed to include the bottom slope in Equation (4.2), thus obtaining two different equations (Eq. 4.9), valid in two different ranges of bottom slopes:

$$\begin{aligned} \frac{H_b}{L_b} &= 0.14 \tanh\left[(0.8 + 5m)\frac{2\pi d_b}{L_b}\right] \qquad for\ m \leq 0.1 \\ \frac{H_b}{L_b} &= 0.14 \tanh\left[(0.8 + 0.5)\frac{2\pi d_b}{L_b}\right] \qquad for\ m > 0.1 \end{aligned} \tag{4.9}$$

Another study addressing breaking conditions was that proposed by Moore (1982), who assumed the wave breaker index as a function of the deep wave steepness and of the bottom slope. This led to Equation (4.10), where *a* and *b* are the same previously defined in Equations (4.4) (4.5).

$$\frac{H_b}{d_b} = a - 0.082 + b\left(\frac{H_0}{L_0}\right)^{4/5} \tag{4.10}$$

In 1991 Kamphuis developed a new criteria for identifying the breaking of regular waves, starting from the model of Danel (1952) and introducing the exponential form of the bottom slope into its formulation:

$$\frac{H_b}{L_b} = 0.127 exp(4m) \tanh\left(\frac{2\pi d_b}{L_b}\right) \tag{4.11}$$

Moreover, after calibrating the model for irregular breaking wave data, the Author proposed the following modification:

$$\frac{H_{sb}}{L_p} = 0.095 exp(4m) \tanh\left(\frac{2\pi d_b}{L_p}\right) \tag{4.12}$$

where, H_{sb} is the significant wave height at the incipient braking, and L_p is the wave length calculated as a function of the wave peak period, T_p.

4.1.1.3. Wave breaking classification based on macroscopic wave features

Further to the definition of the breaking condition, Galvin (1968) proposed the following typological classification of the breaker, based on shape and strength of the jet at the incipient breaking.
In particular, the Author distinguished:

- "spilling" breaker;
- "plunging" breaker
- "surging/collapsing" breaker.

Spilling and plunging breakers are both characterized by the same overall mechanism, but they differ for the scale of the process (Basco, 1985).
The plunging breaker is characterized by a so-called "plunging jet" (Figure 4.1a), starting from the crest, overturning, and reaching the water surface at the so-called "plunging point" (Figure 4.1b). This cause a surface disturbance, called "splash", and the entering of the plunging jet in the oncoming wave trough (Figure 4.1c).
Since the horizontal velocity components are opposite to the wave propagation direction, the plunging jet is pushed backwards and towards the crest, where the velocity component and the wave propagation are equally directed. This generates the so-called "plunger vortex" immediately under the wave crest, which traps and compresses an air core. The creation of air bubbles and the sudden air ejection from the breaker follow. The plunger vortex also translates horizontally, pushes on the oncoming trough to create a secondary wave disturbance and increases the size and strength of the so-called "surface roller", which was generated by the splash (Figure 4.2).

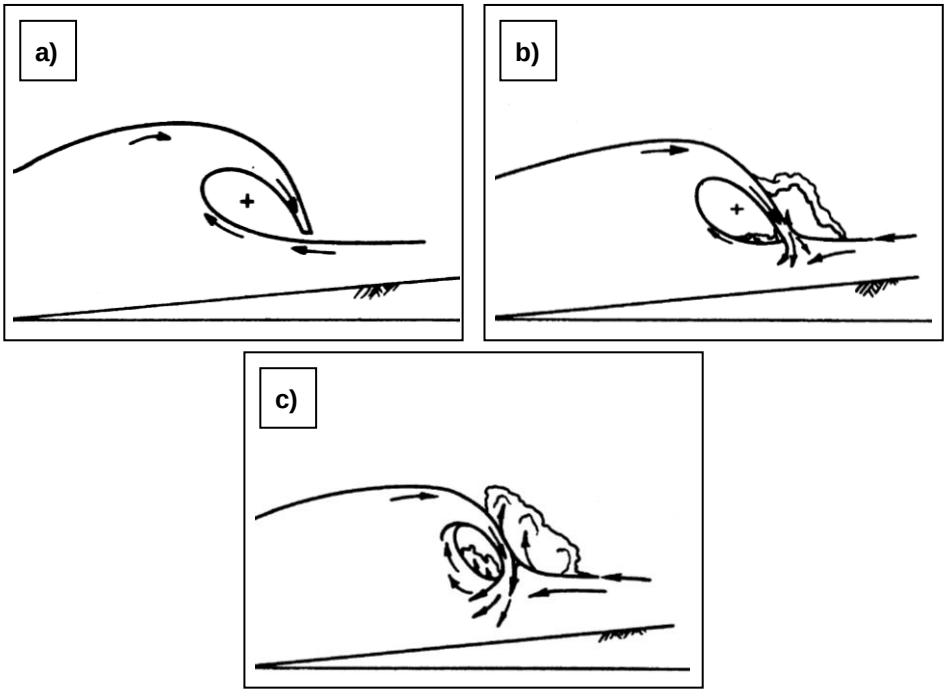

Figure 4.1. Phases of a plunging breakers. (Basco,1985).

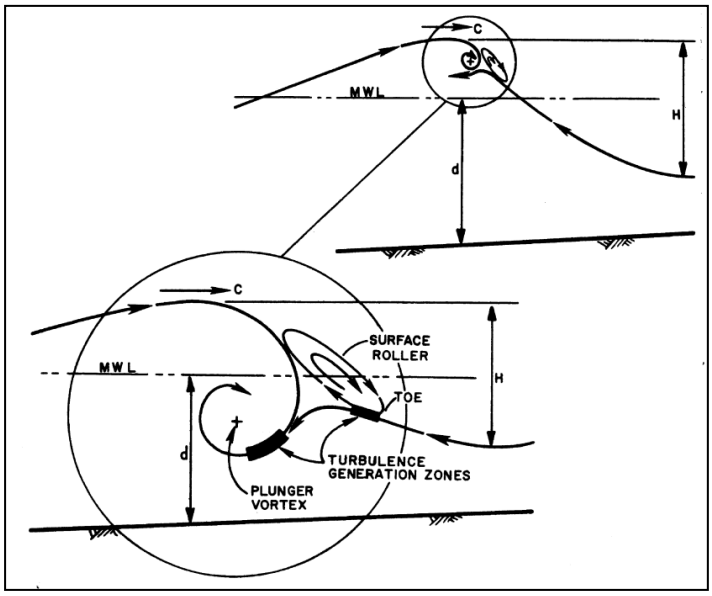

Figure 4.2. Graphical representation of the plunger vortex and of the surface roller (Basco, 1985).

Subsequently, the plunger vortex tents to extinguish (Figure 4.3a) while the toe of the surface roller slides down until it reaches the trough of the oncoming wave ("equilibrium position", Figure 4.3b). After this, the shape of the breaker changes very slowly.

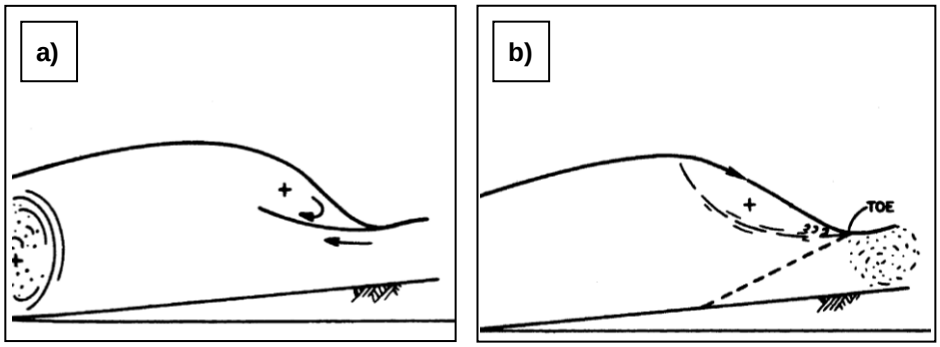

Figure 4.3. Plunging breakers toward the equilibrium position. (Basco, 1985).

As discussed by Galvin (1968), four characteristic sections can be identified in a plunging breaker (Figure 4.4):

1. section at which the wave becomes instable;
2. section at which the wave front becomes vertical (incipient wave breaking condition);
3. section at which the plunging jet impacts on the oncoming wave trough;
4. section at which the splash impacts on the free surface.

These sections also allow to define the approach distance, x_a, the plunge distance, x_p, and the splash distance, x_s.

The main differences between plunging and spilling breaking are related to the strength of vortexes and the consequent presence of air accompanying the macro-feature of wave breaking. In fact, while plunging is characterized by a plunger vortex stronger than the surface roller and by air bubbles (Figure 4.5), in the spilling breaking the plunging jet impacts with the free surface very close to the wave crest (Figure 4.6). This causes that no air is entrapped by the plunger vortex that is weaker than the surface roller.

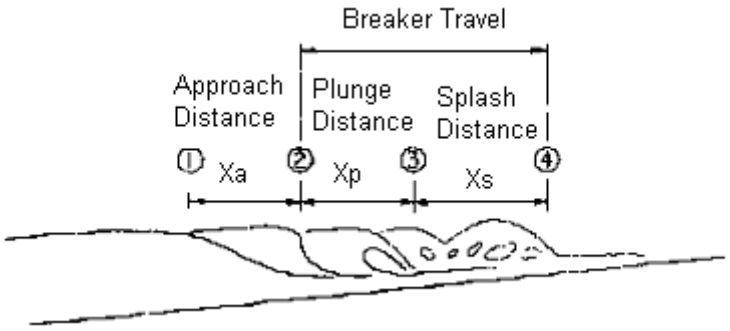

Figure 4.4. Breaker travel. (Galvin, 1968).

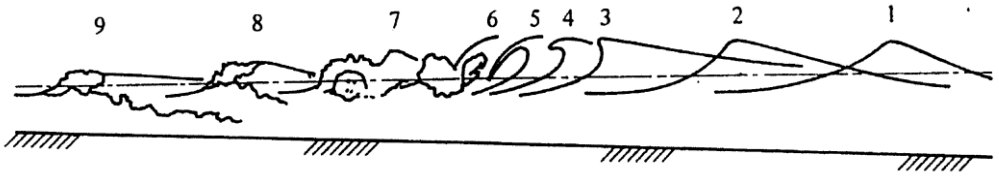

Figure 4.5. Evolution of a plunging breaker.

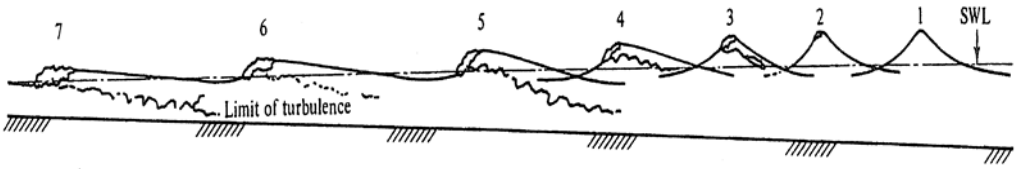

Figure 4.6. Evolution of a spilling breaker.

Differently from the two abovementioned types of breaking, the collapsing one (Figure 4.7) is characterized by a wave break that occurs at the wave's toe, accompanied by the creation of foam and air bubbles.

As regards the surging breaking, it is quite similar to the previous one but, instead of the collapse of the wave, it shows an unbroken wave profile, with the lower part of the wave characterized by some air running up to the shore (Figure 4.8).

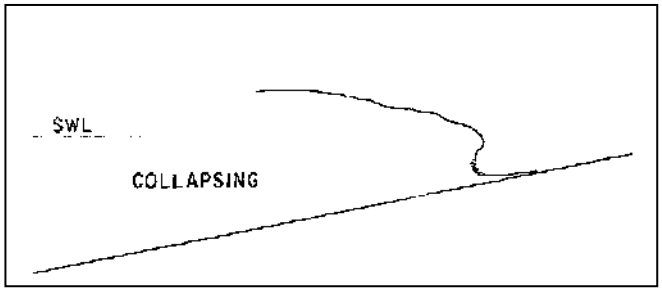

Figure 4.7. Collapsing breaker. (Galvin, 1968).

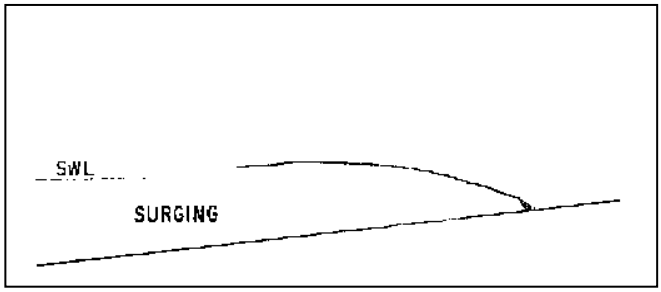

Figure 4.8. Surging breaker. (Galvin, 1968).

In addition to the above, Galvin (1968) observed that the spilling generally occurs in the case of gentle sloped bottoms and steep waves. Furthermore, spilling breaker tends to a plunging or a collapsing/surging one as the bottom slope increases and the wave steepness decreases.
More specifically, the Author observed that the wave breaking shape can be classified according to the surf-similarity parameter (Battjes, 1974):

- Spilling $\xi_0<0.5$;
- Plunging $0.5<\xi_0<3.3$;
- Collapsing/surging $\xi_0>3.3$;

4.1.2. Wave breaking for submerged breakwaters

Several studied are available in literature for the prediction of wave breaking induced by submerged breakwaters. In fact, the main purpose of a conventional breakwater is to force the breaking of higher waves, to induce a turbulent energy dissipation phenomenon, which is generally accompanied by a reduction of the transmission coefficient. Nevertheless, wave breaking often determines a

scour at the toe of the structures and the suspension of sedimentary material, which is often carried away by coastal currents. Moreover, it is able to induce hydraulic gradients, which may lead to erosive currents in the nearshore area.

For all the reasons above, the wave breaking represents one of the most important aspects to define for a proper design of a structure. One of the first studied aimed at the prediction of wave breaking occurrence for submerged breakwaters was that proposed by Nakamura et al. (1966). The Authors, analyzing 2D experimental data conducted with regular waves and impermeable structures, proposed the graph shown in Figure 4.9, allowing to distinguish breaking from non-breaking waves. The thresholds given in the graph depend on three main parameters: the deep wave steepness, H_0/L_0; the ratio between the submergence of the structure, Rc (defined as the difference between the water depth, d, and the height of a structures, h_s) and structure width, B; and Rc/L_0.

In particular, as it is possible to observe from Figure 4.9, the curves characterized by a constant value of Rc/B allow to define an upper region, characterized by the absence of wave breaking, and a lower one, where the wave breaking occurs. Furthermore, Figure 4.9 shows that an increase of the width of the structure (i.e. lower Rc/B values) corresponds to upper curves with an increase in the probability of observing the wave breaking.

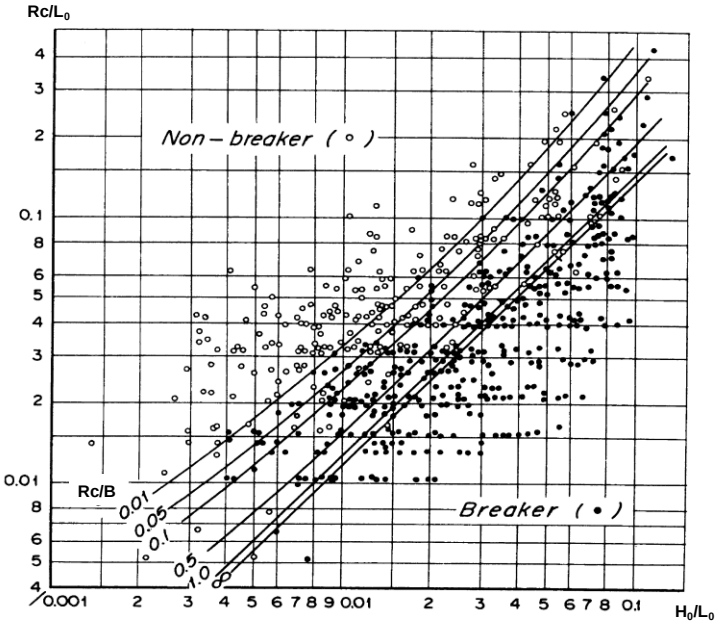

Figure 4.9 Wave breaking limit (Nakamura,1966).

In 1991 Smith and Krouse analyzed the breaking of regular waves in the presence of natural bars and submerged breakwaters. The Authors observed that the breaking index H_b/d_b increases as the Irribarren parameter, ξ_0, increases, until the latter reaches a value of 0.85,while for larger values a decrease in the breaker index was observed (Figure 4.10).

This different behaviour was attributed to the influence on incipient wave breaking condition of an offshore current velocity. In particular, it was observed that, for higher values of the aforementioned current velocity, the wave breaking occurred before the attainment of the limit value of the wave height to depth ratio.

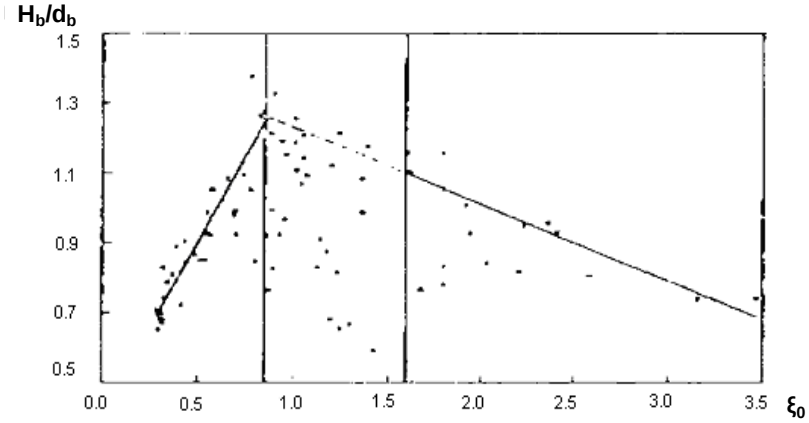

Figure 4.10 Wave breaking index for bar profiles (Smith and Kraus, 1991).

Moreover, according to the Authors, the aforementioned current had a destabilizing effect at low values of ξ_0. In fact, as it is possible to observe in Figure 4.11, the $x_p/H_{b,}$ ratio decreases as ξ_0 increases, until it reaches a constant value for higher ξ_0. The Figure also shows that flat bottoms are characterized by higher values of the plunge distance than the sloped ones. An influence of the Iribarren parameter was also observed on the ratio between the plunge point and the splash one, x_s. In fact, the ratio x_p/x_s decreases as ξ_0 increases in case of bar profiles, while a unit value was obtained in the case of a flat bottom. It was also observed that for a given wave steepness, the H_b/H_0 ratio decreases as the bar

slope increases; while for low values of the wave steepness the same ratio assumes higher values than those retrieved for high wave steepness.

In the same study, a classification of the wave breaking was conducted according to that proposed by Galvin for natural beaches (Galvin, 1968). The results, summarized in Figure 4.12 show that in case of bar profiles the transition between different types of wave breaking occurs at values of the Iribarren parameter lower than those referred to flat bottoms.

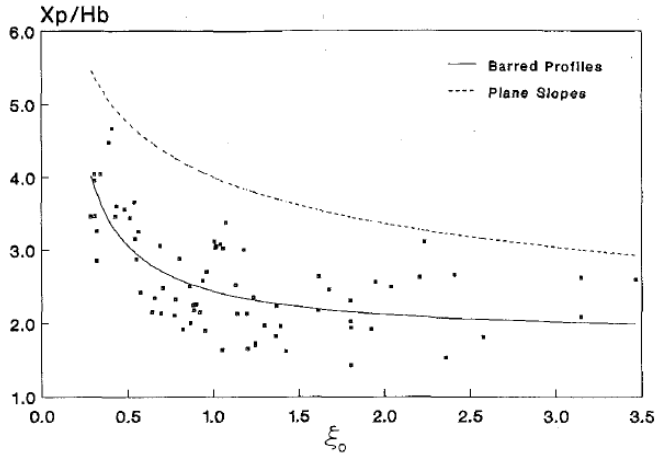

Figure 4.11. Influence of the Iribarren parameter on the x_p to H_b ratio (Smith and Kraus, 1991).

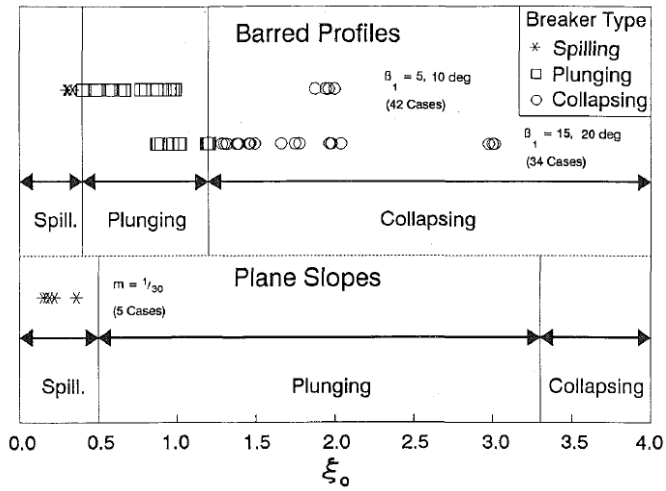

Figure 4.12. Types of breaking for plane slopes and for barred profiles. (Smith and Kraus, 1991).

In 1992 Hara et al. analysed the occurrence of wave breaking performing extensive numerical experiments on the transformation of a solitary wave, passing across an impermeable trapezoidal type breakwater, located on horizontal sea bottom. After regression analyses of the numerical computations, the study demonstrated that an increment of the barrier's slope corresponds to a larger probability of wave breaking, while the wave morphology plays a minor role.

Differently from natural beaches, where the breaking was assumed to be a function of the slope of the bottom and of the wave steepness only (through the Iribarren parameter), in the case of structures, the dependency on the submergence must also be taken into account. In particular, the Authors modified the surf-similarity parameter according to the following Equation for trapezoidal structures with height h_s and width B:

$$\xi' = \left(\frac{B}{d} + \frac{h_s/d}{3.5\tan\alpha}\right)^{0.2} \frac{h_s/d}{(H/d)^{0.4}} \tag{4.13}$$

In the previous Equation, d and H were computed at the offshore toe of the structures. differently from what discussed

Differently from what observed for natural beaches, the breaking probability increases with the modified surf-similarity parameter. Moreover, as already observed by Nakamura et al. (1966), the breaking probability increases at increasing crest widths and submergences.

All the studies described above did not explicitly address the influence of the porosity of the barrier on the breaking phenomenon. One of the first studies on this topic was that by Hattori and Sakai (1994), in which the occurrence and the typology of wave breaking for structures characterized by fixed shapes and different porosities (0 to 0.52) were investigated.

The Authors observed that the wave breaking is influenced by an offshore current over the breakwater, the intensity of which decreases as the porosity of the barrier increases. This current determines the collapsing of the waves when the latter achieves a limit steepness, defined by the following Equation: .

$$\frac{H_b}{L_0} = A_b \left(\frac{2B}{5d}\right)^3 \frac{d}{L_0} \xi' \tag{4.14}$$

In this Equation, the hydraulic characteristics are computed at the offshore toe of the structure; ξ' is calculated by means of Equation (4.13); A_b is a function of the relative submergence, *Rc/d*, and of the permeability of the structures, ε, according to Equation (4.15).
As a consequence, the increment of permeability corresponds to an overall reduction of wave breaking probability.

$$A_b = \left(1 - 0.12\frac{Rc}{d} - 0.6\varepsilon\right) exp\varepsilon \tag{4.15}$$

In the addition to the above, the Authors proposed the following two Equations for the definition of the location of the breaker: Equation (4.16) provides the minimum value of wave height necessary for the wave breaking on the crest of the structures, while Equation (4.17) returns the maximum value after which breaking occurs on the offshore slope.

$$\frac{H_b}{L_0} = \left(\frac{Rc}{L_0}\right)^{6/7} exp(2.7\varepsilon - 1.8) \tag{4.16}$$

$$\frac{H_b}{L_0} = \left(\frac{Rc}{L_0}\right)^{6/7} exp(1.2\varepsilon - 0.8) \tag{4.17}$$

Furthermore the breaking point was found to be influenced by the permeability of the structure, as well as by H_b/L_0 and Rc/L_0, as per the Equation (4.18). It can be noticed, the breaking moves from the slope of the structures to its crest as the permeability increases.

$$\frac{x_b}{B} = ln\left[\frac{H_b}{L_0}\left(\frac{Rc}{B}\right)^{-6/7}\right] - 1.2\varepsilon + 0.8 \tag{4.18}$$

A subsequent study conducted by Kawasaki and Iwata (1996), on impermeable and rectangular structures with monochromatic waves, underlined the importance of the crest width on the wave breaking phenomenon. In particular, the Authors observed a reduction of breaker index occurring at increasing crest widths and at decreasing relative depths. Moreover, a reduction of the limit of wave breaking leads to a shoreward motion of the breaking point.

Kawasaki and Iwata (2001) further proposed a breaking index based on the ratio between the incident wave height and the submergence of the structure, on the basis of the results of an experimental campaign on impermeable submerged breakwaters with trapezoidal section. According to this study, the offshore slope of the barrier, $tan\alpha$, does not influence the breaker index to a significant extent, but impacts on the position of the breaking point, that moves offshore as the offshore slopes increases.

The H_i/Rc term was assumed to be a function of the ratio between the water depth and the the incident wave length, d/L_i. In particular, the breaker index increases as d/L_i increases, independently from the slope of the barrier.

Subsequently, a new study was conducted by Calabrese et al. (2008a), with the aim of indentifying the macro-features and the incipient condition of wave breaking, in the presence of submerged breakwaters. The Authors classified the wave breaker by means of the visual analysis of 2D regular tests, conducted by varying the permeability and the offshore slope of rubble mound submerged breakwaters

In particular, both hydrodynamics and morphological considerations were employed as discriminating criteria for the identification of: the incipient breaking condition; the shape of wave profile at breaking; and the breaker evolution. On the basis of the first two aforementioned aspects, the Authors identified the following main typologies of wave breaking:

- “spilling” breaker;
- “plunging” breaker;
- “bore” breaker;
- “collapsing-surging” breaker;
- “two-steps” breaker.

While the first two types are characterized by breaking occurring at the wave crest, the others correspond to a rupture at the toe of the wave.
In agreement with the classification proposed by Galvin (1968) for natural beaches, the Authors defined the spilling as the breaking characterized by a plunging jet weakly impacting close to the crest, not accompanied an increment of the wave steepness nor by air bubbles under the wave trough (Figure 4.13). In a similar fashion, the plunging breaking is very similar to that characterizing natural beaches, i.e.it occurs when the presence of air trapped by the plunger vortex is significant (Figure 4.14).

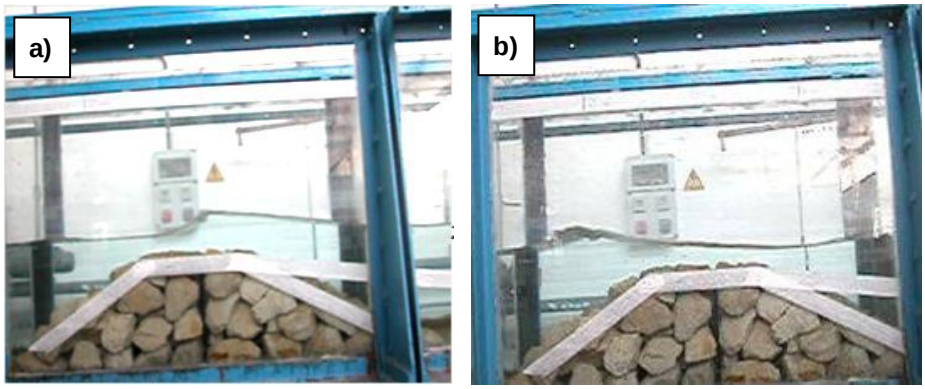

Figure 4.13. Evolution of a spilling breaker on a conventional breakwater. (Courtesy of M. Buccino).

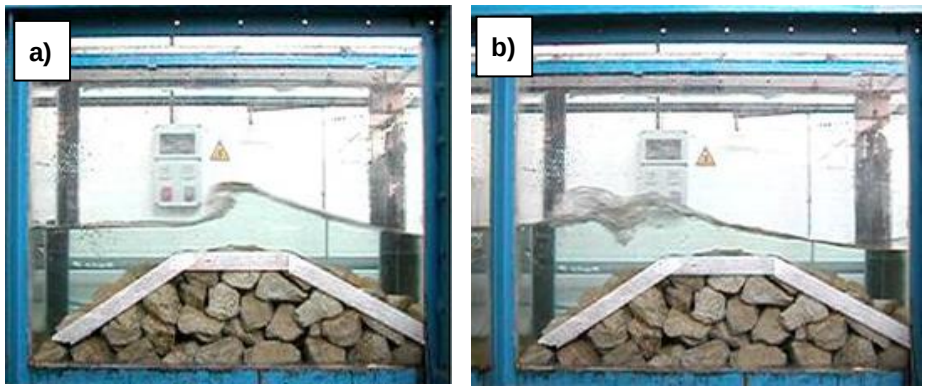

Figure 4.14.Evolution of a plunging breaker on a conventional breakwater. (Courtesy of M. Buccino).

Moreover intermediate cases were also observed and classified as "spilling-to-plunging" breaker. As it can be observed in Figure 4.15, this typology of wave breaking is characterized by a plunging, that detaches from the crest and then impacts very close to the wave crest, similarly to the spilling, as well as by the presence of air under the wave trough, as typical of a plunging. These types of breakers were observed by when the structure was wide enough, compared to the incident wavelength (Calabrese et al., 2008a).

All the previous types of breaker exhibit a steep wave profile; whereas the bore-type one is characterized by a nearly horizontal stretches, connected by a central bore. This bore originates from one or more plunging jets, detaching from the wave crest, and stationary evolves on the crest of the breakwater (Figure 4.16).

In some cases, the Authors observed that, after a first bore-like rupture, the breaker evolves in a way quite similar to the spilling-to-plunging one, i.e. with a descending slope profile in the offshore direction. This hybrid breaking condition was called "Bore – spilling-to-plunging" breaker (Figure 4.17).

Bore breakers were typically observed by the Authors in the case of permeable steep-faced breakwaters (1:2 slope).

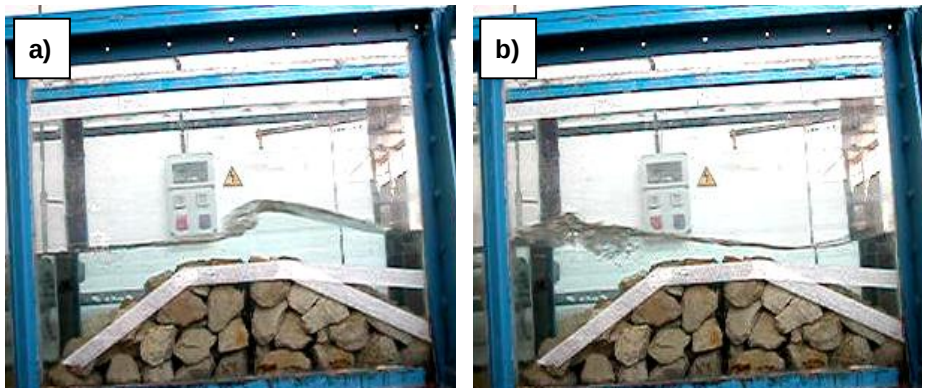

Figure 4.15 Evolution of a spilling-to-plunging breaker on a conventional breakwater. (Courtesy of M. Buccino).

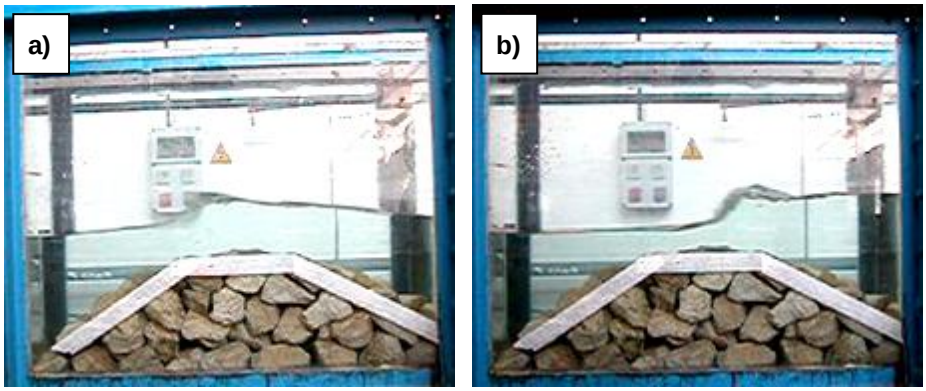

Figure 4.16.Evolution of a bore breaker on a conventional breakwater. (Courtesy of M. Buccino).

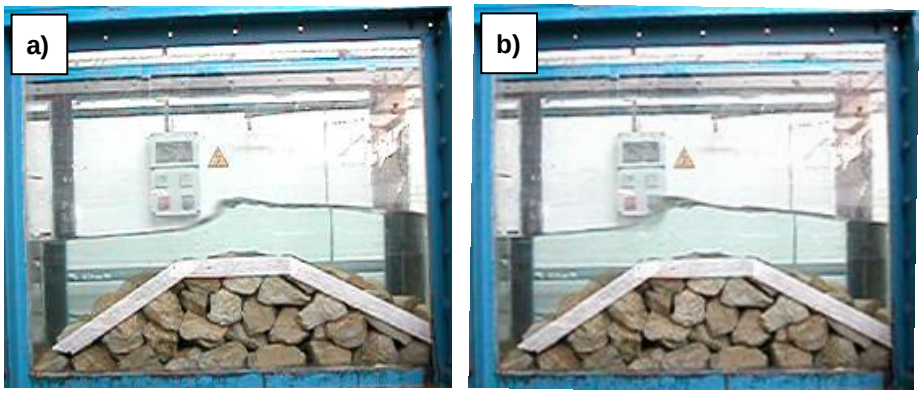

Figure 4.17.Evolution of a bore-spilling-to plunging breaker on a conventional breakwater. (Courtesy of M. Buccino).

The collapsing and the surging breakers are characterized by a plunging jet that detaches from the lower part of the wave profile and by a rise in slope towards offshore direction. In particular, similar to natural beaches, the first breaker was identified by a collapse in the lower part of the wave profile (Figure 4.18 a), while the surging one by an unbroken wave profile (Figure 4.18 b). This type of breaking was observed only for impermeable and steep-faced structures (1:2).

Two different types of intermediate breakings were also identified, namely the "collapsing – bore" and the "collapsing – spilling-to-plunging". The former, typical of lower heights, feature a wave profile on the top of the breakwater similar to an hydraulic jump; the latter is characterized by a supplementary jet

projected forward from a skewed wave crest on the crown of the structure, and a wave profile with a descending slope in the offshore direction.
Finally, the Authors identified the so-called "two-step" breaker, made by two different and subsequent wave ruptures: a first characterized by a plunging jet moving from the middle part of the front; and the second, similar to a spilling–to-plunging breaker (Figure 4.19).

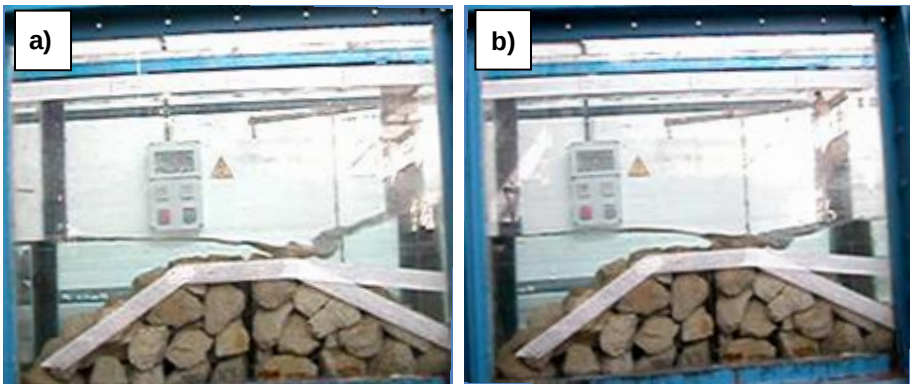

Figure 4.18. a) Collapsing breaker; b) Surging breaker. (Courtesy of M. Buccino).

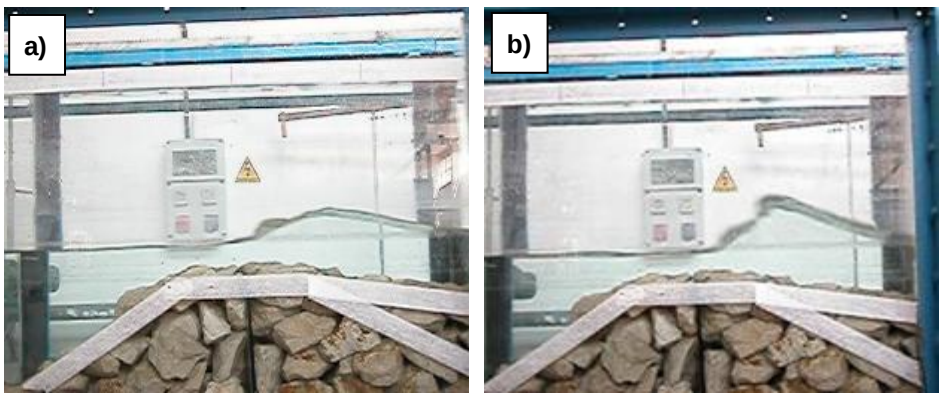

Figure 4.19. Example of a two-step breaker. (Courtesy of M. Buccino).

This type of braking was observed only for 1:10 seaward slope breakwaters, exposed to longer waves.
The Authors also identified the condition of incipient breaking for permeable and impermeable breakwaters, according to the following Equation, originally proposed by Goda (1974):

$$\frac{H_i}{Rc} = A\frac{L_0}{Rc}\left[1 - exp\left(-1.5\frac{\pi Rc}{L_0}\right)\right] \tag{4.19}$$

In the previous Equation, A represents a tuning parameter, which varies with the permeability, P, and with the offshore slope of the structure (Eq. 4.20):

$$A = 0.17exp(0.56P - 0.28\tan\alpha) \tag{4.20}$$

Results of the analyses were summarized in a graph, shown in Figure 4.20, allowing to classify the wave breaker based on two non-dimensional parameters:

$$R_d^* = \xi\frac{H_i}{Rc}\exp(-1.7P) \tag{4.21}$$

$$\xi_B = \frac{h_s}{\frac{h_s}{m} + B}\sqrt{H_i L_0} \tag{4.22}$$

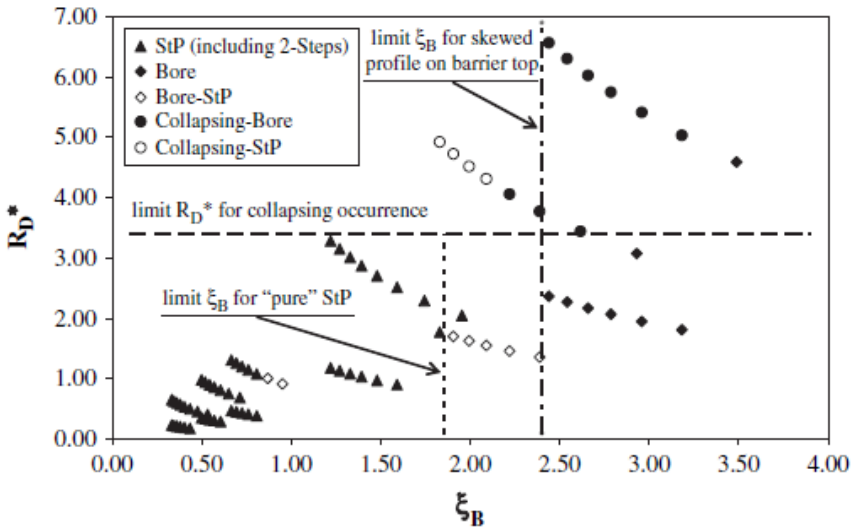

Figure 4.20. Breaker type parameterization.

The Authors observed that the collapsing breaker was the only one occurring for R_d^*>3.5. Conversely, for lower values of R_d^* it was possible to observe

different breaking conditions and to classify them according to the ξ_B parameter. The spilling and plunging breakers occurred for ξ_B approximately less than 1.7÷1.8, while the bore breaker was mainly observed in the case of permeable and steep-faced structures, with $\xi_B > 2.4$. A transition region where bore – spilling-to-plunging breaking is more likely was also observed between 1.8 and 2.4.

4.2 Wave transmission for submerged and low-crested traditional breakwaters

The wave attenuation phenomenon induced by the introduction of a nearshore breakwater is one of the most investigated aspects of the wave-barrier interaction and definitely the primary effect to study from an engineering point of view. This is generally measured by the transmission coefficient, K_T, defined as the ratio between the wave height shoreward the barrier (transmitted wave height, H_t) and that immediately seaward of it (incident wave height, H_i). This coefficient provides a concise measure of the degree of protection afforded to the coast. In the following, a review of the main studies available in the literature for the assessment of the transmission coefficient of conventional submerged and low-crested breakwaters is presented. In Figure 4.21 the main variables that influence the transmission process are shown.

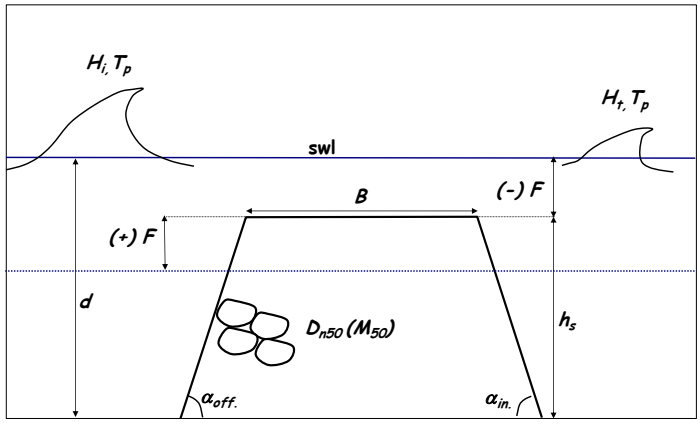

Figure 4.21. Graphic representation of the main geometrical and hydraulic variables influencing the transmission process.

One of the first studies investigating the transmission coefficient at submerged breakwaters was produced by Dattatri et al. (1978). In this study several types and shapes of permeable and impermeable submerged breakwaters were tested with 2D regular waves.

The influence of several geometrical and hydraulic characteristics on K_T was investigated, namely the crest width, B, the crest freeboard (defined as the difference between the height of the structure, h_s, and the water depth, d), F, the incident wave height, H_i, the water depth, d, and the incident wave length, L_i.

Results firstly indicated that the relative depth of the crest submergence, F/d, plays the major role in influencing the performance of an impermeable submerged breakwaters. This results also applies to permeable structures since the energy transmitted across the structure is a small percentage of the energy transmitted over the crest. The study also showed that K_T generally increases as F/d increases. Moreover, for large values of F/d (0.2 to 0.4) an influence of the relative depth of water, d/L_i was also observed (the larger d/L_i, the greater the transmission), as a consequence of deeper water waves and more energy concentrated near the surface, easily transmitted across the structures.

Another significant parameter was identified in the relative crest width, B/L_i. The Authors also observed a decrement of K_T at increasing B/L_i values, until the transmission assumes a minimum value, depending on F/d. After this minimum is reached, K_T tends to further increase with B/L_i, before stabilizing around an asymptotic value (Figure 4.22).

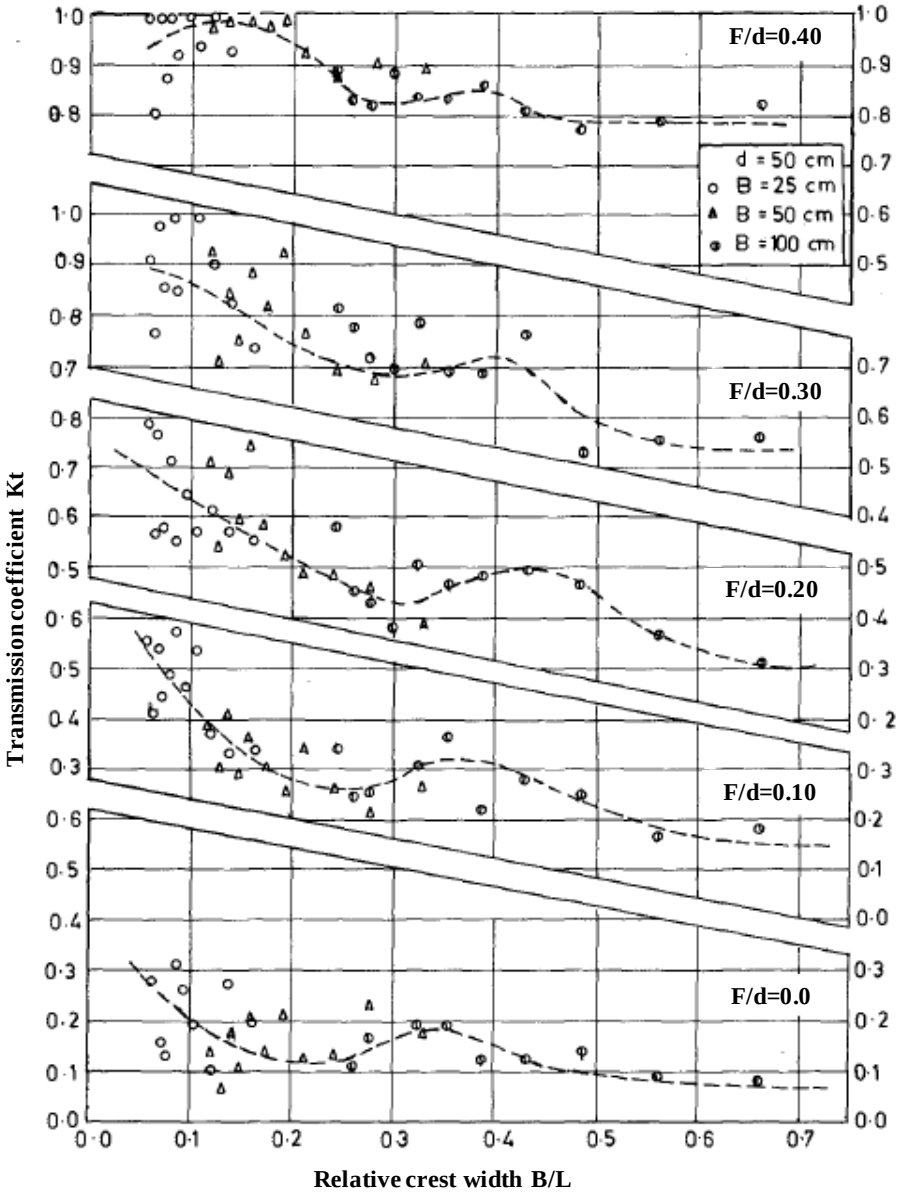

Figure 4.22. Transmission coefficient versus relative crest width for different *F*/*d* values (Dattatri et al., 1987).

Similarly to what observed by Goda et al. (1967) and by Jonson et al. (1951), the transmission coefficient appears to be not significantly influenced by the incident wave steepness, Hi/L_i when this parameter reaches high values (0.037-0.083 according to Dattatri et al., 1978).

On the bases of about 108 tests performed on submerged breakwaters, Gómez and Valdéz (1990) confirmed the dependence of K_T on the ratio between the crest width, B, and the deep wave length, L_0. Furthermore the dimensionless parameter H_i/d was observed to influence the amplitude of the transmission coefficient (K_T increases at increasing H_i/d), as shown in Figure 4.23.

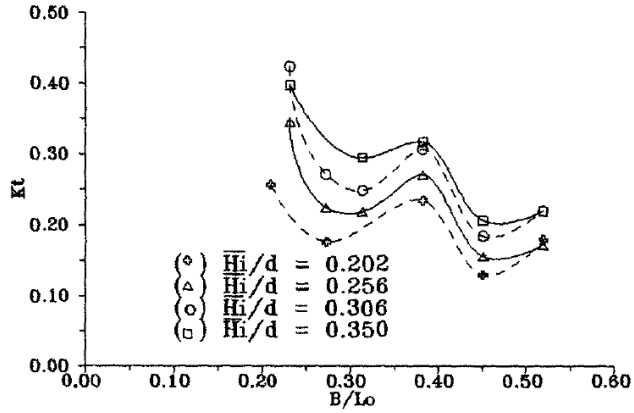

Figure 4.23. Transmission coefficient versus relative crest width for different H_i/d values (Gomez and Valdès, 1990).

In order to take into account the wave breaking, a new parameter was introduced by Gomez and Valdès, namely $\xi B/F$, where ξ is the Iribarren parameter, computed according to the following equation:

$$\xi = \frac{tg\alpha_{off}}{s_0^{0.5}} \tag{4.23}$$

In the previous equation $tg\alpha_{off}$ is the seaward slope of the structure and s_0 is the deep water wave steepness, H_i/L_0.

In 1990 a new formula for the prediction of the K_T was proposed by van der Meer, on the basis of the tests by Seelig (1980), Allsop (1983), Powell and Allsop (1985), Daemrich and Kahle (1985), Ahrens (1987) and van der Meer (1988). In this case, K_T was considered to be a linear function of the dimensionless parameter F/H_{si}, according to the following experimental formula:

$$K_T = a\frac{F}{H_{si}} + b \tag{4.24}$$

where H_{si} is the incident significant wave height and the coefficients of the linear regression, *a*, and *b* are equal to -0.3 and 0.46, respectively.
The Equation (4.24) returns values larger than 1 for low relative submergences ($F/H_{si} < -1.13$) and values slightly larger than 0 for structures characterized by a considerable relative freeboard ($F/H_{si} > 1.2$). For this reasons, the Author suggested to employ the previous equation for the range of values $0.2 < F/H_{si} < 1.13$. In fact, constant values of K_T equal to 0.8 and 0.1 were observed, respectively for $1.13 < F/H_{si} < 2$ and $-2 < F/H_{si} < -1.2$ (Figure 4.24).

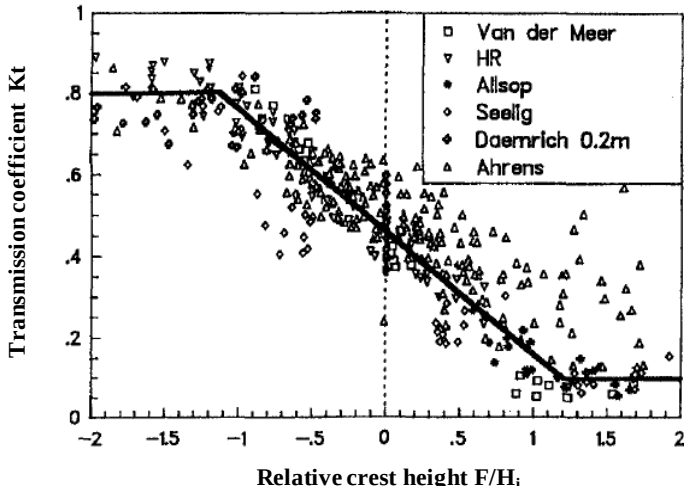

Figure 4.24. Wave transmission versus relative crest height (van der Meer, 1990).

One year later, a new formula for the prediction of wave transmission at permeable low crested structures was presented by Daemen in his Master's thesis (Daemen, 1991) and subsequently published by van der Meer et al. (1991).
The latter was based on 316 tests; in fact the data set employed by van der Meer (1990), was re-analyzed excluding data by Ahrens (1987), due to the different hydraulic response of reef breakwater tested in this study, with respect to that of the others. According to the Authors, part of the scatter previously

observed between predicted and calculated K_T was due to the permeability of armour layer, in particular for structures with crest slightly above m.s.w.l.
The formula proposed had the same linear expression of Equation (4.24), but the ratio between the freeboard and the nominal rock diameter[4] of armour layer, D_{n50}, was introduced (Eq. 4.25).

$$K_T = a\frac{F}{D_{n,50}} + b \tag{4.25}$$

The slope of the previous equation, a, is a function of the relative wave height, H_{si}/D_{n50}:

$$\mathrm{a} = 0.031\frac{\mathrm{H_{si}}}{\mathrm{D_{n50}}} - 0.24 \tag{4.26}$$

Intercept b depends on $H_{si}/D_{n,50}$, B and on the wave steepness, s_{0p}:

$$\mathrm{b} = 0.51 - 5.42\mathrm{s_{0p}} + 0.0323\frac{\mathrm{H_{si}}}{\mathrm{D_{n50}}} - 0.0017\left(\frac{\mathrm{B}}{\mathrm{D_{n50}}}\right)^{1.84} \tag{4.27}$$

The wave steepness is defined as $s_{0p} = 2\pi\, H_{si}/g\, T_{pi}^2$, i.e. the ratio between the significant incident wave height and the deep water wave length, L_{0p}, calculated in function of the incident peak wave period, T_{pi}.
The validity of Eq. (4.25) is limited to $1 < H_{si}/D_{n50} < 6$; $0.01 < s_{op} < 0.05$ and $0.075 < K_T < 0.75$. A comparison between the measured and predicted transmission coefficient is shown in Figure 4.25.

[4] The nominal rock material is defined as the cubic square of the ratio between the 50% value of rock mass distribution curve, M_{50}, and the rock density, ρ_r.

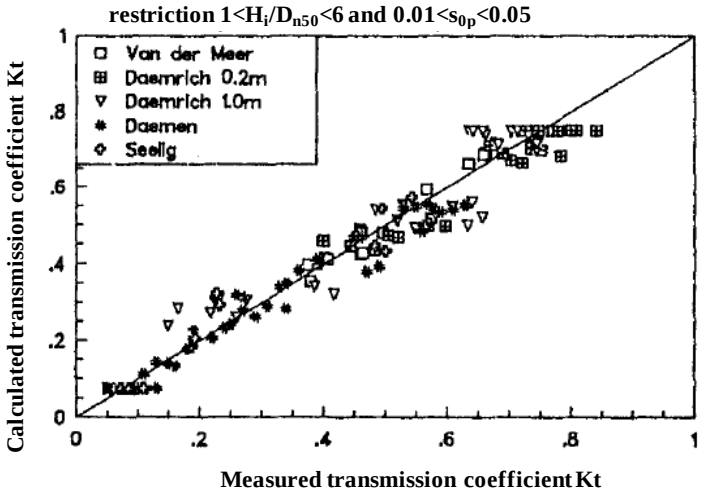

Figure 4.25. Comparison between measured and calculated transmission coefficient (Deamen, 1991)

One of the most employed design equations is that proposed by d'Angremond et al. (1996). The Authors extended the database employed in Daemen (1991) with 82 tests conducted at the Delft Hydraulics. Including impermeable structures and considering only data characterized by $-2.5 < F/H_{si} < 2.5$; $s_{0p} < 0.6$ and $H_{si}/d < 0.54$, the Authors developed the following predictive transmission formula:

$$K_T = -0.4\left(\frac{F}{H_{si}}\right) + x\left(1 - e^{-0.5\xi_p}\right)\left(\frac{B}{H_{si}}\right)^{-0.31} \tag{4.28}$$

where x is a coefficient equal to 0.64 for permeable structures and 0.8 for impermeable ones. ξ_p is the Iribarren parameter, given in Equation (4.29), where s_{0p} is computed using the wave peak period.

$$\xi_p = \frac{tg\alpha_{off}}{s_{0p}^{0.5}} \tag{4.29}$$

Results of the comparison between computed and predicted K_T are shown in Figure 4.26 and Figure 4.27, respectively for permeable and impermeable

structures and d'Angremond et al. (1996) proposed an applicability range of $0.075 < K_T < 0.8$, that is similar to that defined by Daemen (1991).

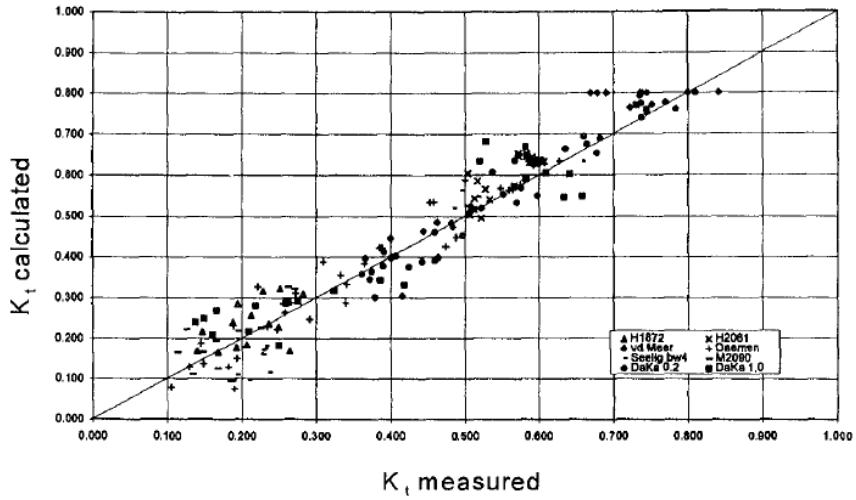

Figure 4.26. Comparison between measured and calculated transmission coefficient for permeable structures (d'Angremond, 1996).

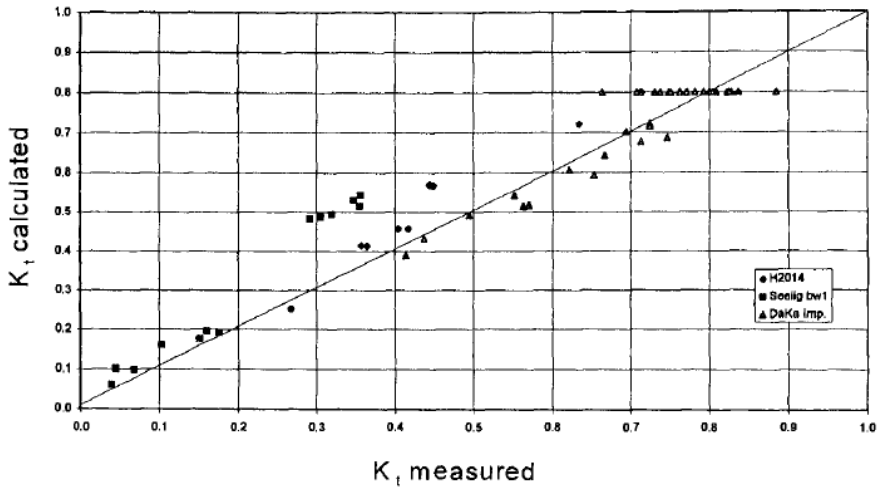

Figure 4.27. Comparison between measured and calculated transmission coefficient for impermeable structures (d'Angremond, 1996).

Few years later, in 1998, Seabrook and Hall (1998) performed an experimental study at the Queen's University Coastal Engineering Research Laboratory in Kingston, Canada, on submerged rubblemound breakwaters. In these tests,

conducted in two-dimensional and three-dimensional conditions, a wide range of the geometrical characteristics was investigated including several crest widths. The Authors considered the relative submergence, the incident wave height and the crest width as the main variables that influence the transmission process (Eq.(4.30) and Figure 4.28).

$$K_T = 1 - \left\{ \exp\left[-0.65\left(\frac{F}{H_i}\right) - 1.09\left(\frac{H_i}{B}\right)\right] + 0.047\left(\frac{BF}{L_{ip}D_{n50}}\right) - 0.067\left(\frac{FH_i}{BD_{n50}}\right)\right\} \quad (4.30)$$

In the previous Equation, L_{ip} represents the incident peak wave length, $BF/L_{ip}D_{n50}$ identifies load losses connected to the water flow, while the ratio FH_{si}/BDn_{50} represents energy dissipations due to the structure roughness.
The applicability range was fixed to $0 \leq BF/L_{ip}D_{n50} \leq 7.08$ and $0 \leq FH_{si}/BD_{n50} \leq 2.14$.

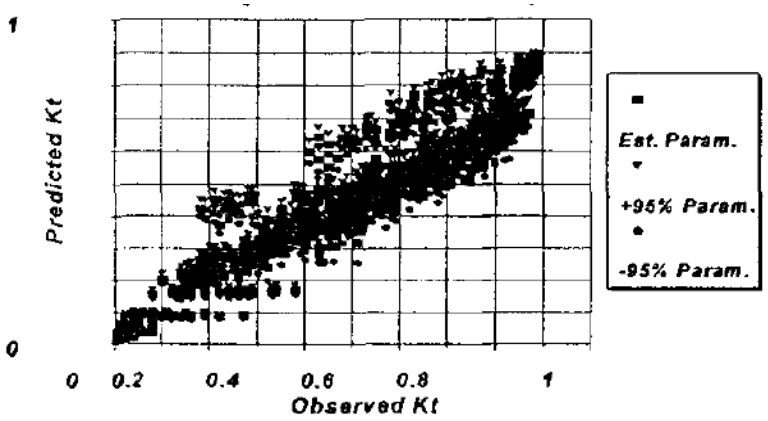

Figure 4.28. Comparison between the observed and the predicted transmission coefficient (Seabrook and Hall, 1998).

The previous predictive equations ware applied by Calabrese et al. (2003) on 48 large-scale experiments carried out at the "Grosser WallenKanal" of Hannover, Germany, on low-crested and submerged breakwaters in shallow water (in the following referred to as GWK data set). In particular, it was observed that for structures with a small crest width ($B/D_{n50} = 4$) the equations proposed by van der Meer (1990), Daemen (1991), d'Angremond et al. (1996) and Seabrook and Hall (1998) return similar values of bias (close to 1), while a minimum Root

Mean Squared Error (RMSE) was observed for van der Meer's ones (8.5%). The latter was 50% less than that obtained by Seabrook and Hall (16.4%). Conversely for large crest width ($B/D_{n50} = 16$), the equation proposed by van der Meer (1990) significantly overestimates the data, while the formulae of Daemen (1991) and Seabrook and Hall (1998) underestimate them. The model by d'Angremond et al. (1996), characterized be the lower values of RMSE, was found to be almost undistorted, although a certain scatter was observed.
The Authors considered that a better prediction of the transmission coefficient could be obtained considering a reduction rate that is function of *B* instead a constant one.
The developed model is expressed by Equation (4.31):

$$K_T = a\frac{F}{B} + b \tag{4.31}$$

where the slope, *a*, and the intercept, *b*, are defined according to the following equations:

$$a = a_1 \exp\left(0.2568\frac{B}{H_{m0i}}\right) \tag{4.32}$$

$$b = b_1 \exp\left(-0.08545\frac{B}{H_{m0i}}\right) \tag{4.33}$$

The term a_1 is a function of the breaking index, the latter expressed as the ratio between the incident significant spectral wave height, H_{m0i}, and the water depth, *d*:

$$a_1 = 0.6957\frac{H_{m0i}}{d} - 0.7021 \tag{4.34}$$

While b_1 is an exponential function of the Iribarren parameter:

$$b_1 = 1 - 0.562\exp\left(-0.0507\xi_p\right) \tag{4.35}$$

In this case the application range is: $-0.4 \leq F/B \leq 0.3$; $1.06 \leq B/H_{moi} \leq 8.13$; $0.31 \leq H_{moi}/d \leq 0.61$ and $3 \leq \xi_p \leq 5.20$.

In Figure 4.29 and Figure 4.30 the comparison between the measured and predicted K_T are shown respectively for the tests GWK data set and for the entire database.

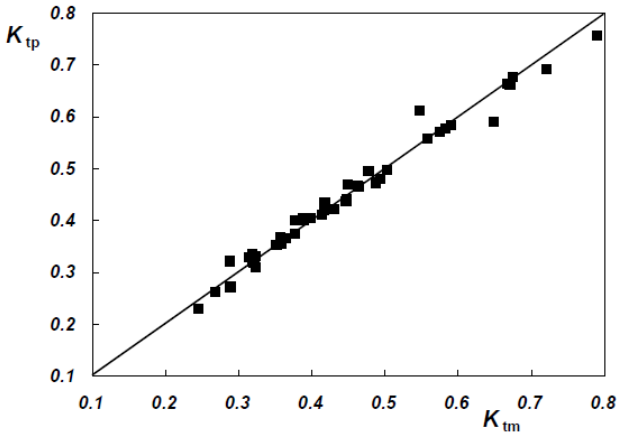

Figure 4.29. Comparison between the measured and predicted transmission coefficient for the GWK dataset (Calabrese et al., 2003).

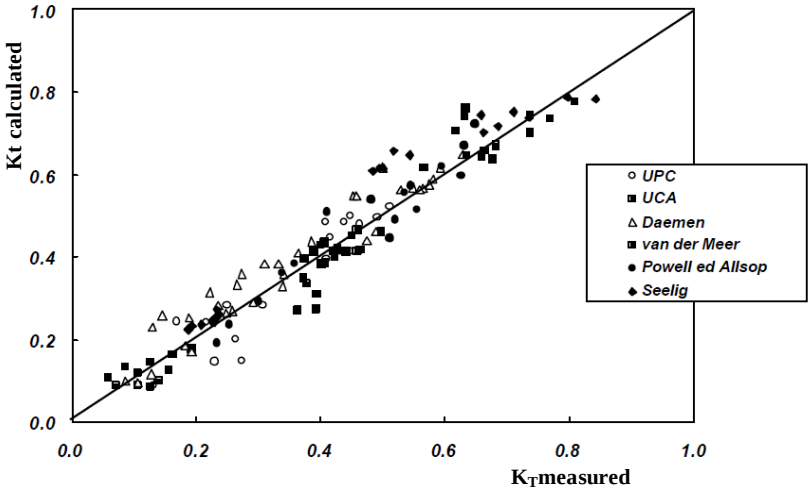

Figure 4.30. Comparison between measured and predicted transmission coefficient for the entire analysed database (Calabrese et al., 2003).

Wemsley and Ahrens in 2003 proposed an alternate formula for the prediction of K_T, defined as the Square Root of the Sum of Squares (SRSS) of two separate contributions: the first one related to the energy transfer through the porous structure, $K_{t,thru}$, and a second one related to the energy transfer over the barrier, $K_{t,over}$:

$$K_T = \sqrt{K_{t,thru}^2 + K_{t,over}^2} \tag{4.36}$$

The two partial transmission coefficients are:

$$K_{t,thru} = \frac{1}{1 + f_{thru}} \tag{4.37}$$

$$K_{t,over} = \frac{1}{1 + f_{over}} \tag{4.38}$$

According to the Authors the two terms f_{thru} and f_{over} can be calculated, for low-crested breakwaters, by means of the following Equations:

$$f_{thru} = \left(\frac{H_s}{D_{n50}}\right)^{0.982} \exp\left[0.433 + 2.35\left(\frac{A_t}{L_0 h_s}\right)\right] \tag{4.39}$$

$$f_{over} = \exp\left[0.465 + 12.7\frac{F}{\sqrt{H_{si}L_0}} - \frac{17.4}{\frac{A_t}{h_s D_{n,50}}} + \frac{0.00118}{\frac{H_{si}}{L_0}}\right] \tag{4.40}$$

H_s/D_{n50} allows to consider that the transmission process becomes inefficient if the disturbance exceeds the size of void spaces in the structures, while the ratio between the cross-section area of the breakwater, A_t, and the height of the structures, h_s, takes into account the influence of an equivalent crest width.
The Authors also considered that the transmission process is dominated by runup and overtopping in case of low-emergent breakwaters, while in case of submerged ones, the transmission over the structures is the prevalent

contribution. In this case a value of 9.0 is assumed for f_{thru} while the following expression is provided for f_{over}:

$$f_{over} = \exp\left[-0.646 + 0.631\frac{F}{H_{si}} - 0.00137\frac{A_t}{D_{n50}^2}\right] \quad (4.41)$$

In the same study, the performance of the predictive formulae proposed by van der Meer et al. (1991), d'Angremend et al. (1996) and Seabrook and Hall (1998) were compared with the curves of Tanaka (1976). These curves, developed for submerged and emergent structures through the use of monochromatic wave tests, allow to calculate a transmission coefficient defined as the ratio between the transmitted wave height and the deep water one, H_0. These are given as a function of the relative freeboard, F/H_0, (Figure 4.31a) and of the relative crest width, B/L_0 (Figure 4.31b).

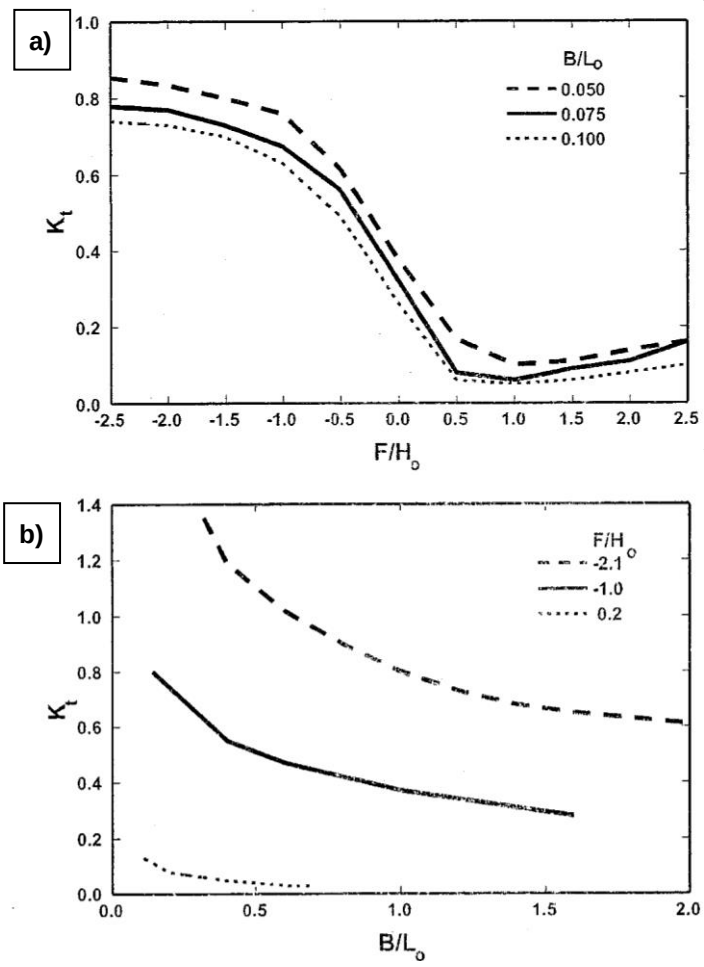

Figure 4.31. Curves providing the transmission coefficient as a function of: a) relative freeboard; b) relative crest width (Tanaka, 1976).

An inverted S-shape function, similar to that shown in Figure 4.31a, was observed in van der Meer (1991) and Wamsley and Ahrens (2003). Moreover, the same qualitative trend was exhibited by equations proposed by van der Meer and d'Angremond in the range $0.1 < K_T < 0.7$ and by Seabrook and Hall, in case of submerged structures.

A comparison between the above-mentioned predictive formulae in the B/L_0 vs K_T plane showed similar trends for the equations proposed by Seabrook and Hall and that by d'Angremond, in the range $-0.75 < F/H_0 < 0.5$.

The Authors considered the van der Meer formula suitable for narrow-crested breakwaters with a freeboard close to zero only. Furthermore, advise is given against the use of their formula (Eq. (4.36) in the specific case of submerged structures.

A new predictive formula (Eq. (4.42) was proposed by Friebel and Harris in 2004, developed from the analysis of experimental data provided by Seelig (1980), Deamirich and Kahle (1985), van der Meer (1988), Deamen (1991) and Seabrook e Hall (1998):

$$K_T = -0.4969\exp\left(\frac{F}{H_i}\right) - 0.0292\frac{B}{d} - 0.4257\frac{h_s}{d} - 0.0696\log\left(\frac{B}{L}\right) + \\ +0.1359\frac{F}{B} + 1.0905 \tag{4.42}$$

The validity of the previous formulation is limited to the following restrict ranges: $-8.696 < F/H < 0$; $0.286 < B/d < 8.750$; $0.440 < h_s/d < 1$; $0.024 < B/L < 1.89$ and $-1.05 < F/B < 0$.

An extensive study on the prediction of transmission coefficient past low-crested and submerged breakwaters was made by van der Meer et al. (2005) on more than 2,300 tests. The wide database employed consisted of data previously analyzed by d'Angremond (1996), Seabrook and Hall (1998) and Calabrese et al. (2002), with the addition of the experiments conducted on behalf of the DELOS project at the University of Cantabria (Garcia et al., 2004) and at the Polytechnic of Catalonia, Spain (Gironella, 2002). Moreover, the results of tests performed on artificial reefs by Hirose et al. (2002) and Melito and Melby (2002) were considered, respectively on Acquareef and Coreloc-armoured breakwaters.

The equation proposed by d'Angremond (1996) resulted to adequately fit data characterized by $B/H_i < 8$. In the range $B/H_i > 12$ the following modified equations was proposed:

$$K_T = 0.35\frac{F}{H_i} + 0.51\left(\frac{B}{H_i}\right)^{-0.65}\left(1 - e^{-0.41\xi}\right) \tag{4.43}$$

A linear interpolation between the Equations (4.28) and (4.43) was proposed in the range $8 < B/H_i < 12$.
The upper limit, K_{Tu}, was assumed as a linear function of the relative crest width, according to the Equation (4.44) and the lower limit was fixed at 0.05.

$$K_{Tu} = -0.006\frac{B}{H_i} + 0.93 \tag{4.44}$$

Buccino and Calabrese (2007a) considered a wide database composed of about 1,200 experimental data obtained from Loveless et al. (1997), Pilarczyk (2003) and those tests conducted on traditional submerged and low-crested breakwaters from the dataset analysed in van der Meer (2005).
Differently from the major part of the equations describe above, which were experimentally derived, the model by Buccino and Calabrese (2007a), called "Conceptual Approach" (CA), is theoretically deduced. The model was developed under some simplifying assumptions and has different formulations depending on the submergence of the structures. In particular, the model assumes that in the transmission process the wave breaking represents the dominating factor in case of submerged structures. In case of deep water the predominant factor is considered to be the mass flux over the structure, and for low-crested structures the overtopping and wave runup.
The CA for submerged breakwater will be presented in the Section 4.2, whilst.
The model developed by Buccino and Calabrese (2007a) for emerged breakwater is briefly discussed hereinafter.
The Auhtors, following the approach of Wamsley and Ahrens (2003), suggested the following formula for the prediction of the transmission coefficient:

$$K_T = \sqrt{\Pi^2 \exp\left(-b\frac{R^*}{\gamma_f}\right) + \left(\frac{1}{1+\upsilon}\frac{\min(F; R_{us})}{H_{si}}\right)^2} \tag{4.45}$$

where Π is the transmission coefficient for null freaboard, expressed by Equation (4.56), γ_f represents the surface roughness, R^* is the dimensionless crest height, R_{us} is the significant wave runup, which can be computed as a function of the Iribarren parameter (van der Meer, 1992), and υ is a coefficient

depending on the incident wave height, the water depth, the width of the rectangular structure and of the friction factor for trough-passing. The latter was assumed as a function of the porosity of the structure and of the diameter of the porous material.

4.2.1. Conceptual Approach for traditional submerged breakwaters

The Conceptual Approach (Buccino and Calabrese, 2007a) assumes the wave breaking on the crest of a submerged breakwater is the main energy dissipation mode. The energy loss is macroscopically modelled using the bore-like breaker approach, originally developed by Le Mehautè (1962) and subsequently employed by several Authors, such as Battejes and Stieve (1985), Thornton and Guza (1983), Svendsen and Petrevu (1993).
Under the hypotheses of wave attack normal to the breakwater and negligible mean currents over the crest, the model is developed starting from the following time-average energy balance equation:

$$\frac{\mathrm{dPle}}{\mathrm{db}} = \Delta \tag{4.46}$$

where *Ple* represents the wave power per unit of span at the landward edge of the crest; *db* is an infinitesimal increase of the crown width (Figure 4.32) and Δ is the mean dissipated power per unit area of horizontal surface.

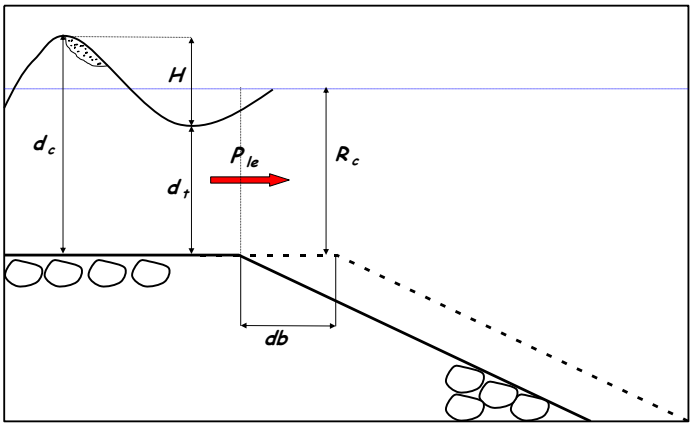

Figure 4.32. Main parameters employed in the energy balance at the basis of the Conceptual Approach for rubble mound submerged breakwaters.

According to the 'bore breaker' theory, Δ can be computed as follows:

$$\Delta = -\frac{\rho_w g}{4}\frac{{H_i}^2 c}{\sqrt{g H_i T}}\frac{H_i}{R_c}\frac{\Phi}{\left(1+\frac{R_c}{H_i}\right)^{0.5}\left(1+\frac{H_i}{R_c}\right)} \tag{4.47}$$

where g is the gravity acceleration, c is the wave phase speed, Φ is the dissipation factor for breaking waves ($\Phi \approx 1$) and R_c is the submergence of the breakwaters, defined as the difference between the water depth and the height of the structures (Figure 4.33).

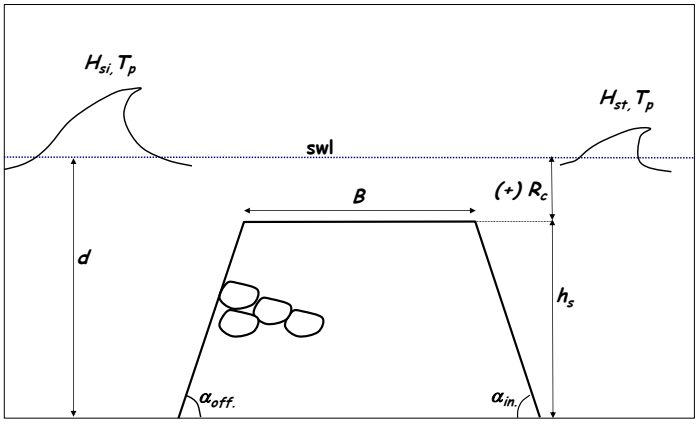

Figure 4.33. Main parameters of the Conceptual Approach.

After same algebra, a nonlinear differential equation is derived, which links the transmission coefficient to the main structure and wave quantities, such as the crest level, the crown width, the incident wave height and the peak period:

$$\frac{dK_T}{db} = -\frac{1}{G'} \cdot \frac{K_T^{5/2}}{\sqrt{H_i L_0}} \cdot \frac{H_i}{Rc} \cdot \frac{1}{\left(1 + \frac{\eta Rc}{K_T H_i}\right)^{0.5} \left(1 + \frac{K_T H_i}{\eta Rc}\right)} \tag{4.48}$$

In the previous equation, η is the ratio between the transmitted wave height and wave height at the landward edge of the breakwater crown and G' is a global dissipation factor which accounts for a number of constants.
The differential equation has been found to have two asymptotic solutions. The first applies to the case of deeply submerged structures, $Rc/H_{si} >> 1$, and reads as follows:

$$K_T = \frac{1}{(K_{t0}^s)^{-1} + G_1 \frac{B}{\sqrt{H_{si} L_{0p}}} \left(\frac{H_{si}}{Rc}\right)^{1.5}} \tag{4.49}$$

where K_{t0}^s is the transmission coefficient obtained for triangular breakwaters ($B = 0$), function of the relative submergence (H_{si}/R_c), and G_1 is the dissipation factor.
For shallow relative submergences, $R_c/H_{si} << 1$, the second asymptotic solution applies, which is independent from R_c/H_{si}:

$$K_T = \left(\sqrt{K_{t0}^n} - G_2 \frac{B}{\sqrt{H_{si} L_{0p}}}\right)^2 \tag{4.50}$$

In the equation above, K_{t0}^n and G_2 represent, respectively, the transmission coefficient for $B = 0$ and the dissipation factor.
In both the asymptotic solutions the effect of the structure crown is represented by $B/(H_{si}L_{0p})^{0.5}$, which can be considered as the geometrical mean of the two

most popular crown widths employed in existing transmission models, namely B/H_{si} '(d'Angremond et al., 1996)' and B/L_0 (Tanaka, 1976).

Equation (4.50) describes a parabola, i.e. the transmission coefficient decreases until it reaches a zero value and then unrealistically increases with the crown width (Figure 4.34).

For this reason the Authors suggested to horizontally cut the curve at the value of $B/(H_{si}L_{0p})^{0.5}$, referred to as B^* hereafter, beyond which the transmission coefficient is reduced to less than 5%. Accordingly, the following expression is obtained:

The two asymptotic solutions described in the Equations (4.50) and (4.51) respectively apply to deeply submerged structures and low submergence ones, i. e. for values of R_c/H_{si} respectively grater and less than two thresholds, S_1 and S_2. These can be define after a calibration of the theoretical model on real experimental data. A linear interpolation is suggested for intermediate situations, i.e. for $S_1<R_c/H_{si}<S_2$ (Eqs. 4.52-4.54).

The CA model assumes that the relationship between K_T and the main predictors depends on the relative submergence. This is believed to be related to a change in the dissipation mechanism that would occur when the water depth over which waves propagate reduces. Overall, the model has 6 parameters to be calibrated, namely two K_{t0}, two G, S_1 and S_2.

$$K_T = \left[\sqrt{{K_{t0}}^n} - G_2 \min\left(B^*; \frac{B}{\sqrt{H_{si}L_{0p}}}\right)\right]^2 \tag{4.51}$$

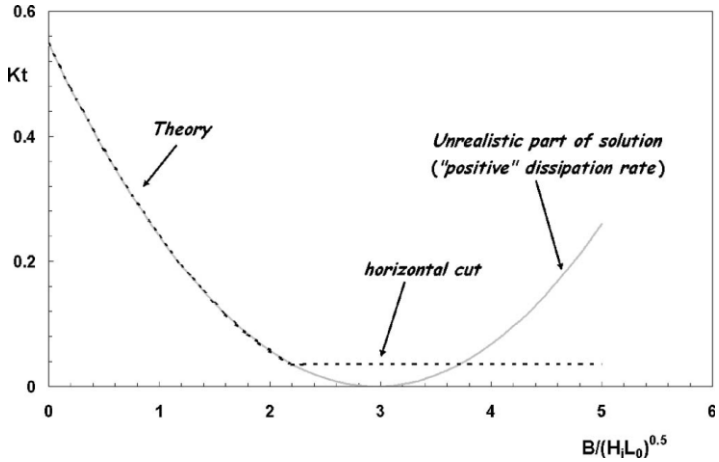

Figure 4.34. Theoretical cut of Equation (4.50). (Buccino and Calabrese 2007a).

$$K_T = \frac{1}{(K_{t0}^s)^{-1} + G_1 \frac{B}{\sqrt{H_{si} L_{0p}}} \left(\frac{H_{si}}{Rc}\right)^{1.5}} \qquad \text{for } \frac{R_c}{H_{si}} \geq S_1 \tag{4.52}$$

$$K_T = \left[\sqrt{{K_{t0}}^n} - G_2 \min\left(B_1; \frac{B}{\sqrt{H_{si} L_{0p}}}\right)\right]^2 \qquad \text{for } \frac{R_c}{H_{si}} \leq S_2 \tag{4.53}$$

$$K_T = a\frac{Rc}{H_{si}} + b \qquad \text{for } S_1 \leq \frac{R_c}{H_{si}} \leq S_2 \tag{4.54}$$

The calibration was performed by the Authors on a dataset of about 1,000 data specifically dedicated to submerged breakwaters, composed as follows:

- The data set used for the calibration of the Seabrook and Hall formula (Seabrook and Hall, 1998); acronym SH;
- Results of physical model tests conducted at the Coastal Engineering Laboratory of the University of Cantabria, Spain, (Garcia et al., 2004); UCA;
- Data from tests carried out at the CIEM wave flume of the Laboratori d'Enginyeria Maritima of Barcelona, Spain, (Gironella et al., 2002); UPC;
- Results of experiments conducted at the Grosser WellenKanal of Hannover, Germany (Calabrese et al., 2002); GWK;

- Data from experiments performed at the University of Bristol, U.K. (Loveless et al., 1997); UBr;
- Data from physical model tests conducted at Delft Hydraulics for the Amwaj Islands Development project (Pilarczyk, 2003); AID.
- The database used for calibration of d'Angremond et al. formula (de Jong, 1996). This database collects a number of studies from 1980 to 1991 (among which Seelig, 1980; Daemrich and Kahle, 1985; Powell and Allsop,1985; van der Meer, 1988, Daemen, 1991 were employed for calibrating CA for submerged breakwaters) and tests conducted at Delft Hydraulics, (acronym H2061 from the report number).

Results of the calibration are summarized in the following equations:

$$K_T = \frac{1}{1.18\left(\frac{H_{si}}{Rc}\right)^{0.12} + 0.33\frac{B}{\sqrt{H_{si}L_{0p}}}\left(\frac{H_{si}}{Rc}\right)^{1.5}} \qquad \text{for } 0.83 \le \frac{R_c}{H_{si}} \le 2 \qquad (4.55)$$

$$K_T = \left[min\left(0.74; 0.62\xi_{0p}^{0.17}\right) - 0.25min\left(2.2; \frac{B}{\sqrt{H_{si}L_{0p}}}\right)\right]^2 \qquad \text{for } \frac{R_c}{H_{si}} = 0 \qquad (4.56)$$

$$K_T = a\frac{Rc}{H_{si}} + b \qquad \text{for } 0 < \frac{R_c}{H_{si}} < 0.83 \qquad (4.57)$$

The upper limit of validity of Equation (4.55), $R_c/H_{si} < 2$, represents a threshold beyond which it is reasonable to assume that the breaking waves occur in the crest of the structures. However, employing data from Seabrook and Hall (1998), the Authors showed the applicability of the model until R_c/H_s reaches values around 3 (Buccino and Calabrese 2007b).

As far as K^s_{t0} is concerned, a slight dependence on R_c/H_{si} has been found for deeply submerged breakwaters. K^n_{t0} has been shown to be related to the Iribarren number. This is deemed to be related to the influence of the run-up height on the transmission process at low-submerged structures. In particular, for triangular structures it is assumed that:

$$K_{t0}^{n} = \frac{H_t}{H_i} \propto \frac{R_u}{H_i} \tag{4.58}$$

In fact, from Equation (4.56) it can be noticed the K^{n}_{t0} increase at increasing Iribarren parameter, ξ. A similar trend is also shown by R_u/H_i. at increasing ξ, as results from experimental tests. Furthermore, as already observed in other models, this trend should approach a constant value for high values of ξ.
B_1 in Equation (4.53) was conventionally assumed equal to 2.2, because for $B/(H_{si}L_{0p})^{0.5} \geq 2.2$ the transmission coefficient assumes values less than 0.05, so that it can be considered negligible. Coefficient *b* of the linear Equation (4.57) is the same reported in Equation (4.56), while the slope *a* is:

$$a = 0.833(b - f) \tag{4.59}$$

where:

$$f = \frac{1}{1.206 + 0.434\dfrac{B}{\sqrt{H_{si}L_{0p}}}} \tag{4.60}$$

A comparison between the measured and calculated transmission coefficients is shown in Figure 4.35. In this case the index of linear determination, R^2, is slightly greater than 95% and the standard error is less than 0.05.

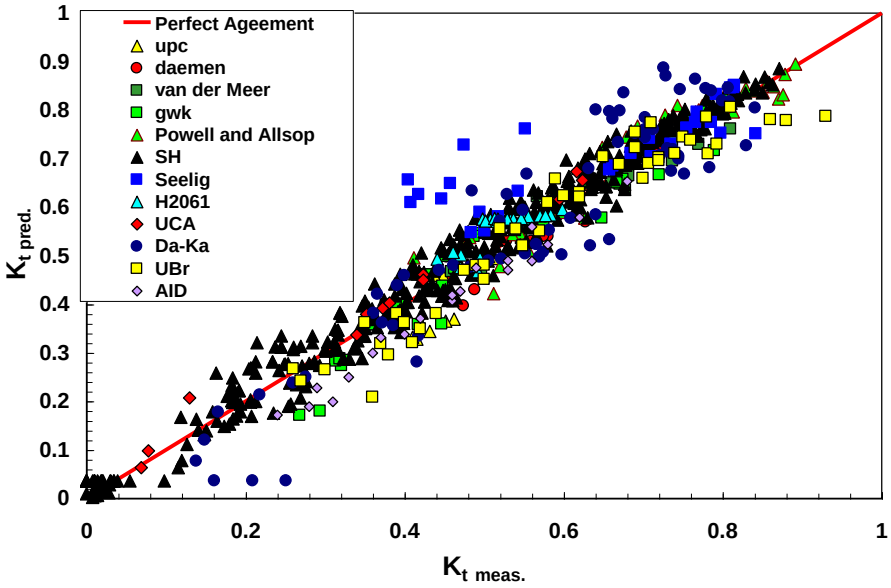

Figure 4.35. Comparison between measured and predicted K_T (Buccino and Calabrese, 2007a).

4.3 Wave Set-up for submerged and low-crested conventional breakwaters

Since the 1960's, the scientific community has dedicated several efforts to the study of the wave-barrier interaction, especially regarding the transmission coefficient, while few studies have been conducted in order to investigate the the increment of the medium sea water level following the introduction of a submerged or low-crested breakwaters, also known as "setup". Indeed, the knowledge of this phenomenon is important for a full comprehension of shadow zone hydrodynamic.

In fact, due to the reduction of the momentum flux caused by wave breaking and the mass transport process associated with wave overpassing, the wave setup behind the structures influences longhshore currents and the occurrence of dangerous rip currents. These are currents directed seaward, that may cause both an intense localized erosions and a serious risk for the safety of people (MacMahan et al., 2006).

First studies providing a qualitative description of these phenomena are those by Homma and Sokou (1959) and Homma and Hoikawa, (1961).

Longuet-Higgins in 1967 aimed at establishing the main parameters influencing the phenomenon, providing an analytical equation for the quantitative prediction of the water setup (Eq. (4.61). The latter allowed to estimate the difference, δ', between the water level shoreward and seaward of a submerged breakwater. The equation was developed, according to second order theory (Longuet-Higgins and Stewart, 1962), under the hypothesis of small amplitude waves and irrotational motion, considering the time-average flux of a vertical momentum into a column of water delimitated by the still water level and the free surface.

$$\delta' = \frac{H_i^2(1+K_R^2)k_I}{8sinh(2k_I d_I)} - \frac{H_i^2 K_T^2 k_{II}}{8sinh(2k_{II} d_{II})} \tag{4.61}$$

In Equation (4.61) k_I and d_I represent, respectively, the offshore wave number and water depth; k_{II} and d_{II} the same parameters evaluated inshore the

structures; K_R is the reflection coefficient, defined as the ratio between the reflected wave height, H_R, and incident one (Figure 4.36). Worth noting, in the previous equation, δ' increases with the reflection coefficient, while the transmission coefficient plays the opposite role.

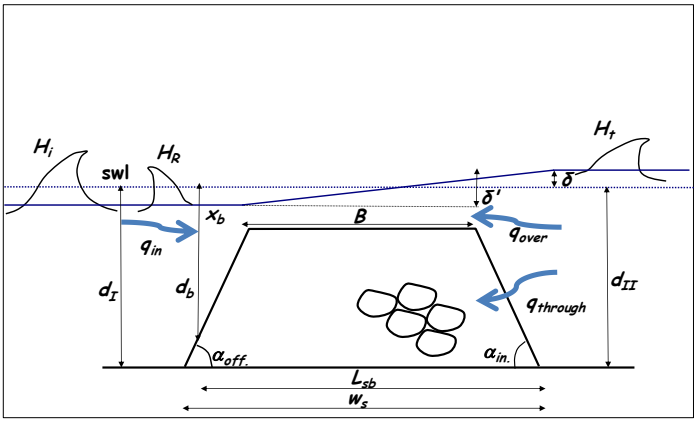

Figure 4.36. Definition of the main parameters used in wave setup models.

A comparison between the predictions obtained through the previous model and experimental tests conducted on impermeable rectangular breakwaters under 2D regular waves was performed by Dick (1968), who founded a substantial underestimation of real data.

In 1970, Diskin et al. developed an empirical formula (Eq. (4.62) based on about 190 regular wave experiments, performed in a flume at the Technion Israel Institute of Technology of Haifa (Israel). These tests were carried out using homogeneous trapezoidal breakwaters with fixed slopes, crest width and rock diameter. For this reason, the influence of porosity and side slope was not investigated. Conversely several F values were considered, in order to investigate the wave setup for both submerged and emerged structures.

$$\frac{\delta}{H_0} = 0.60e^{-\left[0.70-\left(F/H_0\right)\right]^2} \tag{4.62}$$

According to Equation (4.62) the set-up, δ, is a function of two parameters: the difference between the height of the structure and the water depth, F, and the

deep water height, H_0, calculated as the ratio between H_i and the linear shoaling coefficient.

The equation provides a maximum value for $F = 0.7H_i$, i.e. structures with crest elevation just above the sea level. For water levels above and below, δ decreases and tends to zero. The validity of this equation is limited in the range $-2.0 < F/H_i < 1.5$ and for d_I/H_0 variable between 0.1 and 0.83.

As reported in the discussion note following the Diskin et al. (1970) paper, Dalrymple and Dean (1971) attributed the scatter between experimental data and Equation (4.62) to the influence of K_R and K_T on the setup process, which were neglected by Diskin et al. (1970).

Besides, the Authors proposed a predictive equation (Eq. 4.63), according to which the setup is the sum of two contributions: δ_{mf}, representing the momentum flux due to wave collapsing on the seaward slope of the breakwater; and δ_c, that is the mass flux caused by a return current over the structure, which equilibrates the flux entering into the control volume. The latter extends for the structure width and is delimitated by the bottom and free surface.

$$\delta = \delta_{mf} + \delta_c \tag{4.63}$$

In particular, δ_{mf} is considered as the wave setup at the beach. This can be computed from the conservation of the horizontal momentum, under the hypotheses of shallow water and constancy of wave height to depth ratio:

$$\delta_{mf} = 0.15(d_b + F) \tag{4.64}$$

In the previous Equation the water depth at incipient breaking, d_b, can be computed according to the solitary waves breaking criterion:

$$d_b = 1.28H_i \tag{4.65}$$

The setup on the crest of the structure was not considered in Equation (4.64). In fact, the formula returns $\delta_{mf} = 0$ for waves breaking on the structures ($d_b = F$).

As regards δ_c, it is calculated as a function of the mass flux balance equation, according to which the entering mass flux, q_{in}, is equal to the sum of outgoing

fluxes passing through the barrier, $q_{through}$ (this term is generally omitted in the practical applications) and that over the structure, q_{over} :

$$q_{in} = q_{through} + q_{over} \tag{4.66}$$

q_{in} is considered as a fraction of the incident wave Stokes drift and can be computed according to the Equation (4.67):

$$q_{in} = \beta \frac{E}{\rho_w c} \tag{4.67}$$

where E is the incident wave energy; ρ_w is the water density; c represents the phase speed of incident waves, calculated according to the linear theory at the offshore toe of the barrier. β is a factor less than 1, depending on the time interval, calculated in a wave period in which the water surface exceeds the crest of the structure.

Using the small amplitude wave theory, Dalrymple and Dean (1971) obtained the following expression of the β factor:

$$\beta = \frac{1}{\pi}\left\{cos^{-1}\left[2\frac{F-(\delta_{mf+}\delta_c)/2}{H_i}\right] + \frac{1}{2}sin\left[2cos^{-1}\left(2\frac{F-(\delta_{mf+}\delta_c)/2}{H_i}\right)\right]\right\} \tag{4.68}$$

where the quantity $\frac{F-(\delta_{mf+}\delta_c)/2}{H_i}$ represents the relative crest freeboard, in which the setup, δ, is included.

The following equation was proposed to calculate the flux over the structure:

$$q_{over} = \sqrt{2g\delta_c}\left(\frac{\delta_{mf} + \delta_c}{2} - F\right) \tag{4.69}$$

in which δ_c was considered as an hydraulic head, converted into kinetic energy. The overall wave set-up, δ, can be obtained via the iterative solution of Equation (4.66).

An extensive test campaign was conducted by Loveless and Debski (1997) on permeable submerged and low-crested breakwaters in the flume of the

Hydraulic Laboratory of Civil Engineering Department at the University of Bristol. In these 253 tests, conducted with regular and irregular waves, eight homogenous structures with different crest width, front slope angle and rock diameter were investigated.

Based on the assumption that the wave setup essentially represents the mean hydraulic gradient needed to drive back the net inshore rate, pumped by waves by a dominant turbulent flow through the structure, Loveless et al. (1998) developed the following expression for regular waves:

$$\frac{\delta}{B} = \frac{\left(\frac{H_i L}{dT\pi}\right)^2}{gD_{n50}}\ 1.23\exp\left[-20\left(\frac{F}{h_s}\right)^2\right] \tag{4.70}$$

in which the setup is a function of both the hydraulic characteristics (i.e. the incident wave height, the period, the wave length and the water depth at the toe of the structure) and of the geometric parameters of the breakwater (i.e. the height of the structure, the water freeboard and the diameter of the rouble mound material).

In agreement with Diskin et al. (1970), the influence of F was modelled through the Gauss function, the maximum value of which was reached for F=0 instead of $0.7H_0$, as in Equation (4.62).

In the same study a comparison between the Equation (4.70) and the formula proposed by Diskin et al. (1970) Equation (4.62) was also presented. In particular, the Authors founded that Equation (4.63) is able to accurately predict the wave setup for submerged structures, whereas it largely overestimates data in the other cases. This gap was essentially related to the different size of the material employed in the two different experimental campaigns. In fact, in the tests conducted by Diskin et al. (1970) this was 40% less than the smallest model employed in the Lovelless et al. (1998) ones.

The Authors also suggested the use of the average wave height in the Equation (4.70) for irregular sea states.

Subsequently, Ruol et al. (2003) carried out about 60 two-dimensional irregular wave tests on low-crested rubble mound structures, in order to investigate the influence of the flux passing over and through the breakwaters on the setup. In this experimental campaign, conducted in the flume of the Hydraulic, Maritime,

Geotechnical and Environmental Engineering of the University of Padua (Italy), isolated and segmented breakwaters, with different porosities, were both investigated. In order to study the influence of the gap between structures, the recirculation flow rate, previously stored in a reservoir, was changed. The setup measured for permeable structures was compared with that provided by Diskin et al. (1970) formula, resulting into an overestimation of about 30% with respect to the previous formula. This was due to the different sea states employed in the two studies: regular according to Diskin et al. and irregular for Ruol et al. Conversely, the application of the model by Loveless et al. (1998) resulted in a significant underestimation of data.

Afterward, the models by Diskin et al. (1970) and Loveless et al. (1998) were applied by Calabrese et al. (2003) to a database composed by 48 irregular-waves experiments, performed in the large-scale (1:2) flume of the Grosser WellenKanal, Coastal Research Centre of Hannover (Germany). In this study the influence of both crest width and permeability, on submerged and low-crested rubble mound breakwaters, was investigated.

In order to apply the aforementioned models and considering the close link between the wave setup and the energy loss due to the passage of waves over the structure, the Authors employed the equivalent energetic wave, H_{en}, as a characteristic one. The latter was defined as the ratio between the significant spectral wave height, H_{mo}, and the square root of 2. H_{mo} was computed integrating the power spectrum for frequencies larger than 0.5 times the peak ones.

Calabrese et al. (2003) found that Equations (4.62) and (4.70) adequately reproduce the trend of measures, both for submerged and low-crested structures. However, the model by Diskin et al. overestimated data with low crest widths and underestimated the others, while Loveless' formula greatly overestimated the wave setup in case of wide structures. Furthermore, a lack of fit was observed for low values of B, in case of low-crested structures.

For these reasons, following the scheme proposed by Dalrymple and Dean (1971), a new formula for the prediction of wave setup was proposed by the same Authors, starting from the following assumptions: constancy of the wave period; impermeable and non-reflecting submerged breakwater; average hydrostatic distribution of forces acting onto the structure. In addition, the

Authors considered that wave setup presents a linear trend in the surf zone, delimited seaward from the breaking point and shoreward from the toe of the structure.
Under these simplifying hypotheses, the Authors calculated δ_m from the momentum balance, projected in the horizontal direction, applied to the control volume delimited by the sea bottom, the free surface and by two vertical sections taken at the toe of the structure. The equation proposed is the following:

$$\delta_m = 0.5[-b + (b^2 - 4c)^{0.5}] \tag{4.71}$$

where

$$b = 2d - a \tag{4.72}$$

$$c = \frac{3}{8} H_{eni}\left(1 - K_T^2\right) \tag{4.73}$$

In Equation (4.72) *a* is assumed as a function of the geometric parameters of the structure, i.e. crest width and height, and of the breaking characteristics, namely: x_b, i.e. the distance between the breaking depth (d_b) and the seaward crest edge; and L_bs, i.e. the distance between d_b and the landward toe of the breakwater (Eq. (4.74).

$$a = \left(1 + \frac{x_b + B}{L_{bs}}\right) h_s - \frac{x_b}{L_{bs}}(d_b + F) \tag{4.74}$$

Equation (4.73) accounts for the influence of K_T on δ_m, in fact the *c* term is a function of the incident energetic wave height, H_{eni}, and of the so-called transmitted coefficient, defined as the ratio between the transmitted H_{mo} and the incident one.
In order to estimate the breaking water depth, the Authors proposed to combine the linear shallow water shoaling theory with the breaking criterion of Kamphuis (1991), thus obtaining the following expression:

$$d_b = \left[\frac{H_{moi}}{0.56\exp(3.5\tan\alpha_{off})}\right]^{4/5} d^{0.2} \tag{4.75}$$

Assuming the total setup is a function of the sole momentum flux contribution, so that it can be computed by means of Equation (4.71), a good agreement was found for submerged structures with low values of crest width. Conversely, a significant underestimation was observed for structures characterized by greater values of B and for low submergences. In order to reduce this lack of fit, a contribution δ_c was added to δ_m, calculated employing the formula of Gauckler-Strickler for uniform turbulent flows:

$$\delta_c = \frac{q_{in}^2}{f^2|F|^{10/3}} B_{eq} \tag{4.76}$$

In the previous equation, f is the friction parameter and F represents the hydraulic radius. The flow rate, q_{in}, and the rectangular equivalent crest width, B_{eq}, are respectively computed according to the following Equations:

$$q_{in} = \frac{1}{8} H_{eni}^2 \sqrt{g/d} \tag{4.77}$$

$$B_{eq} = B + \frac{h_s\left(ctg\alpha_{off} + ctg\alpha_{in}\right)}{2} \tag{4.78}$$

The friction parameter f accounts for the energy loss due to the interaction between the breakwater and the return flow, as well as the permeability of the structure. Its value has to be calibrated on the basis of experimental data. As suggested in Calabrese et al. (2008b), f can be calculated by equating the following two expressions for the determination of the unitary shear stress at bottom, τ_b:

$$\tau_b = \rho_w g F S_w \tag{4.79}$$

$$\tau_b = \frac{1}{2}\rho_w \lambda U_b^2 \tag{4.80}$$

where S_w is the slope of the energy grade line, computable by means of Glaukler-Strickler formula, U_b is the bottom velocity and λ is the dimensionless friction. The latter can be retrieved from Nelson (1996) for coral reefs or from Lamberti et al. (2007) for low-crested breakwaters.

Substituting Equations (4.71) and (4.76) in Equation (4.63), the final model can be obtained. Its application to the abovementioned dataset returned a good agreement.

Bellotti (2004) proposed a new model for the prediction of the wave setup for submerged and impermeable detached breakwaters interrupted by gaps. The conceptual model assumed that incident short waves cause a current over the structures that transport water at the back of the breakwater. This phenomenon is partially compensated by an offshore undertow current (Svendsen and Bhur Hansen, 1986), while the remaining quantity of water is forced by the sloping water level (so-called feeders) toward rip channel, thus returning offshore. This model is based on four main equations employed: depth-integrated continuity and momentum equation across the structure, a free discharge relationship at the gap, and a barrier-shore system continuity equation. After several algebra steps, the following expression was proposed:

$$\frac{\delta^2}{2} + \delta\left(d_{gI} C_v \frac{L_g}{L_S}\right)^2 \left[\frac{2}{d_{sII}+\delta} - \frac{2}{d_{sI}} + w_S f' \left(\frac{1}{d_{sII}+\delta} + \frac{1}{d_{sI}}\right)^2\right] + \delta(d_{sII} - G) + \\ + \frac{3}{16}(H_{II}^2 - H_I^2) = 0 \tag{4.81}$$

where, *g* and *s* subscripts indicate quantities respectively referred to the gap and to the structure; *I* and *II* refer to the offshore and onshore quantities, calculated at the toe of the breakwater (Figure 4.37).

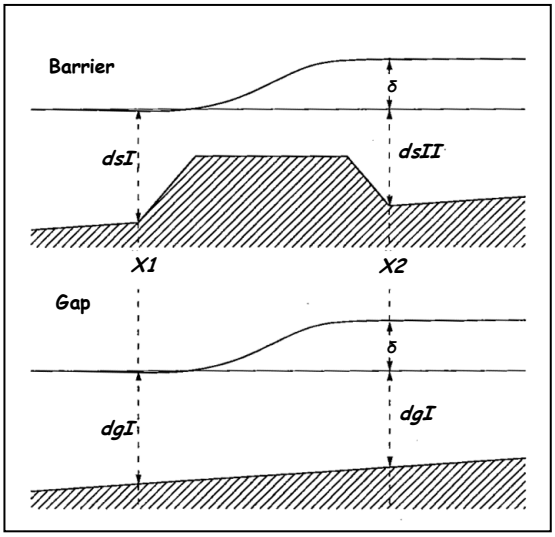

Figure 4.37. Representation in section of the main variables of Bellotti's model (adapted from Bellotti 2004).

In addition to the aforementioned quantities, L_s and L_g respectively represent the alonghshore length of the structures and of the gap; w_s the base width of the breakwaters; C_v is a discharge coefficient; and f' the bottom friction factor, which is assumed to be negligible. The geometrical quantity G, related to the equivalent water thickness over the breakwater, can be computed by the following expression:

$$G = \int_{x_1}^{x_2} \frac{x - x_1}{x_2 - x_1} \frac{\delta d}{\delta x} dx \tag{4.82}$$

in which x_2 and x_1 are, respectively, the distance from the shoreline of the inshore and the offshore toe of the structure, hence the difference between the two quantities represent w_s (Figure 4.38).

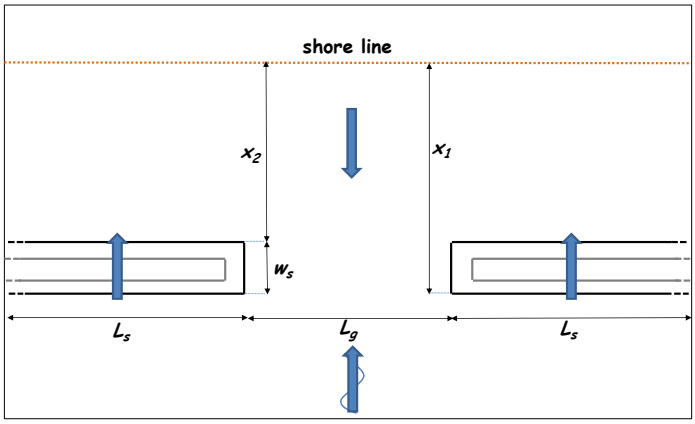

Figure 4.38. Plan view of the main variable of the Bellotti's formula.

In case of continuous breakwaters, i.e. not interrupted by gaps, the term $L_g$is zero and Equation (4.81) assumes the simplified expression reported in Equation (4.83). The latter can be also employed as a first attempt in the iterative solution of Equation (4.81).

$$\delta_{1DH} = G - d_{sII} + \frac{1}{4}\sqrt{-6H_{II}^2 + 6H_I^2 + 16d_{sII}^2 - 32Gd_{sII} + 16G^2} \tag{4.83}$$

Bellotti (2004) also stated that the effect of the rip currents on setup can be better supported neglecting O(δ^2) terms providing the following approximate expression:

$$\delta = \frac{{}^{3}/_{16}\,(H_I^2 - H_{II}^2)}{d_{sII} - G + \left(d_{gI}C_v\frac{L_g}{L_s}\right)^2\left(\frac{2}{d_{sII}} - \frac{2}{d_{sI}}\right)} \tag{4.84}$$

The discharge coefficient, representing the hydraulic head loss coefficient, is considered as a tuning parameter which can be computed employing standard methods for open channels.
Once the setup has been calculated by means of Equation (4.84), the depth-integrated velocity of rip currents can be determined as follows:

$$u_{gI} = C_v\sqrt{2g\delta} \tag{4.85}$$

The model was validated on experiments performed by Haller et al. (1997) in the basin of the Center for Applied Coastal Research of the University of Delaware (USA). These tests were conducted on submerged structures, characterized by a parabolic cross-section shape, under six sea state conditions and with monochromatic waves.

The application of the model on this database showed a dependence of the Equation (4.81) on the friction parameter and discharge coefficient. However, Bellotti (2004) founded that the variation in the rip currents' velocity was less than 2% and, therefore negligible for $-0.02<f'<0.02$, while C_v and L_g/L_s had a greater influence.. In particular, the best performance of the model was obtained for $L_g<0.5L_s$, due to the better evaluation of so-called "confined" rip current flow (Bellotti, 2004).

In 2005 Calabrese et al., applied the model previously developed in 2003 on a database composed of about 300 experimental tests, from three different laboratories (Calabrese et al., 2005): 253 tests carried out at the Hydraulic Laboratory of Bristol's Civil Engineering Department, including the regular ones employed by Loveless et al. (1998) for the calibration of the Equation (4.70); 25 tests previously employed for the calibration of the model of Calabrese et al. (2003); and 21 tests conducted with 2D regular waves at the University of Naples "Federico II".

The model was firstly applied on regular data only, for which the braking criteria proposed by Moore in 1982 was adopted:

$$\left(\frac{H}{d}\right)_b = b - 0.0827as_0^{4/5} \tag{4.86}$$

In the previous Equation, *a* and *b* are functions of the bottom slope, *m*, and the deep water wave height is calculated from the incident one employing the linear shoaling coefficient.

The application of the model to the regular tests showed an underestimation of experimental data, which was particularly evident for the data from Bristol.

The reason for these different behaviours was attributed by the Authors to the different positioning of structures employed in the tests, which was deeper for those performed in Bristol with respect to those carried out in Naples. In fact, an increment of water depth corresponds to a decrease of the mass drift (Eq. 4.77) and of δ_c, with a consequent increasing in the error (Calabrese et al., 2005). Moreover, an increasing in the difference between the measured and the calculated setup was observed at decreasing relative crest freeboard.
In order to take in account these parameters, a new expression for q was proposed by the Authors, according to the Svendsen's theory (1984). The latter considers the total drift as the sum of the Stokes drift, that is connected to the orbital motion, and the contribute due to the surface roller. Furthermore, using the shallow water theory, the Equation (4.87) was proposed for the estimation of q_{in}.

$$q_{in} = \sqrt{gd}\frac{\overline{H}^2}{d}\left(B_0\frac{A_1}{\overline{H}^2}\frac{d}{L}\right) \tag{4.87}$$

In the Equation above the water depth was assumed equal to the absolute value of the submergence of the structures and the wave height was calculated as the average wave height across the structure:

$$\overline{H} = \frac{H_i(1 + K_T)}{2} \tag{4.88}$$

The A_1 term in Equation (4.87) is the area of the surface roller in the vertical plane, which can be computed by means of the following expression (Okayasu, 1989):

$$A_1 = 0.06HL \tag{4.89}$$

The term B_0 is a shape factor to be calibrated on the base of experimental data. Calabrese et al. (2008b) considered this factor as a function of the Ursell's parameter, U_R, for a wave breaking located near the crest:

$$U_R = \frac{2\pi}{s_0}\left(\frac{H_i}{|R_c|}\right)^2\left(1+\frac{H_i}{|R_c|}\right) \tag{4.90}$$

Substituting the Eq. (4.87) in the Eq. (4.76) it is possible to determine the continuity contribution.

The model was calibrated on the database employed by Loveless et al. (1998) and was applied on the experimental data from Naples, leading to a good agreement between measured and estimated values.

A similar good agreement also resulted from the application of Equation (4.75) to irregular data. In this case the peak wave period and the Kamphuis' breaking criteria were considered for the application of the model. Moreover, by assuming random sea states as the sum of regular waves and employing the Rayleigh distribution, the incident wave height, was calculated, as in the following Equation:

$$H_{mi} = \frac{\sqrt{2\pi}}{4} H_{m0} \tag{4.91}$$

The model proposed by Calabrese et al. (2005), was subsequently applied by the same Authors (Calabrese et al., 2008b), but employing the breaking criteria of Iwata and Kiyono (1985) for the determination of the incident wave height:

$$H_i = \frac{1}{1+K_R}\left(0.218 - 0.076\frac{1-K_R}{1+K_R}\right) L_b tanh\left(2\pi\frac{d_b}{L_b}\right) \tag{4.92}$$

where L_b represents the wave length at the incipient breaking. The Equation (4.92) returns the Miche criteria (1944) for progressive waves and the model of Daniel (1952) for standing waves.

The application of this model, under the hypothesis of shallow water, returned a breaking index H/d=0.88, which is larger than the one found by Sawaragi (1995) in the analyses of submerged breakwaters, which was H/d=0.625. This suggested to employ another breaking criteria for breaking waves on the crest of the structure. In fact, Calabrese et al. (2008b) assumed that the breaking

occurs for H_i larger than the limit wave height expressed by the relationship proposed by Hur et al. (2003):

$$H_b^{cr} = 0.095 L_0 tanh\left(\frac{2\pi|R_c|}{L_0}\right) \tag{4.93}$$

The equation above returned a shallow water breaking index H/d = 0.6, which was deemed to be in good agreement with that found by Sawaragi (1995).

The model was applied on the same database employed by Calabrese et al. (2005) widen with other 63 regular tests conducted at the University of Naples (described in Pasanisi et al., 2006 and Di Pace, 2006).
The application of the aforementioned model on regular experimental data returned a good agreement, with a determination index, $R,^2$ equal to 0.89. The model was compared with the formulae proposed by Loveless et al (1998), Dalrymple and Dean (1971) and Diskin (1970) resulting to be the fitting one. Moreover a significant underestimation was found applying Equation (4.70) to the database already employed by Calabrese et al. (2005), while a certain overestimation was observed employing the model by Dalrymple and Dean (1971) and that by Diskin (1970). A more reliable predictive capability of the Equation (4.62) was found employing the incident wave height instead of the deep water one.
The results obtained for monochromatic waves were transferred to spectral ones employing the peak period and defining two heights, namely H_{rms} and the average wave height H_μ.
The Kamphuis (1991) breaking criteria was assumed for computing H_{rms} and H_μ:

$$\left(\frac{H_{rms}}{h}\right)_b = 0.4\exp(3.5m) \tag{4.94}$$

$$\left(\frac{H_\mu}{h}\right)_b = 0.35\exp(3.5m) \tag{4.95}$$

In the previous two Equations, m was assumed equal to zero if the wave breaking occurred on the crown of the breakwaters, otherwise it was equal to $tan\alpha_{off}$.

The application of the model suggested a recalibration of the f term when H_{rms} was employed. On the contrary, the model resulted to be able to predict the wave setup when H_{μ} was adopted.

A comparison between the previously presented formulae can be found in Soldini et al. (2009). In this study a database of about 40 experimental tests conducted in four different European and American laboratories was employed.

The Italian tests were partially carried out in portioned basin of the Polytechnic of Bari, where segmented submerged rubble mound structures were investigated with regular and irregular waves (as described in Lorenzoni et al. 2004), and partially conducted in the flume of Coastal Laboratory of Civil Engineering Department of the Florence University, where both submerged and low-crested structures were tested with monochromatic waves. In the last tests several berm widths, structure heights and offshore slopes were investigated. In addition to the above, tests conducted at the Alborg University for the European Project DELOS (Kramer et al., 2005) were considered. In particular only those aimed at investigating the hydrodynamic of submerged and low-crested breakwaters with a central rip channel were considered.

The American experiments, described in Haller et al. (2000), were conducted on bar systems with regular waves in the wave basin of the Ocean Engineering Laboratory of the University of Delaware (USA).

As reported in Soldini et al. (2009), the application of the model by Diskin et al. (1970) provided a substantial overestimation of data, probably due to the differences in F/H_0 and in wave characteristics employed in the studies. Conversely, an over-prediction was found for the data from Delaware, ascribed by the Authors to the inability of the Diskin's model to represent the horizontal flume.

In agreement to what observed by Calabrese et al. (2003), an overestimation of data was also found applying the Loveless' formula to tests performed in Bari and in Florence while a good agreement was observed for data from Alborg. Finally, the inapplicability of the model resulted from the use of Delaware data, due to different experimental conditions.

In the same study, results obtained from the application of the model proposed by Bellotti (2004) were also discussed and a good agreement was found employing the simplified Equation (4.84). A good interpretation of the data was also found employing the model of Calabrese et al. (2005), in which the only momentum flux contribution was employed.

Chapter 5 – REVIEW OF STUDIES ON REEF BALL BREAKWATERS

In recent years, few studies have been dedicated to the analysis of the transmission coefficient at breakwaters made of RB modules.

Early studies aimed at the characterization of the wave transmission of Reef Ball structures were performed by Armono in 2003, further developed and published, with some modifications, by Armono and Hall (2003). These studies were aimed at developing a predictive equation for different types of Reef Ball breakwaters, based on the results of an experimental campaign. The Authors investigated two different Reef Ball layouts, namely modules placed directly on the bottom and on the crest of a mound, and several configurations, including multi-layered ones.

More recently, Ward (2011) performed an experimental campaign in order to optimize the design of an offshore submerged breakwater in Florida (USA). In these tests, RB units were arranged according to one layout only, i.e. in a single layer and directly placed on the bottom, while different configurations were obtained by varying the distance between the units.

As result of the rising interest in the use of RB modules for shore protection purposes, the aforementioned studies were analysed by Del Vita in 2012, and a new model for the prediction of the transmission coefficient was proposed by Buccino et al. (2014).

In the following, a description of the studies performed by Armono (2003) and Ward (2011) are presented, whereas findings of Buccino et al. (2014) will be discussed in the next Chapter.

5.1 The Armono (2003) study

5.1.1. Description of the experimental campaign

The database employed in Armono (2003) was composed of about 300 two-dimensional random tests, conducted at the Queen's University Coastal Engineering Research Laboratory (QUCERL, Canada).

These experiments, hereafter referred to as *QUCERL* data, were performed in a 47 m long, 0.9 m wide and 1.2 m deep flume, provided with a flap-type wave-maker (Figure 5.1). Reef Balls were placed on an horizontal bottom, at a distance of 17 m from the paddle. The modules were characterized by an height, h_R, equal to 0.13 m and by a base diameter, D_R, of 0.20 m; the weight of the units ranged from 2.189 to 2.944 Kg and the number of holes over the lateral surface was averagely 20.

These characteristics correspond to Pallet Balls (Table 2.1), scaled down at a 1:7 ratio.

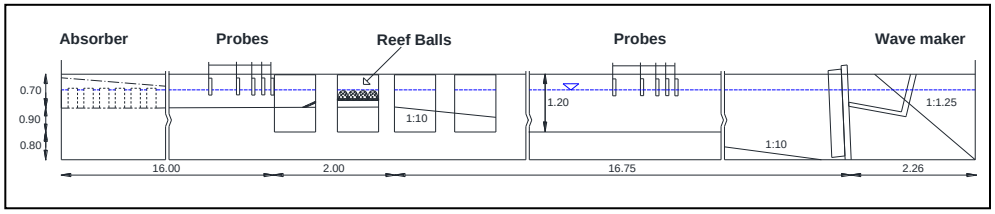

Figure 5.1. Cross-section of the flume at QUCERL.

RBs modules were arranged in two different layouts:

- "Bottom Seated" (BS) layout, with modules seated directly on the horizontal bottom;
- "Berm layout" (B), with modules placed onto the crown of a conventional mound.

In each of the layouts above, the number of RB layers was varied from one to three, to create different configurations.

Configurations investigated for the BS layout are shown in Figure 5.2. In particular, the configuration *BS-3* (Figure 5.2a) was composed of 3 RB levels, with the second layer arranged upside-down to improve the interlocking with the first one and provide a planar base for the top level (Armono and Hall,

2003). The *BS-2* configuration (Figure 5.2b) was obtained from *BS-3* by simply removing the upper layer.

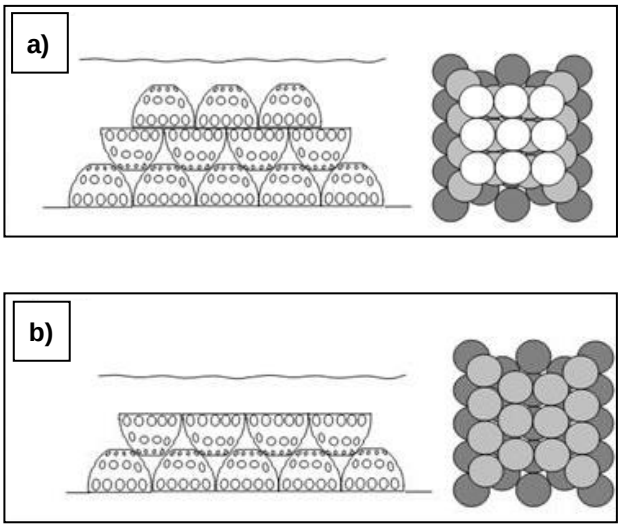

Figure 5.2. Representation of BS layout. a) Configuration BS-3;b) Configuration BS-2.

As far as the type "*B*" layout is concerned, Reef Balls were assembled in 1 or 2 levels. In the former case, modules covered the entire crown (configuration referred to as *B-F1*, where "*F*" stands for "full cover", Figure 5.3a) or only part of it (configuration referred to as *B-P1*, where "*P*" stands for "partial cover", Figure 5.3b). Finally, in the configuration *B-F2*, RBs were arranged in two levels, to cover the entire crest of a berm (Figure 5.3c).

The rubble mound was made of a core with D_{n50} =0.01 m and two armour layers with D_{n50} =0.037 m. The height of the berm, h_m, the crown width of the mound, B_m, and the slope angles (α_{off}. and α_{in}.) were kept constant for all the tests.

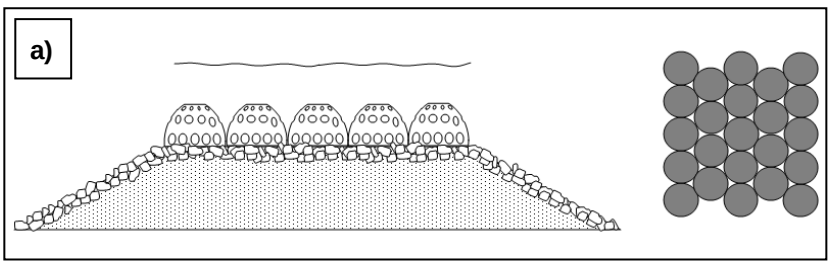

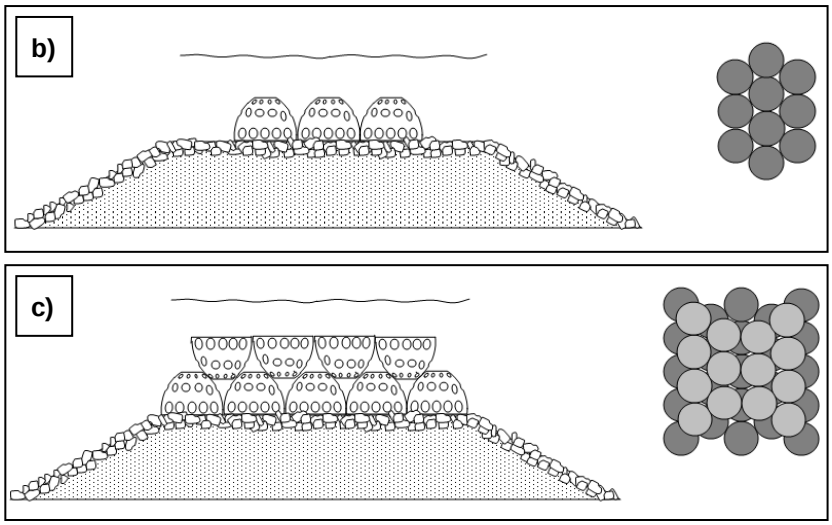

Figure 5.3. Representation of B layout: a) configuration BF-1; b) configuration BP-1; c) configuration BF-2.

Table 5.1 shows, for each configuration tested, the number of observations (#data); the number of RB rows at the top of the structure, *n*; and the variation ranges of the hydraulic characteristics observed during the tests, i.e. water depth, significant incident wave height, peak period and measured transmission coefficient, $K_{T,meas}$. The transmitted wave height, used in the computation of the transmission coefficient, was calculated by means of two arrays of five probes, placed 13 m away from the toe of the structure and 2 m behind the reefs.

Configuration	**# data**	**n**	**d [m]**	**H_{si} [m]**	**T_p [s]**	**$K_{T,meas}$**
BS-3	54	3	0.35-0.45	0.05-0.20	1.0-3.5	0.56-1.06
BS-2	60	4	0.21-0.30	0.05-0.20	1.0-3.5	0.33-0.99
BF-2	49	4	0.43-0.60	0.05-0.20	1.0-2.5	0.37-0.89
BF-1	56	5	0.35-0.50	0.05-0.20	1.0-2.5	0.33-0.95
BP-1	56	3	0.35-0.50	0.05-0.20	1.0-2.5	0.39-0.95

Table 5.1. Summary of *QUCERL* tests.

5.1.2. Description of the model

From the analysis of *QUCERL* data, Armono (2003) developed the following predictive model for RB submerged breakwaters, via a linear regression analysis at least squares:

$$K_T = \frac{1}{1 + A_0 \left(\frac{H_{si}}{gT_p^{\,2}}\right)^{0.901} \left(\frac{B_{bR}}{gT_p^{\,2}}\right)^{-0.413} \left(\frac{h_s}{B_{bR}}\right)^{-1.013} \left(\frac{h_s}{d}\right)^{4.392}} \tag{5.1}$$

where h_s is the total height of the structure; B_{bR} is the crest width of Reef Ball structures, computed as the sum of RBs' base diameters, D_R, at the lower layer (Eq. 5.25.2); and A_0, is a scale factor, assumed as a function of the analysed configuration.

According to Equation (5.1), the transmission coefficient is related to four fundamental parameters, each one raised to a different constant exponent: the wave steepness (H_{si}/gT_p^2); the relative depth (h_s/d); the ratio between the geometric characteristics of the structure (h_s/B_{bR}); and the ratio between the crest width and the period (B_{bR}/gT_p^2).

$$B_{bR} = nD_R \tag{5.2}$$

In Table 5.2 the value of the A_0 coefficient, the determination index, R^2, and the Standard Error, *SE*, are summarized, for each configuration.

Configuration	A_0	R^2	SE
BS-2	10.719	0.922	0.049
BS-3	7.949	0.867	0.042
B-F2	15.318	0.856	0.058
B-F1	14.527	0.953	0.036
B-P1	14.527	0.953	0.036

Table 5.2. Values of the scale factor, determination index and standardized error according to the Armono model (2003).

Subsequently, Armono and Hall (2003) proposed the modification of the previous model reported in Equation (5.3) to be applied only for configurations *B-F1* (Figure 5.3a) and *B-P1* (Figure 5.3b):

$$K_T = 1.616 - 31.322\left(\frac{H_{si}}{gT_p^2}\right) - 1.099\left(\frac{h_s}{d}\right) + 0.265\left(\frac{h_s}{B_{bR}}\right) \quad (5.3)$$

In the previous Equation, instead of four parameters, only three were considered to be significant for the prediction of the transmission coefficient, because the influence of B_{bR}/gT_p^2 was deemed to be negligible.
The model described by Equation (5.3) is characterized by a R^2 value of 0.841, resulting to be lower than that found by Armono (2003), which was equal to 0.95 for the same configurations.

5.2 The Miami Beach 63rd Street Hotspot case-study

The project of the Miami Beach 63rd Street "Hotspot" was part of the National Shoreline Erosion Control Development and Demonstration Program - Section 227, developed by the U.S. Army Engineer Research and Development Center (*ERDC*) with the objective of advancing the state of the art of shoreline protection, through a series of demonstrative projects of innovative and non-tradition solutions.
The project site extended along the 63rd Street of Miami, for approximately 762 m (Figure 5.4). This site had experienced a significant shoreline retreatment, with a rate exceeding those observed on adjacent shorelines.

Figure 5.4. Beach near 63rd Street (Ward, 2011).

The main goal of the project was to measure the energy reduction corresponding to different arrangements of RB units and to identify the best configuration to employ for the shoreline stabilization.
Because of the sand bottom, Reef Balls were placed on Armorlefex mattress (Figure 2.15). The latter allowed to avoid silting phenomena, working as a sand trap. As a final result, the protection of the site was achieved, mainly due to wave dissipation and reduction of the near-shore slope of the bottom.
On behalf of this project, 64 experiments were carried out at the USACE Engineering Research and Development Centre Coastal and Hydraulics Laboratory (*ERDC/CHL*, USA), to investigate the effectiveness of different RB configurations.
These experiments were conducted in a wave basin 51.82 m long, 30.48 m wide and 1.21 m deep, provided with a 27 m wide multi-directional wave generator. The tank was partitioned at nearly 15 m from the paddle to form a 20.73 m by 2.44 m flume, normal to the generator. The flume's profile, which reproduced the topography of the site at a 1:10 length-scale, included a 1:20 slope, for the first 4.87 m, followed by a 1:250 slope, for 9.75 m, and finally a 1:7.5 slope, for 4.87 m (Figure 5.5).

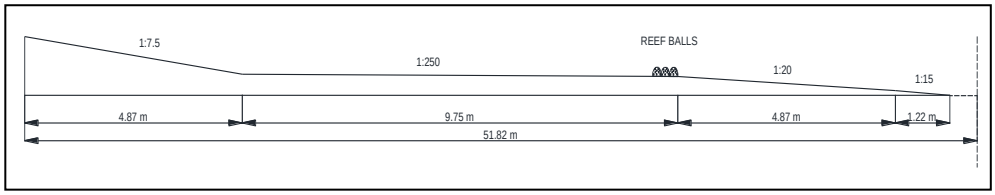

Figure 5.5. Profile of the flume employed in the *ERDC/CHL* tests.

1:10 models of Goliath Balls (Table 2.1) were arranged in a single layer and placed directly on the bottom, according to a layout typically employed in the practical applications. The modules were placed in different rows on the 1:250 slope, with the offshore row beginning where the slope transitioned from 1:20 to 1:250. Different configurations were obtained by varying the spacing between the units, both in the direction of the wave propagation (cross-shore) and the normal one (along-shore). Moreover, the number of rows was changed to investigate the influence of the structure width.

The configuration *BS-1a* was made up of 10 modules in each row, with an alongshore spacing of 0.55 m in the prototypal scale (Figure 5.6). Up to 7 rows were used, with the cross-shore spacing also set at 0.55 m. RB rows were realized in such a way that the centre of each unit was aligned with the gap between two units in the preceding and following row. The configuration *BS-1b* was obtained from *BS-1a* by removing the even rows. Consequently, the modules appear perfectly aligned cross-shore (Figure 5.7).

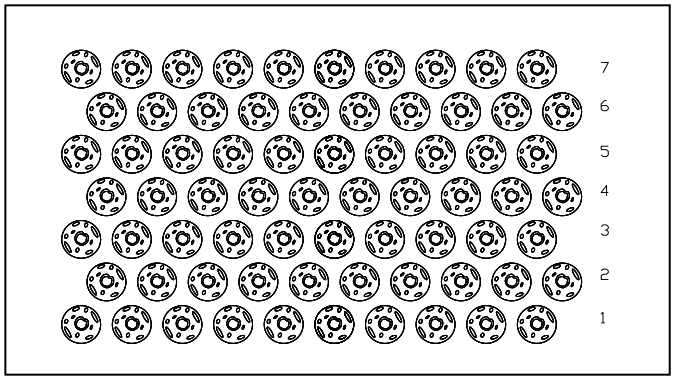

Figure 5.6. Plan view of the configuration *BS-1a*.

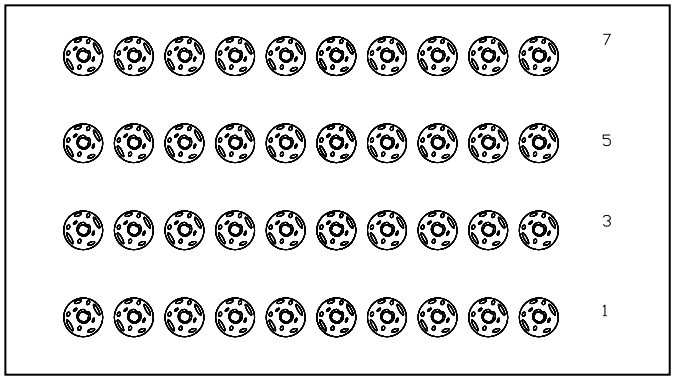

Figure 5.7. Plan view of the configuration *BS-1b*.

The configuration *BS-1c* was obtained from the *BS-1a* one, with a number of rows equal to 7, after eliminating row number 2 (Figure 5.8).
The configuration *BS-1d* was identical to *BS-1b*, but the modules were not aligned (Figure 5.9). The structure *BS-1e* included 3 rows with no spacing

between the units (Figure 5.10). Finally, the configuration *BS-1f* was obtained from *BS-1b*, by halving the number of modules in each row (Figure 5.11).

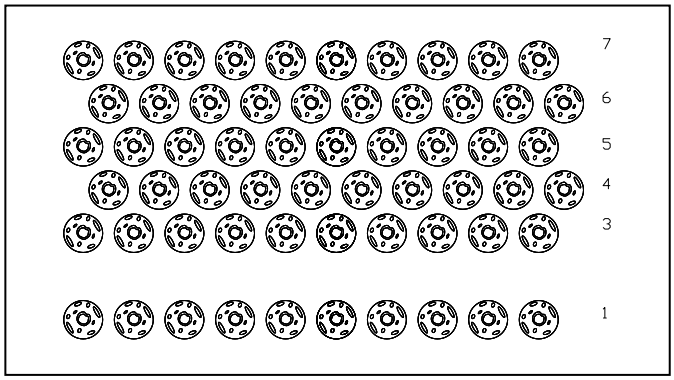

Figure 5.8. Plan view of the configuration *BS-1c*.

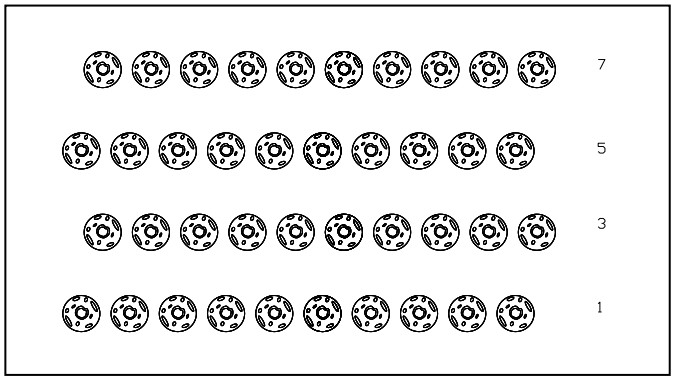

Figure 5.9. Plan view of the configuration *BS-1d*.

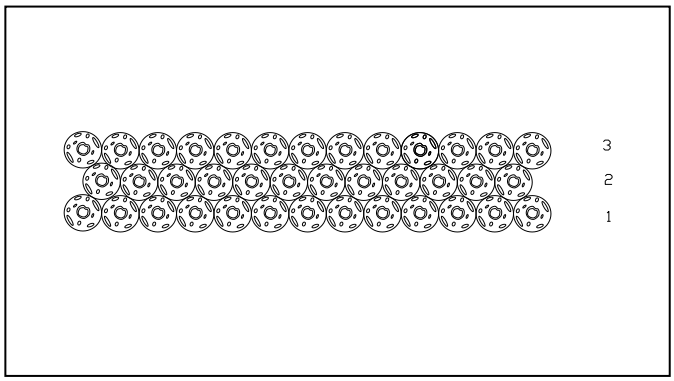

Figure 5.10. Plan view of the configuration *BS-1e*.

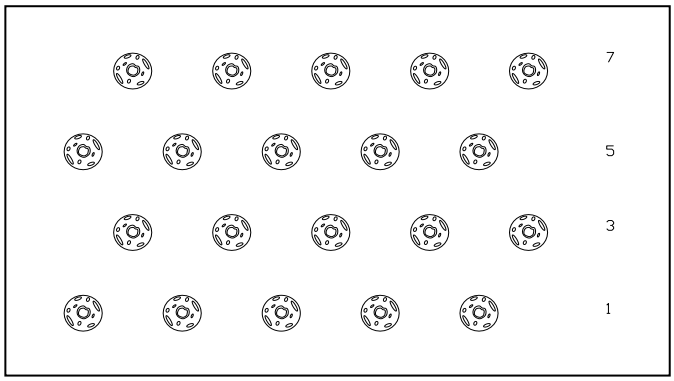

Figure 5.11. Plan view of the configuration *BS-1f*.

Reef Ball breakwaters were placed at a submergence of about 30 cm under the mean sea water level, so that the major part of the tests were referred to a depth of 0.183 m. Moreover, some tests were also performed at a depth of 0.256 m. This allowed to take into account for the average tide variation and the maximum sea level oscillation at the site, which were about 0.7 m and 0.8 m, respectively.

In Table 5.3 the investigated configurations, the number of observations, the main hydraulic characteristics and the measured K_T are summarized.

Configurations	**#data**	**n**	**d [m]**	**H_{si} [m]**	**T_p [s]**	**$K_{t,meas}$**
BS-1a	28	1÷7	0.183;0.256	0.076;0.152	1.58;2.53	0.50;0.99
BS-1b	12	2÷4	0.183	0.076;0.152	1.58;2.53	0.62;0.92
BS-1c	4	5	0.183	0.076;0.152	1.58;2.53	0.59;0.77
BS-1d	12	3÷4	0.183;0.256	0.076;0.152	1.58;2.53	0.60;0.91
BS-1e	4	3	0.183	0.076;0.152	1.58;2.53	0.63;0.84
BS-1f	4	4	0.183	0.076;0.152	1.58;2.53	0.81; 0.92

Table 5.3. Summary of *ERDC/CHL* tests for each configuration investigated.

The transmitted and incident wave heights were measured, respectively with and without the breakwater, by means of three probes placed shoreward the structure. Accordingly, K_T was expressed as follows:

$$K_{T,meas} = \frac{H_{m,0(with\ structure)}}{H_{m,0(without\ structure)}} \tag{5.4}$$

where $H_{m,0}$ is the spectral significant wave height.
The study resulted in a transmission coefficient variable between 0.5 and 0.99. The maximum wave attenuation was observed for the configuration *BS-1a* with 7 rows of Reef Ball modules. Moreover, no significant variation of K_T was observed by changing the distance between the units.

Chapter 6 – ANALYSIS OF THE TRANSMISSION COEFFICIENT BASED ON LITERATURE DATA (BUCCINO ET AL., 2014)

In 2014, Buccino, Del Vita and Calabrese analysed the results of the two previously-discussed experimental campaigns (Sects. 5 and 5.2) and applied two different approaches for the development of new predictive models for the transmission of RB barriers.

The first model was directly derived from the one by Armono (2003), described by Equation (5.1). The result was characterized by a relatively high determination index ($R^2 = 0.80$) and by normality of the residuals, but it was less able to interpret the *ERDC/CHL* data than the *QUCERL* ones. The main reasons were attributed by the Authors to the peculiar functional relationship of the Armono's model, which was considered to be unable to adequately reproduce the physics governing the wave dissipation process.

For these reasons, a new model was developed, starting from the so-called "Conceptual Approach" (Buccino and Calabrese, 2007a), previously proposed for traditional submerged breakwaters.

In the following, the study by Buccino et al. (2014) is described starting from the analyses of the *QUCERL* and the *ERD/CHL* datasets (see Chapter 5). Subsequently, the application of the Conceptual Approach (Buccino and Calabrese 2007a) is presented.

6.1 Analysis of QUCERL and ERDC/CHL data

The starting point of the study by Buccino et al. (2014) was the analysis of the functional form of the model by Armono (2003) .

The Equation (5.1) was assumed by the Author as a function of B_{bR}/gT_p^2 which is, except the constant term π, equal to the ratio between the width of the structure and the deep wave length. This variable had been often employed as a main predictor of the transmission coefficient for traditional breakwaters (e.g.

Tanaka, 1976). Generally speaking, a decrement of the energy dissipation was observed for structures characterized by a crest width less stretched than the wave length. Thus, an increment of the transmission coefficient is expected for structures characterized by low values of the B/L_0 ratio and, therefore, also of B_{bR}/gT_p^2. Contrariwise, the B_{bR}/gT_p^2 term in Equation (5.1) was raised to a negative exponent, so that the transmission coefficient increased as the above-mentioned term did. As an example, this trend is shown in Figure 6.1, where the transmission coefficient, calculated by means of Equation (5.1) for $h_s/B_{bR} = 0.32$, $H_{si}/gT^2 = 0.157$, $h_s/d = 0.8$, $h_s/B_{bR} = 0.32$ and $A_0 = 7.949$, is plotted against B_{bR}/gT_p^2.

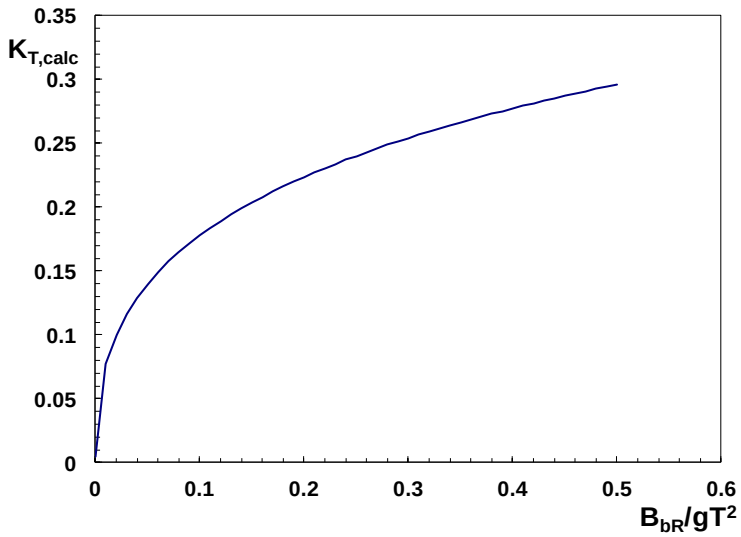

Figure 6.1. Increment of the transmission coefficient calculated by means of Eq. (5.1) with B_{bR}/gT_p^2 (Del Vita, 2012).

The model of Armono was linearized according to the following expression:

$$Y = 1 + A_0 X \tag{6.1}$$

where Y and X are respectively expressed by means of the Equations (6.2) and (6.3).

$$Y = \frac{1}{K_T} \tag{6.2}$$

$$X = \left(\frac{H_{si}}{gT_p{}^2}\right)^{0.901} \left(\frac{B_{bR}}{gT_p{}^2}\right)^{-0.413} \left(\frac{h_s}{B_{bR}}\right)^{-1.013} \left(\frac{h_s}{d}\right)^{4.392} \tag{6.3}$$

Figure 6.2 shows the results of the application of the Armono's model in the plane of the transformed variables (*X*, *Y*) for the configuration *BS-2* (Figure 5.2b) and *BS-3* (Figure 5.2a).

It is worth noticing that the *QUCERL* data exhibits a certain curvature around the mean trend line, especially for small values of *X*. Moreover, in case of the configuration *BS-2*, a certain scatter is exhibited for large *X* values (Figure 6.2a).This suggests that Armono's equation might suffer some lack of fit, at least with respect to the BS arrangements.

In addition to the above, Figure 6.3 shows the errors, e_i, associated to Armono's model versus *X*, which were estimated as the difference between measured and predicted *Y* values.

From the Figure 6.3, a dependence of the residuals on *X* emerges, suggesting the presence of a non-linear term, omitted in the model by Armono.

The application of the linearized model (Eq.6.1) on *ERDC/CHL* data revealed that, differently from the *QUCERL* experiments (Figure 6.2), this data are not adequately fitted by the Armono's model (Figure 6.4). In fact, when plotted on the *X*-*Y* plane, *ERDC/CHL* data splits into two distinct sub-arrays. Furthermore, a clear lack of correlation between *X* and *Y* emerges for the configurations *BS-1c*, *BS-1e* and *BS-1f* (Figure 6.5).

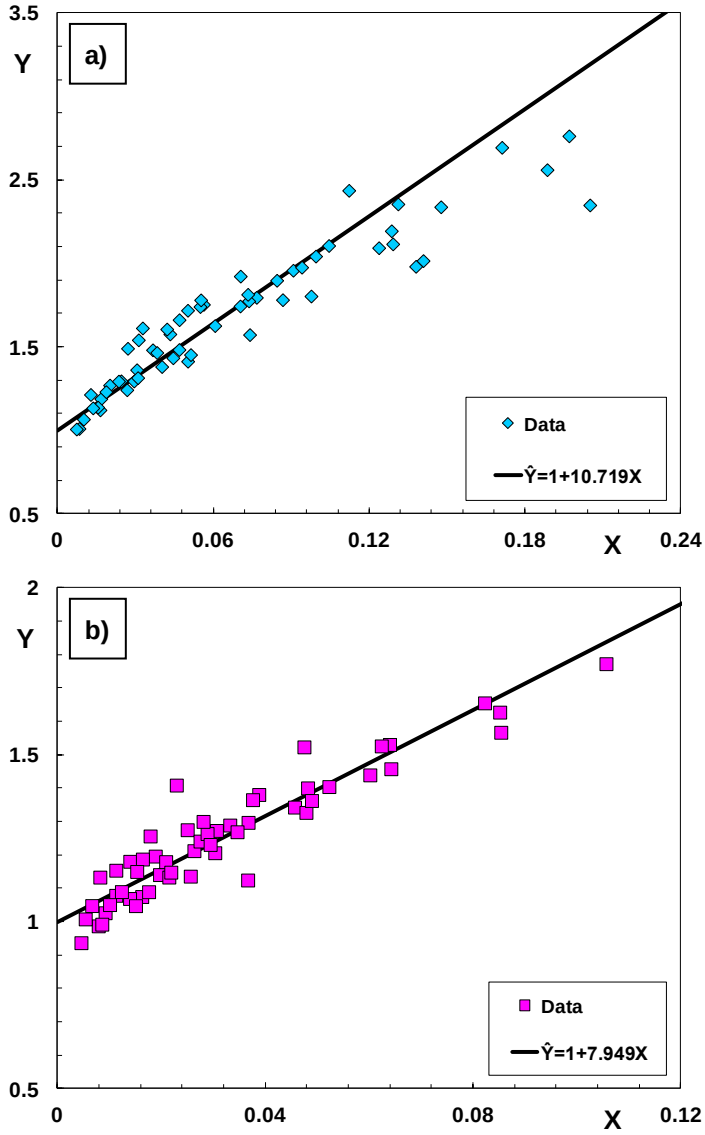

Figure 6.2. Comparison between Equation (6.1) and *QUCERL* data: a) configuration *BS-2*; b) configuration *BS-3*.

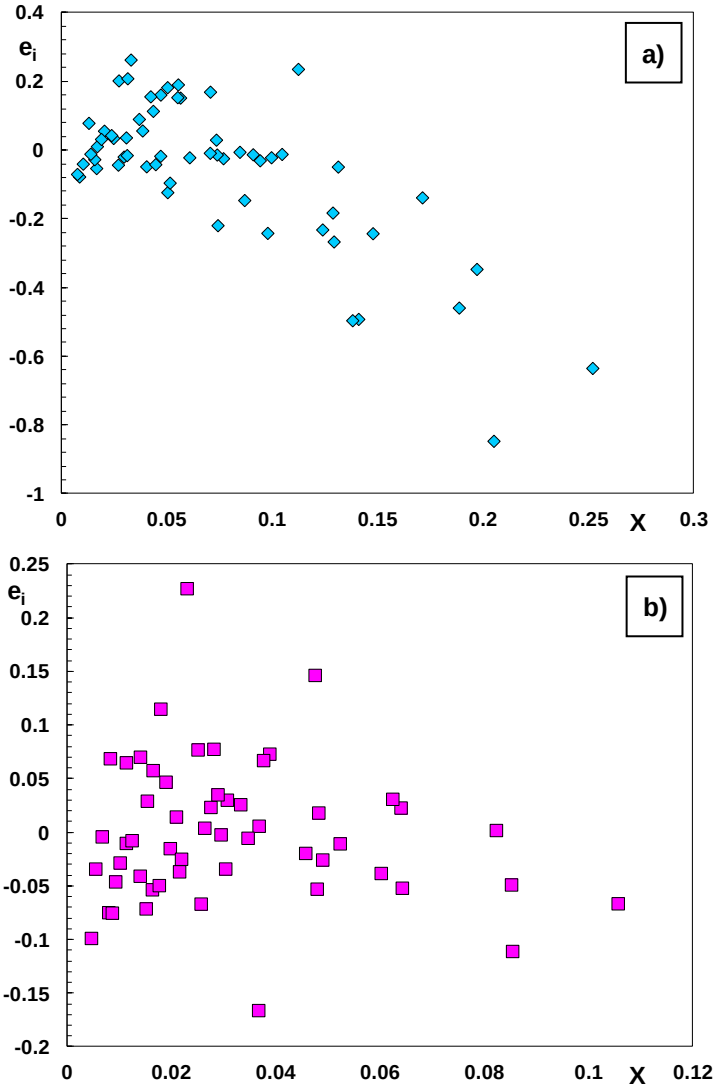

Figure 6.3. Scatter plot of errors e_i vs. X: a) configuration *BS-2*; b) configuration *BS-3*.

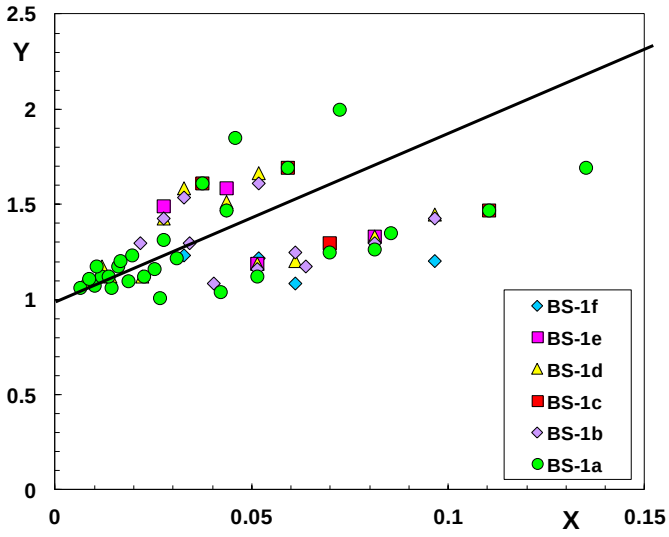

Figure 6.4. Application of Eq. (6.1) to *ERDC/CHL* data.

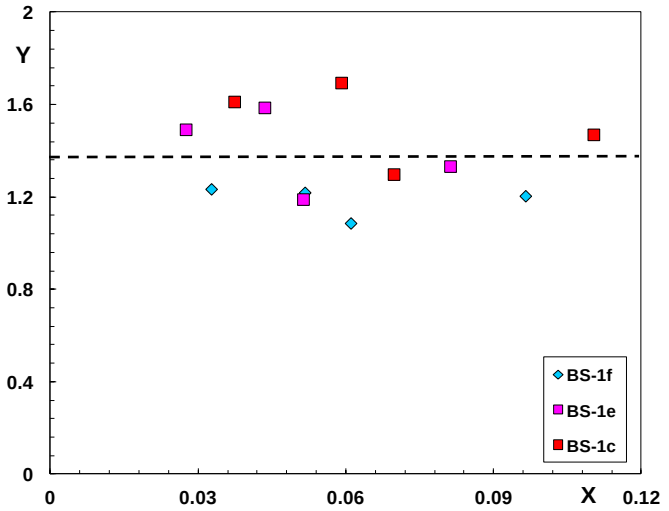

Figure 6.5. Application of Eq. (6.1) to *BS-1c*, *BS-1e* and *BS-1f* data.

In order to understand the possible reasons for the above, the statistical technique known as "Added Variable Plot" (AVP) (Draper and Smith, 1981), was applied. This technique, generally used in the field of regression analyses, consists in the evaluation of the effect of the predictors on the model, by

performing subsequent partial regressions with respect to each variable and then plotting the residuals against the remaining ones.
To this purpose, the model by Armono was again linearised according to the following equation:

$$Y_T = a_0 + a_1 X_1 + a_2 X_2 + a_3 X_3 + a_4 X_4 \tag{6.4}$$

where, Y_T is the transformed dependent variable:

$$Y_T = ln\left(\frac{1}{K_T} - 1\right) \tag{6.5}$$

while the predictors are:

$$X_1 = ln\left(\frac{h_s}{d}\right);\ X_2 = ln\left(\frac{h_s}{B_{bR}}\right);\ X_3 = ln\left(\frac{H_{si}}{gT_p^2}\right);\ X_4 = ln\left(\frac{B_{bB}}{gT_p^2}\right) \tag{6.6}$$

By applying the AVP technique on the BS-subset of *QUCERL* data, Buccino et al. (2014) observed that the X_3 predictor is not sufficient to completely describe the effect of the wave period on the transmission process. Therefore, a tentative correction of the model by Armono was performed, including both *QUCERL* and *ERDC/CHL* data, which resulted into a R^2 of 0.8 and a standard error of 0.071.
Moreover, by observing that the wave steepness influenced the *ERDC/CHL* data less than the *QUCERL* ones, the Authors concluded that the *BS-1* configuration differs from the others in the mechanisms underlying the attenuation of the incoming waves. This could represents the reason why the Armono's approach fails in capturing the mean features of the interaction between waves and modules.
For this reasons, the same Authors proposed another model for the prediction of transmission coefficient, based on the Conceptual Approach (Buccino and Calabrese 2007a), presented in the next Section.

6.2 Conceptual Approach for Reef Ball submerged breakwaters (Buccino et al., 2014)

The "Conceptual Approach" (Buccino and Calabrese, 2007a; see Section 4.2) was chosen as an alternate model for the prediction of the transmission coefficient of submerged breakwaters made of Reef Balls, both placed on the bottom and on the crown of a conventional rubble mound.
In the following the model developed and the procedure employed for its calibration will be explained.

6.1.1. Conceptual Approach for Bottom Seated Reef Balls

In order to calibrate the *CA* model, a preliminary redefinition of the main structural variables, namely the crown width and the height of the structure, was considered to be necessary, due to the different characteristics of the RBs with respect to common armour units, as well as to the heterogeneity of the investigated configurations.

6.1.1.1. Variable redefinition

In those cases in which the upper layer of the structure was made of modules placed upright (configurations *BS-1* and *BS-3*), the nominal crown width, B_t, was defined as follows:

$$B_t = (n-1)D_R \tag{6.7}$$

On the contrary, when RBs were placed with the base upwards (configuration *BS-2*), B_t was simply assumed as the sum of the base diameter of the modules:

$$B_t = nD_R \tag{6.8}$$

Moreover, the equivalent structure height, h_{se}, was introduced. This was considered equal to the height of the units, h_R, for the configuration *BS-1* (Eq. 6.9), while for configuration *BS-2* it was assumed to be computable by means of the Eq. (6.10).

$$h_{se} = h_R \tag{6.9}$$

$$h_{se} = (2\varphi_p - 0.5)h_R \tag{6.10}$$

In the previous Equation, φ_p is a thickness coefficient, equal to the ratio between the total height of the stricture and $2h_R$.
Finally, because the layout *BS-3* originates from *BS-2* after adding a third level of RBs in the normal (upright) position, h_{se} was set as follows:

$$h_{se} = (2\varphi_p + 0.5)h_R \tag{6.11}$$

Obviously, the introduction of an equivalent structure height corresponds to the definition of an equivalent crest level, R_{ce}:

$$R_{ce} = d - h_{se} \tag{6.12}$$

A graphic representation of the above-defined variables is shown in Figure 6.6 for the configurations *BS-1* (Figure 6.6a) and *BS-2* (Figure 6.6b), respectively.

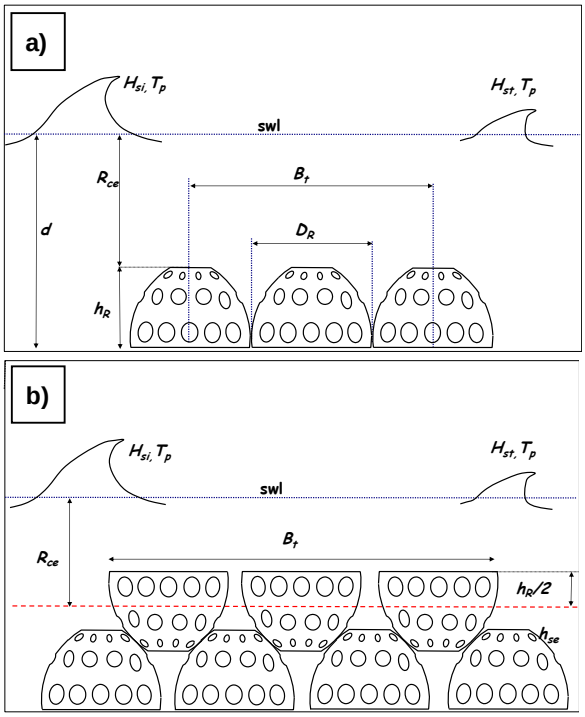

Figure 6.6. Representation of the variables used in the application of *CA* to RB barriers for the configuration *BS-1*(a) and configuration *BS-2* (b).

6.1.1.2. Calibration of the asymptotic solution for low-submerged structures

The calibration of the CA in the case of bottom-seated layout started from the calibration of the Eq. (4.53). The latter, hereunder reported for the reader's convenience, represents the asymptotic solution of the Buccino and Calabrese (2007a) model, for low-submerged structures.

$$K_T = \left[\sqrt{{K_{T,0}}^n} - G_2 \min\left(B_1; \frac{B}{\sqrt{H_{si} L_{0p}}}\right)\right]^2 \qquad \text{for } \frac{R_c}{H_{si}} \leq S_2 \qquad (4.53)$$

In a plane defined by $B_t/(H_{si}L_{0p})^{0.5}$ as the abscissa and $K_T^{0.5}$ as the ordinates, the aforementioned Equation represents a straight line with intercept ${K^n}_{T,0}^{0.5}$ and slope G_2 (see Sect. 4.2). However, a significant dispersion in data was found by the Authors, due to the different responses of *ERDC/CHL* and *QUCERL*

experiments. This problem was solved by introducing a dissipation factor, *ν,* varying according to Table 6.1.

Configurations	**ν**
BS-1a	0.6
BS-1b	0.6
BS-1c	0.6
BS-1d	0.6
BS-1e	1
BS-1f	0.25
BS-3	1.4
BS-2	1.5

Table 6.1. Configuration factor, *ν*, for Bottom Seated configurations.

The introduction of this factor allowed to correct the width of the structure B_t, via the definition of an effective crown width, B_t^*:

$$B_t^* = \nu \cdot B_t \tag{6.13}$$

By employing this parameter, instead of the nominal crest width, the previous plane was transformed into a $B_t^*/(H_{si}L_{0p})^{0.5}$ vs. $K_T^{0.5}$one. The plotting of data in this plane (Figure 6.7), allowed to obtain a satisfactory grouping around the trend line expressed by Equation (6.14), testified by a determination index R^2 =0.90.

$$\sqrt{K_T} = -0.2496\mathrm{b}^* + 0.9474 \tag{6.14}$$

In the Equation above b^* is a dimensionless variable expressed as follows:

$$b^* = \frac{B_t^*}{\sqrt{H_{si}L_{0p}}} \tag{6.15}$$

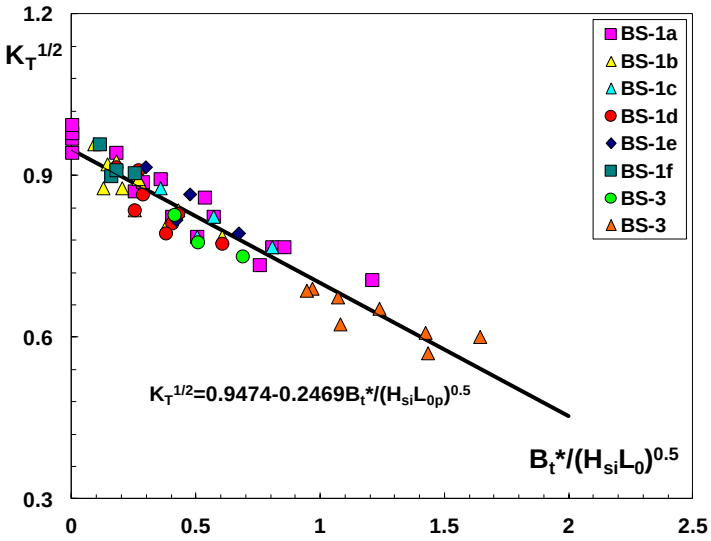

Figure 6.7. Calibration of Eq. (4.53) on all BS data (*QUCERL* and *ERDC/CHL* data).

As it can be observed from Equation (6.14), the Authors obtained a dissipation index, G_2, of 0.25, identical to that found by Buccino and Calabrese (2007) for conventional breakwaters. The value of $K^n_{T,0}$ retrieved from the analysis was close to the unit ($K^n_{T,0}$ = 0.95), that represents the transmission rate for structures made by one row of RBs. In order to verify the linear relationship between b^* and $K_T^{0.5}$, as well as the negligible role of R_{ce}, the residuals, e_i, computed as the difference between $K_{T,meas}$ and $K_{T,calc}$, were plotted against b^* (Figure 6.8) and R_{ce}/H_{si} (Figure 6.9).

Although the previous two graphs don't exhibit a clear trend, the Authors observed some heteroskedasticity for R_{ce}/H_{si}

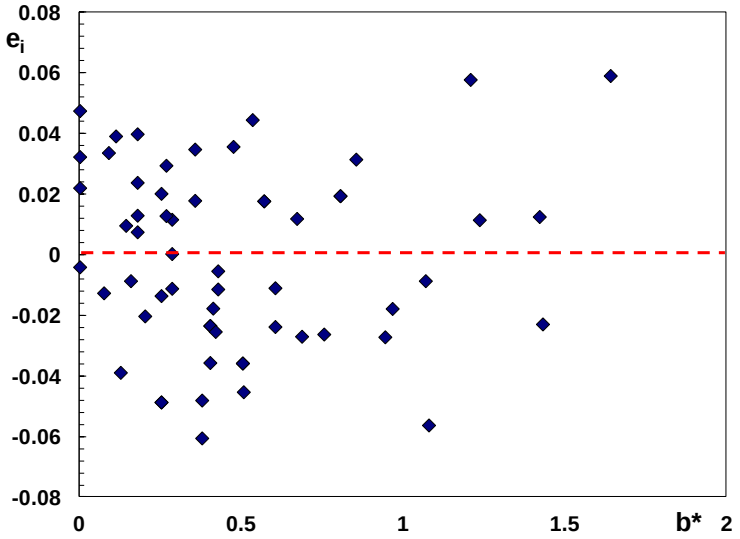

Figure 6.8. Plot of the residuals of Eq. (6.14) vs b^*.

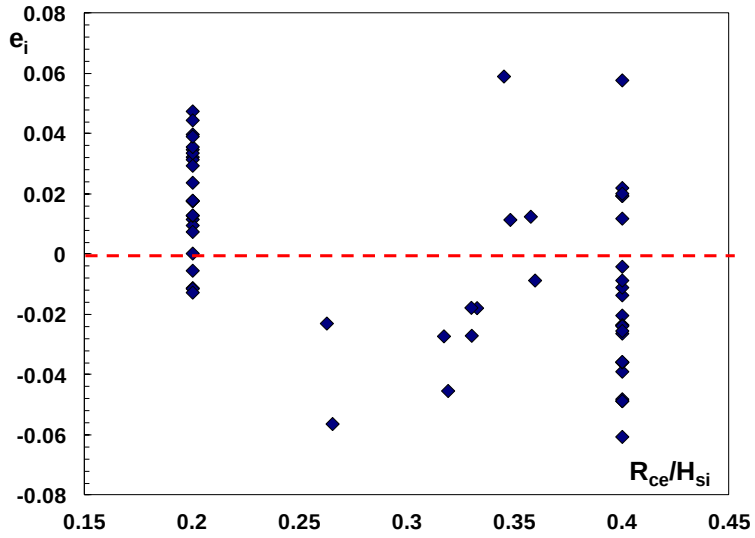

Figure 6.9. Residuals of Eq. (6.14) vs R_{ce}/H_{si}.

6.1.1.3. Calibration of the asymptotic solution for deeply-submerged structures

The calibration of the Eq. (4.52), providing the asymptotic solution of the Buccino and Calabrese (2007a) model for deeply-submerged structures,

required the application of a procedure different from that employed by the Authors for conventional submerged breakwaters.
In fact, the RB database (*QUCERL* and *ERDC/CHL* data) was not as large as the one by Seabrook and Hall (1998), which was employed by Buccino and Calabrese (2007a) for the calibration of the CA model on conventional breakwaters.
For the reason above, the calibration of the Equation (4.52) was conducted by firstly linearising it as follows:

$$Y = 1 + BZ \tag{6.16}$$

where,

$$Y = \frac{1}{K_T} \tag{6.17}$$

and

$$Z = b^* \left(\frac{H_{si}}{R_{ce}}\right)^{1.5} \tag{6.18}$$

In order to define whether any agreement exists with the Equation (6.16) and obtain the eventual limit of application, data was grouped in classes of breaker index, H_{si}/R_{ce}, and progressively plotted in the plane (Z,Y). Results showed a curvature of the fitting line in the interval $0.29 \leq H_{si}/R_{ce} < 0.68$ (Figure 6.10). The Authors attributed this behaviour to the progressively loss of dependence of K_T form the leading variables, as the probability of wave breaking decreases.
Conversely, a linear trend was obtained for $0.68 \leq H_{si}/R_{ce} < 1.1$ (Figure 6.11). In this range of values, the Equation (6.16) resulted to be reasonably verified, as shown by a determination index of 0.90. Moreover, by extending the interval up to a value of about 1.4, the linear trend still persisted (Figure 6.12), in face of a slight reduction of the determination index (R^2 =0.88).
For higher values of the breaker index a significantly loss of linearity emerged (Figure 6.13), similarly to what already observed in Figure 6.10.

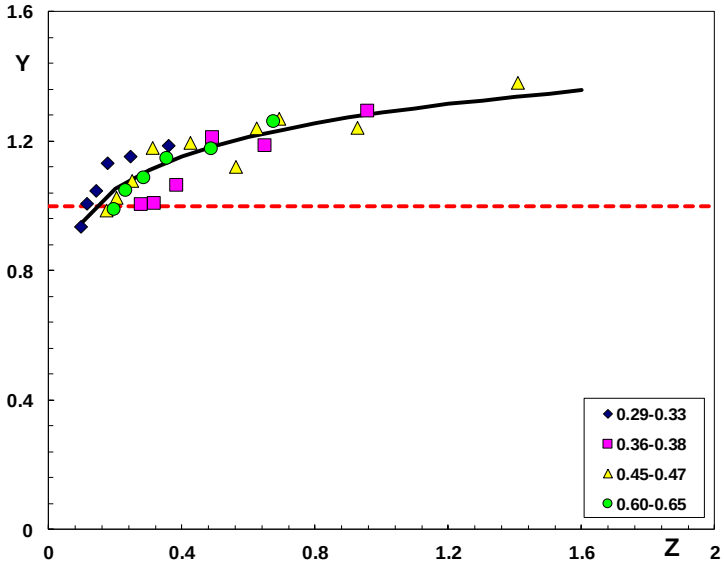

Figure 6.10. Plot of experimental data in the (*Z*-*Y*) plane for H_{si}/R_{ce} <0.68.

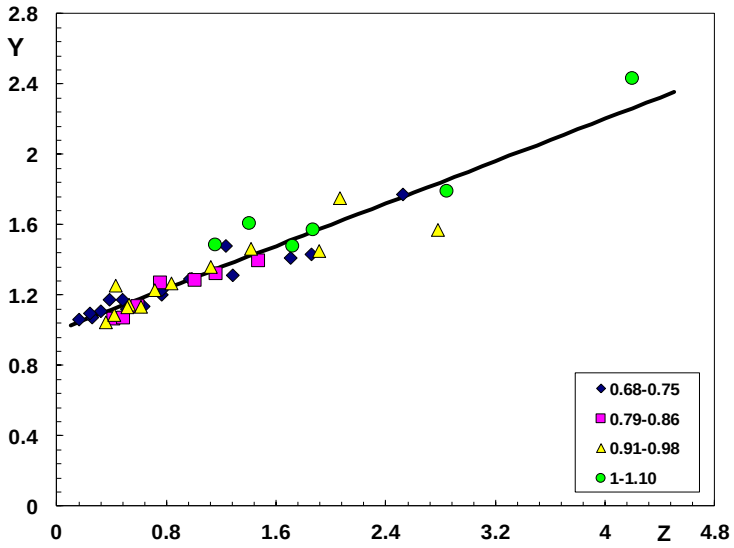

Figure 6.11. Plot of experimental data in the (*Z*-*Y*) plane for 0.68≤ H_{si}/R_{ce} ≤1.1.

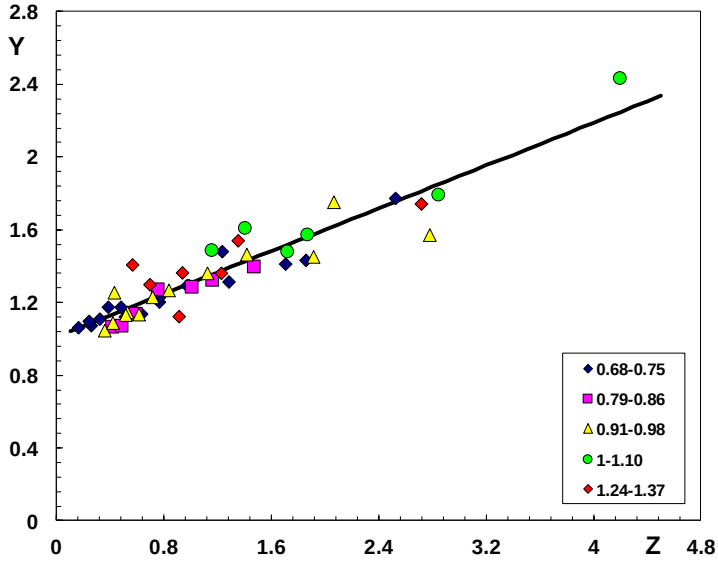

Figure 6.12. Plot of experimental data in the (Z-Y) plane for $0.68 \leq H_{si}/R_{ce} \leq 1.4$.

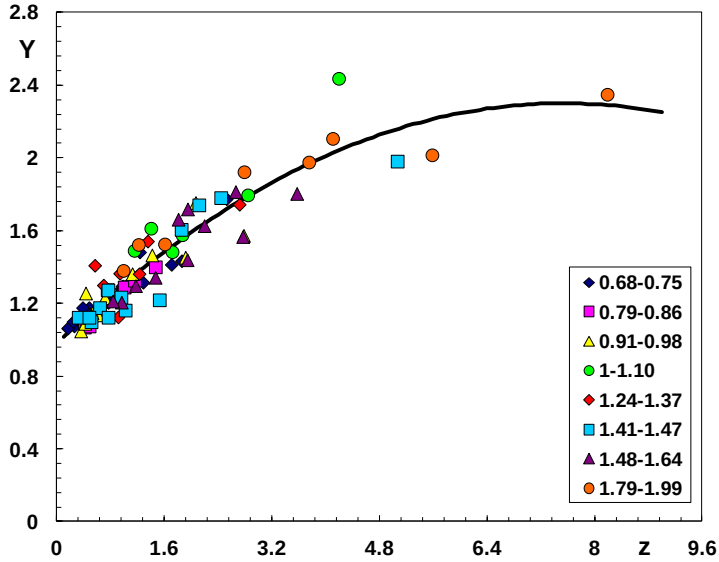

Figure 6.13. Plot of experimental data in the (Z-Y) plane for $0.68 \leq H_{si}/R_{ce} \leq 2$.

On the basis of the previous discussion, the Authors concluded that the Equation (6.16) can be reasonably assumed to be valid for breaker indexes between 0.68 and 1.4, corresponding to relative submergences, R_{ce}/H_{si}, between 0.71 and 1.47.

The calibrated form of the mode is given by the following Equation:

$$K_T = \frac{1}{1 + 0.3\left(\frac{H_{si}}{R_{ce}}\right)^{1.5} b^*} \tag{6.19}$$

Similarly to what already retrieved from the calibration of Equation (4.53), the dissipation factor was 0.3, i.e. a value similar to that found for conventional breakwaters (0.33). It is worth noting that the minimum breaker index (0.68) for Equation (6.18) is 36% larger than that estimated for conventional breakwaters (0.5). This delay in wave breaking occurrence can be likely explained by the larger porosity of the RB barriers with respect to traditional ones (Buccino et al. 2014).

In order to verify the dependence of K_T on $(H_{si}/R_{ce})^{1.5}$ and on b^*, the model was firstly linearised in the logarithmic plane according to Equation (6.20), and subsequently a regression analyses was performed at a 5% significance.

$$Y' = \beta_0 + \beta_1 X' + \beta_2 X'' \tag{6.20}$$

In Equation (6.20) the predictors *X'* and *X''* were respectively defined by the following logarithmic expressions:

$$X' = ln\left(\frac{H_{si}}{R_{ce}}\right) \tag{6.21}$$

$$X'' = ln(b^*) \tag{6.22}$$

and

$$Y' = ln\left(\frac{1}{K_T}\right) \tag{6.23}$$

Results of the regression analysis are summarized in Table 6.2. As it can be observed from this Table, p-values lower than 0.05 ensure that both the relative

submergence and the relative structure width are significant to the prediction of K_T. Moreover, the theoretical values of β_1 and β_2, respectively 1.5 and 1, resulted to be included in the 95% confidence interval (β_1 = 1.27÷2.21; β_2 = 0.81÷1.09). As far as the parameter β_0 is concerned, its value varies between -1.29 and -1.08, which approximately corresponds to the *ln*(0.3).

Coefficients		SE	T-stat	p-value	95% confidence bands	
$\boldsymbol{\beta_0}$	-1.187	0.0526	-22.587	7.01×10^{-27}	-1.293	-1.081
$\boldsymbol{\beta_1}$	1.736	0.234	7.4316	1.82×10^{-09}	1.266	2.206
$\boldsymbol{\beta_2}$	0.950	0.069	13.7054	4.91×10^{-18}	0.811	1.090

Table 6.2. Results of the regression analyses.

Finally, the calibrated CA model for the BS configuration is expressed by the following Equations:

$$K_T = \frac{1}{1 + 0.3\left(\frac{H_{si}}{R_{ce}}\right)^{1.5} b^*} \qquad \text{for } 0.71 \leq \frac{R_{ce}}{H_{si}} \leq 1.47 \tag{6.24}$$

$$K_T = [-0.249 min(4; b^*) + 0.9474]^2 \qquad \text{for } \frac{R_{ce}}{H_{si}} \leq 0.4 \tag{6.25}$$

$$K_T = a\frac{R_{ce}}{H_{si}} + b \qquad \text{for } 0.4 \leq \frac{R_{ce}}{H_{si}} \leq 0.71 \tag{6.26}$$

The Equation (6.24) applies in the case of deeply-submerged breakwaters ($0.71 \leq R_{ce}/H_{si} \leq 1.47$); Equation (6.25) is valid in the opposite cases ($R_{ce}/H_{si} \leq 0.4$), and a linear interpolation (Eq. 6.26) is proposed for the intermediate cases ($0.4 \leq R_{ce}/H_{si} \leq 0.71$).

In the Equation (6.25) an empirical threshold of 4 was introduced, corresponding to the zero value of a parabola (see Sect.4.2).

A comparison between the predicted and measured transmission coefficient is shown in Figure 6.14. The data show a good agreement, apart from two outliers, relative to the *BS-2* configuration, which are circled in red in the Figure.

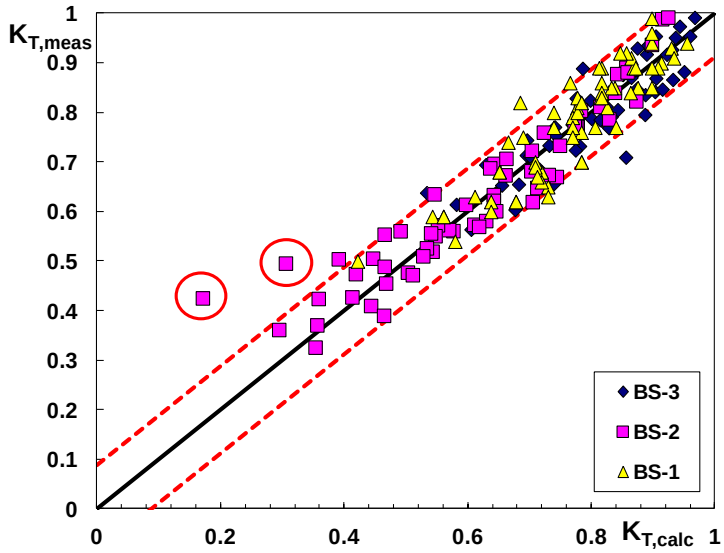

Figure 6.14. Comparison between calculated (Eqs. 6.24- 6.26) and measured transmission coefficient.

Data exhibits a high K_T value in spite of the relatively low submergence (R_{ce}/H_{si} = 0.5) and the large value of b^* (between 2 and 3). However, an overall R^2 of 0.90 was obtained, which indicates good prediction capabilities, 10% larger than that found for the corrected Armono's Equation. The residuals resulted to be Gaussian, with a zero mean and a standard deviation equal to 0.054.

On one hand, this implies that the measured value of the transmission coefficient has a 90% probability of being included in an interval of +/- 0.088 around the predicted one (Figure 6.14); on the other hand, the normality of the residuals ensures, in virtue of the central limit theorem, that all the sources which rule the scatter between measurements and predictions have, more or less, the same importance.

The obtained standard error of 0.054 is slightly larger than that found for conventional breakwaters (0.047). However, after removing the two outliers, a value of 0.049 was obtained which is in a satisfactory agreement with previous findings. Furthermore, the standard error is similar for the three layouts, being 0.052 for *BS-3*, 0.060 for *BS-2* (including the two outliers; 0.046 without them)

and 0.052 for *BS-1*. The values relative to the *QUCERL* datasets resulted to be slightly larger than those returned by the formula of Armono (Eq. 5.1) which was 0.044 and 0.048 for *BS-3* and *BS-2*, respectively.

6.1.2. Conceptual Approach for Bermed Reef Balls

According to the *CA* model, two different solutions were calibrated in case of low and deep submergences. The transition between these two conditions was defined trough an empirical threshold, i.e. the ratio between the submergence of the mound, R_{cm}, and its height, h_m, (Figure 6.15).

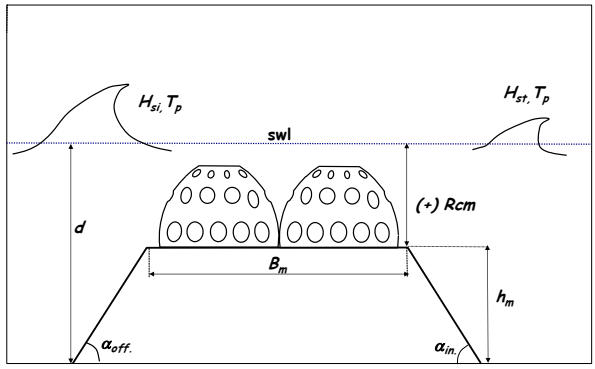

Figure 6.15. Representation of the main variables of the *CA* for bermed configurations.

More precisely, a structure was considered to be deeply submerged when $R_{cm}/h_m \geq 0.95$. In this range of values, it was assumed that the *CA* model calibrated for *BS* layouts still reasonably predicts K_T. On the contrary, a behaviour similar to that of conventional breakwaters was assumed for low-submerged structures. In Figure 6.16, the application of the Equations (6.24) to (6.26) on deeply submerged structures is shown. As it is possible to observe in the graph, a good agreement was found, even though nearly 12% of the 105 data exceed the 90% confidence intervals (red dotted lines). Furthermore, a slight overestimation of calculated values can be observed, which was attributed to the effect of the berm, reducing the permeability of the structure and thus increasing both reflection and dissipation. In this case, a value of the determination index of 0.90 was found, similar to that found by Armono in 2003 ($R^2 = 0.92$).

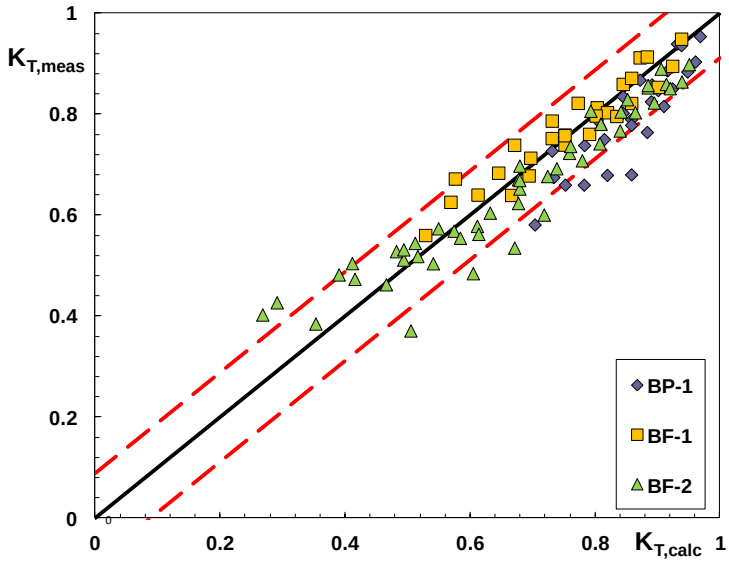

Figure 6.16. Comparison between calculated (Eqs. 6.24-6.26) and measured transmission coefficient, for bermed layouts with $R_{cm}/h_m \geq 0.95$.

In the case of low-submerged structures ($R_{cm}/h_m < 0.95$), the whole structure (berm and RBs) was modelled as a submerged conventional breakwater characterized by a submergence R_{cm} and a crown width B_m (Figure 6.15). RB modules were supposed to be an added resistance, so that their role was taken into account by the dissipation factor, G_R.
Under this assumption, the model was expressed by the following Equation:

$$K_T = \frac{1}{1.18\left(\frac{H_{si}}{R_{cm}}\right)^{0.12} + G_R\left(\frac{H_{si}}{R_{cm}}\right)^{1.5}\frac{B_m}{\sqrt{H_{si}L_{0p}}}} \tag{6.27}$$

The dissipation factor, G_R, was calibrated on the bases of about 55 data, and resulted to be:

$$G_R = 0.33exp\left(\frac{nD_R}{B_m}\right) \tag{6.28}$$

In the Equation above, the exponential term represents the percentage of the berm crown occupied by RBs.

The comparison between the calibrated model and the experimental data is shown in Figure 6.17. This model was assumed valid in the range $0.6 \leq R_{cm}/H_{si} \leq 3.5$, which is broader than the one typically used for conventional breakwaters.

A determination index of 0.90 was found, that is slightly larger than the 0.85 value, found by Armono and Hall (2003) on the same database.

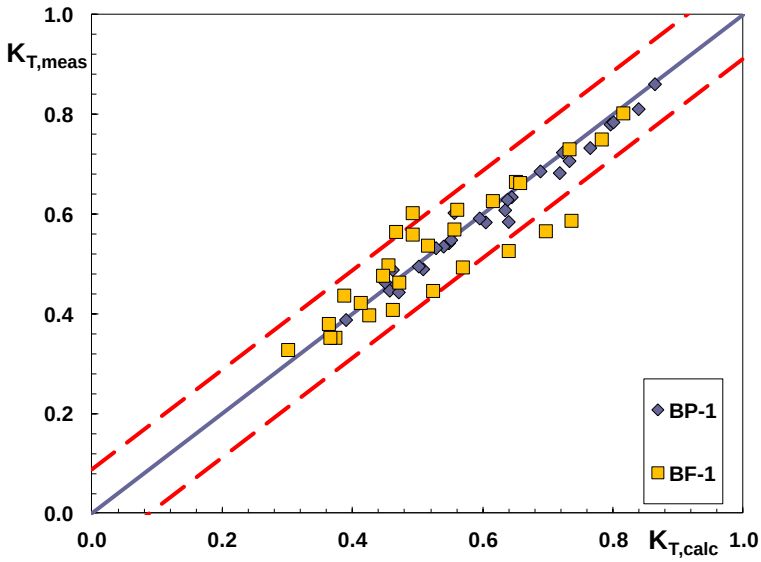

Figure 6.17. Comparison between calculated (Eqs. 6.27 and 6.28) and measured transmission coefficient, for bermed layouts with $R_{cm}/h_m < 0.95$.

The prediction capacity of this model was compared to that of Equation (5.3), proposed by Armono and Hall (2003) for *B-F1* and *B-P1* configurations. A determination index of 0.90 was found, vs. 0.85 of the Equation (5.3).

Moreover, the performance of a conventional breakwater (Figure 6.18a) was compared to that of a barrier made of Reef Balls, arranged according to the configuration *BF-1* and placed on a low berm (Figure 6.18b).

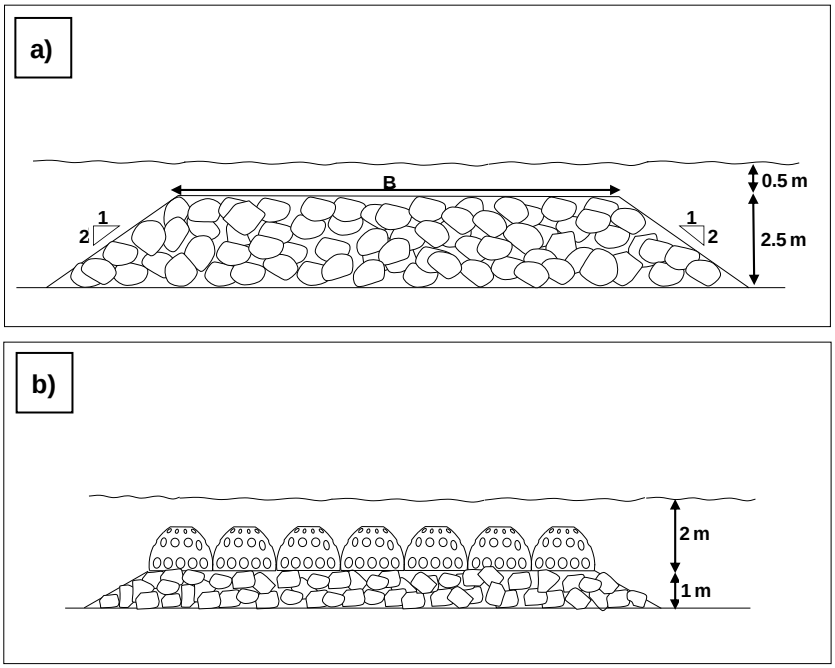

Figure 6.18. Main characteristics of the barriers employed for the comparison: a) conventional breakwater; b) Reef Ball structure.

The mean water depth was 3 m, the submerged depth was 0.5 m and the slopes of the mound were both 1:2. Moreover, the significant wave height was 1.8 m with a peak period of 7 s. The results of the comparison are shown in Figure 6.19, where the transmission coefficient is plotted vs. the structural width. As it is possible to observe, the RB barrier dissipates less than the traditional one because of its larger porosity and lower slope, nonetheless a 50% reduction in the incoming wave height is reached for RB structure realized with 7 rows. Such a rate of dissipation may be appropriate for many situations of practical interest. Besides, this could be increased employing additional rows of Reef Balls.

The same target could be reached by a conventional breakwater characterized by a crown width of 5 m, which on the other hand would require a significant amount of quarried rocks.

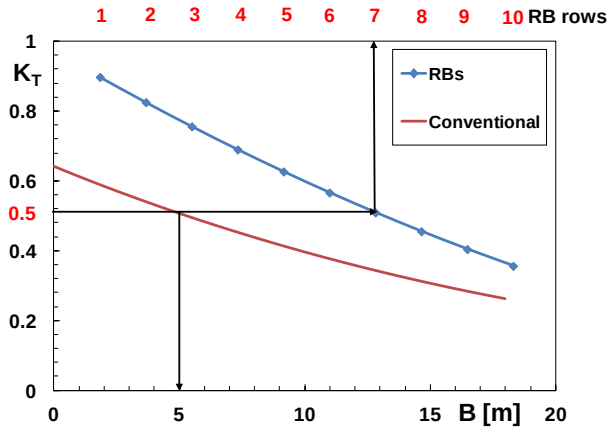

Figure 6.19. Comparison between a conventional breakwater and a structure made of Reef Ball (values of K_T for the conventional breakwater were estimated by means of Eqs. 4.55-4.57).

As a final result of the analyses described above (Buccino et al., 2014), it can be noticed that the predictive model shows, on the one hand, encouraging properties, such as an high determination indexes. Nevertheless, on the other hand, the dataset employed for the calibration of the model appears to be not wide enough to guarantee a sufficient reliability of the predictions; moreover, the base hypothesis of the model, i.e. breaking occurring on the crest of the breakwaters, requires to be further investigated by means of dedicated tests.
The *DICEA* experimental campaign, described in the following Chapter, was expressly designed to address, among the others, the aforementioned issues and to overcome the previous shortcomings

Chapter 7 – THE *DICEA* EXPERIMENTAL CAMPAIGN

In order to investigate the main aspects of wave-structure interaction and compare the macroscopic behaviour of RB barriers to that of conventional breakwaters, an extensive experimental campaign was performed at the Department of Civil, Architectural and Hydraulic Engineering (*DICEA*) of the University of Naples "Federico II", Italy. This campaign was designed to overcome the limitations affecting previously described studies (see Chapter 6) and extend the range of configurations analyzed through experimental tests. For these reasons, about 1,500 experiments were carried out in the flume of the *DICEA* laboratory.

7.1 Experimental set-up

7.1.1. Flume and main equipment features

The flume of the *DICEA* laboratory employed in the experimental campaign is a 0.80 m high and 26 m long structure with a variable section. The first 13.6 m, starting from the wave maker, are characterized by a width progressively decreasing from 80 cm to 50 cm; thereafter the section remains constant for all the remaining part. This portion of the flume is characterized by 11 glass windows from which visual observations can be made (Figure 7.1).

Starting from the wave maker, the flume profile is characterized by a 8.23 m long horizontal bottom, connected to a steel flat by a 1:18 slopped junction. The flat was *ad-hoc* realized for the *DICEA* experimental campaign, with a length of 4 m and a distance of 0.32 m from the flume bottom. This was used as a foundation for Reef Balls structures (Figure 7.2).

The wave maker is a piston-type one located at 3 m from the end of the channel (Figure 7.3a), controlled by a position sensor. It is moved by an oildynamic pump powered by an electric motor, allowing a maximum semi-stroke of 20 cm. Signals generated by the software WAVEGEN (developed by HR Wallingford) are sent to the control cabinet (Figure 7.3b), and then transferred to the wave maker, allowing to reproduce regular and irregular sea states.

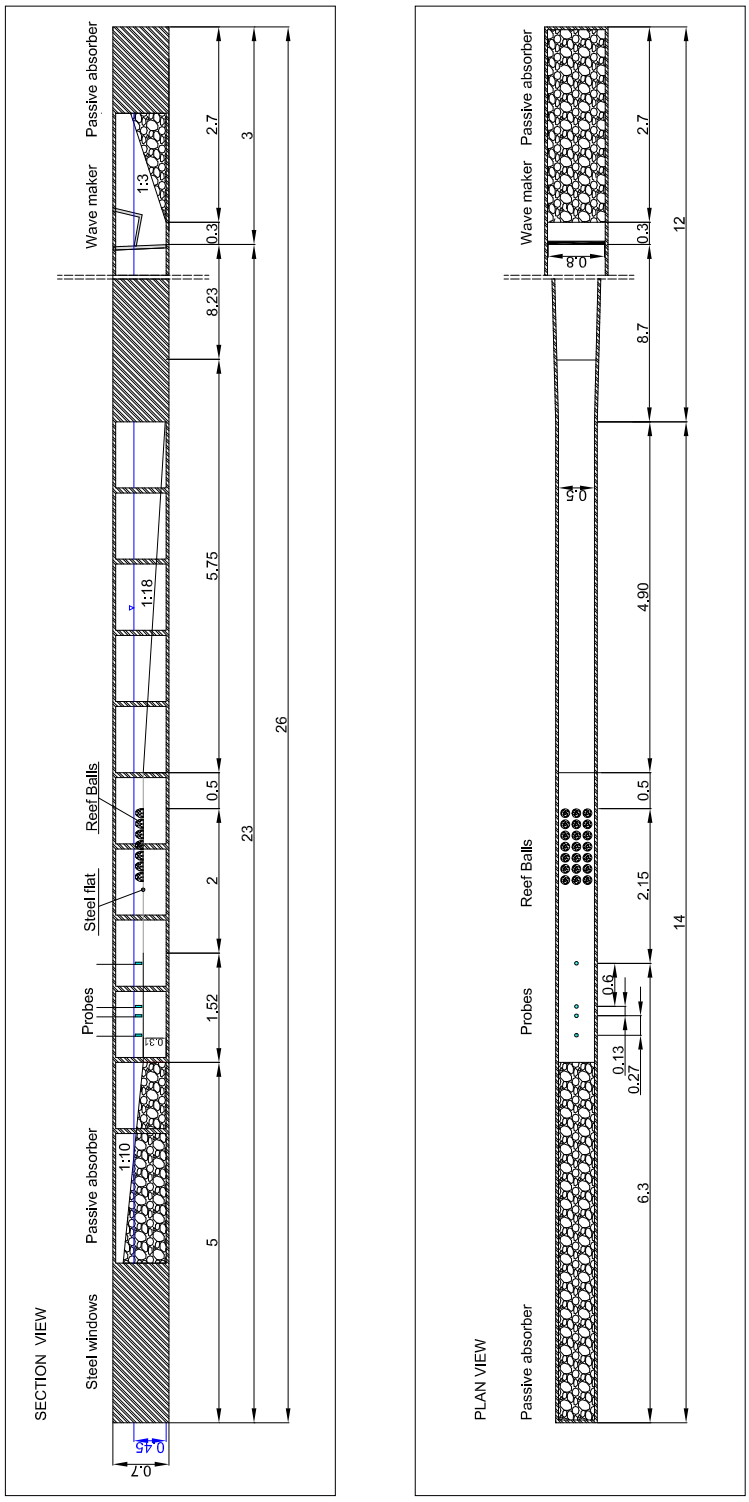

Figure 7.1.Cross-section and plan view of the flume.

Figure 7.2. Reef Balls arranged on a steel flat in the *DICEA* flume.

With specific reference to the *DICEA* campaign, irregular waves were employed, generated according to a medium Jonswap spectrum. Moreover, in order to minimize the effect of wave reflection, two passive absorbers were placed on the back of the wave generator and at the other end of the channel, respectively with a slope of 1:3 and 1:10.

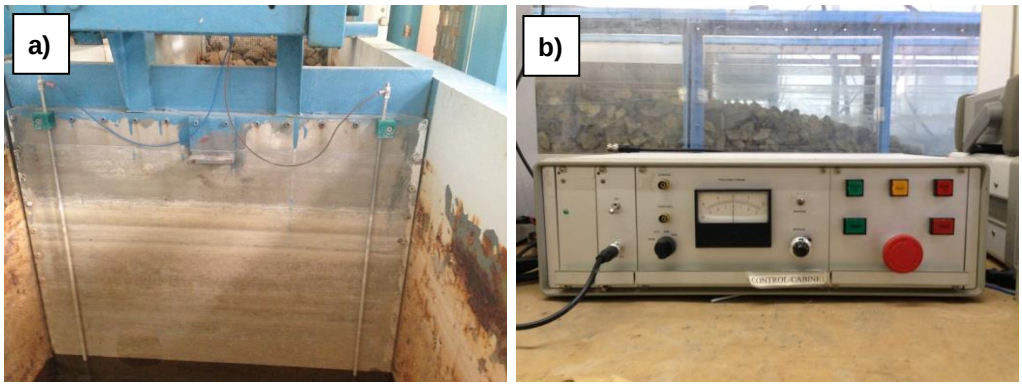

Figure 7.3. a) Wave maker; b) control cabinet.

Measures of the water level and wave characteristics were conducted by means of 4 “twin wire” resistive probes (Figure 7.4a), powered by a dual-power supply (Figure 7.4b) operating at a differential voltage of about ±15V.

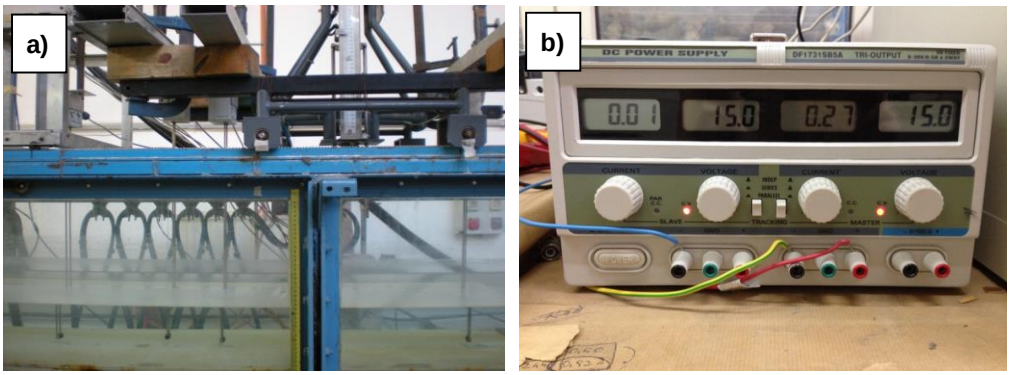

Figure 7.4. a) Array of probes; b) dual power supply.

The differential voltage returned by the sensors is transformed into a 16 bit digital signal through an Analogical Digital Converter (ADC) and stored in a PC by means of an acquisition card.

7.1.2. Probes' positioning

The mutual position of the probes was established as result of a reflection analysis, conducted by means of the "REL-RIFLINC" software, aimed at minimizing the interaction between incident and reflected waves.

Given the number and position of probes, the water depth, the duration of the test and the sampling frequency (25 Hz), the program returned a reliability versus frequency graph. In such a graph peaks greater than 1.2 represent ideal resonance frequencies, where the interactions are greater.

The optimal mutual position of probes was therefore obtained via an iterative procedure for the different wave depths and series lengths of interest.

As an example, Figure 7.5 shows the reliability graphs returned by the program for a series length of 600 sec and for local water depths equal to 0.1 m. These water depth values correspond to a submergence of Reef Ball structures equal to 0, 0.20 m, 0.50 m and 1 m in the prototype scale.

Worth noting, a good reliability index was obtained for frequencies between 0.25 and 2.2 Hz. The suitability of this range of values was evaluated in the light of wave peak frequencies, f_p, employed in the tests, which are, as it will be discussed more in detail in Section (7.2) , equal to 0.5, 0.67, 1 and 1.43 Hz.

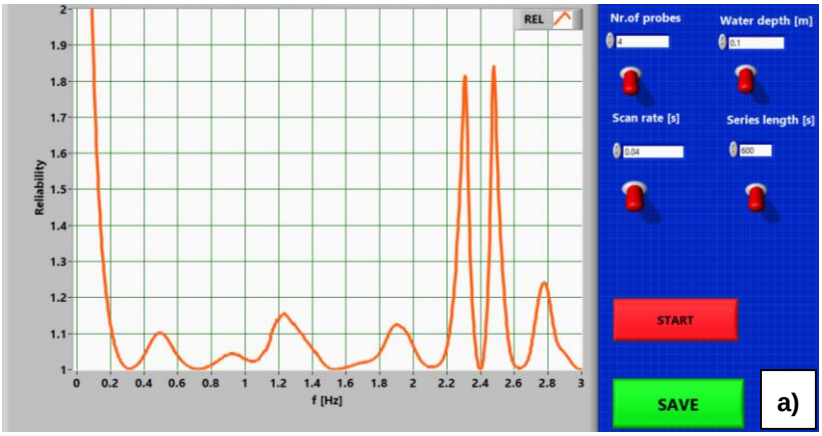

Figure 7.5. Reliability index returned by the program Rel-reflinc for a submergence of 0.1 m.

Based on the above, a good reliability was observed in the range 0.5 f_p and 1.5 f_p. This allowed to find a unique relative position of probes, for all of the tests. The four probes were finally arranged over a length of 1 m, at a distance of 60 cm, 13 cm and 27 cm from one another.

Furthermore, the probes were located behind the RB modules, with the first one at a distance of 16.48m form the wave maker. This position was kept constant for all the tests (Figure 7.1).

7.1.3. Probes' calibration

On a daily base, or whenever required by external conditions, a check of the probe's signals and their subsequently calibration were performed.

The signal test was done by means of the "Measurement and Automation Explorer" program (by National Instruments), allowing to identify any eventual noise or drift during an acquired continuous signal. Figure 7.6 shows an example of the acquired signal for the four probes employed. The absence of drift for all the probes can be noticed, while some noise affects the fourth one (red signal in Figure 7.6).

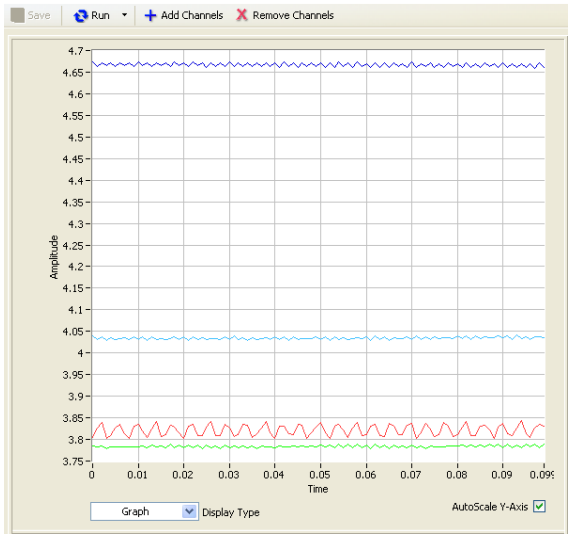

Figure 7.6. Example of acquired signal.

After eliminating such a noise, generally due to the accumulation of calcium carbonate on the immerged portion of the probe, it was possible to proceed with the calibration.

This operation required to establish a correspondence between the position of the probes (with respect to the water level) and the voltage returned. Starting from a given position of the probes, each one was moved with incremental steps of 2 cm and the correspondent voltage returned by probes was read.

The calibration was conducted by means of the "Calibration Define" software (Figure 7.7), employing 8 calibration points corresponding to moving probes in a range of ± 6 cm around the initial position.

The same software also allowed to verify that probes were properly working, by computing the signal to noise ratio, *S*/*N*, expressed by the Equation (7.1).

$$\frac{S}{N} = 20log_{10}\left(\frac{\mu}{\sigma}\right) \tag{7.1}$$

In the previous equation, μ represents the average of the signals acquired for 5 seconds with a sampling frequency of 25 Hz, while σ is standard deviation, i.e. the noise of the signals.

The minimum value of *S*/*N* calculated during the experimental campaign was about 45 db, that ensured the correct operation of probes.

Subsequently, for each probe, the calibration points were fitted with a liner regression line, with a determination index, R^2, always greater than 0.99 (Figure 7.8).

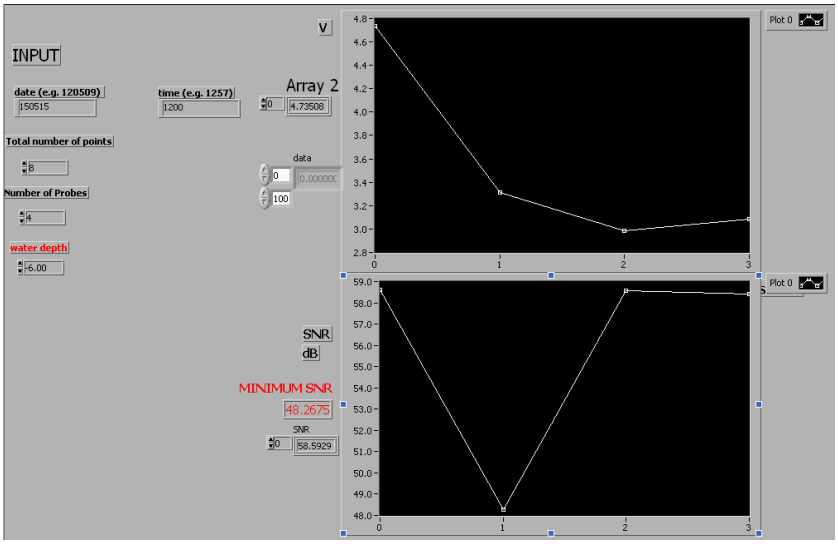

Figure 7.7. Probes calibration.

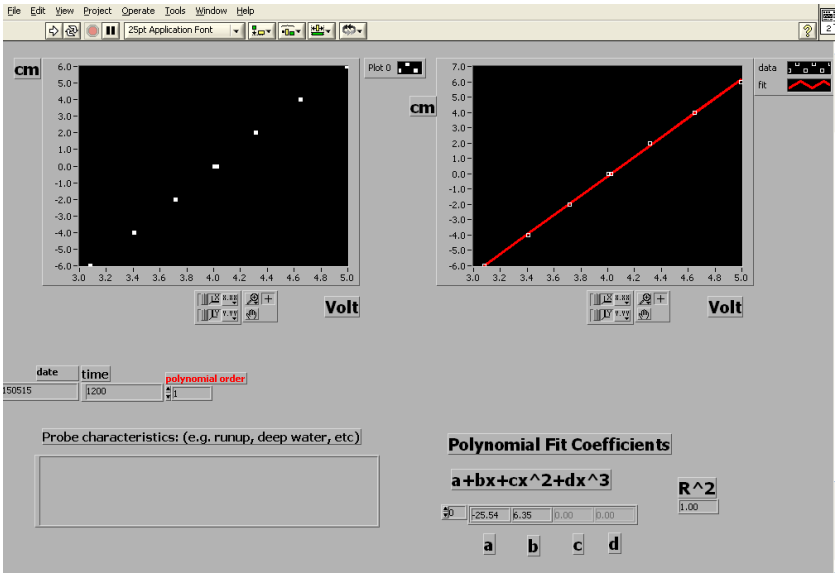

Figure 7.8. Fitting of the calibration points

7.2 Description of the DICEA tests

Reef Balls employed in the *DICEA* tests were characterized by a base diameter, D_R, of 12 cm, by an height, h_R, of 10 cm and by a weight of 0.78 Kg (Figure 7.9), corresponding to 1:15 models of Goliath Ball (Table 2.1).

Each module was equipped with 3 magnets under the base, to anchor it to the steel flat and avoid any type of displacement during the tests (Figure 7.9).

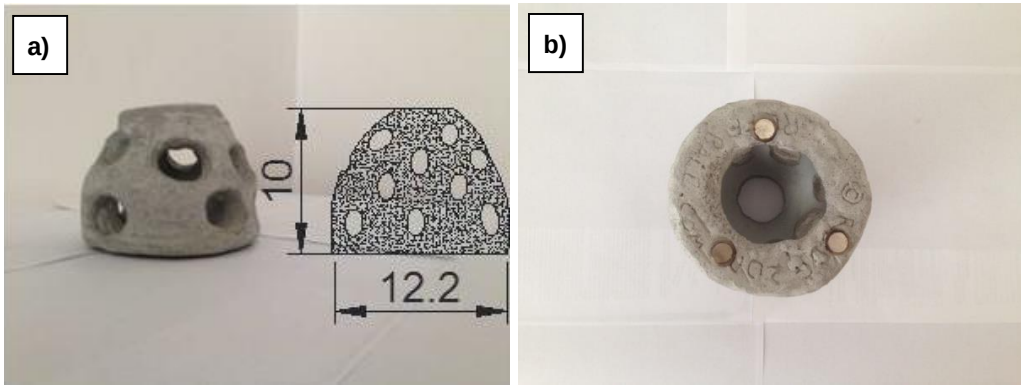

Figure 7.9. a) Reef Ball model employed in the *DICEA* tests; b) magnets placed under the base of model.

In all the tests carried out, RB units were placed in a single layer, in order to reproduce the most common layout employed in the practical applications, which is the one with bottom-seated Reef Balls. Modules were arranged in a variable number of rows, with the first one always placed 14.1 m far from the wave maker.

Three main configurations were investigated, namely *DICEA-A*, *DICEA-B* and *DICEA-C*

The *DICEA-A* configuration (Figure 7.10) was obtained by arranging modules side-by-side, to form structures with a number of rows variable between 1 and 10. Each row was composed by 4 RB units.

The remaining configurations were obtained by arranging Reef Balls respectively in 3, 5 and 7 rows, each one composed by 3 modules. In particular, a distance between units of 3.3 cm (50 cm in the prototype scale) was assumed

for the *DICEA-B* configuration (Figure 7.11), while 6.6 cm (1 m in the prototype scale) was fixed for the *DICEA-C* one (Figure 7.12).

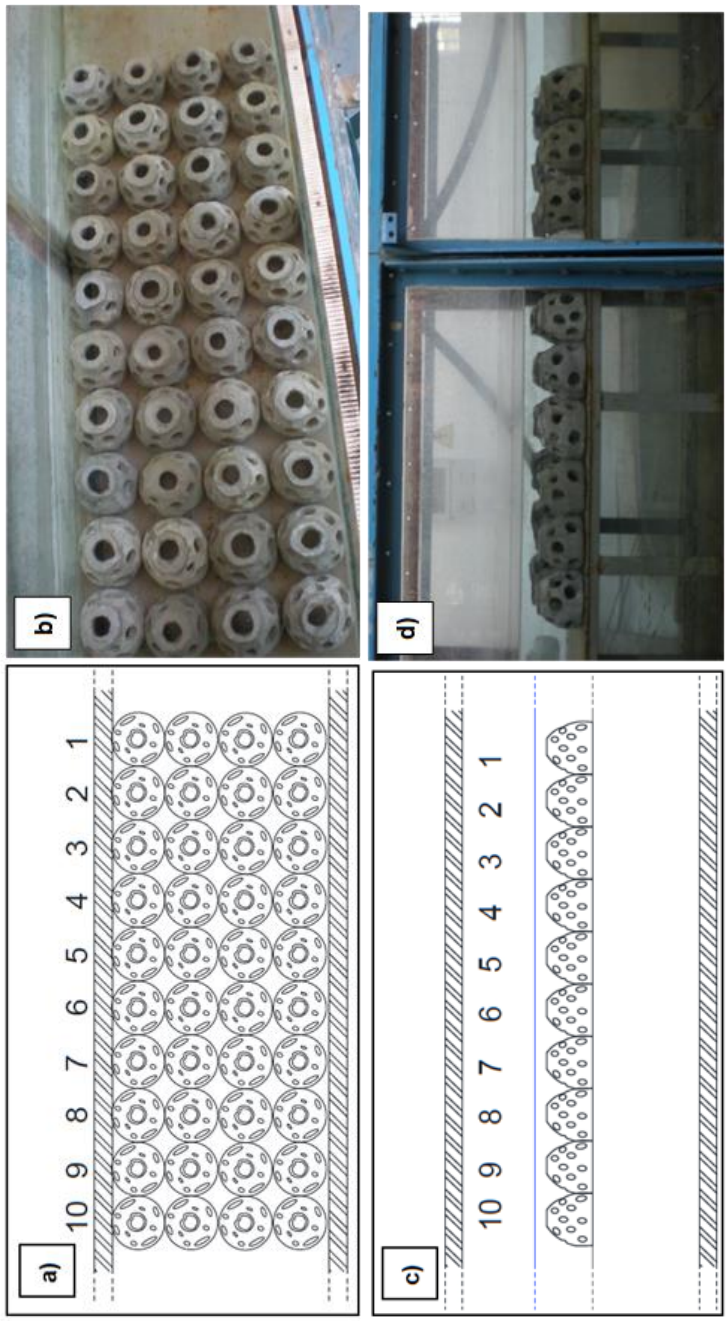

Figure 7.10. Configuration *DICEA-A*: a) plan representation; b) the plant view; c) cross section representation; d) the cross-section view

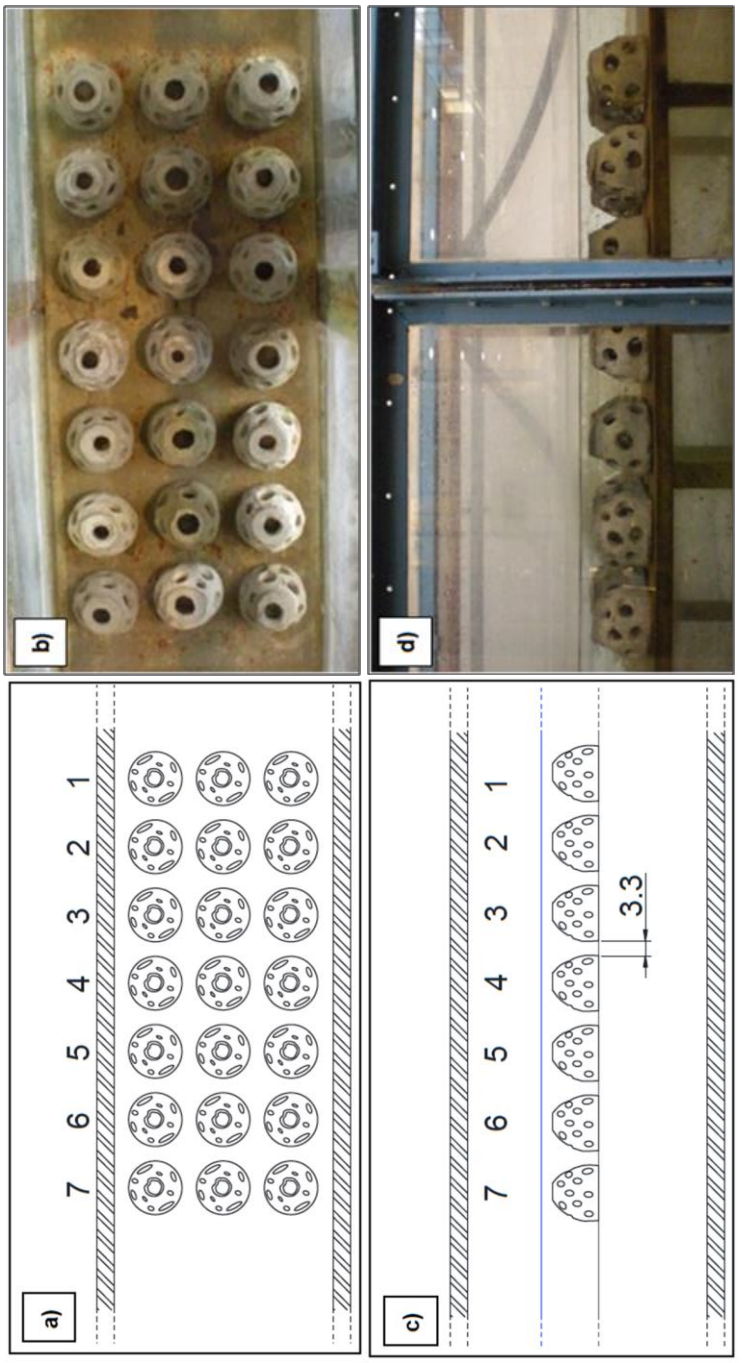

Figure 7.11.Configuration *DICEA-B*: a) plan representation; b) the plant view; c) cross section representation; d) the cross-section view

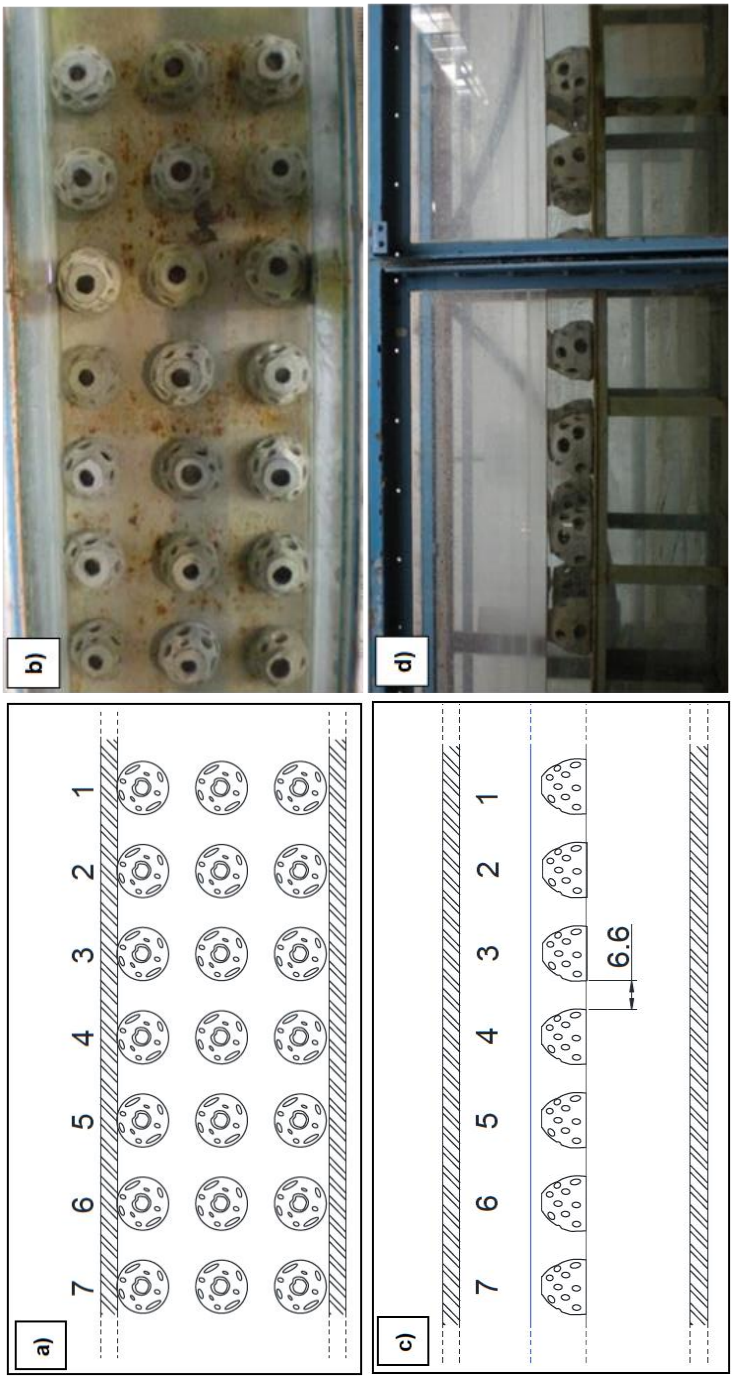

Figure 7.12. Configuration *DICEA-C*: a) plan representation; b) the plant view; c) cross section representation; d) the cross-section view.

As previously stated, the main objective of this Thesis is the characterization of Reef Ball barriers for what concerns wave breaking, transmission and set-up.

While wave breaking was analyzed through visual observations, measures of wave characteristics were required to investigate the other two aspects.

In particular, to evaluate wave transmission and set-up in the presence of RB modules, tests were conducted with (Figure 7.13a) and without the structures (Figure 7.13b). This way, it was possible to measure, respectively, the transmitted and the incident wave height, as well as the variation of the medium water level due to the RB structures.

Accordingly, the position of the probes was set behind the barrier and kept constant in all the tests (Figure 7.14).

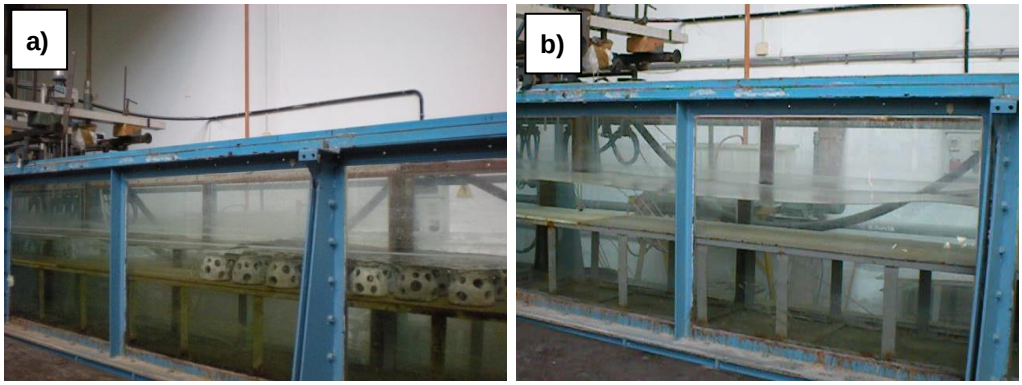

Figure 7.13. Test conducted with and without RB modules to determine the characteristics of the transmitted wave (a) and of the incident one (b).

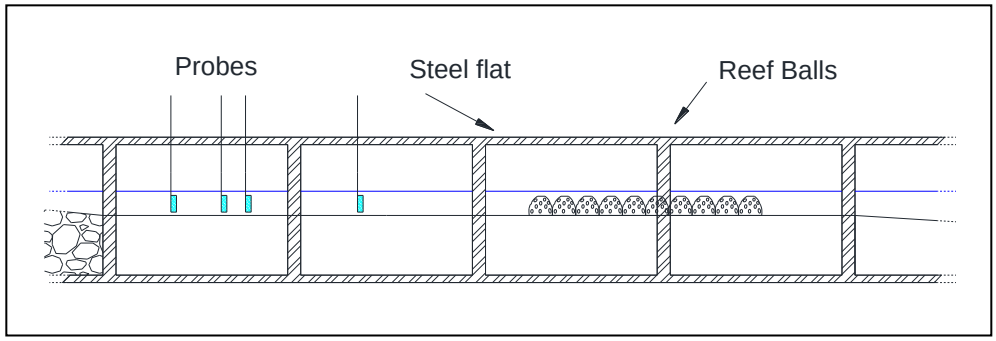

Figure 7.14. Position of probes for investigating transmission and wave set-up due to RB modules.

In order to cover a wide range of design conditions, involving breaking and non-breaking waves, the tests without the barrier were carried out for six wave heights, four peak periods and four water depths, leading to an overall number of 96 tests. Tests were conducted for a variable duration, to collect 300 waves independently from the peak frequency employed.

Table 7.1 shows the target wave characteristics, the local water depths, and the duration of tests performed without the barrier.

f_p (Hz)	H_i (m)	d (m)	Duration (sec)
0.13	0.3, 0.6, 0.9, 1.2, 1.5, 1.8	0.1, 0.11, 0.13, 0.17	600
0.17	0.3, 0.6, 0.9, 1.2, 1.5, 1.8	0.1, 0.11, 0.13, 0.17	450
0.26	0.3, 0.6, 0.9, 1.2, 1.5, 1.8	0.1, 0.11, 0.13, 0.17	300
0.37	0.3, 0.6, 0.9, 1.2, 1.5, 1.8	0.1, 0.11, 0.13, 0.17	210

Table 7.1.Summary of the tests conducted without structure. Measures are reported in the prototype scale.

The same tests were conducted in the presence of RB structures, except for the *DICEA-A* configuration composed by 8 and 10 rows, for which only the two submergences Rc = 0.5 m and Rc = 1 m were investigated. Worth recalling, the submergence of the barrier is defined as the difference between the local water depth, d, and the height of Reef Ball modules, h_R. For each configuration, Table 7.2 shows the numbers of rows employed, the submergences investigated and the total number of test performed. The overall number of tests carried out on behalf of the *DICEA* experimental campaign was 1,440.

Configurations	# rows	Rc (m)	# tests
DICEA A	1-7, 9	0.0, 0.2, 0.5, 1	768
	8, 10	0.5, 1	96
DICEA B	3, 5, 7	0.0, 0.2, 0.5, 1	288
DICEA C	3, 5, 7	0.0, 0.2, 0.5, 1	288
			Total=1,440

Table 7.2. Summary of the *DICEA* tests. Measures are reported in the prototype scale.

Chapter 8 – ANALYSIS OF THE WAVE BREAKING FOR THE *DICEA* TESTS

As discussed in Section (1), the wave breaking is a complex phenomenon, able to impact on wave transmission and set-up and cause different, often contrasting, effects, such as energy dissipation, scour and erosion.
For these reasons, the first objective of the *DICEA* experimental campaign was to assess whether RB structures are able to determine the wave breaking, its significance and typology.
Before analyzing in detail the results, it is required to preliminarily define the wave breaking condition considered in this study. In fact, because random waves were employed during the tests, the condition of incipient breaking was identified by the presence of at least one breaking wave during the whole duration of the experiments. The identification of this state required a detailed visual observation of the tests and the visual examination of camera recordings. Although a frame-by-frame analysis was carried out, the assessment is qualitative in nature and, therefore, intrinsically affected by some uncertainties and subjectivity.
The analysis was performed for the tests of *DICEA-A* configuration only, for which a sufficient number of observations was available.

8.1 Wave breaking without RB structures

Tests conducted without the structures were firstly investigated, with the aim of differentiating the cases in which the breaking condition occurred from those where it did not. In Table 8.1 to Table 8.4, breaking and non-breaking tests are reported, for each target peak frequency investigated. As it is possible to deduce from the Tables, about 78% of the tests was characterized by wave breaking occurring without the RB barrier.

H_i (m)	Rc=1 (m)	Rc=0.5 (m)	Rc=0.2 (m)	Rc=0 (m^3)
0.3	-	-	-	-
0.6	-	-	-	x
0.9	-	-	-	x
1.2	-	x	x	x
1.5	x	x	x	x
1.8	x	x	x	x

Table 8.1. Summary of the breaking (x) and non-breaking (-) tests, conducted without the barrier, for a peak frequency equal to 0.37 Hz (values given in the prototype scale).

H_i (m)	Rc=1 (m)	Rc=0.5 (m)	Rc=0.2 (m)	Rc=0 (m^3)
0.3	-	-	-	-
0.6	-	x	x	x
0.9	x	x	x	x
1.2	x	x	x	x
1.5	x	x	x	x
1.8	x	x	x	x

Table 8.2.Summary of the breaking (x) and non-breaking (-) test, conducted without the barrier, for a peak frequency equal to 0.26 Hz (values given in the prototype scale).

H_i (m)	Rc=1 (m)	Rc=0.5 (m)	Rc=0.2 (m)	Rc=0 (m^3)
0.3	-	-	-	-
0.6	-	-	-	x
0.9	x	x	x	x
1.2	x	x	x	x
1.5	x	x	x	x
1.8	x	x	x	x

Table 8.3. Summary of the breaking (x) and non-breaking (-) test, conducted without the barrier, for a peak frequency equal to 0.17 Hz (values given in the prototype scale).

H_i (m)	Rc=1 (m)	Rc=0.5 (m)	Rc=0.2 (m)	Rc=0 (m^3)
0.3	-	-	-	-
0.6	-	-	x	x
0.9	x	x	x	x
1.2	x	x	x	x
1.5	x	x	x	x
1.8	x	x	x	x

Table 8.4. Summary of the breaking (x) and non-breaking (-) test, conducted without the barrier, for a peak frequency equal to 0.13 Hz (values given in the prototype scale).

Data from the previous Tables have been plotted in a plane reporting $H_{m0,i}/d$ on the horizontal axis and h_R/d on the vertical one (Figure 8.1).

$H_{m0,i}$ represents the spectral significant wave height, in the following referred to as H_i for brevity; d is the water depth; h_R is the height of RB modules. Worth noting, h_R is constant for all performed test and the all the investigated configurations are made of a single layer, therefore h_R coincides with the height of the structure, h_s.

In Figure 8.1, the outcomes of the tests are depicted with different marks (crosses identify the breaking condition in the absence of the structure: "NO STRUCTURE BR"; blue diamond marks address the absence of breaking for tests conducted without the structure: "NO STRUCTURE N-BR").

In the same Figure, it is possible to observe the presence of two clusters of data, roughly separated by a value of H_i/d equal to 0.28. This value is deemed to be the threshold of the incipient breaking condition.

The previous distinction is also evident from Figure 8.2, reporting the same data in a H_i/d versus d/L_0 plane.

It is worth noting that according to the definition of wave braking employed in this study, i.e. the presence of at least one breaking wave during tests, it is reasonable to assume that the wave breaking occurred for the highest waves of the irregular wave train. Under the Reyleigh hypothesis, this corresponds to assuming that the condition of incipient breaking occurs for $H_{max}/d > 0.56$, that is a value very similar to that proposed by Le Méhauté (Allsop, 1998) for natural beaches (Sect. 1).

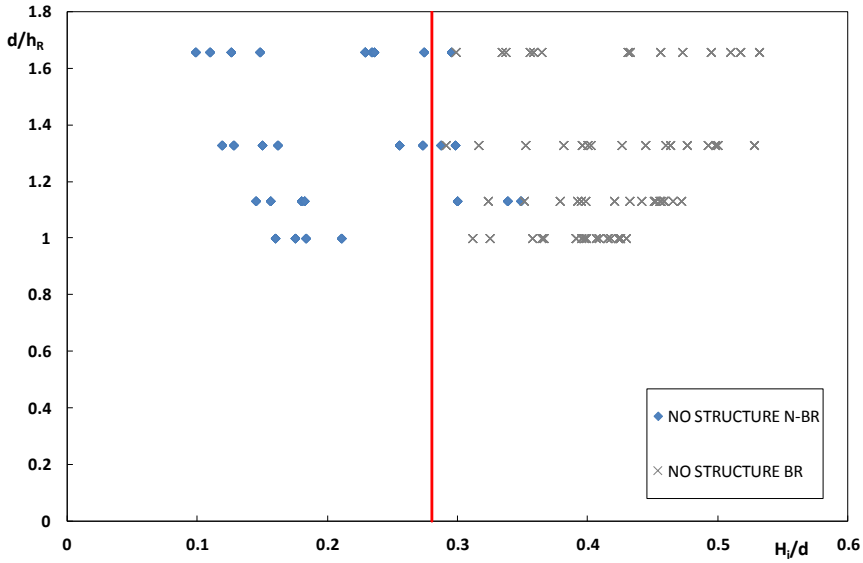

Figure 8.1. Breaking and non-breaking tests conducted without structures, plotted in a H_i/d vs d/h_R plane. The red line identifies the incipient breaking condition (H_i/d =0.28).

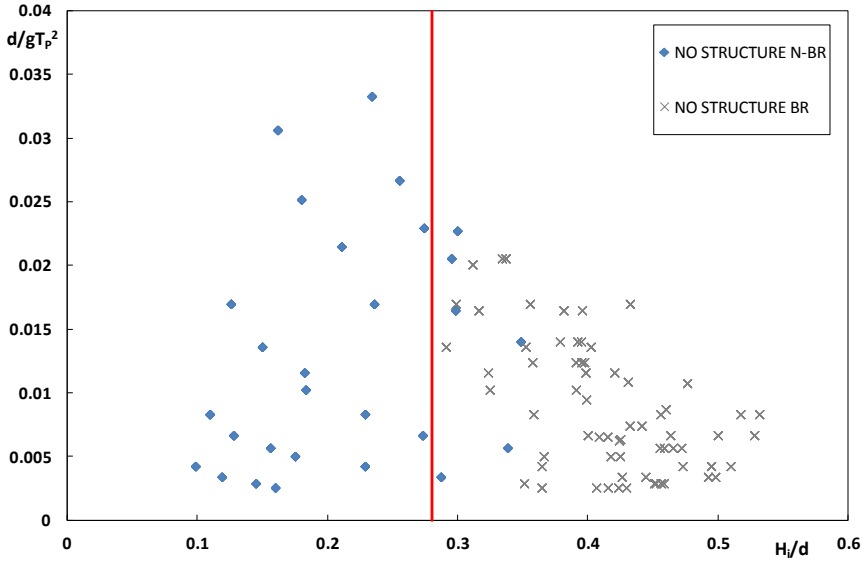

Figure 8.2. Breaking and non-breaking tests conducted without structures, plotted in a H_i/d vs d/L_0 plane. The red line identifies the incipient breaking condition (H_i/d =0.28).

In particular, results show that the probability of wave breaking is equal to 0% for values of $H_i/d \leq 0.28$ and 100% for $H_i/d > 0.365$. Thus, a condition of

breaking was observed for H_{max}/d >0.73, quite close to the breaker index proposed by Danel (1952).

The condition of incipient breaking was observed for values included in the aforementioned limits, where the breaking probability is equal to 72%.

Table 8.5 summarizes the number of breaking and non-breaking tests included in the aforementioned bands.

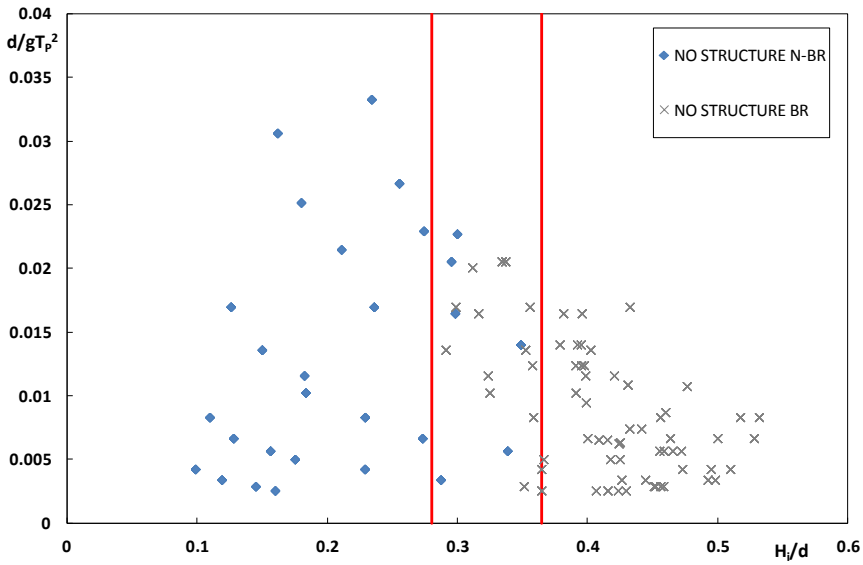

Figure 8.3. Bands identifying different probabilities of breaking for tests conducted without structures in the H_i/d vs. d/L_0 plane.

	$H_i/d \leq 0.28$	$0.28 < H_i/d \leq 0.365$	$H_i/d > 0.365$
# Breaking tests	0	16	52
# No-breaking tests	22	5	0

Table 8.5. Summary of tests conducted without the structures and relevant H_i/d classes.

8.2 Wave breaking in the presence of RB structures

The influence of RB structures was investigated following the same approach previously employed for tests performed without the structures.

In particular, a comparison between no-structure and no-breaking tests and those conducted with RBs arranged according to the *DICEA-A* configuration is shown in Figure 8.4.

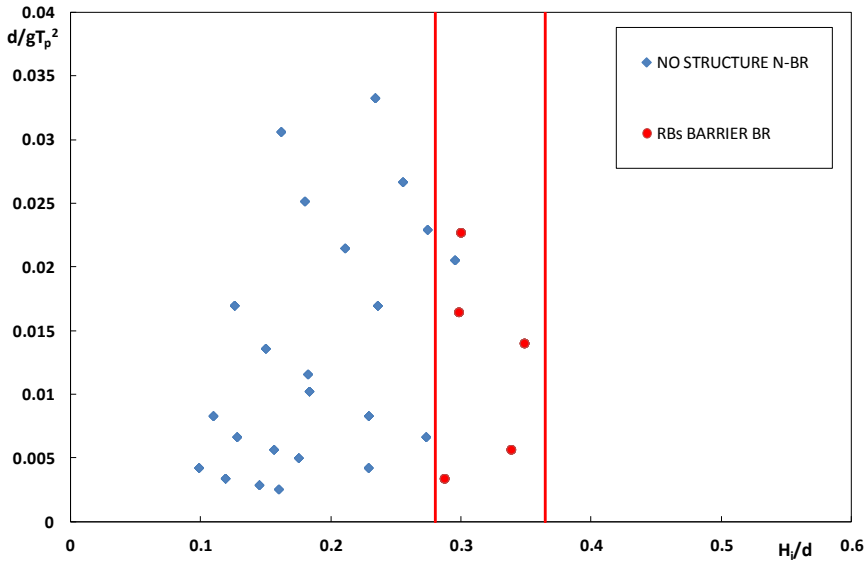

Figure 8.4. Breaking tests conducted without structures (blue dots) and with RB structures (red dots), plotted in a H_i/d vs d/L_0 plane. The red lines (H_i/d =0.28 and H_i/d =0.365) identify different probabilities of breaking.

As shown in the graph above, the presence of Reef Ball barriers does not influence the occurrence of breaking for $H_i/d \leq 0.28$, while it increases the probability of breaking in the range $0.28 < H_i/d \leq 0.365$.
In the following Tables a summary of the number of the breaking tests for each region is reported.

	$H_i/d \leq 0.28$	**$0.28 < H_i/d \leq 0.365$**	**$H_i/d > 0.365$**
# without structures	0	138	458
# with RB barrier	0	192	458

Table 8.6. Summary of tests conducted with the structures and relevant H_i/d classes.

As it is possible to observe from Figures 8.5 to 8.8, where RB-breaking tests are represented by red marks, RB barriers don't influence the wave breaking in

the case of deeply submerged structures (Figure 8.5) nor for Rc=0 m (Figure 8.6), independently from the number of rows employed to build the structure. Contrariwise, they are able to induce the wave breaking in case of intermediate submergences (Figure 8.7 and Figure 8.8).

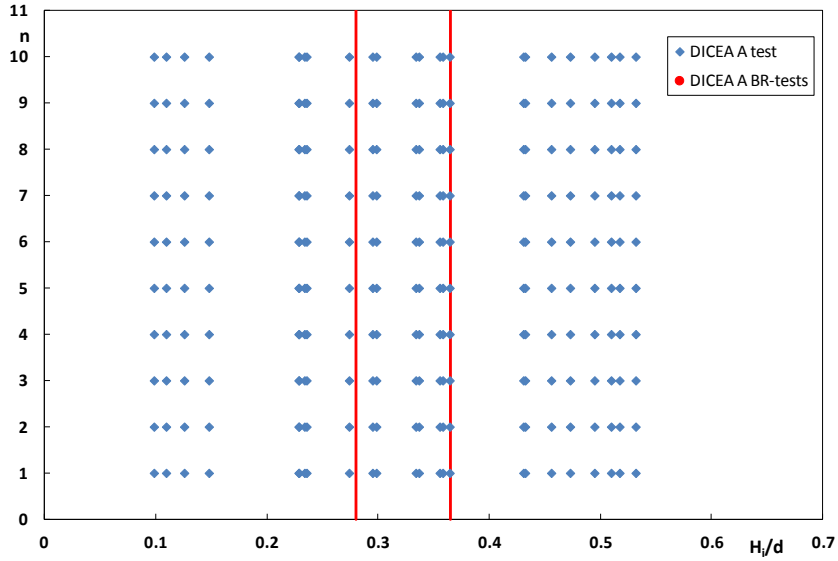

Figure 8.5. Comparison between breaking (red dots) and non-breaking (blue dots) tests for the *DICEA-A* configuration and for a submergence equal to 1 m.

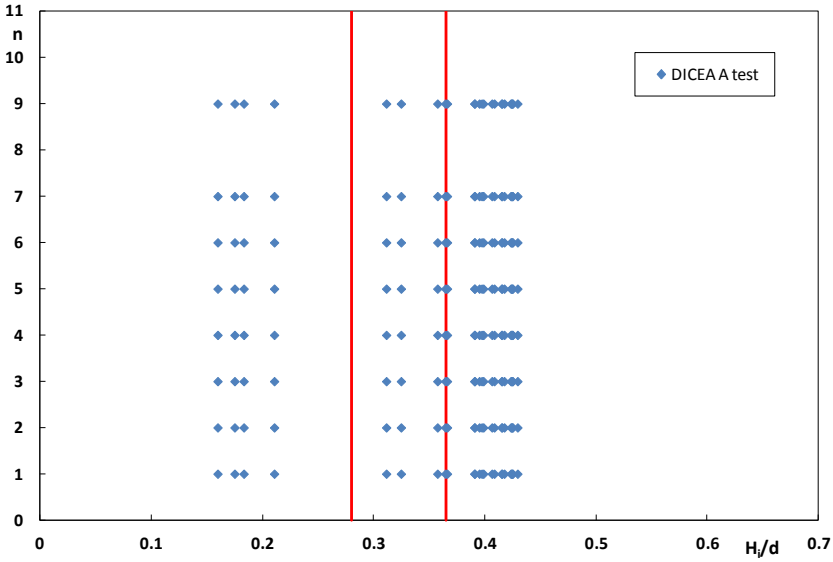

Figure 8.6.Comparison between breaking (red dots) and non-breaking (blue dots) tests for the *DICEA -A* configuration and for a submergence equal to 0 m.

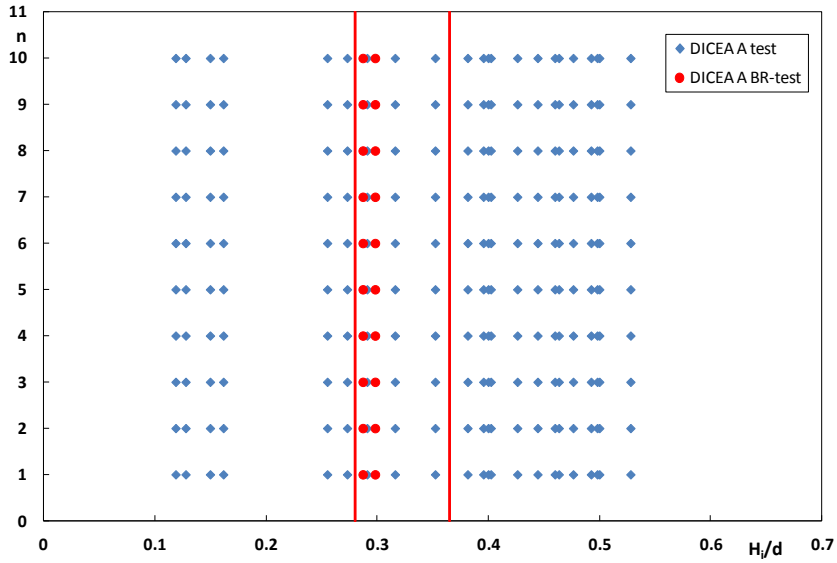

Figure 8.7. Comparison between breaking (red dots) and non-breaking (blue dots) tests for the *DICEA-A* configuration and for a submergence equal to 0.5 m.

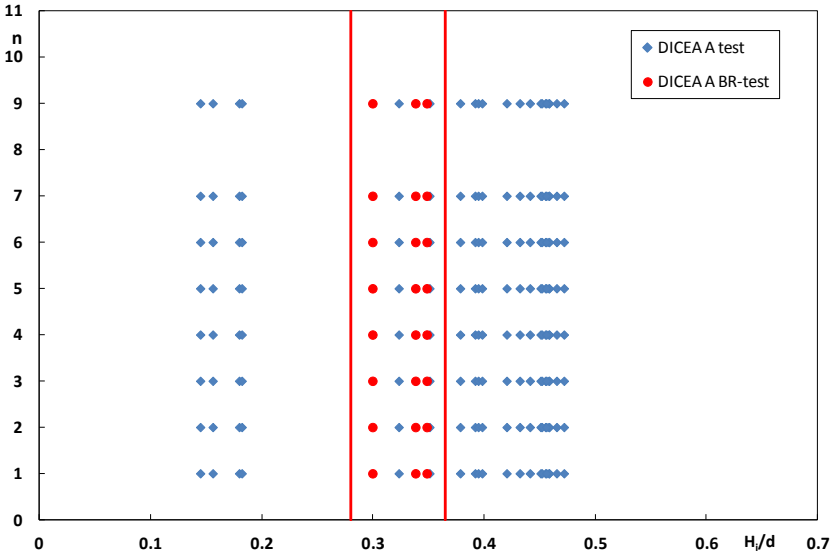

Figure 8.8.Comparison between breaking (red dots) and no-breaking (blue dots) tests for the *DICEA-A* configuration and for a submergence equal to 0.2 m.

Starting from the above considerations, the presence of Reef Balls seems to not able to systematically induce the wave breaking, but rather to destabilize waves shoaling in a condition of incipient breaking. In particular, RB structures are able to increase the breaking probability up to 95% for $0.28<H_i/d \leq 0.365$.
As a general result of the breaking analysis in the presence of RB modules, three main classes of breaking conditions can be distinguished:

- *non-breaking waves*, observed for $H_i/d \leq 0.28$;
- *slightly-breaking waves*, observed in the range $0.28<H_i/d \leq 0.365$;
- *hardly-breaking waves*, observed for $H_i/d > 0.365$.

This distinction will be employed in the following analyses of the transmission as different breaking condition are likely associated to different dissipation mechanisms and, therefore, K_T values.

8.2.1 Classification of breaking based on macroscopic features

A classification of breakers was conducted according to Calabrese et al. (2008), who distinguished different typologies of wave breaking occurring in the presence of traditional submerged breakwaters (see Sect 4.1.2). This classification is mainly based on the characterization of breaker shape, via visual analysis.
In the following, some figures deemed to be the most representative of the evolution of wave breaking on RB barriers are shown.
The condition of incipient breaking for structures made of one row of modules, has been identified by the rupture at the toe of the incident wave (Figure 8.9), according to a classical mechanism of “collapsing” breaking (Figure 4.18a).

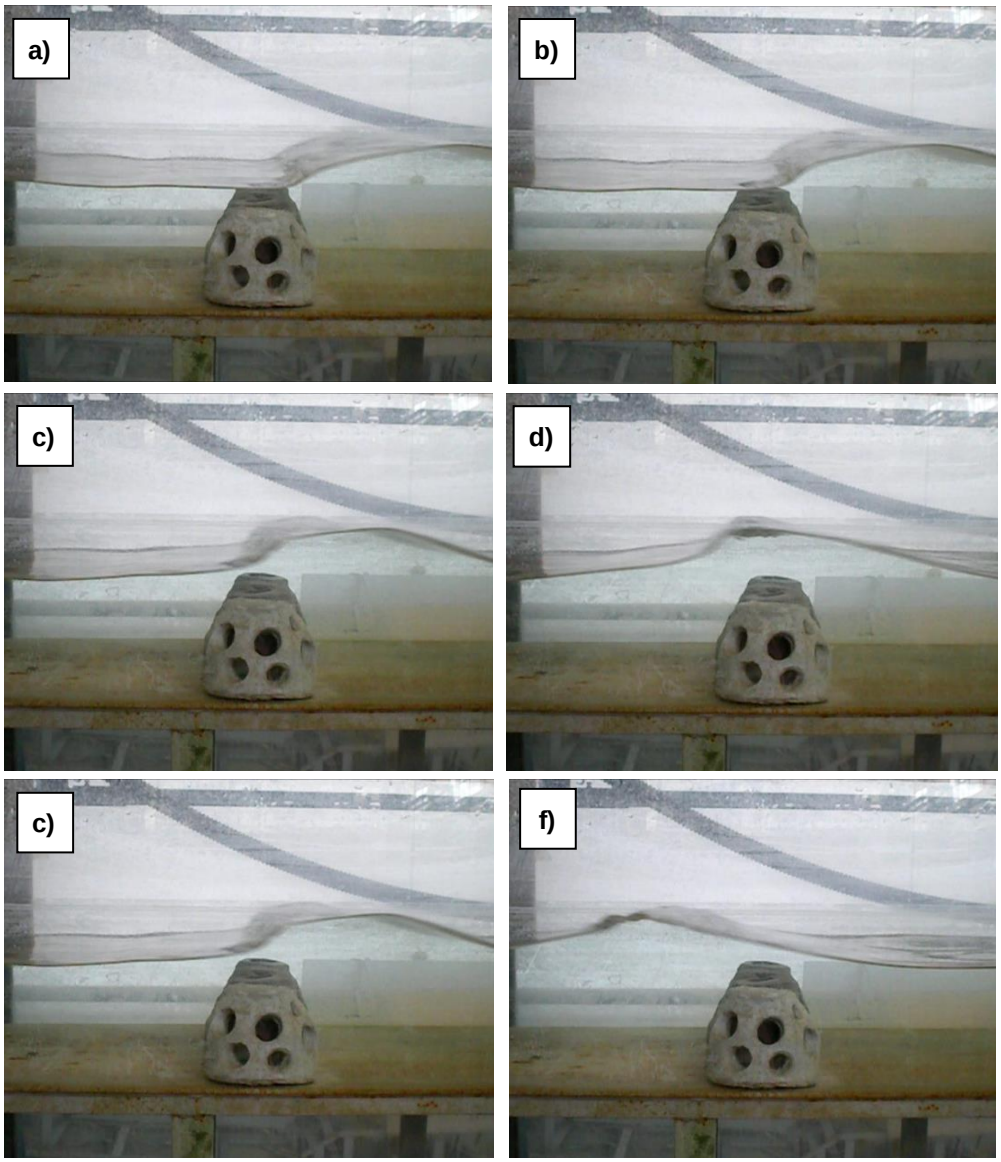

Figure 8.9. Example of collapsing breaker for structures made of 1 row (Rc= 0.5 m, f_p= 0.37 Hz and H_i= 0.9 m).

In particular, for Rc=0.5 m a gradual transition from a "collapsing" to a "collapsing – spilling-to-plunging" breaker was observed, moving from one-row structures to multiple-rows ones (Figure 8.10 and Figure 8.11). This is even more evident for wider structures (Figure 8.12 and Figure 8.13).

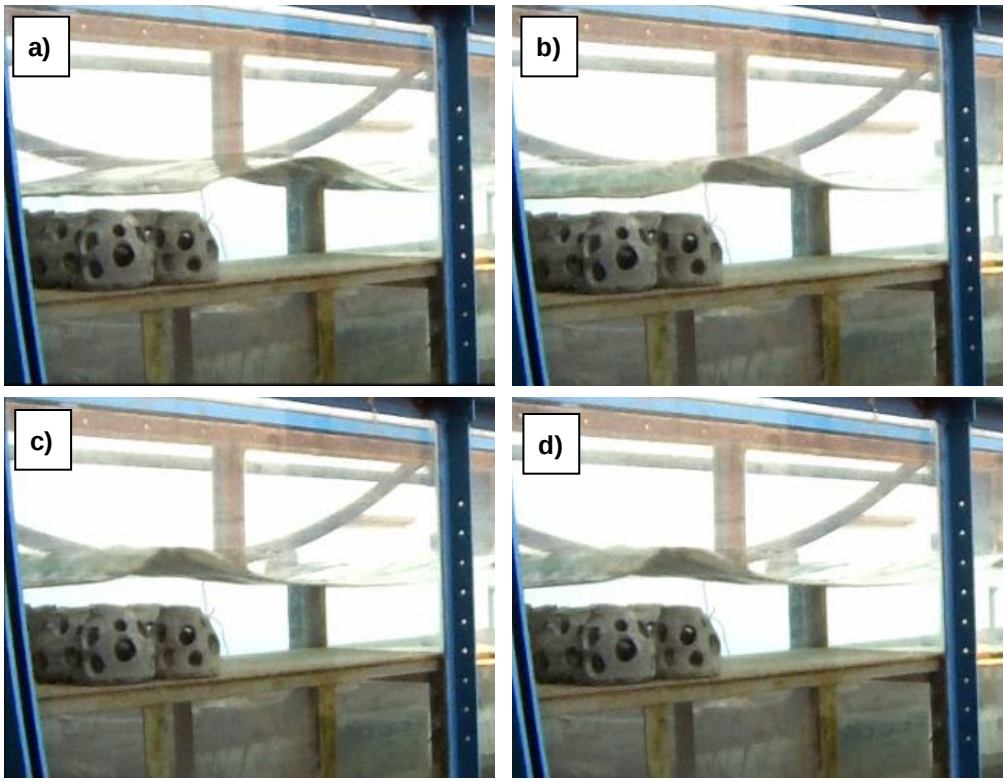

Figure 8.10. Example of a collapsing – spilling-to-plunging breaker for structures made of 2 rows (Rc= 0.5 m, f_p= 0.37 Hz and H_i= 0.9 m).

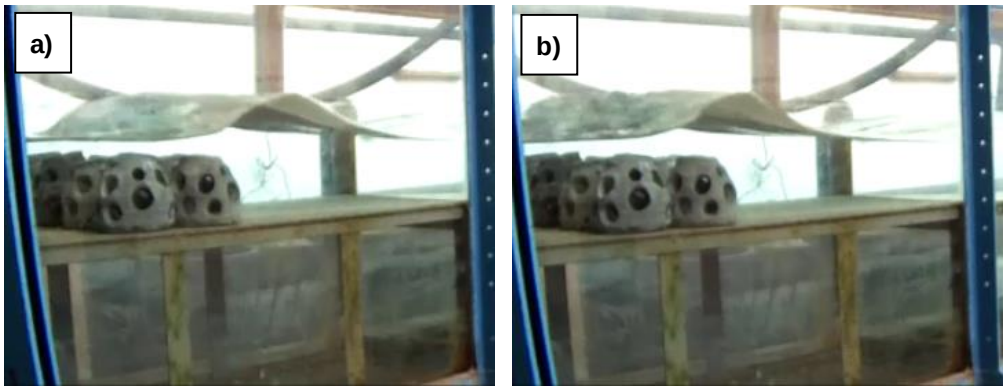

Figure 8.11.Example of a collapsing – spilling-to-plunging breaker for structures made of 2 rows (Rc= 0.5 m, f_p= 0.13 Hz and H_i= 0.6 m).

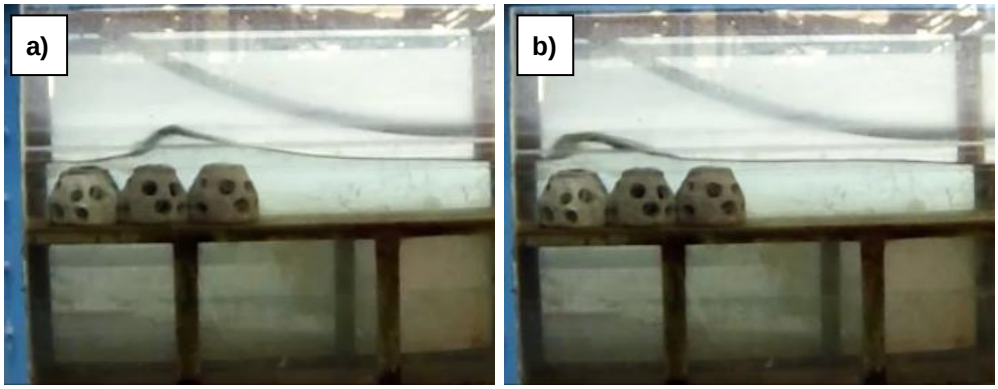

Figure 8.12. Plunging breaker for structures made of 3 rows (Rc= 0.5 m, f_p= 0.13 Hz and H_i= 0.6 m).

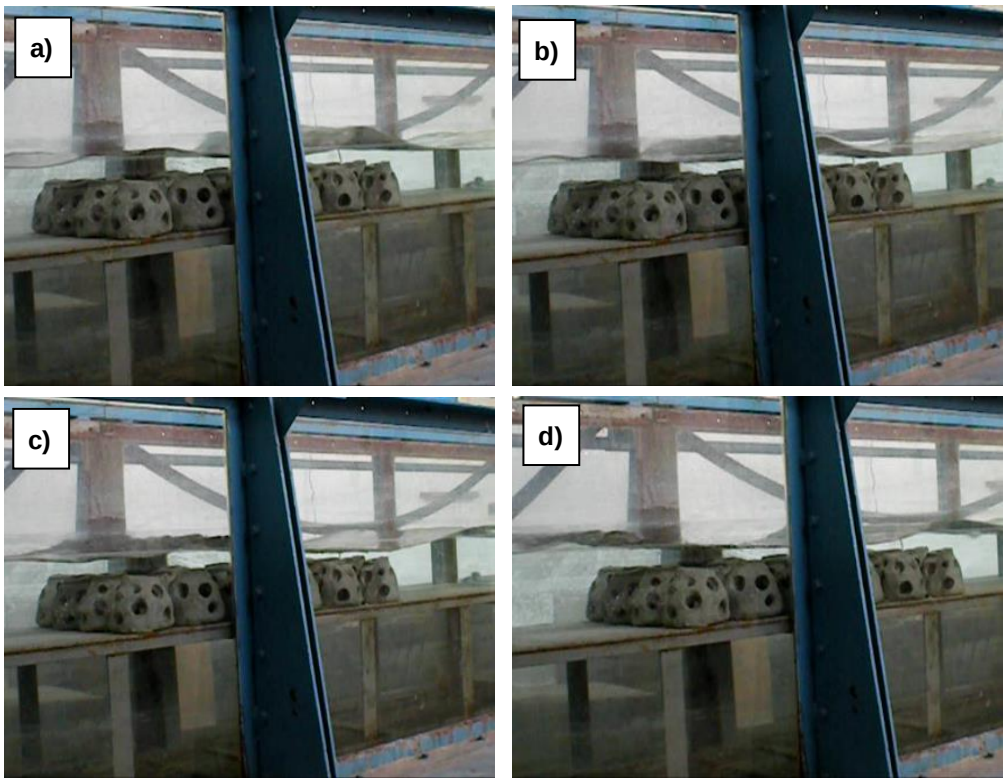

Figure 8.13. Evolution of a plunging breaker for structures made of 6 rows (Rc= 0.5 m, f_p= 0.37 Hz and H_i= 0.9 m).

On the contrary, in case of Rc= 0.2 m, wave breaking generally occurred according to a "collapsing" breaker, for structures composed by 2 rows (Figure 8.14). This typology generally turned into a "spilling-to-plunging" breaker (Figure 4.15) starting from structures composed by 3 rows; although collapsing was still observed for wider barriers, as it is possible to observe in Figure 8.16.

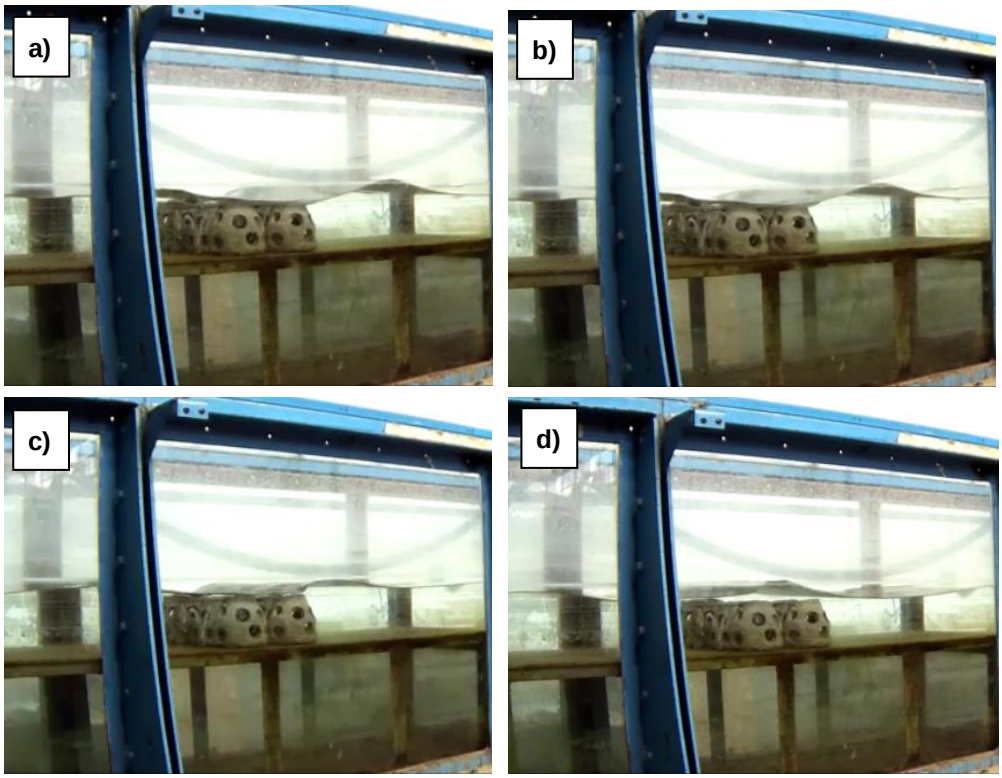

Figure 8.14. Example of evolution of a collapsing breaker for Rc= 0.2 m, f_p= 0.37 Hz and H_i= 0.6 m.

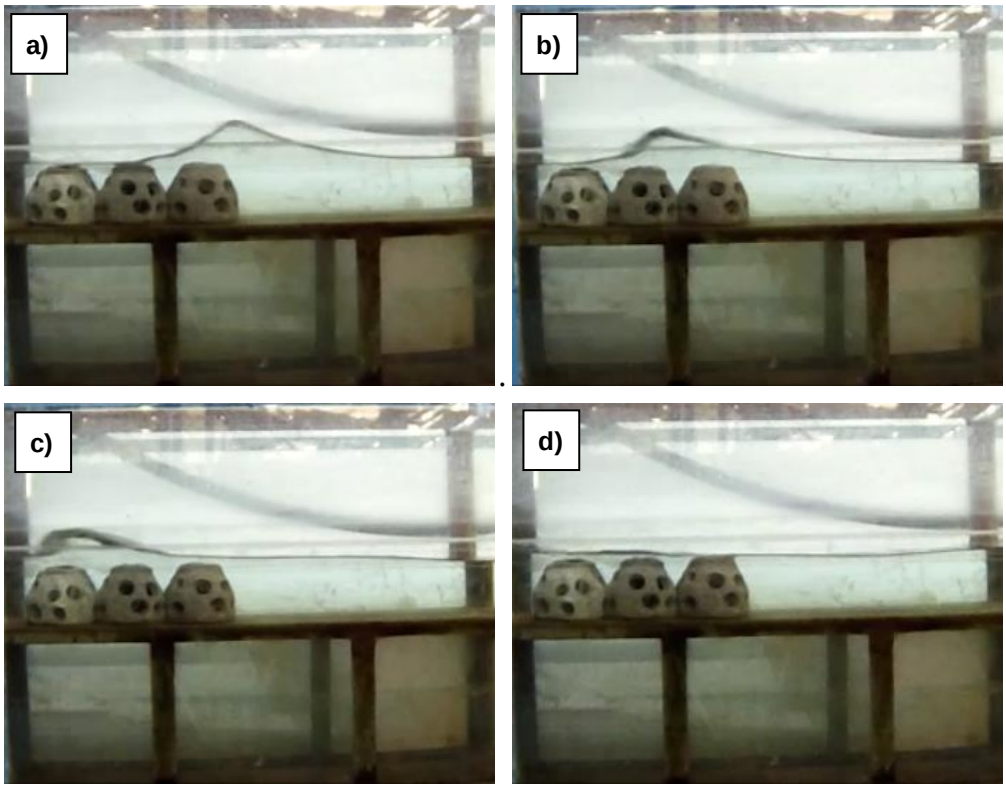

Figure 8.15.Example of evolution of a spilling-to-plunging breaker for Rc= 0.2 m, f_p= 0.17 Hz and H_i= 0.6 m.

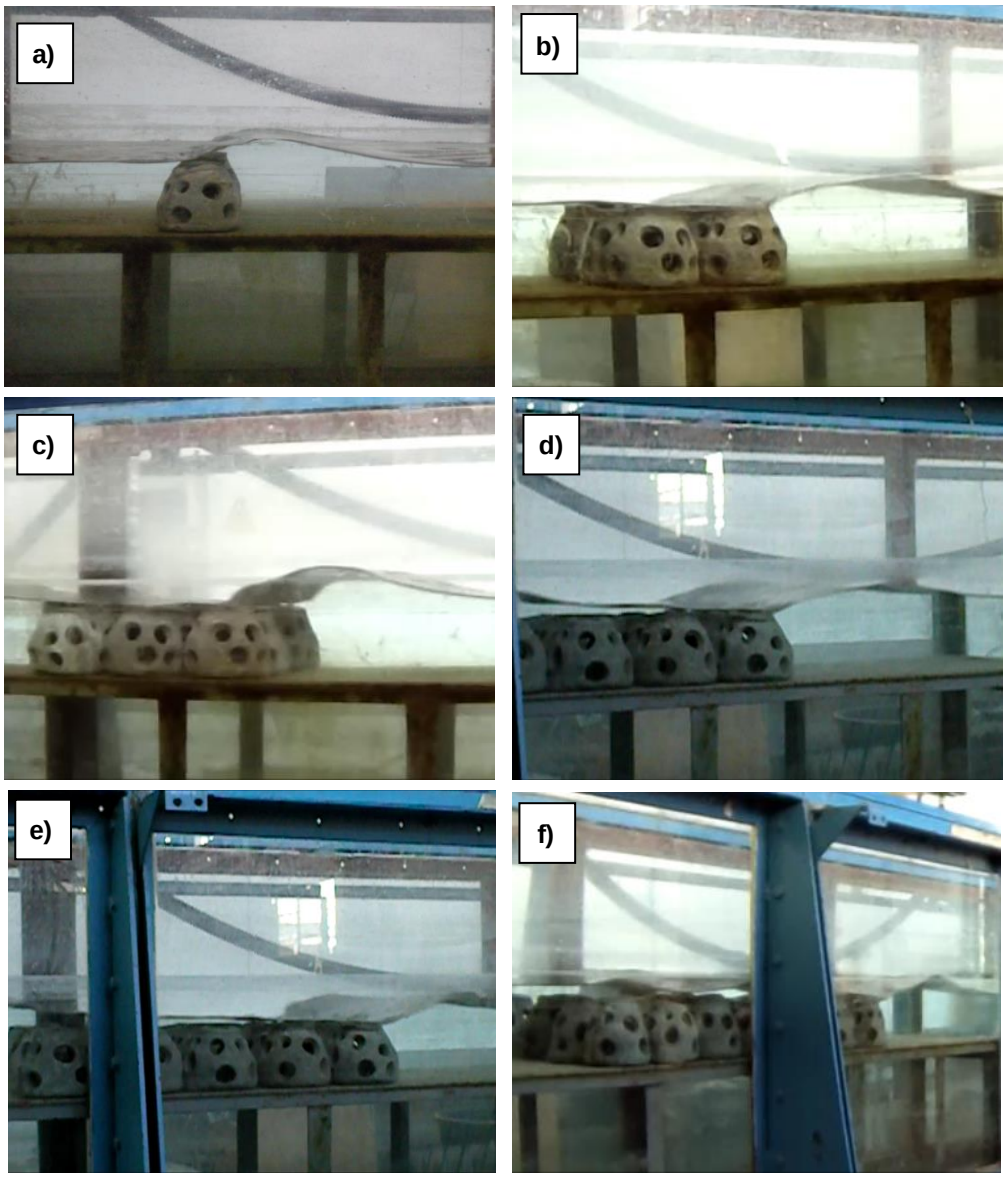

Figure 8.16. Collapsing breaker for structures with a number of rows variable between 1 to 7; (Rc= 0.2 m, f_p= 0.37 Hz and H_i= 0.9 m).

Chapter 9 – ANALYSIS OF THE WAVE TRANSMISSION FOR THE *DICEA* TESTS

This Chapter deals with the application of existing and new methods to the results of the *DICEA* experimental campaign, for the prediction of the rate of wave energy transmitted in the lee of submerged barriers composed of Reef Ball modules.
In the following Sections, criteria for the definition of a suitable transmission coefficient and for the applicability of a predictive model will be given first. Subsequently, the results of the random wave experiments described in Chapter 7 will be analysed via literature predictive models, suited for Reef Ball barriers; finally new models will be proposed and analysed.

9.1 The measure of the transmission coefficient

It is worth recalling that the rate of energy dissipation is usually measured via the so-called transmission coefficient, K_T, which equals the root square of the transmitted to incident wave energy ratio:

$$K_T = \sqrt{\frac{E_T}{E_I}} = \sqrt{\frac{m_{0,t}}{m_{0,i}}} \tag{9.1}$$

where m_0 represents the zero order spectral moment and the suffixes i and t stand for "incident" and "transmitted", respectively.
K_T can also be defined as the ratio between the spectral significant wave height rear the structure and that just seaward of it (Eq. 9.2).

$$K_T = \frac{H_{m0,t}}{H_{m0,i}} \tag{9.2}$$

In both the experiments conducted at the *DICEA* and *ERDC/CHL*, the transmission coefficient has been calculated according to Equation (9.2), as the ratio between the significant spectral wave height leeward the structure, and the wave height measured at the same position, without the structure in place. For brevity, $H_{m0,t}$ and $H_{m0,i}$ have been, in the following, referred to as H_T and H_i.
This method allows assessing the real effectiveness of the barrier in damping the wave motion, especially in the surf zone, where the "natural" transmission coefficient, $K_{T,n}$, (i.e. without the structure) between "in front" and "at rear" is less than one (Figure 9.1):

$$K_{T,n} = \frac{H_{rear}}{H_{front}} \tag{9.3}$$

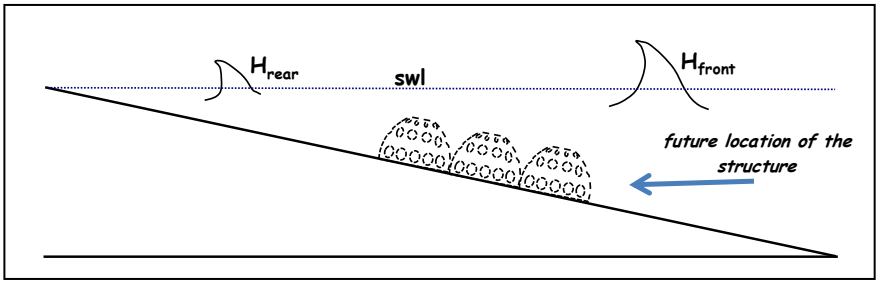

Figure 9.1. Natural transmission coefficient, $K_{T,n}$.

It is then obvious that

$$K_T = \frac{H_{with}}{H_{without}} = \frac{H_{with}}{K_{T,n}H_{front}} = \frac{K_{T,c}}{K_{T,n}} \tag{9.4}$$

where $K_{T,c}$ is the transmission coefficient, as usually calculated. It follows that, if $K_{T,n} \cong 1$ (i.e. no natural dissipation occurs between in front and at rear), then $K_T \cong K_{T,c}$; whereas, if $K_{T,n} < 1$ (e.g. within a surf zone, or due to frictional effects for a very long structure), then $K_T > K_{T,c}$.
The values of K_T calculated at each probe have been averaged to obtain a single value, representative of a given test.

9.2 On the accuracy of a predictive model

When comparing a predictive model with experimental data, the question arises as to the produced estimates are accurate enough. This depends, of course, on the specific variable under consideration, e.g. the reflection coefficient, the rate of overtopping, the wave run-up, etc.

As for the transmission coefficient, a conventional threshold of accurateness may be established, based on the results of the former analyses conducted on a great deal of data with conventional breakwaters. In this respect, the Standard Error (*SE*) between predictions and measures can be used, defined as follows:

$$SE = \sqrt{\frac{\sum_{i=1}^{n}(e_i - \overline{e_i})^2}{N}} \tag{9.5}$$

where e_i indicates the difference between the measured and the predicted values of the output variable (residual), $\overline{e_i}$ represents the average of the residuals (or bias) and N is the number of observations.

As mentioned in Section (4.2), the first systematic analysis on wave transmission at rubble mound breakwaters was conducted by d'Angremond et al. (1996). The Authors proposed a formula, based on 328 data, which produced a *SE* of 0.060. Lately, Seabrook and Hall (1998) performed a multiple regression analysis on nearly 670 results of experiments conducted at *QUCERL* and their predictive equation had *SE*=0.063.

Among the most recent studies, Van der Meer et al. (2005) modified the d'Angremond et al. (1996) formula and obtained a *SE* =0.074, with respect to a wide database of nearly 2,000 points. Furthermore, the Conceptual Approach by Buccino and Calabrese (2007 a) yielded to $SE \cong 0.05$ on a 1,000 experiments dataset.

From the previous review, one may conclude that a reasonable threshold for the accurateness of a prediction model for the transmission coefficient is of the order of 0.06.

It is useful to highlight that if the residuals were randomly distributed and the model was undistorted ($\overline{e_i}$ =0) then *SE* =0.06 would imply that 90% of the measurements would be included in a band of amplitude ±0.1 around the

predictions. As shown in Figures from 9.2 to 9.4, this is approximately verified for Seabrook and Hall (1998), Van der Meer et al. (2005) and Buccino and Calabrese (2007 a).

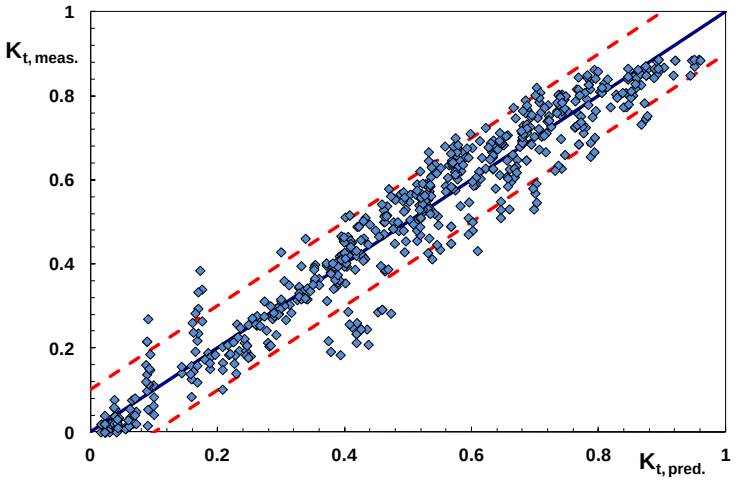

Figure 9.2. Comparison between measured and predicted transmission coefficient according to Seabrook and Hall (1997) and 90% confidence bounds (dotted lines) .

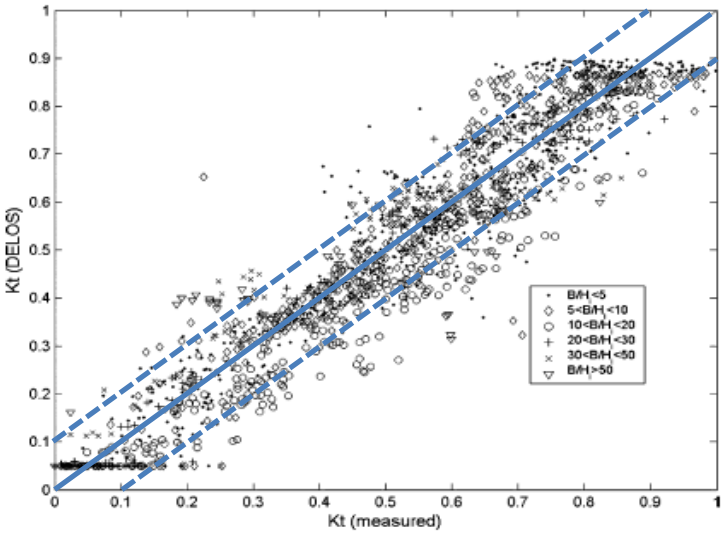

Figure 9.3. Comparison between measured and predicted transmission coefficient according to Van der Meer (2005) and 90% confidence bounds (dotted lines).

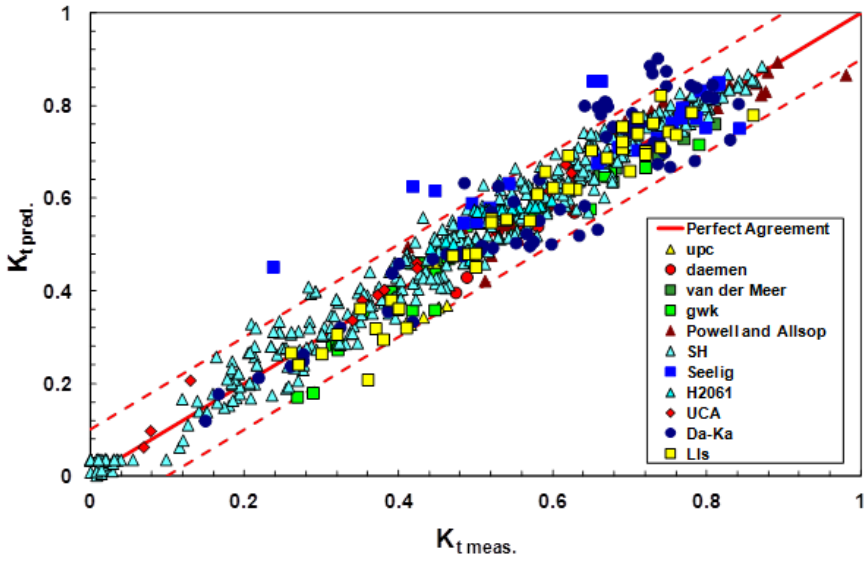

Figure 9.4. Comparison between measured and predicted transmission coefficient for submerged structures according to Buccino and Calabrese (2007a) and 90% confidence bounds (dotted lines).

It is interest to discuss that, to test the accurateness of a prediction model, the *SE* seems to be more appropriate than the determination index, R^2. The latter is, in fact, defined as:

$$R^2 = 1 - \frac{SE^2}{S^2} \tag{9.6}$$

in which S^2 is the total variance of measurements (i.e. the variance of the measured transmission coefficients).

It follows that, for a given standard error, the higher S^2, the higher R^2. In the case of Reef Balls, the values of the transmission coefficient are generally higher than conventional rubble mound breakwaters, due to their larger permeability. Thus, the variance of data is far lower than ordinary structures and consequently lower values of R^2 are expected. Figures from 9.5 to 9.7 show K_T for the *DICEA* data, against the number of rows, *n*. It is found that 95% of the points is included in the range of 0.5÷1 for the *DICEA-A* and *DICEA-C* configurations, whilst the range is 0.65÷1 for *DICEA-B*.

Conversely, the 95% range is 0.02÷0.89 for the Seabrook and Hall (1998) data and 0.08÷0.95 for Buccino and Calabrese (2007 a), referred to submerged structures only. As a consequence, the values of S^2 reported in Table 9.1 have been obtained.

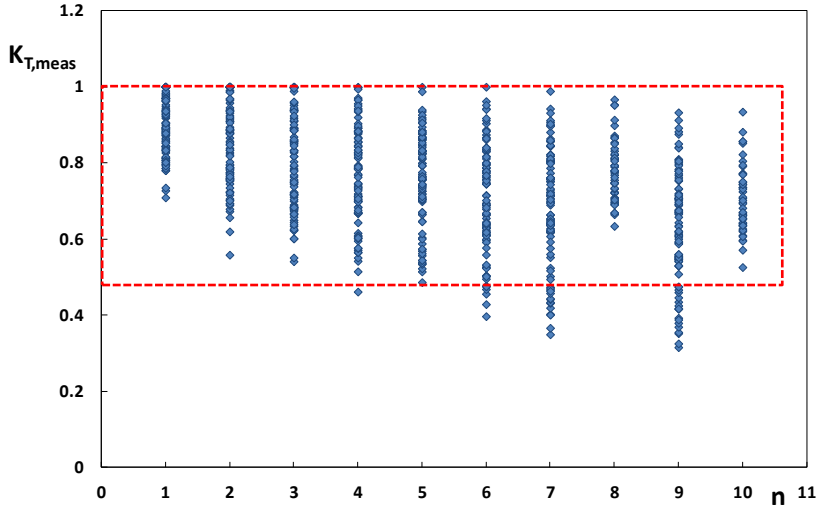

Figure 9.5. Measured transmission coefficient vs. number of rows, for the *DICEA-A* configuration.

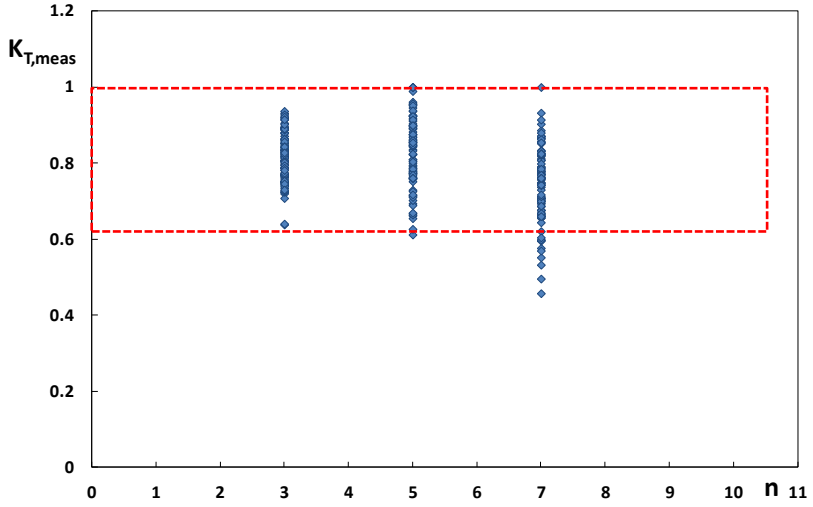

Figure 9.6.Measured transmission coefficient vs. number of rows for the *DICEA-B* configuration.

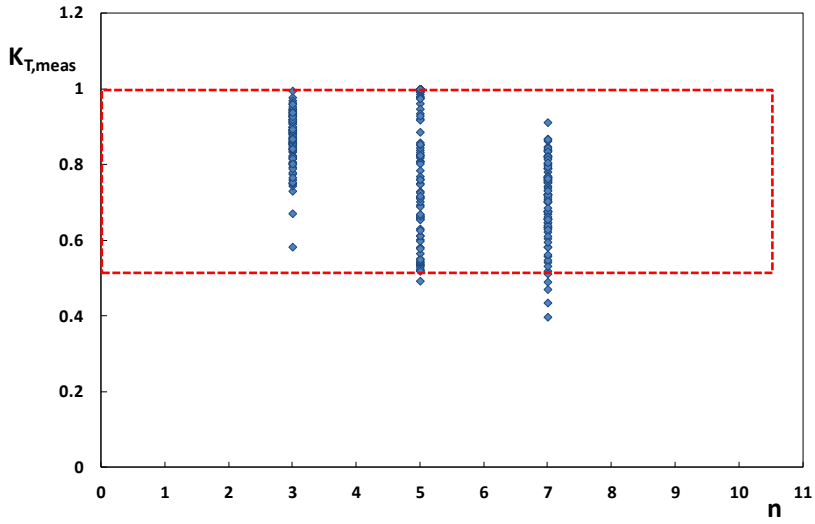

Figure 9.7.Measured transmission coefficient vs. number of rows for the *DICEA-C* configuration.

Studies		S^2	# data
Seabrook and Hall (1998)		0.063	633
Buccino and Calabrese (2007 a)		0.047	1,000
DICEA	DICEA-A	0.021	864
	DICEA-B	0.009	288
	DICEA-C	0.019	288

Table 9.1. S^2 values and number of observations for Seabrook and Hall (1997), Buccino and Calabrese (2007 a) and *DICEA* experimental campaign.

It is seen that the variance of the *DICEA-A* data is 1/3 of that from Seabrook and Hall and 1/2 of that from Buccino and Calabrese, which have a R^2 statistic of 0.93 and 0.96, respectively.

Another relevant issue in computing the determination index is related to the so-called "influential points", which are measurements rather far from the bulk of observations, that lead to an unrealistic increase in R^2. As an example, in Table 9.2 the case of a model returning a constant value for most of the

predictions and only two points far from the bulk of data is given. As shown in Figure 9.8, a linear regression on these data would lead to R^2 =0.95, which is very high notwithstanding the poor overall fitting .

Measured	Predicted
0.5	5
1	5
1.5	5
….	…
10	5
45	44
60	51

Table 9.2. Example of a model giving two predictions far from the bulk of data.

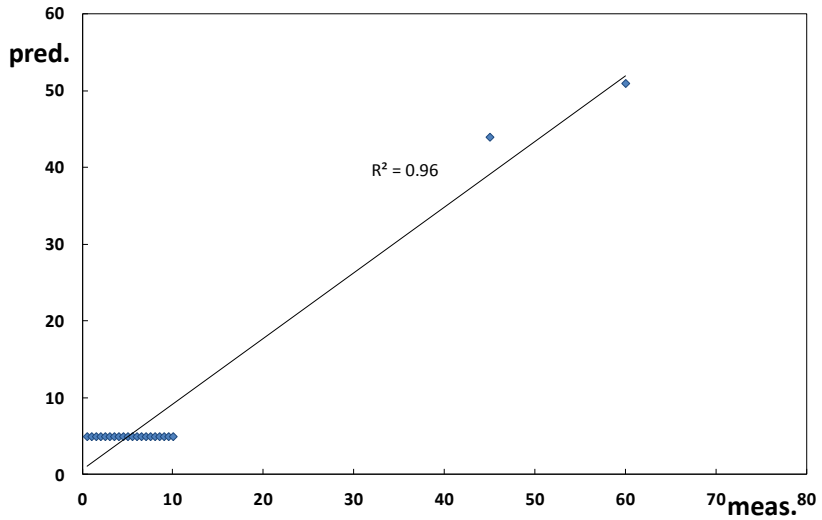

Figure 9.8. Linear regression of data reported in Table 9.2.

9.3 Application of existing models to the DICEA data

In this Section, the application of existing models developed for Reef Balls, namely Armono (2003) and Buccino et al. (2014), to the *DICEA* experimental data is presented, along with a calibration of their parameters.

More specifically, the two existing models have been firstly applied to the *DICEA* dataset only and, subsequently, compared to the *ERDC/CHL* data.
To perform such a comparison it is necessary to introduce a configuration density, φ, allowing to discriminate among the different placements of RB units. The latter is calculated as follows:

$$\varphi = \frac{n_r}{n_t} \tag{9.7}$$

where n_r is the "real" number of RB modules employed and n_t is the "theoretical" one. The latter is defined as the ratio between the area of the rectangle inscribing the configuration, A_{rect}, and the base area of one RB module, A_{RB} (Figure 9.9).

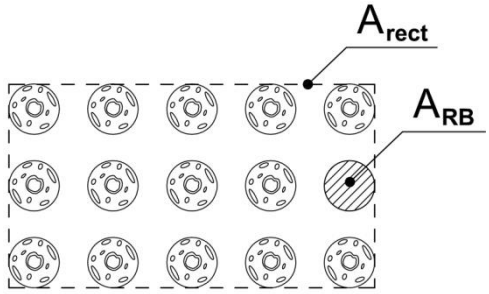

Figure 9.9. Example of density computation

The abovementioned densities have been subsequently averaged ($\bar{\varphi}$) for each configuration (Table 9.3).
It might be useful to remark that the *DICEA* tests represent the sole ensemble of data systematically collected on Reef Ball units, composed of 1,440 data. In fact, as already mentioned, the Armono's (2003) work focused on uncommon configurations (modules placed on the top of each other), which can be hardly compared to the *DICEA* data, whilst the *ERDC/CHL* campaign only included 64 experiments. Furthermore 24 out of these 64 tests were characterized by H_i/d =0.83 which was considered to be far high for irregular waves on mild foreshores. It is in fact likely that such a value includes infragravity waves, which have been not addressed in this Study. For this reason the comparison with *ERDC/CHL* has been performed considering only 40 data. This suggests

that a validation of the *DICEA* tests should be performed against future experimental campaigns.

Laboratory	Configurations	$\bar{\varphi}$
ERDC/CHL	BS-1a	0.54
	BS-1b	0.35
	BS-1c	0.44
	BS-1d	0.31
	BS-1e	0.80
	BS-1f	0.26
DICEA	DICEA-A	0.79
	DICEA-B	0.55
	DICEA-C	0.41

Table 9.3. Average density for each configuration,.

9.3.1 Application of the Armono (2003) formula to the DICEA dataset

As already mentioned in Section (5), Armono (2003) proposed the following approach for the prediction of K_T:

$$K_T = \frac{1}{1 + A_0 \left(\frac{H_{si}}{gT_p^{\,2}}\right)^{0.901} \left(\frac{B_{bR}}{gT_p^{\,2}}\right)^{-0.413} \left(\frac{h_s}{B_{bR}}\right)^{-1.013} \left(\frac{h_s}{d}\right)^{4.392}} \tag{5.1}$$

in which A_0 is a scale parameter depending on the layout and arrangement of modules. The Author found that Equation (5.1) provides good estimates for multi-layered configurations, with values of A_0 of the order of 10. Conversely, a significant spread around the prediction curve was observed by Buccino et al. (2014) for the 64 *ERDC/CHL* experiments, where Reef Balls were arranged in single-layered layouts.

For this reason it seems worth to investigate the applicability of the Armono's model to the *DICEA* dataset, which is composed of about 1,440 tests performed on single-layered structures.

As already discussed in Section (6), the most immediate way to check the validity of Equation (5.1) is to plot the experimental data in a plane of transformed variables, reported below for the Reader's convenience.

$$Y = \frac{1}{K_T} \tag{6.2}$$

$$X = \left(\frac{H_{si}}{gT_p{}^2}\right)^{0.901} \left(\frac{B_{bR}}{gT_p{}^2}\right)^{-0.413} \left(\frac{h_s}{B_{bR}}\right)^{-1.013} \left(\frac{h_s}{d}\right)^{4.392} \tag{6.3}$$

In such a plane, the points should draw a straight line passing through one and with an A_0 slope.

Figures from 9.10 to 9.12 display the *DICEA-A* data series on the aforementioned plane, respectively for all the data, for $H_i/d \leq 0.28$ (i.e. non breaking waves) and for $H_i/d > 0.28$ (i.e. breaking waves). Figures from 9.13 to 9.18 report the same information for *DICEA-B* and *DICEA-C* configurations.

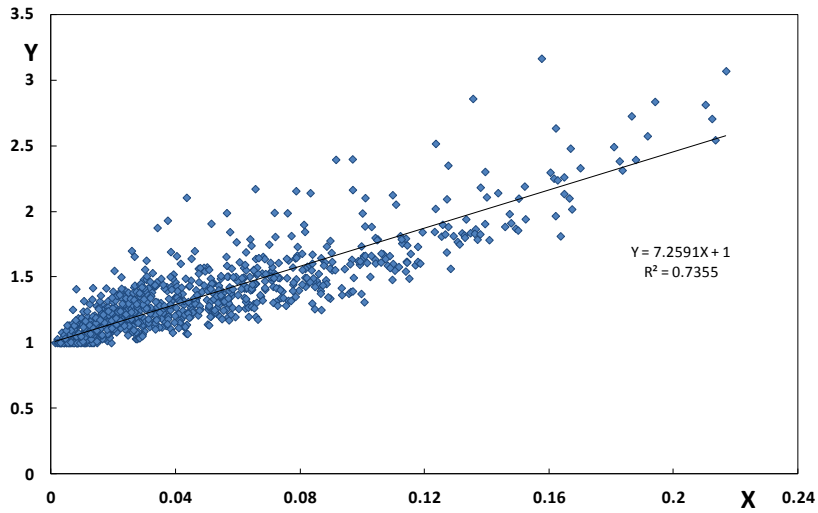

Figure 9.10. Plot of the *DICEA-A* data in the plane of transformed variables (Eqs. 6.2-6.3).

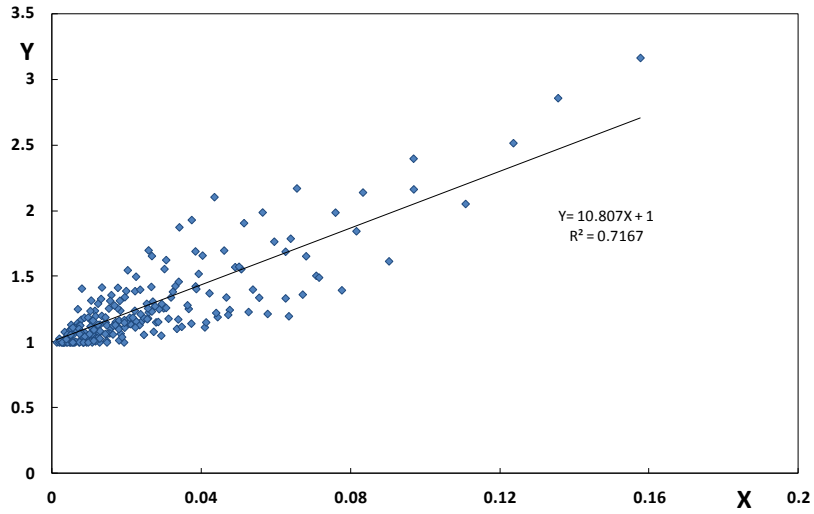

Figure 9.11. Plot of the *DICEA-A* data with $H_i/d \leq 0.28$ in the plane of transformed variables (Eqs. 6.2-6.3).

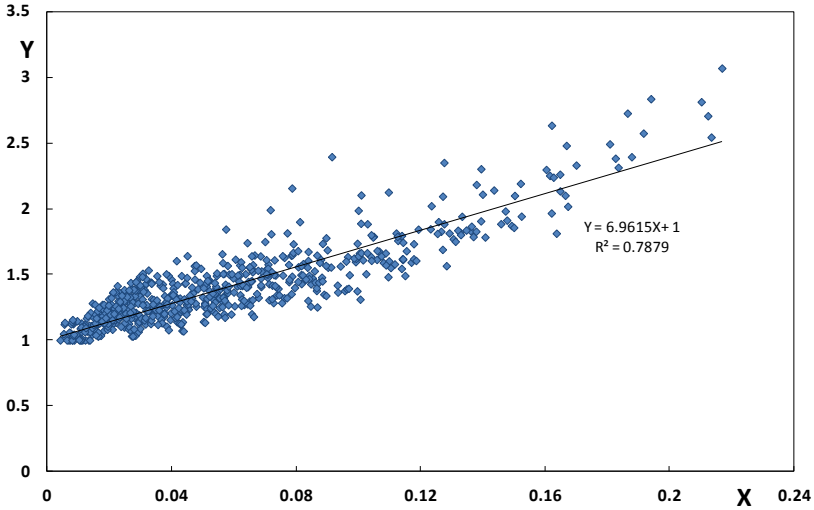

Figure 9.12. Plot of the *DICEA-A* data with $H_i/d > 0.28$ in the plane of transformed variables (Eqs. 6.2-6.3).

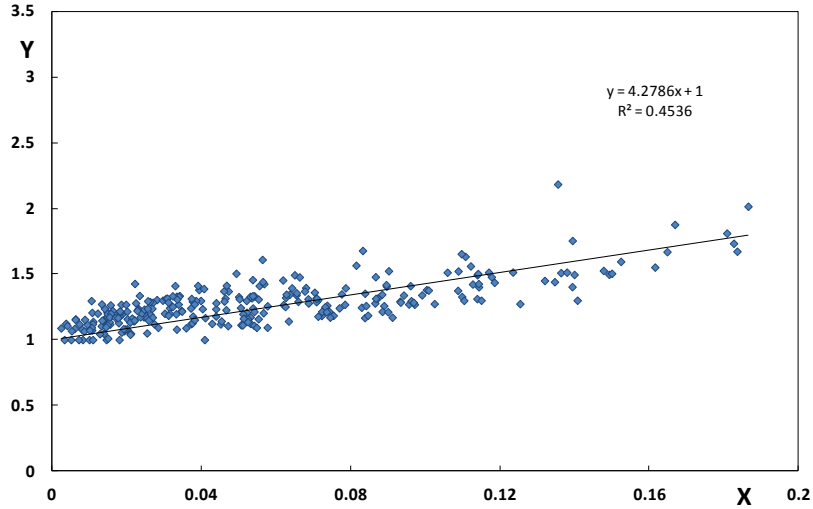

Figure 9.13. Plot of the *DICEA-B* data in the plane of transformed variables (Eqs. 6.2-6.3).

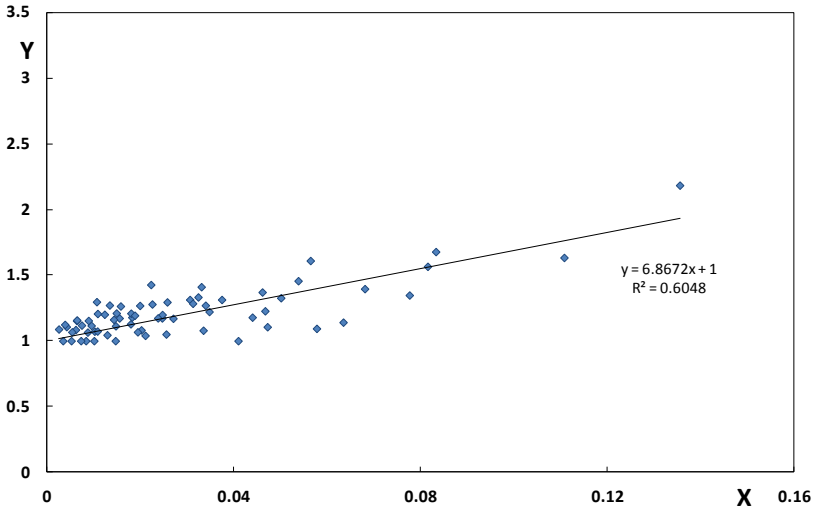

Figure 9.14. Plot of the *DICEA-B* data with $H_i/d \leq$ 0.28in the plane of transformed variables (Eqs. 6.2-6.3).

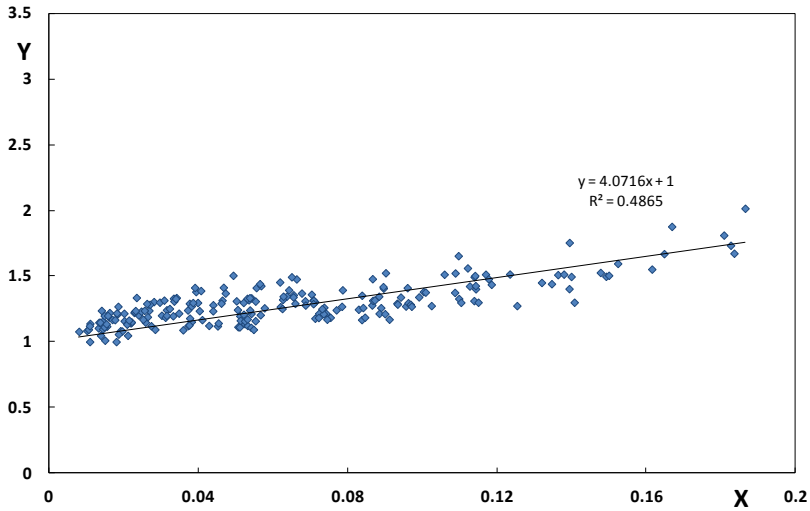

Figure 9.15. Plot of the *DICEA-B* data with H_i/d>0.28 in the plane of transformed variables (Eqs. 6.2-6.3).

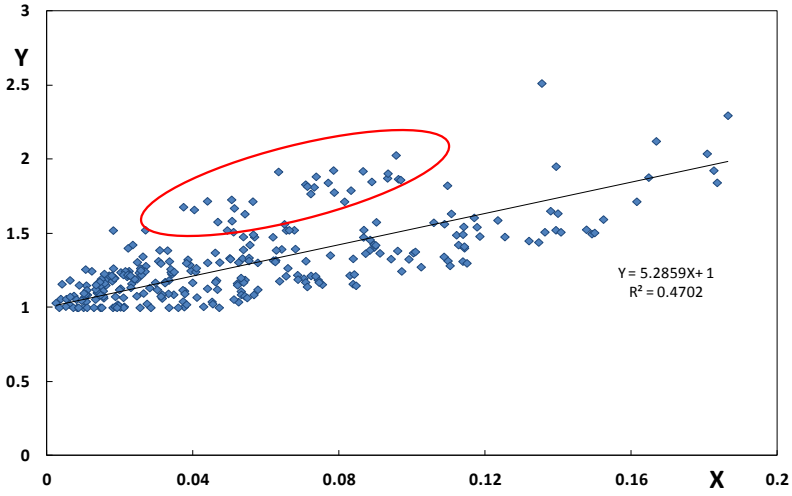

Figure 9.16. Plot of the *DICEA-C* data in the plane of transformed variables (Eqs. 6.2-6.3).

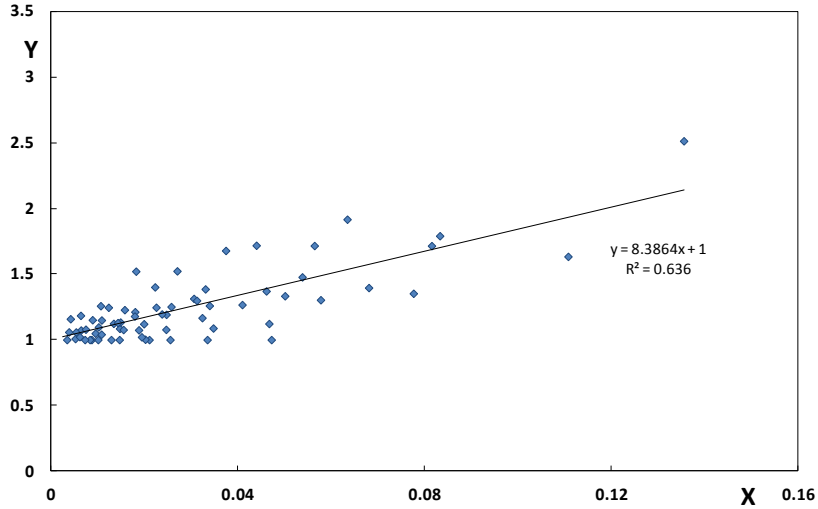

Figure 9.17. Plot of the *DICEA-C* data with $H_i/d \leq 0.28$ in the plane of transformed variables (Eqs. 6.2-6.3).

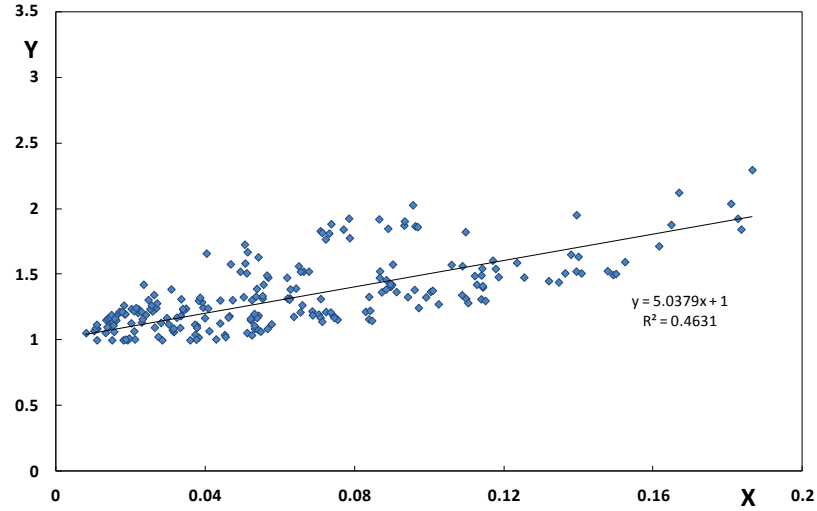

Figure 9.18. Plot of the *DICEA-C* data with $H_i/d > 0.28$ in the plane of transformed variables (Eqs. 6.2-6.3).

After fitting the straight lines forced to 1, the values of A_0 reported in Table 9.4 have been obtained. In the same Table, the statistical characteristics, R^2 and *SE*, are reported, as obtained from the comparison of the measured and predicted transmission coefficient.

Configurations	H_i/d	#data	A_0	R^2	SE
DICEA-A	All	864	7.26	0.73	0.076
	≤0.28	214	10.81	0.66	0.088
	>0.28	650	6.96	0.75	0.069
DICEA-B	All	288	4.28	0.56	0.073
	≤0.28	69	6.87	0.47	0.081
	>0.28	219	4.07	0.57	0.067
DICEA-C	All	288	5.29	0.51	0.099
	≤0.28	69	8.39	0.56	0.095
	>0.28	219	5.04	0.49	0.097

Table 9.4. Summary of results for each configuration investigated.

The inspection of Table 9.4 suggests that:

- the standard errors are all larger than 0.06, indicating an unsatisfactory degree of accurateness, according to what discussed in Section (9.2);
- the *DICEA-C* configuration exhibits a larger scatter compared to that of *-A* and *-B*;
- the model seems more effective for breaking waves (H_i/d >0.28) than non-breaking ones (H_i/d ≤0.28);

The Table also shows that A_0 coefficients for the *DICEA-A* are larger than the corresponding ones for *-B* and *-C*. This is obviously due to the fact that a most scattered arrangement of modules leads to a reduction in the dissipation. However, the values for *DICEA-C* appear slightly larger than those characterizing *-B*. This unexpected, and possibly fortuitous, result deserves to be deepened through supplementary data analyses.

Figure 9.16 highlights the presence of possible outliers (circled in red), which correspond to the experiments performed with n =5 and Rc =0.2 m. When these data are removed, the scatter plot on the *X-Y* plane suggests that the response of the configuration *-B* and *-C* are quite similar each other (Figure 9.19).

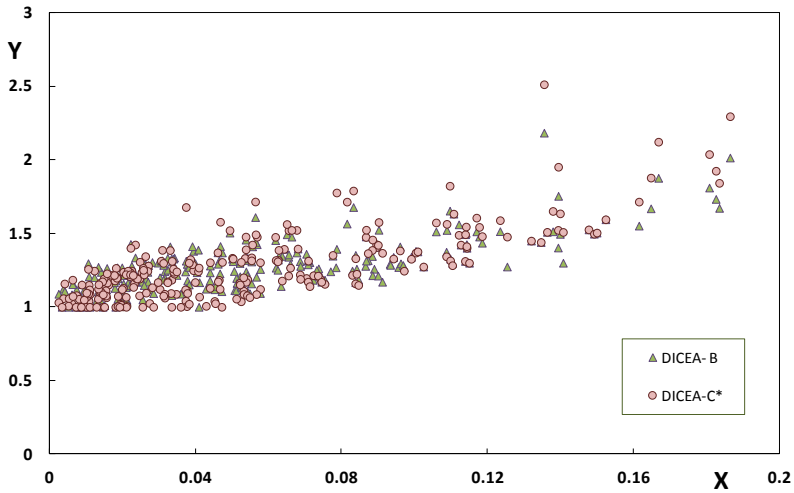

Figure 9.19. Plot of the *DICEA-C** (without outliers) and *DICEA-B* data in the plane of transformed variables (Eqs. 6.2-6.3).

9.3.1.1 Comparison with ERCD/CHL data

As a matter of fact, *ERCD/CHL* data are very few compared to those of the *DICEA* campaign and this practically limits the significance of the comparison reported below.

The density of the *ERCD/CHL* arrangements (Table 9.3) is such that the configurations *BS-1a* and *BS-1c* have values of $\bar{\varphi}$ respectively close to the *DICEA-B* and the *DICEA-C*, whereas *BS-1e* (crossed rows with no-distance) is similar to *DICEA-A*. On the other hand, the densities of *BS-1b* and *BS-1d* are slightly less than that of *DICEA-C*, while *BS-1f* has a minimum density $\bar{\varphi}$ =0.26. The fundamental difference between *BS-1a* and *DICEA-B* is that in the former case the rows are "crossed", leading to a lower distance along the wave direction (0.22 cm, vs. 0.5 cm in *DICEA-B*). Conversely, in case of *BS-1b*, the analogy with *DICEA-C* data is more stringent, as the rows are aligned in both the cases. Figure 9.20 shows the results obtained for *BS-1e* data together with *DICEA-A* ones. Figure 9.21 and Figure 9.22 plot *BS-1a* vs. *DICEA-A* and vs. *DICEA-B*, respectively. Figure 9.23 shows *BS-1c* vs. *DICEA-C*.

Figures from 9.24 to 9.26 display the low density data, *BS-1b*, *BS-1d* and *BS-1f*, vs. *DICEA-C*. It is useful to remark that all the *ERDC/CHL* data have H_i/d larger than 0.28.

The inspection of the graphs suggests that the *ERDC/CHL* data are generally located upwards the *DICEA* ones which corresponds to a dissipation associated to the former case larger than that observed for the latter. An exception to the above is represented by *BS-1f*, nevertheless it should be considered that only two data are available, besides characterized by the lowest density value.

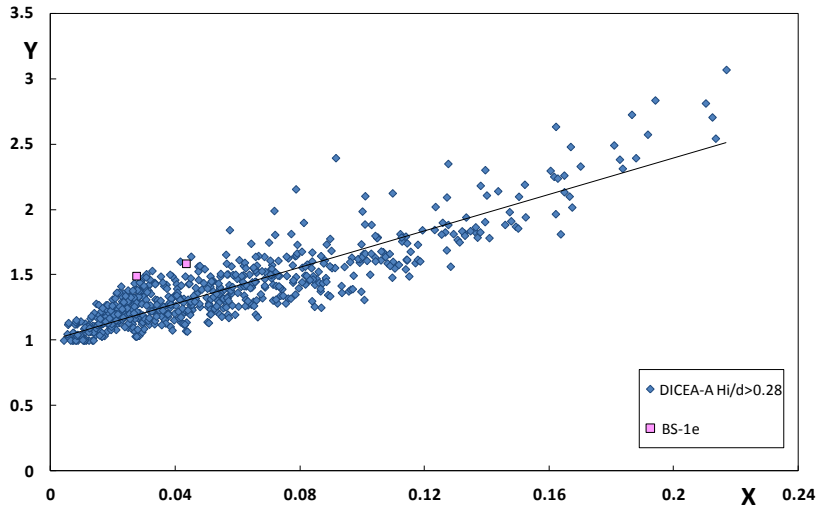

Figure 9.20. Plot of the *DICEA-A* and *BS-1e* in the plane of transformed variables (Eqs. 6.2-6.3).

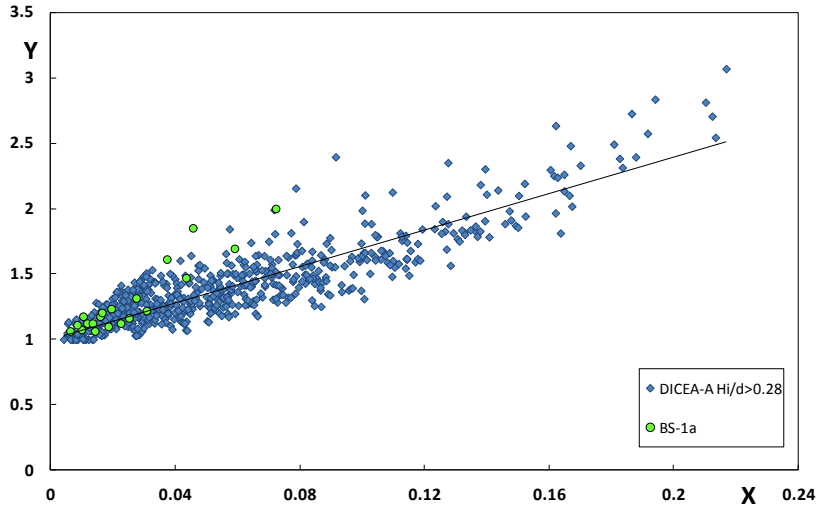

Figure 9.21. Plot of the *DICEA-A* and *BS-1a* in the plane of transformed variables (Eqs. 6.2-6.3)

.

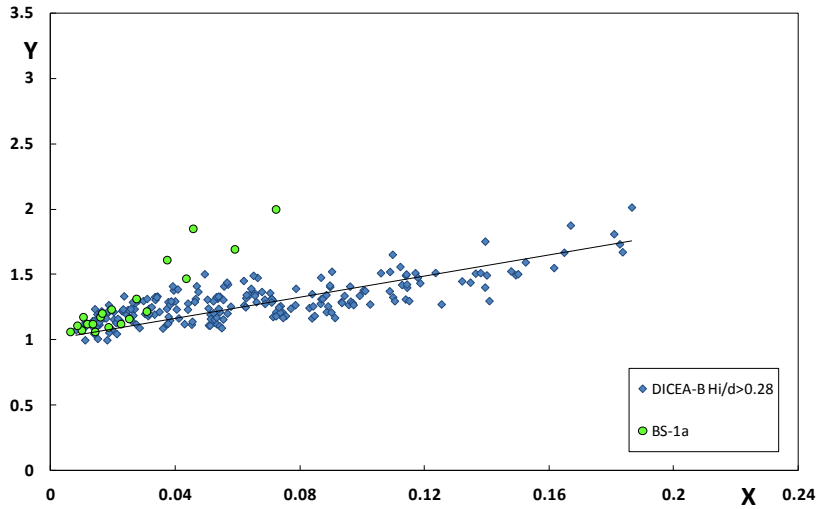

Figure 9.22. Plot of the *DICEA-B* and *BS-1a* in the plane of transformed variables (Eqs. 6.2-6.3).

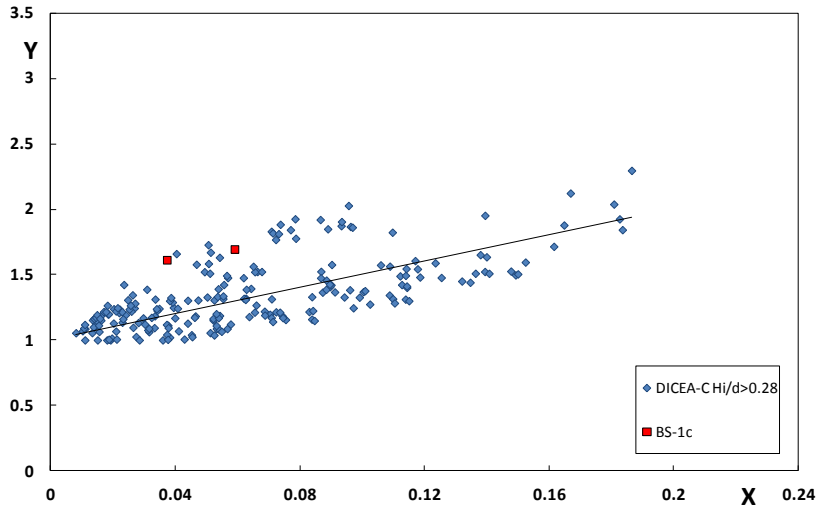

Figure 9.23. Plot of the *DICEA-C* and *BS-1c* in the plane of transformed variables (Eqs. 6.2-6.3).

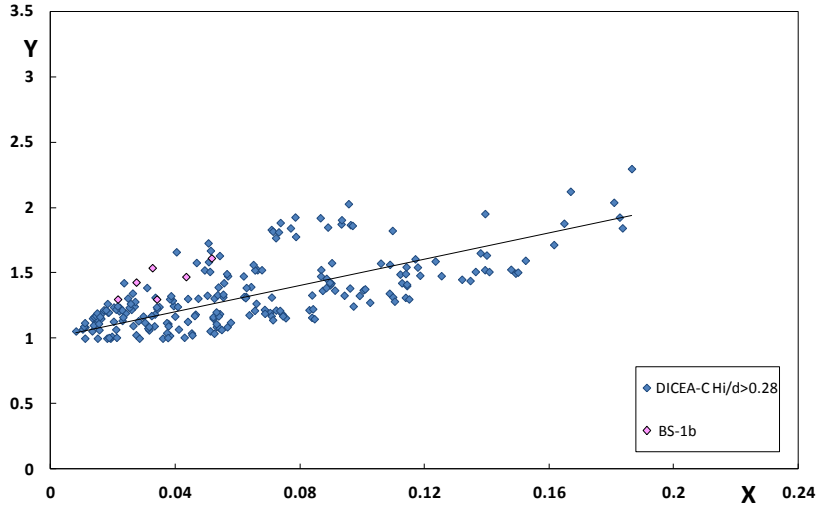

Figure 9.24. Plot of the *DICEA-C* and *BS-1b* in the plane of transformed variables (Eqs. 6.2-6.3).

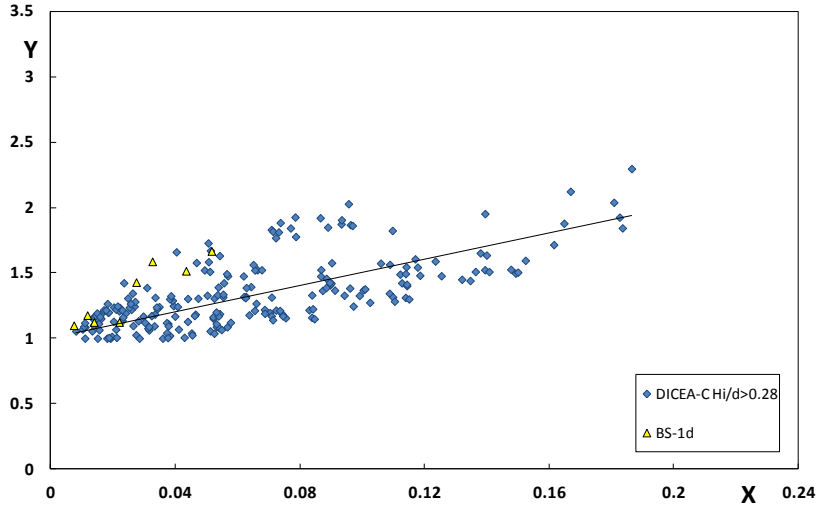

Figure 9.25. Plot of the *DICEA-C* and *BS-1d* in the plane of transformed variables (Eqs. 6.2-6.3)

.

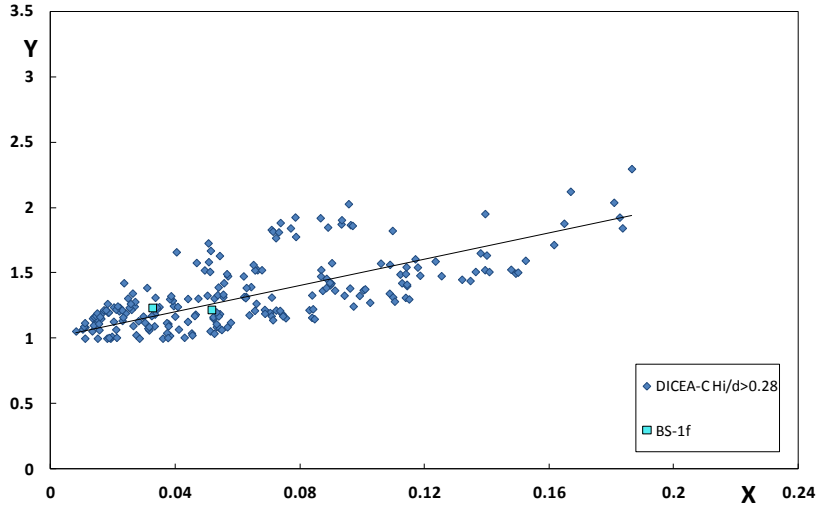

Figure 9.26. Plot of the *DICEA-C* and *BS-1f* in the plane of transformed variables (Eqs. 6.2-6.3)

9.3.2 Application of the Buccino et al. (2014) formula to the DICEA dataset

As discussed in Section (4.2), the leading hypothesis of the Buccino et al. (2014) method is that the barrier always causes waves to break on the crest. This has been demonstrated to be not necessarily true in case of *DICEA* tests (see Chapter 8), in fact the measures indicate that RB modules may force the occurrence of breaking only in situations where waves are about to break on the shoal without the structure ($0.28 < H_i/d \leq 0.365$). Therefore, the model can be considered to be:

- not justified for $H_i/d \leq 0.28$;
- partially justified for $H_i/d > 0.28$.

This means that while for $H_i/d \leq 0.28$ the dissipation occurs via macro-roughness, for larger waves RBs may enhance the strength of breaking, leading to a damping mechanism similar to that imagined by Buccino et al. (2014) (see Sect. 6.2).

In Figures from 9.27 to 9.29 the results obtained via the prediction model are compared to the *DICEA-A* data. In these Figures, points have been partitioned depending on the value of H_i/d. A value of berm correction factor $v = 0.6$ has been used, which corresponds to that of the majority of data analysed in Buccino et al., 2014 (see Sect. 6.1).

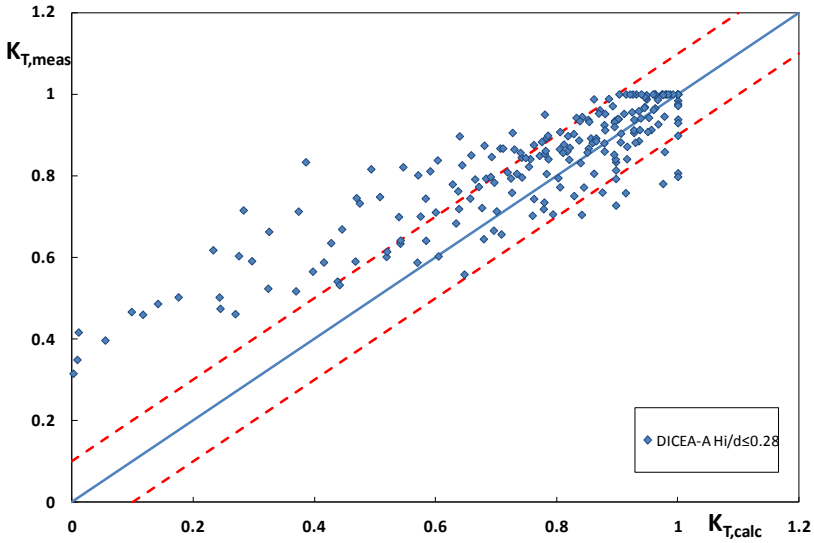

Figure 9.27. Comparison between the measured transmission coefficient and the predicted one according to Buccino et al. (2014) assuming $\nu = 0.6$: *DICEA-A* data with $H_i/d \leq 0.28$.

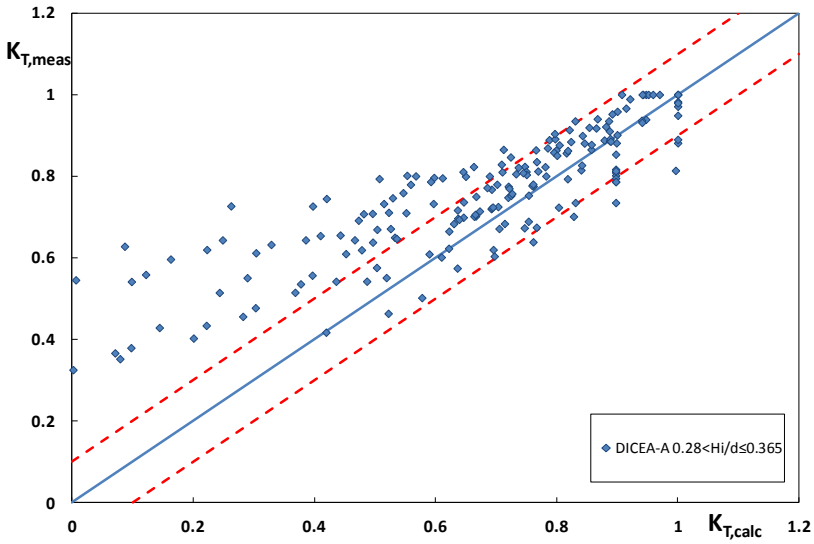

Figure 9.28. Comparison between the measured transmission coefficient and the predicted one according to Buccino et al. (2014) assuming $\nu = 0.6$: *DICEA-A* data with $0.28 < H_i/d \leq 0.365$.

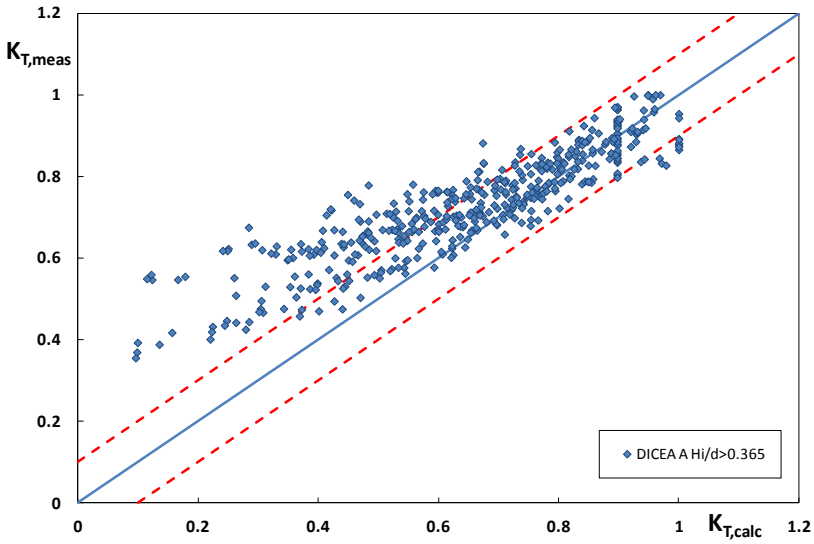

Figure 9.29. Comparison between the measured transmission coefficient and the predicted one according to Buccino et al. (2014) assuming $v = 0.6$: *DICEA-A* data with $H_i/d > 0.365$.

Surprisingly, the trend is almost the same for the three groups, even if some less scatter is detected for $H_i/d > 0.365$. The physical meaning of these results might be that vortices originated by macro-roughness have the same macroscopic effect as breaking, as discussed by the Authors in Buccino et al. (2014). However, it seems clear that the model provides acceptable results for higher values of K_T, when the structures are deeply submerged or include a small number of rows.

On the other hand, as the width of the structure increases and/or the submergence reduces, the prediction heavily underestimates the measures, indicating that the rate of dissipation is greatly overestimated.

It of interest to highlight that the failure of the model becomes more evident for K_T less than approximately 0.6; as it can be observed from Figure 9.30 where all the *DICEA-A* data are plotted. In fact, it is seen that most of data for $K_T > 0.6$ are internal to the ideal acceptance bands $\pm$ 0.1.

In this regard, it can be observed that in the original database of Buccino et al. (2014) nearly 80% of data (142 out of 178) had a measured value of $K_T > 0.6$.

In the following a tentative adjustment of the aforementioned model is presented, consisting in a simple recalibration of the width factor, v.

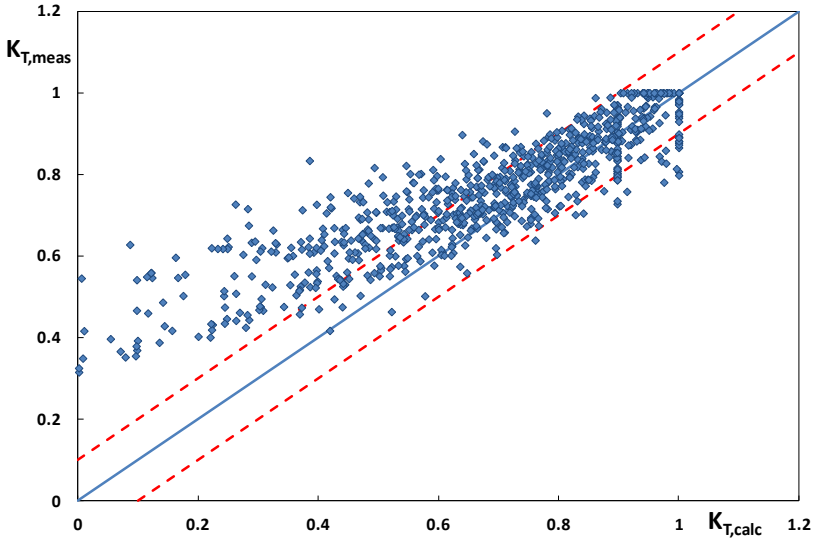

Figure 9.30. Comparison between the measured transmission coefficient and the predicted one according to Buccino et al. (2014) assuming $v = 0.6$: all *DICEA-A* data.

9.3.2.1 Recalibration of the Buccino et al. (2014) model on the DICEA data

For each *DICEA* configuration, the value of the width factor has been changed by imposing a minimum standard error, *SE*, with the constraint of an almost undistorted model. The latter means that the average of residuals has to be included between -0.01 and +0.01.

Accordingly, the values reported in Table 9.5 have been obtained.

Configuration	v	SE
DICEA-A	0.35	0.076
DICEA-B	0.24	0.072
DICEA-C	0.24	0.084

Table 9.5 Values of the width factor, *v*, and of the standard error, *SE*, after calibrating the Buccino et al. (2014) model.

As it is possible to observe from the previous Table, the behaviour of configurations *DICEA-B* and *-C* is nearly the same. Despite the values of the standard errors are well beyond the acceptance limits, it has been observed the *CA* model to become particularly effective when the wave height to depth ratio

exceeds 0.365, i.e. under rough breaking. This result appears to be physically consistent. In Figures from 9.31 to 9.33, the measured transmission coefficients are plotted against the predicted ones for the three configurations and, respectively, for $H_i/d \leq 0.28$; $0.28 < H_i/d \leq 0.365$ and $H_i/d > 0.365$. Figure 9.34 shows all the data in the aforementioned plane.

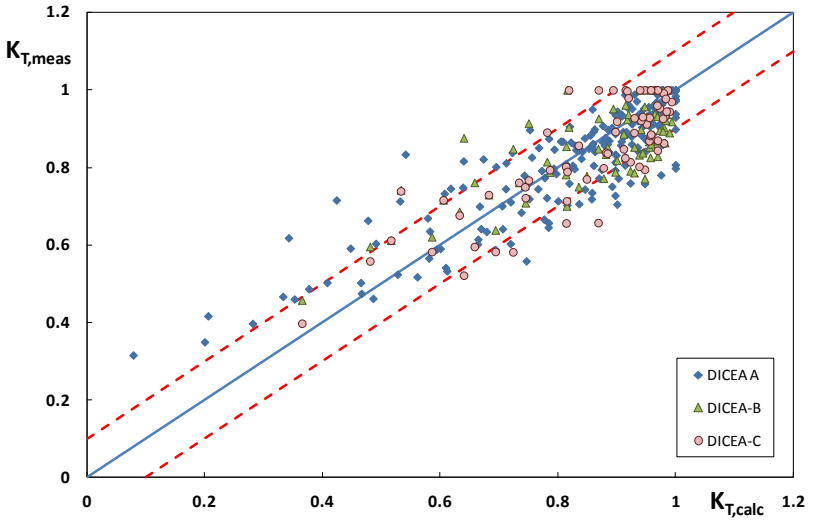

Figure 9.31. Comparison between the measured transmission coefficient and the predicted one according to Buccino et al. (2014), after v calibration, for $H_i/d \leq 0.28$.

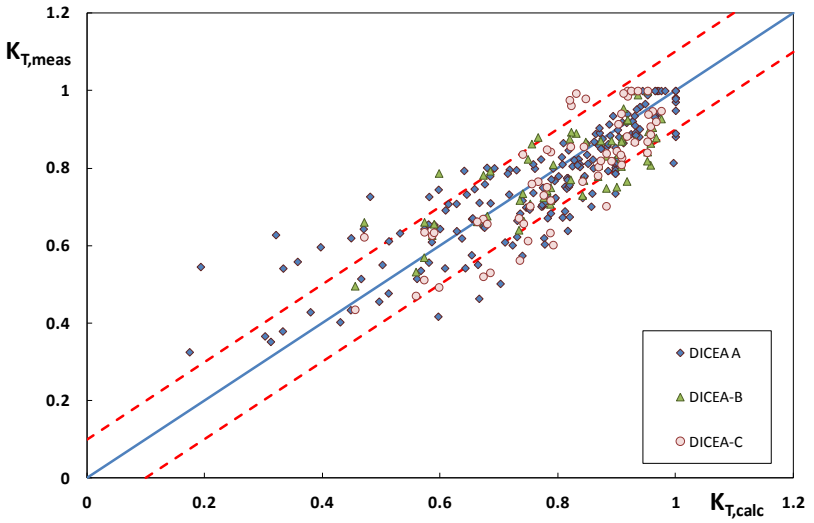

Figure 9.32. Comparison between the measured transmission coefficient and the predicted one according to Buccino et al. (2014), after v calibration, for $0.28 < H_i/d \leq 0.365$.

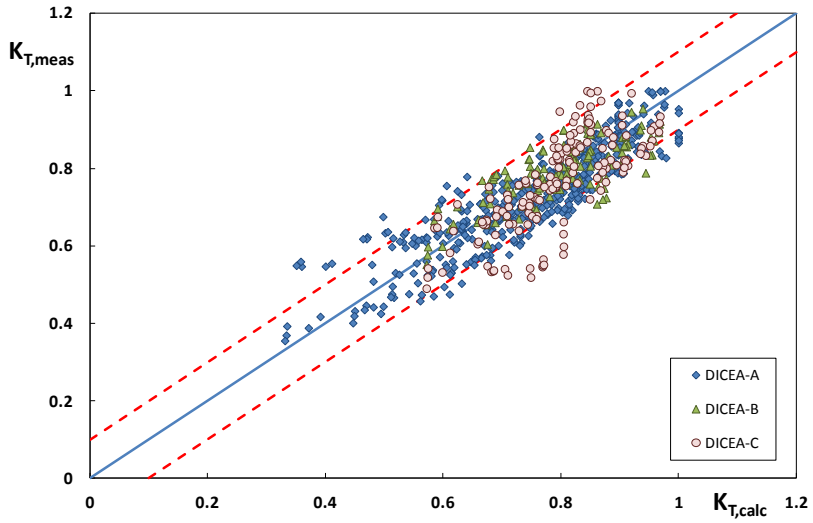

Figure 9.33. Comparison between the measured transmission coefficient and the predicted one according to Buccino et al. (2014), after v calibration, for H_i/d >0.365.

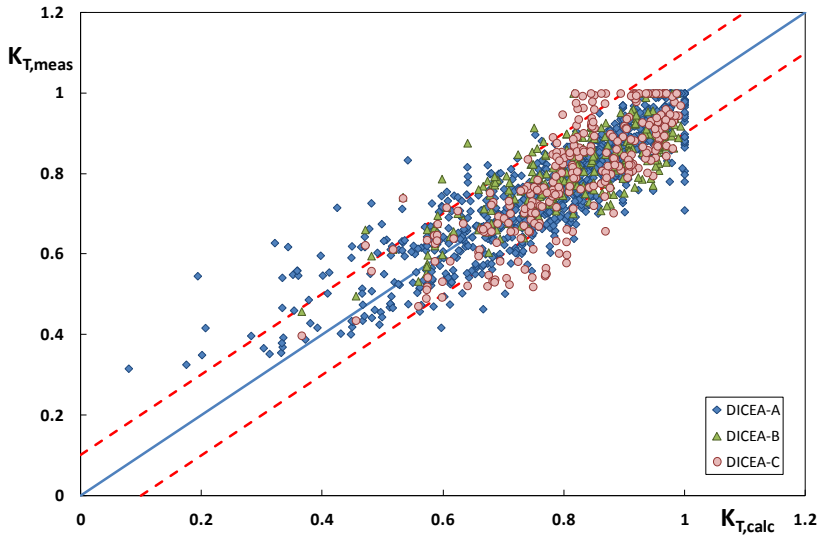

Figure 9.34. Comparison between the measured transmission coefficient and the predicted one according to Buccino et al. (2014), after v calibration.

The usefulness of *CA* for large broken waves (H_i/d >0.365) is evident for *DICEA-A* and *DICEA-B*. As far as *DICEA-C* is concerned, it does not appear any real improvement, unless the outliers with Rc =0.2 and n =5 are removed (Figure 9.35). These points were found to behave differently from the others

also for the Armono's model, as discussed in the previous Section. The Table 9.6 summarizes the values of the *SE* and R^2 for the various groups of data.

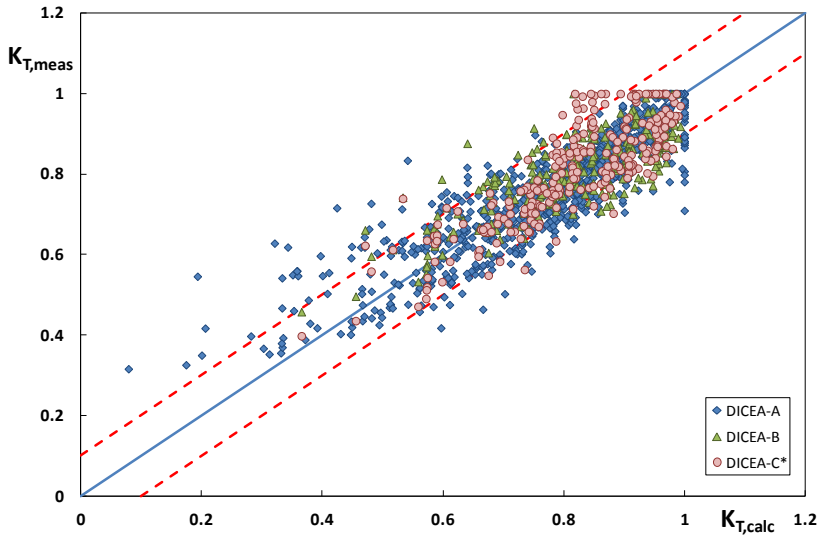

Figure 9.35. Comparison between the measured transmission coefficient and the predicted one according to Buccino et al. (2014), after *v* calibration and outliers removal.

Data-set	H_i/d	# data	R^2	SE
DICEA-A	All	864	0.78	0.076
	≤0.28	214	0.77	0.086
	0.28÷0.365	192	0.75	0.088
	>0.365	458	0.80	0.064
DICEA-B	All	288	0.63	0.071
	≤0.28	69	0.60	0.090
	0.28÷0.365	63	0.64	0.079
	>0.365	156	0.61	0.058
DICEA-C	All	288	0.64	0.083
	≤0.28	69	0.70	0.081
	0.28÷0.365	63	0.69	0.086
	>0.365	156	0.55	0.083
DICEA-C*	All	264	0.72	0.077
	≤0.28	65	0.69	0.080
	0.28÷0.365	58	0.74	0.075
	>0.365	141	0.64	0.065

Table 9.6. Summary of the statistical characteristics for each group of the *DICEA* data according to Buccino et al. (2014), after *v* calibration.

9.3.2.2 Comparison with ERCD/CHL data

The comparison between the Buccino et al. (2014) recalibrated model with *ERDC/CHL* is shown in Figure 9.36. As it can be observed, the outcome is similar to that obtained from the Armono's model (Sect. 9.3.1.1). In fact, the transmission coefficients for the Miami Beach project are generally lower than those measured at the *DICEA* and data is generally overestimated.

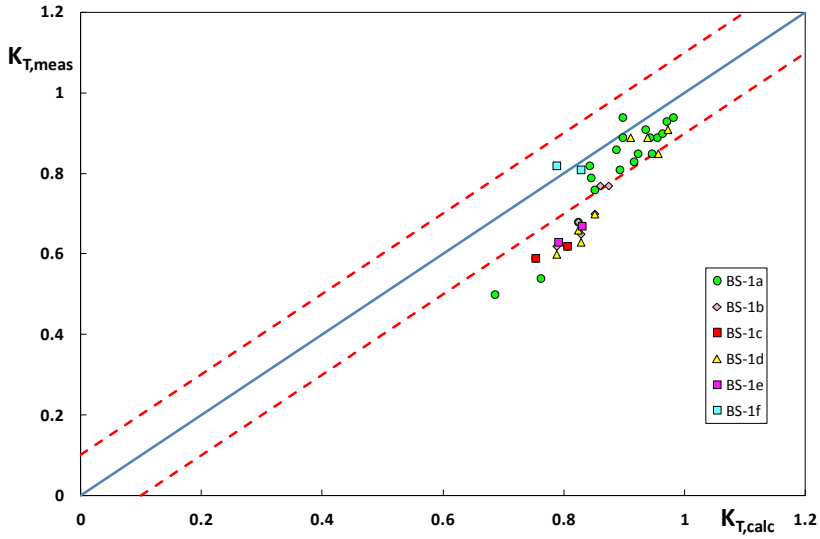

Figure 9.36. Comparison between the measured transmission coefficient and the predicted one according to Buccino et al. (2014), after *v* calibration, for *ERDC/CHL* data.

9.4 Development of a predictive model based on DICEA experimental campaign

So far, it has been observed that slight modifications of the existing predictive models don't lead to the desired accurateness in the prediction of the transmission coefficient. For this reason, existing models from the literature have been firstly adapted and partially modified and, subsequently, new ones have been proposed.

9.4.1 Generalized Armono's model

In the present Section, the Armono's model has been simply generalized, by keeping the same regressors, as well as the same structure of the design Equation (5.1). The latter can be written as follows:

$$K_T = \frac{1}{1 + A_0 \left(\frac{H_{si}}{gT_p^{\,2}}\right)^{\beta_1} \left(\frac{B_{bR}}{gT_p^{\,2}}\right)^{\beta_2} \left(\frac{h_s}{B_{bR}}\right)^{\beta_3} \left(\frac{h_s}{d}\right)^{\beta_4}} \tag{9.8}$$

and arranged into the following linear model:

$$Y = \ln\left(\frac{1}{K_T} - 1\right) = \ln(\mathrm{A}_0) + \beta_1 \cdot \mathrm{X}_1 + \beta_2 \cdot \mathrm{X}_2 + \beta_3 \cdot \mathrm{X}_3 + \beta_4 \cdot \mathrm{X}_4 \tag{9.9}$$

where:

$$\mathrm{X}_1 = \ln\left(\frac{H_{si}}{g{T_p}^2}\right); \mathrm{X}_2 = \ln\left(\frac{B_{bR}}{g{T_p}^2}\right); \mathrm{X}_3 = \ln\left(\frac{h_s}{B_{bR}}\right); \mathrm{X}_4 = \ln\left(\frac{h_s}{d}\right) \tag{9.10}$$

In the fitting of Equation (9.9) to the experimental data, K_T values larger than 0.95 have been initially censored, to avoid Y to diverge, as its argument tends to zero ($K_T \cong 1$).

9.4.1.1 Calibration on DICEA-A data

As a first step of the analysis, the Equation (9.9) has been calibrated on the *DICEA-A* data. Results of the regression analyses for the three groups of H_i/d are reported in Table 9.7 to Table 9.9.

Coefficients		SE	T-stat	p-value	95% confidence bands	
ln(A$_0$)	-0.1872	0.254	-0.736	0.462672	-0.689	0.315
β$_1$	0.484	0.128	3.782	$2.19\text{x}10^{-4}$	0.231	0.737
β$_2$	-0.434	0.152	-2.864	$4.742\text{x}10^{-3}$	-0.734	-0.135
β$_3$	-0.938	0.160	-5.857	$2.6\text{x}10^{-08}$	-1.255	-0.622
β$_4$	4.404	0.224	19.673	$1.45\text{x}10^{-44}$	3.962	4.846

Table 9.7. Results of the regression analysis for *DICEA-A* and $H_i/d \leq 0.28$.

Coefficients		SE	T-stat	p-value	95% confidence bands	
ln(A$_0$)	1.162	0.480	2.419	0.01673	0.213	2.110
β$_1$	1.428	0.356	4.008	$9.53\text{x}10^{-05}$	0.724	2.132
β$_2$	-1.221	0.354	-3.445	$7.37\text{x}10^{-4}$	-1.921	-0.521
β$_3$	-1.88	0.360	-5.229	$5.49\text{x}10^{-07}$	-2.59	-1.169
β$_4$	4.603	0.3819	12.053	$5.52\text{x}10^{-24}$	3.849	5.358

Table 9.8. Results of the regression analysis for *DICEA-A* and $0.28 < H_i/d \leq 0.365$.

Coefficients		SE	T-stat	p-value	95% confidence bands	
$\ln(A_0)$	0.445	0.273	1.63	0.104	-0.092	0.982
β_1	0.386	0.196	1.972	0.049	0.001	0.771
β_2	0.008	0.185	0.046	0.964	-0.356	0.372
β_3	-0.769	0.188	-4.098	$4.94\text{x}10^{-05}$	-1.137	-0.400
β_4	2.404	0.261	9.198	$1.36\text{x}10^{-18}$	1.890	2.917

Table 9.9. Results of the regression analysis for *DICEA-A* and H_i/d >0.365.

It is seen that data referring to non-breaking and slightly breaking experiments ($H_i/d \leq 0.365$) may belong to the same population. This is clear from the inspection of the confidence intervals of the coefficients shown in Table 9.7 and Table 9.8. In fact, for $H_i/d \leq 0.28$ and $0.28 < H_i/d \leq 0.365$, the intervals overlap for all the variables $X_1 \div X_4$, indicating that some common values of the parameters may exist. For example, the range of variation of β_1 for $H_i/d \leq 0.28$ is $0.23 \div 0.74$, whereas for $0.28 < H_i/d \leq 0.365$ is $0.72 \div 2.13$. Hence, an overlap exists in the interval $0.72 \div 0.74$.

On the contrary, no overlapping is observed for all the variables when comparing the first two groups (Table 9.7 and Table 9.8) with H_i/d >0.365 (Table 9.9); here it is also noticed that the variable X_2 is not even significant.

Accordingly, slightly breaking and non-breaking wave data have been gathered to get the predictive Equation (9.11), which produces a *SE* of 0.06.

$$K_T = \frac{1}{1 + 0.865\left(\frac{H_{si}}{gT_p^{\,2}}\right)^{0.486}\left(\frac{B_{bR}}{gT_p^{\,2}}\right)^{-0.385}\left(\frac{h_s}{B_{bR}}\right)^{-0.962}\left(\frac{h_s}{d}\right)^{4.123}} \tag{9.11}$$

The Figure 9.37 shows the comparison between measures and predictions, along with the acceptance bands ±0.1 around the line of perfect agreement. Table 9.10 reports the results of the regression analysis for $H_i/d \leq 0.365$.

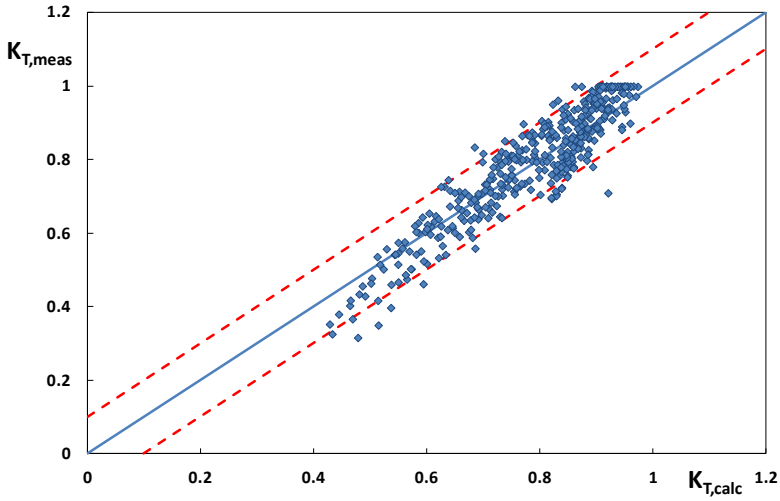

Figure 9.37. Comparison between the measured transmission coefficient and the predicted one, according to the generalized Armono's model, for *DICEA-A* with $H_i/d \leq 0.365$.

Coefficients		Standard Error	T-stat	p-value	95% confidence bands	
$\ln(A_0)$	-0.145	0.164	-0.886	0.376	-0.468	0.178
β_1	0.486	0.06	8.075	1.33×10^{-14}	0.367	0.604
β_2	-0.385	0.073	-5.274	2.44×10^{-7}	-0.529	-0.241
β_3	-0.962	0.082	-11.753	8.13×10^{-27}	-1.123	-0.801
β_4	4.123	0.137	30.044	8.3×10^{-96}	3.853	4.393

Table 9.10. Results of the regression analysis for *DICEA-A* and $H_i/d \leq 0.365$.

From the inspection of the graph above, the residuals seem some structured, with the cloud of points which appears to be rotated compared to the line of perfect agreement. This is clearer in Figure 9.38, where the residuals $e_i = K_{T,meas} - K_{T,calc}$ are plotted against the predictions. The values of e_i are almost all negative for $K_{T,calc} < 0.6$, indicating a lack of fit, the reason of which is not clear till now.

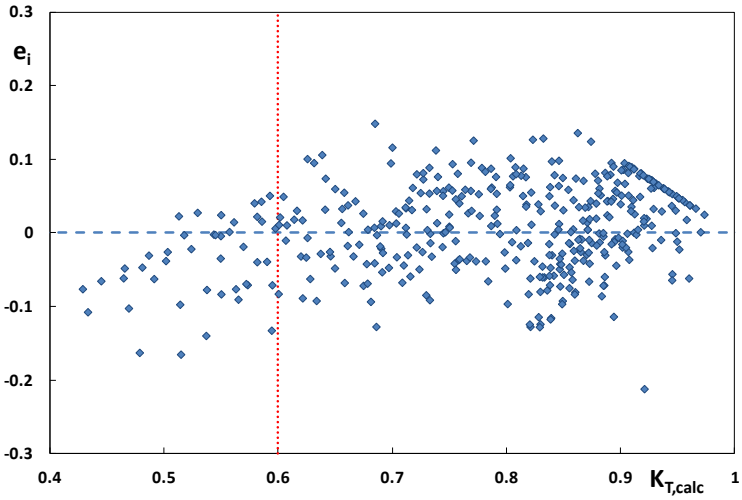

Figure 9.38. Plot of the residuals e_i vs. $K_{T,calc}$ according to Eq. (9.11) for *DICEA-A* with $H_i/d \leq 0.365$.

It is also worth to notice that the ranges of variation of the parameters for $H_i/d \leq 0.365$ (Table 9.10) do not overlap with those related to $H_i/d > 0.365$ (Table 9.9); apart from the not significance of the variable X_2, the values for X_4 are external from one another.

Hence, a new regression analysis has been performed for the data with heavy breaking ($H_i/d > 0.365$), removing the variable X_2 from the predictors set.

The following formula has been obtained:

$$K_T = \frac{1}{1 + 1.577\left(\frac{H_{si}}{gT_p^{\,2}}\right)^{0.395}\left(\frac{h_s}{B_{bR}}\right)^{-0.777}\left(\frac{h_s}{d}\right)^{2.415}} \tag{9.12}$$

which exhibits a standard error of 0.049. Additionally, as shown in Figure 9.39 the cloud of data seems to properly follow the line of perfect agreement; as also clearly shown from the plot of the residuals in Figure 9.40.

Finally, the Table 9.11 reports the results of the regression analysis.

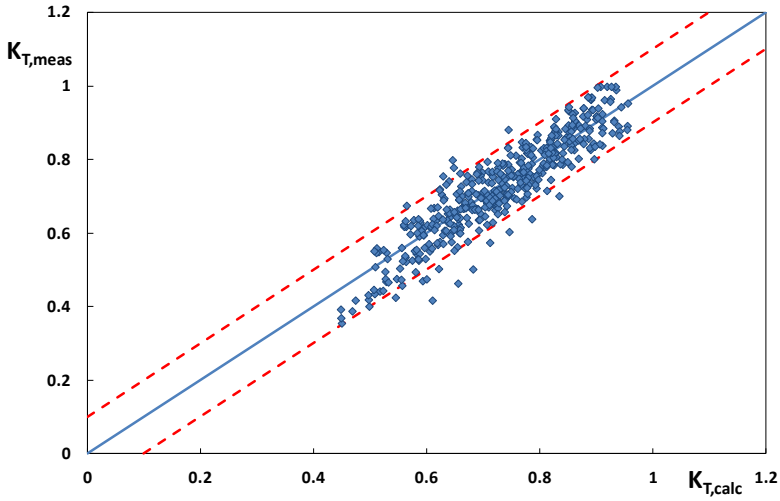

Figure 9.39. Comparison between the measured transmission coefficient and the predicted one, according to the generalized Armono's model, for *DICEA-A* with H_i/d >0.365.

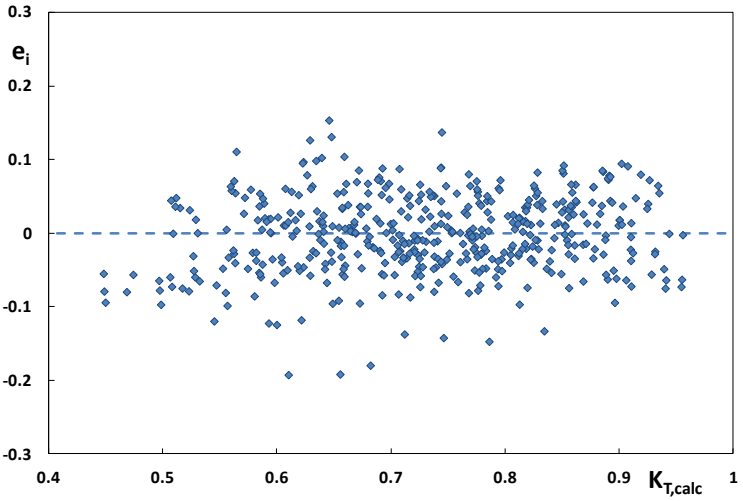

Figure 9.40. Plot of the residuals e_i vs. $K_{T,calc}$ according to Eq. (9.12) for *DICEA-A* with H_i/d >0.365.

Coefficients		Standard Error	T-stat	p-value	95% confidence bands	
$\ln(A_0)$	-0.455	0.169	2.695	7.31×10^{-3}	0.123	0.787
β_1	0.395	0.028	14.312	1.38×10^{-38}	0.341	0.449
β_3	-0.777	0.022	34.582	4.8×10^{-129}	-0.821	-0.733
β_4	2.415	0.087	27.812	6×10^{-100}	2.244	2.586

Table 9.11. Results of the regression analysis for *DICEA-A* and H_i/d >0.365 omitting the variable X_2.

Configurations	H_i/d	# data	R^2	SE
DICEA-A	All	864	0.87	0.054
	≤0.365	406	0.86	0.060
	>0.365	458	0.86	0.049

Table 9.12. Summary of the statistical characteristics for *DICEA-A* data.

9.4.1.2 Inclusion of DICEA-B and DICEA-C data

Before investigating configurations *DICEA-B* and *DICEA-C*, it seems worth to recall that these experiments have not been conducted systematically for all the number of rows; but only for *n* equal to 3, 5 and 7. This renders an *ad-hoc* recalibration of the predictive model somehow questionable.

The behaviour of low-density configurations can be discussed by means of the graphs reported from Figures 9.41 to 9.44, where the transmission coefficient is plotted against the number of rows, for fixed values of the relative submergence, h_s/d. It is seen that the difference in the response is generally small and this practically means that the effect of *n* rows of RB is roughly the same, whatever the distance between the modules. However, from a closer insight, the following considerations can be drawn:

- no relevant difference has been noticed between *DICEA-B* and *-C*;
- the low density data tends to mix into the *DICEA-A* cloud for well submerged barriers (h_s/d =0.60÷1.75);

- on the other side, when the crest of the structure approaches the still water level, the experimental points of *DICEA-B* and *DICEA-C* tend to lie above *DICEA-A* (h_s/d =0.88÷1);
- a group of data belonging to *DICEA-C* and characterized by h_s/d =0.88 and n =5 seems to behave as an outlier. This is particularly evident from the Figure 9.45, where the low density data have been isolated. Since for this group the values of K_T are particularly small, it seemed cautious to exclude them from subsequently analyses.

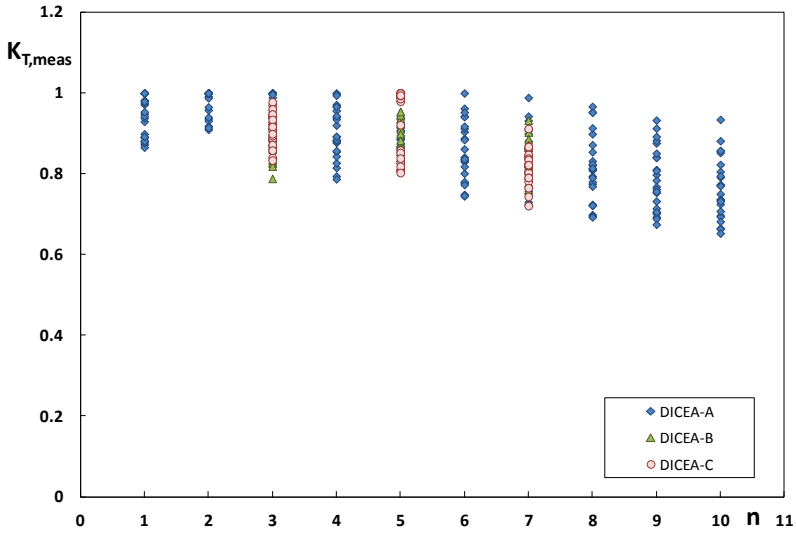

Figure 9.41. Plot of the measured transmission coefficient vs. the number of RB rows for h_s/d =0.60.

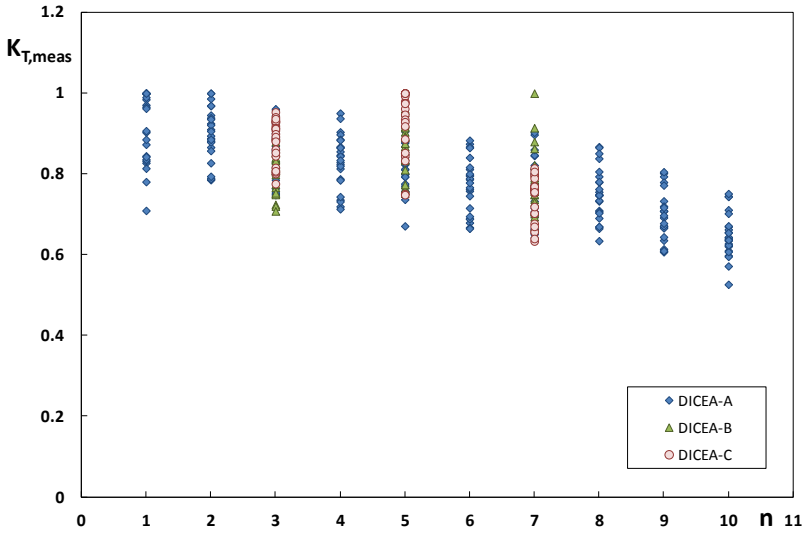

Figure 9.42. Plot of the measured transmission coefficient vs. the number of RB rows for h_s/d =0.75.

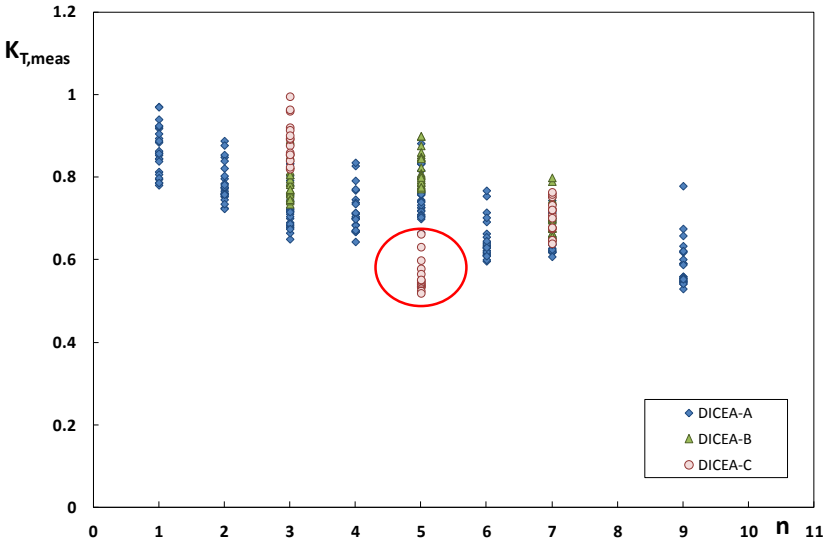

Figure 9.43. Plot of the measured transmission coefficient vs. the number of RB rows for h_s/d =0.88. Outliers are circled in red.

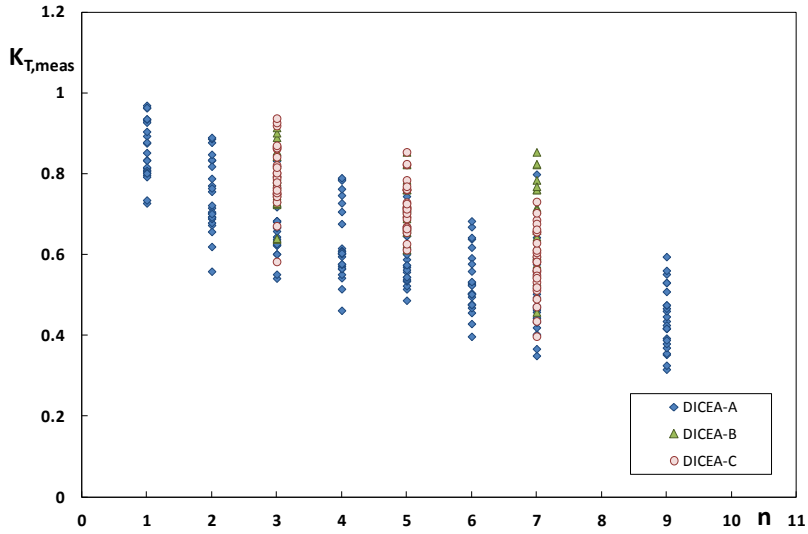

Figure 9.44. Plot of the measured transmission coefficient vs. the number of RB rows for h_s/d =1.

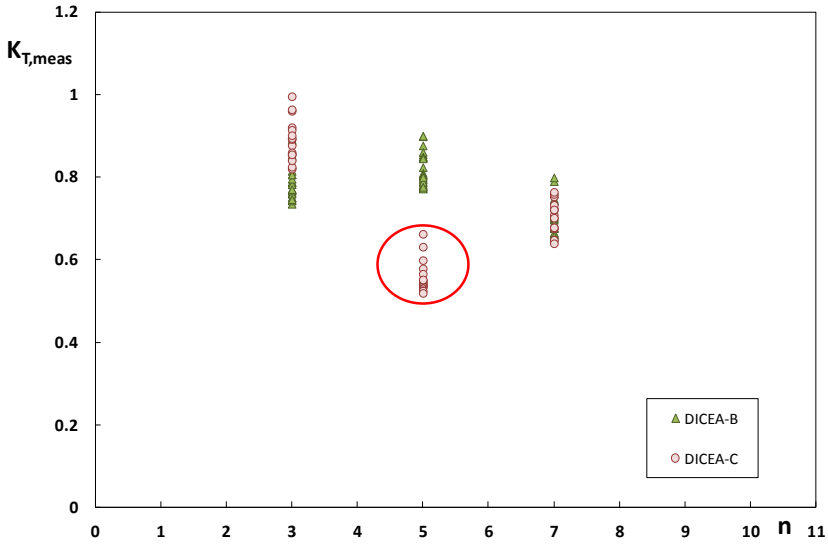

Figure 9.45. Plot of the measured transmission coefficient vs. the number of RB rows for low density configurations with h_s/d =0.88. Outliers are circled in red.

Two different approaches may be followed for deriving a predictive model including low density data:

1. trying to capture the peculiarities of these data, via the application of the previously calibrated equations to low density data;
2. ignoring the differences between the *DICEA* dataset, by refitting the previous predictive equation to all the available experiments.

The first approach represents the simplest way to include the effect of the spacing between modules. In fact, by the application of Equations (9.11) and (9.12) to *DICEA-B* and *–C*, values of K_T were found to be reasonably predicted, apart from an average underestimation, equal to 0.053 for $H_i/d \leq 0.365$ and 0.073 for $H_i/d > 0.365$. Hence the following Equations can be proposed:

$$\begin{aligned} K_T &= \text{Eq. (9.11)} + 0.053 \quad \text{for } H_i/d \leq 0.365 \\ K_T &= \text{Eq. (9.12)} + 0.073 \quad \text{for } H_i/d > 0.365 \end{aligned} \tag{9.13}$$

The comparison between measures and predictions is shown in Figure 9.46 and Figure 9.47. The statistical characteristics of the model are summarized in Table 9.13; as it can be noticed, values of standard error larger than 0.06 have been obtained.

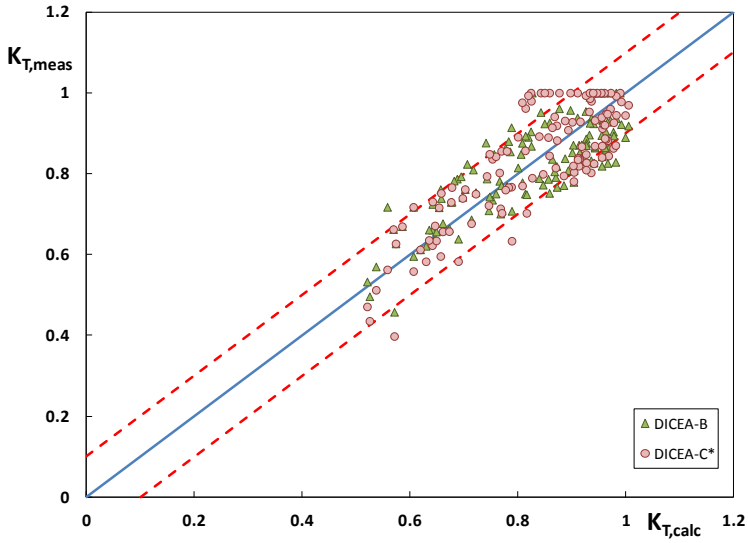

Figure 9.46. Comparison between the measured transmission coefficient and the predicted one, according to Eq.(9.13), for *DICEA-B* and *DICEA-C** data with $H_i/d \leq 0.365$.

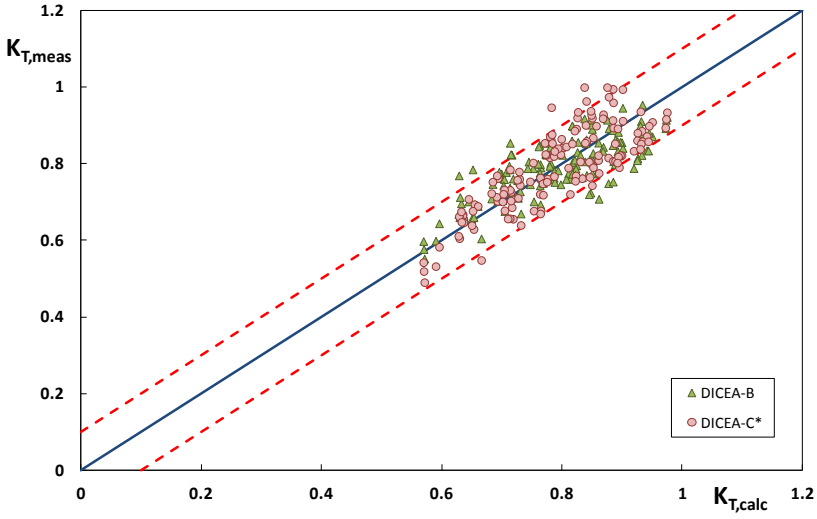

Figure 9.47. Comparison between the measured transmission coefficient and the predicted one, according to Eq. (9.13), for *DICEA-B* and *DICEA-C** data with $H_i/d > 0.365$.

Configurations	H_i/d	# data	R^2	SE
DICEA-B+DICEA-C*	All	552	0.67	0.068
	≤0.365	255	0.68	0.074
	>0.365	297	0.64	0.061
DICEA-B	All	288	0.66	0.067
	≤0.365	132	0.68	0.074
	>0.365	156	0.61	0.060
DICEA-C*	All	264	0.64	0.070
	≤0.365	123	0.69	0.079
	>0.365	141	0.68	0.062

Table 9.13. Summary of the statistical characteristics for *DICEA-B* and *DICEA-C** data.

The second approach (point two of the previous list) consists in neglecting the effect of the spacing and treating all the data as they would come from the same population. After gathering all the datasets, two regressions have been performed depending on whether $H_i/d \leq 0.365$ or $H_i/d > 0.365$; the results of which are reported in Table 9.14 and Table 9.15. It is seen that, for heavy breaking waves, the transmission coefficient is independent from H_i/gT_p^2 and B_{bR}/gT_p^2. In practical terms, this would imply that K_T is not affected by the wave period.

For this reason a new regression analysis has been performed for $H_i/d > 0.365$, neglecting the two abovementioned predictors. The results are shown in Table 9.16.

Finally, the predictive Equations (9.14) and (9.15) have been obtained, valid for $H_i/d \leq 0.365$ and $H_i/d > 0.365$, respectively:

$$K_T = \frac{1}{1 + 0.654\left(\frac{H_{si}}{gT_p^{\,2}}\right)^{0.390}\left(\frac{B_{bR}}{gT_p^{\,2}}\right)^{-0.273}\left(\frac{h_s}{B_{bR}}\right)^{-0.852}\left(\frac{h_s}{d}\right)^{3.519}} \qquad (9.14)$$

$$K_T = \frac{1}{1 + 0.123\left(\frac{h_s}{B_{bR}}\right)^{-0.74}\left(\frac{h_s}{d}\right)^{1.643}} \tag{9.15}$$

Coefficients		Standard Error	T-stat	p-value	95% confidence bands	
$\ln(A_0)$	-0.424	0.141	-3.006	$2.77\text{x}10^{-3}$	-0.701	0.147
β_1	0.390	0.050	7.789	$2.50\text{x}10^{-14}$	0.292	0.489
β_2	-0.273	0.060	-4.538	$7.03\text{x}10^{-6}$	-0.392	-0.155
β_3	-0.852	0.069	-12.285	$9.45\text{x}10^{-31}$	-0.989	-0.716
β_4	3.519	0.109	32.209	0.00	3.304	3.733

Table 9.14. Results of the regression analysis for *DICEA* data with $H_i/d \leq 0.365$.

Coefficients		Standard Error	T-stat	p-value	95% confidence bands	
$\ln(A_0)$	-0.041	0.308	-0.133	0.894	-0.646	0.564
β_1	0.102	0.22	0.466	0.64	-0.329	0.533
β_2	0.286	0.205	1.391	0.165	-0.117	0.688
β_3	-0.47	0.207	-2.267	0.024	-0.876	-0.063
β_4	1.608	0.295	5.45	$6.89\text{x}10^{-8}$	1.029	2.187

Table 9.15. Results of the regression analysis for *DICEA* data with $H_i/d > 0.365$.

Coefficients		Standard Error	T-stat	p-value	95% confidence bands	
$\ln(A_0)$	-2.097	0.052	-40.061	$4.3\text{x}10^{-187}$	-2.20	-1.99
β_3	-0.74	0.029	-25.777	$6.6\text{x}10^{-105}$	-0.797	-0.684
β_4	1.64	0.092	17.56	$5.34\text{x}10^{-59}$	1.461	1.824

Table 9.16. Results of the regression analysis for *DICEA* data with $H_i/d > 0.365$ where X_2 ($H_i/gT_p^{2)}$ and X_3 (B_{bR}/gT_p^2) were neglected.

The comparison between predictions and measures is shown, for different ranges of H_i/d, from Figures 9.48 to 9.50.

Table 9.17 summarizes the statistics of the model, whereas the graphs depicted in Figure 9.51 Figure 9.56 display the residuals vs. the predicted transmission coefficient and the normality plot.

The following items deserve to be highlighted:

- the obtained standard errors slightly exceed the acceptance value of 0.06. The percentage of data exceeding the ±0.1 bands is 16% for both $H_i/d \leq 0.365$ and $H_i/d > 0.365$;
- Compared to the model calibrated on *DICEA-A* only (Sect 9.4.1.1), the inclusion of low density configurations, as expected, increases the scatter.
- the SE are almost uniform for all the three arrangements;
- the residuals are Gaussian distributed;
- the residuals for $H_i/d \leq 0.365$ exhibit a certain curvature, probably due to a lack of fit, which had been already observed for *DICEA-A*.

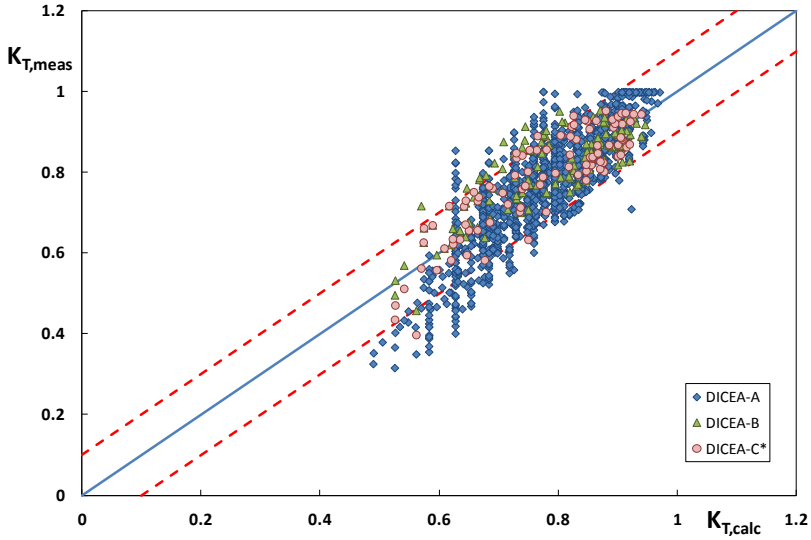

Figure 9.48. Comparison between the measured transmission coefficient and the predicted one, according to Eqs. (9.14) and (9.15), for the whole *DICEA* dataset.

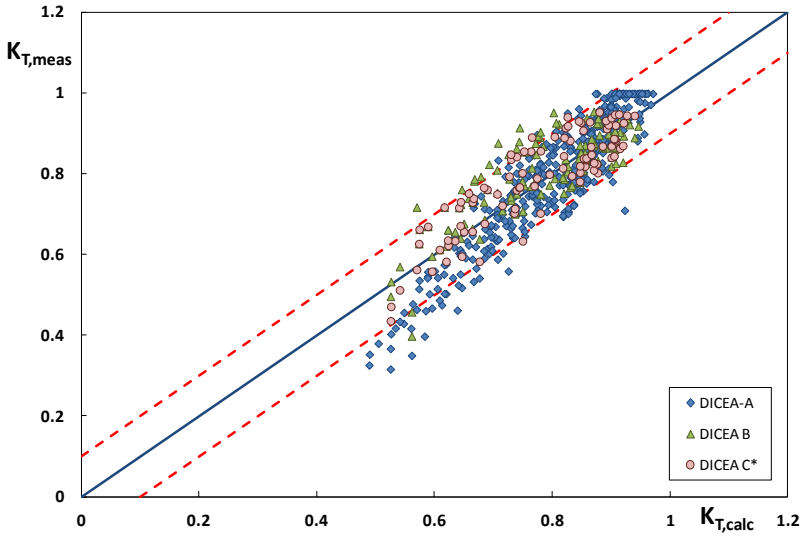

Figure 9.49. Comparison between the measured transmission coefficient and the predicted one, according to Eq. (9.14), for the whole *DICEA* dataset with $H_i/d \leq 0.365$.

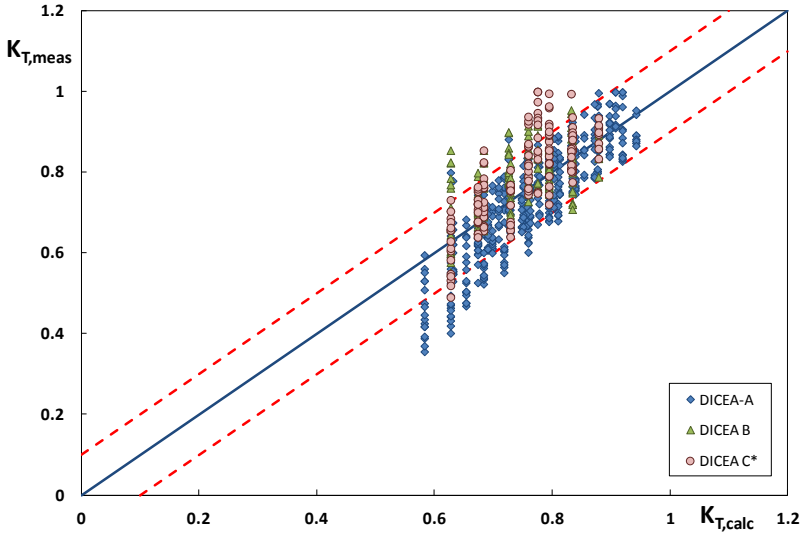

Figure 9.50. Comparison between the measured transmission coefficient and the predicted one, according to Eq. (9.15), for the whole *DICEA* dataset with $H_i/d > 0.365$.

Configurations	H_i/d	# data	R^2	SE
All DICEA	All	1416	0.71	0.074
	≤0.365	661	0.77	0.072
	>0.365	755	0.71	0.076
DICEA-A	All	864	0.82	0.069
	≤0.365	406	0.62	0.067
	>0.365	458	0.76	0.068
DICEA-B	All	288	0.57	0.066
	≤0.365	132	0.68	0.066
	>0.365	156	0.37	0.065
DICEA-C*	All	264	0.66	0.073
	≤0.365	123	0.71	0.076
	>0.365	141	0.57	0.071

Table 9.17. Summary of the statistical characteristics for *DICEA* data.

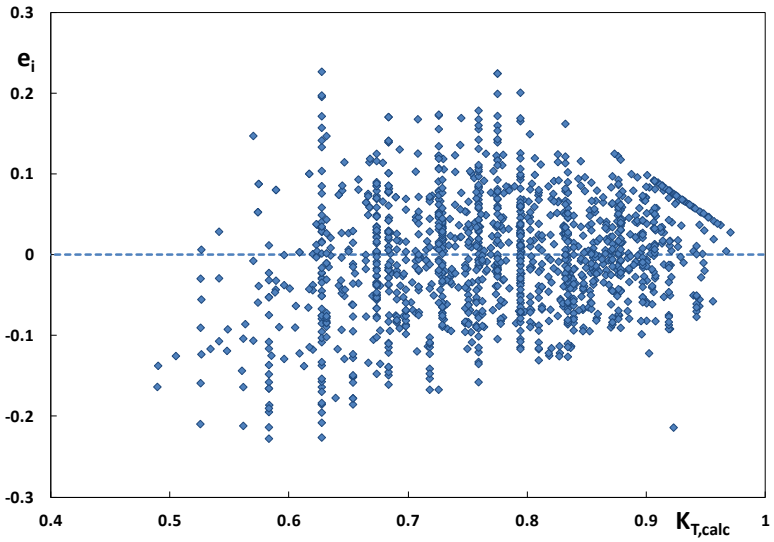

Figure 9.51. Plot of the residuals e_i vs. $K_{T,calc}$ according to Eqs. (9.14) and (9.15), for the whole *DICEA* dataset.

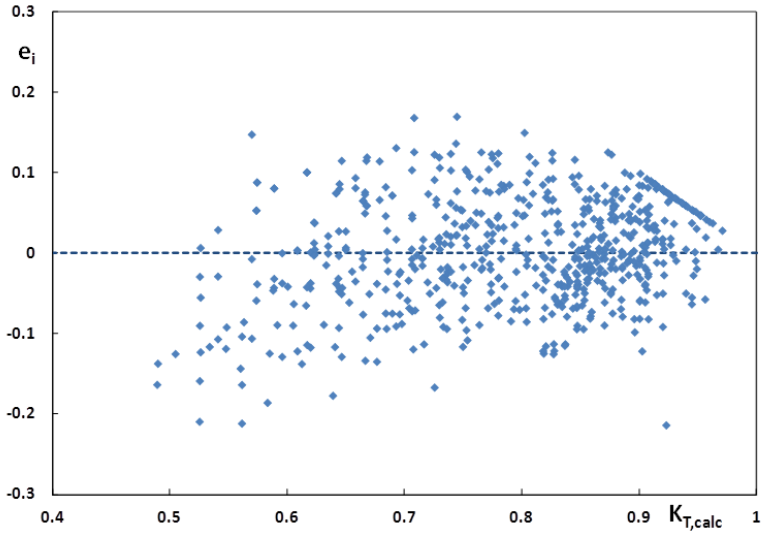

Figure 9.52. Plot of the residuals e_i vs. $K_{T,calc}$ according to Eq. (9.14), for the whole *DICEA* dataset with $H_i/d \leq 0.365$.

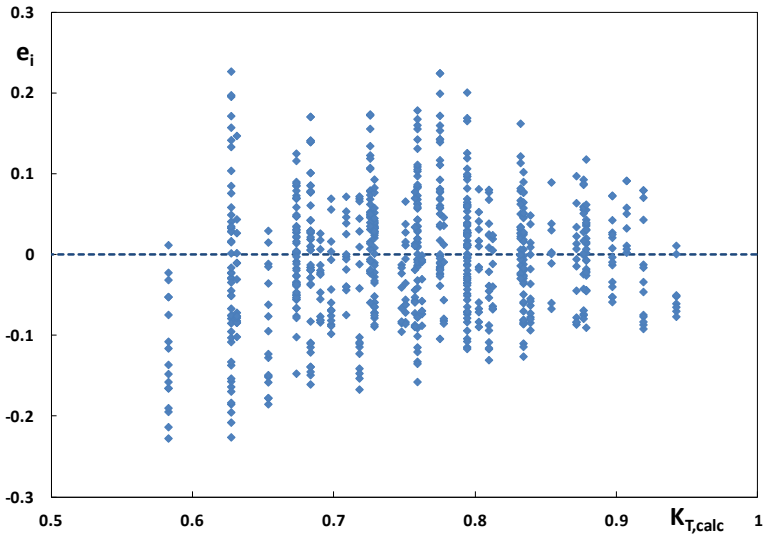

Figure 9.53. Plot of the residuals e_i vs. $K_{T,calc}$ according to Eq. (9.15), for the whole *DICEA* dataset with $H_i/d > 0.365$.

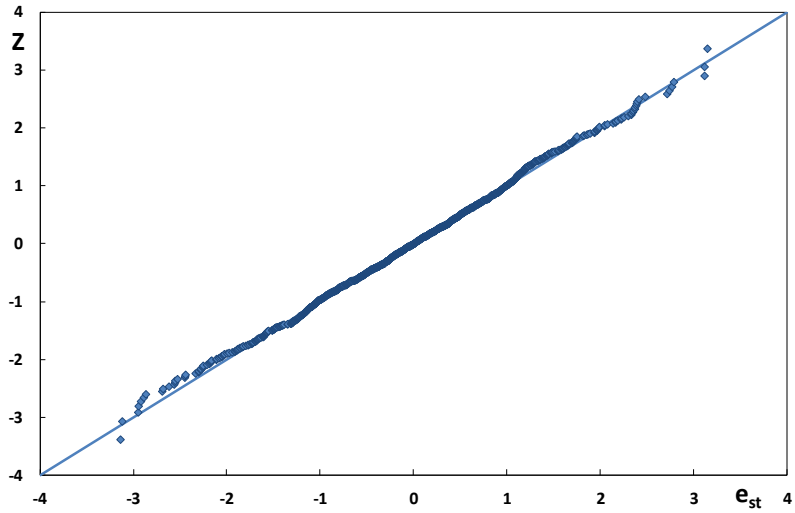

Figure 9.54. Normality plot of the standardized residuals.

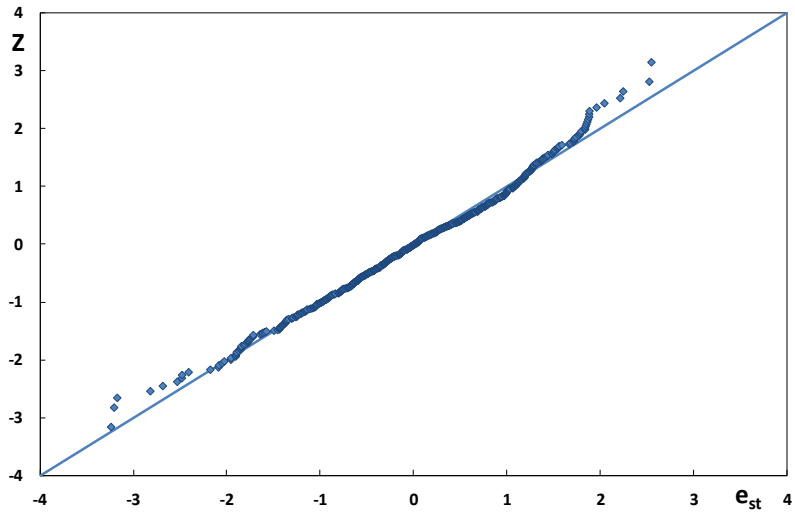

Figure 9.55. Normality plot of the standardized residuals for $H_i/d \leq 0.365$.

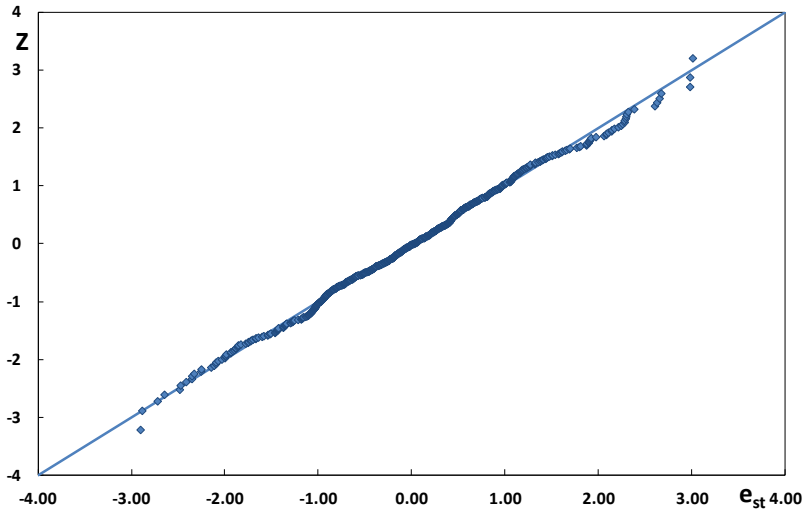

Figure 9.56. Normality plot of the standardized residuals for H_i/d> 0.365.

9.4.1.3 Comparison with ERCD/CHL data

Figure 9.57 shows the *ERCD/CHL* data vs. the prediction obtained from the Armono's generalized model, given in Eqs. (9.14) and (9.15). The experimental points appear largely overpredicted, as already observed after the application of the Armono (2003) and Buccino et al. (2014). In this case the number of points out of the acceptance bands is even larger than what expected (43%).

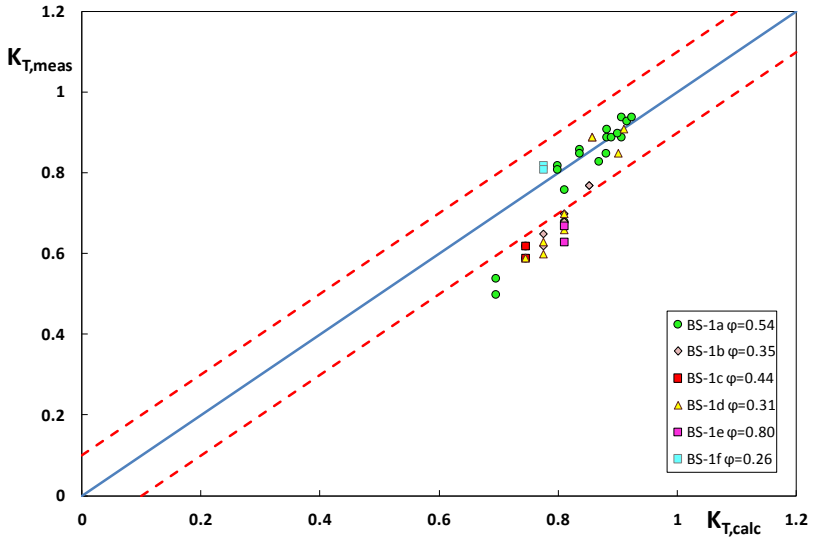

Figure 9.57. Comparison between the measured transmission coefficient and the predicted one, according to Eqs. (9.14) and (9.15), for the *ERDC/CHL* dataset.

9.4.2 Development of a conceptual approach based on friction

In the following paragraphs a conceptual predictive approach is developed, similar to the one suggested by Buccino and Calabrese (2007a) but based on friction as the main mechanism of dissipation. This in order to understand whether a closer modelling of the physics characterising the interaction between modules and waves may lead to more effective predictions. The analysis may also be helpful in clarifying some aspects of the transmission response, such as the effect of spacing.

9.4.2.1 Bases of modelling

The results shown in the Chapter 8 clearly indicate that a barrier in Reef Ball hardly produces the breaking of incoming waves. If the structure is located out of the surf zone ($H_i/d \leq 0.28$), the wave energy is dissipated by macro-roughness; on the other hand the effectiveness of a barrier within the surf zone is probably related either to a friction mechanism or to a breaking enhancement induced by modules.

Here we firstly assume that the leading dissipation mechanism is macro-roughness, so that the presence of broken waves is simply modelled as a variation of the friction factor. Then, the possibility that wave transmission in the surf zone is dominated by breaking effects is explored.

The basic assumption is that, in absence of breaking, the Reef Ball modules can be treated as a bottom friction, with a characteristic dimension h_s.

As shown by Putnam and Johnson (1949), the average rate of energy dissipation per plan area due to bottom friction for shallow water is:

$$\delta_{BT} = \rho \frac{f' H^3}{12\pi} \left(\frac{g}{d}\right)^{3/2} \tag{9.16}$$

in which ρ is the water density and f' is a friction factor (drag coefficient), dependent on flow and bottom characteristics.

The Equation (9.16) can be easily rearranged as follows:

$$\delta_{BT} = \rho g f' \frac{H}{d} \cdot \frac{H^2 \sqrt{gd}}{d} \tag{9.17}$$

where it is seen that the dissipated power is proportional to the energy flux ($\rho g {H_T}^2/\sqrt{gd}$) in shallow water and to the reciprocal of the water depth. The proportionality factor is finally equal to the product of the drag coefficient, *f'*, and the wave height to depth ratio (H_T/d). So, for an infinitesimal trunk of structure of width (∂b), the wave energy balance reads:

$$\frac{\partial P_T}{\partial b} = -\rho g f' \frac{H_T}{d} \cdot \frac{{H_T}^2 \sqrt{gd}}{d} \tag{9.18}$$

where *P* denotes the energy flux. In the Equation (9.18) it has been assumed that no dissipation occurs when the waves travel from the landward end of the structure to the free bottom (see Sect. 4.2).
Remembering that RBs are here modelled as a simple roughness of the bottom at the "constant" depth *d*, we have:

$$\frac{1}{8}\rho g \frac{\partial {H_T}^2}{\partial b}\sqrt{gd} = -\rho g f' \frac{H_T}{d} \cdot \frac{{H_T}^2 \sqrt{gd}}{d} \tag{9.19}$$

and then,

$$\frac{\partial {H_T}^2}{\partial b} = -8 f' \cdot \frac{H_T}{d} \cdot \frac{{H_T}^2}{d} \tag{9.20}$$

After some algebra one gets:

$$\frac{\partial H_T}{\partial b} = -4 f' \cdot \frac{{H_T}^2}{d^2} \tag{9.21}$$

Considering $H_T = K_T H_i$, it follows that:

$$\frac{\partial K_T}{\partial b} = -4 f' \cdot \frac{H_i K_T^2}{d^2} \tag{9.22}$$

and separating the variables,

$$\frac{\partial K_T}{K_T^2} = -4f' \frac{H_i \partial b}{d^2} \tag{9.23}$$

By integrating the previous Equation from zero to *B*:

$$\frac{1}{K_T} = \frac{1}{K_{T,0}} + 4f' \frac{H_i B}{d^2} \tag{9.24}$$

where $K_{T,0}$ represents the transmission coefficient for $B = 0$. If $B = B_t$ is assumed (Eq.6.7, reported below for ease of the reader), consistently with Buccino et al. (2014) , then $K_{T,0}$ is the transmissivity of a single row of Reef Balls.

$$B_t = (n-1)D_R \tag{6.7}$$

In a plane with $1/K_T$ on ordinates and the quantity $B_t H_i/d^2$ on the abscissa, the experimental points are expected to draw straight-line with a slope equal to $4f$ and an intercept of $1/K_{T,0}$. If we assume f' to be of the order 0.1, then the slope of the line would be 0.4 as an order of magnitude. As for $1/K_{T,0}$, we expect it to be slightly larger than 1.

Under the hypothesis of rough turbulent flow, the drag coefficient is assumed as an increasing function of the relative roughness h_s/d, which corresponds to the well-known Nikuradse ratio ε/D (i.e. the ratio between the characteristic dimension of the roughness, ε, and the diameter of a pipe, D). Moreover, it has been assumed that f' is a function of both the RB arrangement (shape of roughness) and the rate of breaking, which affects the characters of the dissipation.

In particular it has been set:

$$f'\left(\varphi; \frac{h_s}{d}; \frac{H}{d}\right) = \nu_\varphi\left(\frac{h_s}{d}; \varphi\right) \cdot \nu_{br}\left(\frac{h_s}{d}; \frac{H}{d}\right) \cdot f_0\left(\frac{h_s}{d}\right) \tag{9.25}$$

where:

- ν_φ is an arrangement correction factor;
- ν_{br} is related to the occurrence of breaking;

- f_0 is a basic drag coefficient, valid for very close modules and absence of breaking.

Since h_s/d also represents the relative submergence of the structure, it can be reasonably assumed that $K_{T,0}$ is a function of this parameter.
In a first approximation, it has been hypothesized that neither φ nor H/d affect $K_{T,0}$. The latter assumption comes from the absence of experiments with a single row in *DICEA-B* and *DICEA-C*; moreover, it is reasonable that $K_{T,0}$ slightly varies around 1, so that a detailed prediction of the latter is not really necessary.
As obvious, the transmission coefficient for a single row will increase with reducing h_s/d.
It is clear that the just derived model is rigorously appropriate in the absence of breaking, i.e. for $H_i/d \leq 0.28$. For structures located within the surf zone, a correction might be introduced through the factor ν_{br}, under the hypothesis that the dissipation mechanism is still dominated by macro-roughness.

9.4.2.2 Calibration of the CA friction model for non- breaking waves

In Figures form 9.58 to 9.61, the reciprocal of the measured transmission coefficient, $1/K_T$, is plotted against the quantity $\nu_\varphi \frac{BH_i}{d^2}$, for $H_i/d \leq 0.28$. The following values of the density factor have been found, with no differences between *DICEA-B* and *DICEA-C*.

$\mathbf{h_s/d}$	ν_φ
0.60	1
0.75	1
0.88	0.5
1	0.4

Table 9.18. Values of the density factor, ν_φ, for *DICEA-B* and *DICEA-C* configurations.

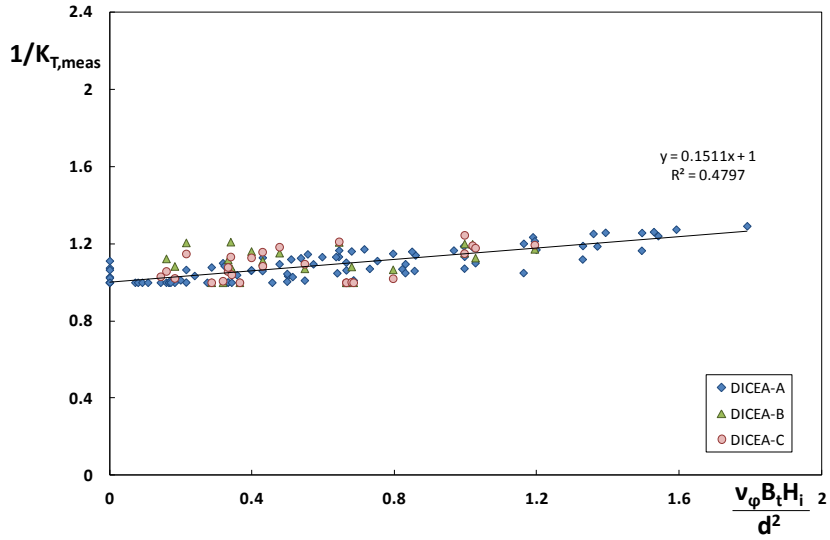

Figure 9.58. Plot of *DICEA* data in the plane ($1/K_{T,meas}$; $\nu_\varphi \frac{B_t H_i}{d^2}$) for $H_i/d \leq 0.28$ and h_s/d =0.6.

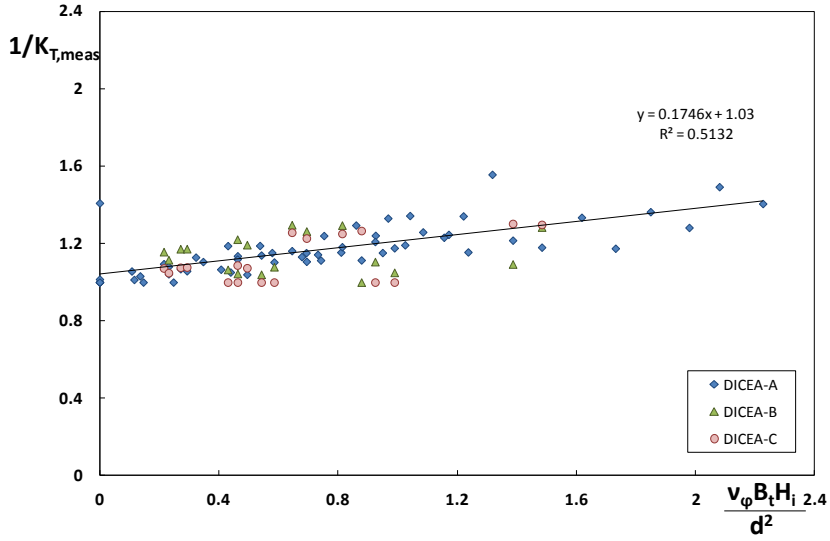

Figure 9.59. Plot of *DICEA* data in the plane ($1/K_{T,meas}$; $\nu_\varphi \frac{B_t H_i}{d^2}$) for $H_i/d \leq 0.28$ and h_s/d =0.75.

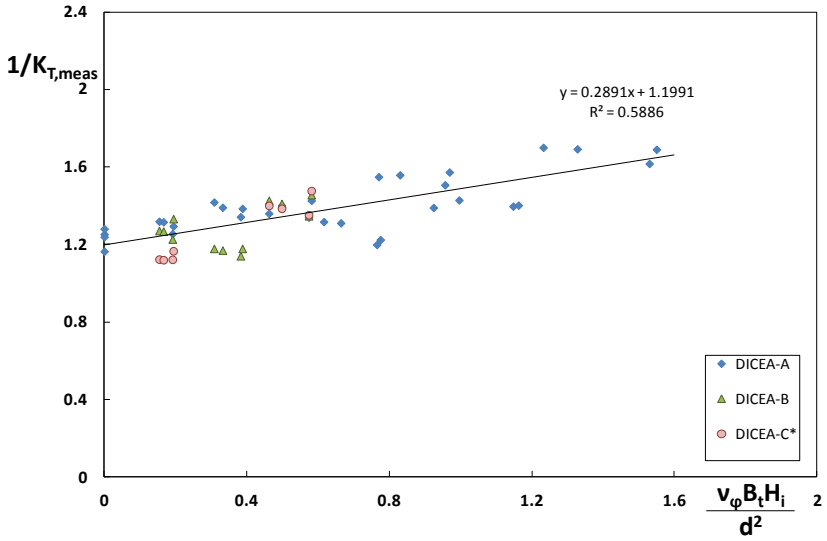

Figure 9.60. Plot of *DICEA* data in the plane ($1/K_{T,meas}$; $\nu_\varphi \frac{B_t H_i}{d^2}$) for $H_i/d \leq 0.28$ and $h_s/d = 0.88$.

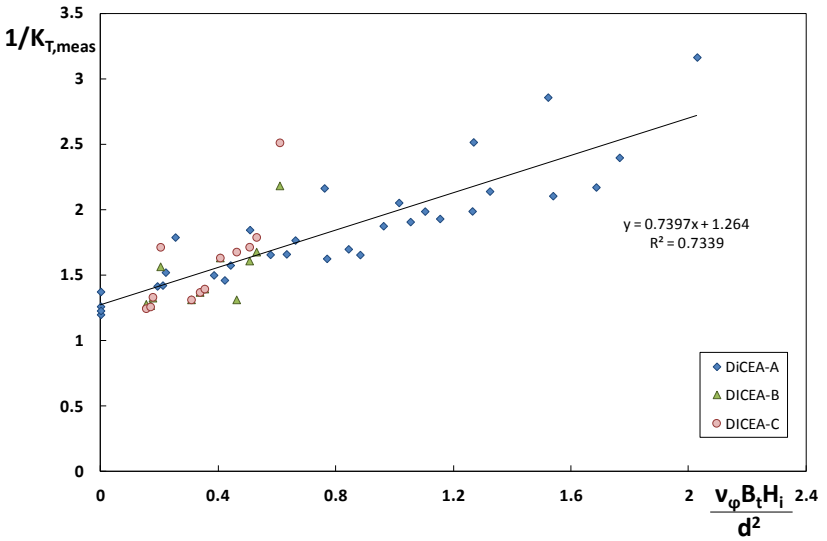

Figure 9.61. Plot of *DICEA* data in the plane ($1/K_{T,meas}$; $\nu_\varphi \frac{B_t H_i}{d^2}$) for $H_i/d \leq 0.28$ and $h_s/d = 1$.

It is seen that the spacing between modules produces a significant effect for structures with crests close to the still water level, whereas the response of submerged barriers is almost the same.

As a general remark, it is to mention that the *DICEA-B* and *DICEA-C* data respond to the variables in a weaker way, compared to the *DICEA-A*, with points the more scattered the smaller the submergence. Form a physical point of view this can be explained considering that when modules are placed very close to each other, they behave "like a structure" (say as single body) and, accordingly, the transmission coefficient appears rather predictable. On the other hand, when the spacing increases, the modules tend to respond like isolated units and the experimental data become more scattered.
Finally, after a least square fitting of the data plotted in Figures from 9.58 to 9.61, the following values of f_0 and $K_{T,0}$ have been found:

$\mathbf{h_s/d}$	$\mathbf{f_0}$	$\mathbf{1/K_{T,0}}$
1	0.74	1.26
0.88	0.29	1.20
0.75	0.17	1.03
0.60	0.15	1

Table 9.19. Values of drag coefficient, f_0, and the reciprocal of the transmission coefficient for a single row of RB modules, $1/K_{T,0}$.

The quantities above can be interpolated through the following relationships:

$$f_0 = 0.1058\left(\frac{d}{h_s} - 0.95\right)^{-0.627} \tag{9.26}$$

$$\frac{1}{K_{T,0}} = 0.9699\left(\frac{d}{h_s} - 0.95\right)^{-0.094} \tag{9.27}$$

As shown in Figure 9.62, the model fits the data rather well, with an R^2 of 0.83 and a global standard error of 0.06, that matches with our target.
The design Equations appear particularly suited to *DICEA-A*, where a standard error of 0.052 and R^2 =0.88 has been detected, although some scatter still exists for low-density configurations (Table 9.20).

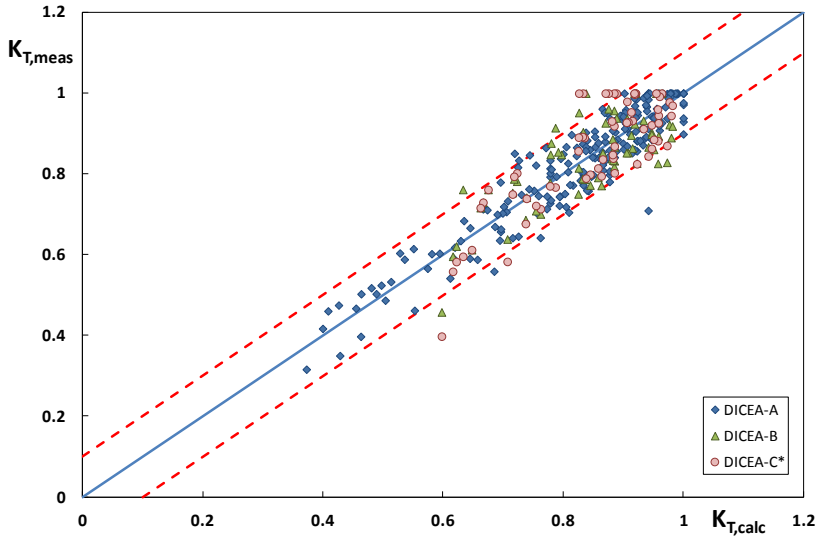

Figure 9.62. Comparison between measured and predicted (Eq. 9.24) transmission coefficients for *DICEA* data with $H_i/d \leq 0.28$.

Configurations	SE	R^2
All	0.060	0.83
DICEA-A	0.052	0.88
DICEA-B	0.070	0.62
DICEA-C	0.075	0.79

Table 9.20. Summary of the statistical characteristics for the *DICEA* data with $H_i/d \leq 0.28$.

9.4.2.3 Calibration of the CA friction model for slightly breaking waves

Appling the same approach described above to slightly breaking waves ($0.28 < H_i/d \leq 0.365$), the following correction factors, ν_{br}, have been found:

h_s/d	ν_{br}
0.60	1
0.75	1
0.88	0.8
1	0.6

Table 9.21. Values of the breaking factor, ν_{br} for $0.28 < H_i/d \leq 0.365$.

Results suggest that the presence of broken waves leads to a reduction of efficiency only for structures with a crest close to the still water level.
The comparison between predictions and measures is shown in Figure 9.63. Like for $H_i/d \leq 0.28$, the model returns a standard error of 0.06 with a R^2 equal to 0.83; in particular, a good performance has been especially found for *DICEA-A*, with R^2=0.88 and *SE*=0.052 (Table 9.22).

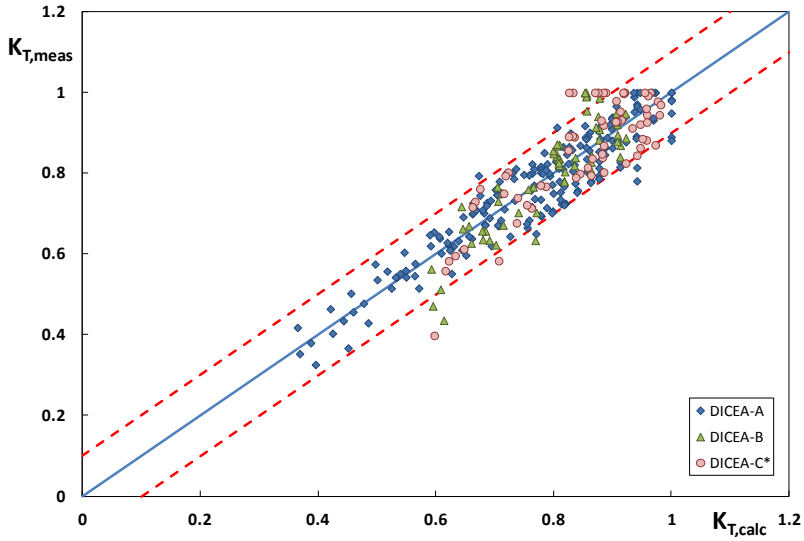

Figure 9.63. Comparison between measured and predicted (Eq. 9.24) transmission coefficients for *DICEA* data with $0.28 < H_i/d \leq 0.365$.

Configurations	SE	R^2
DICEA	0.060	0.83
DICEA-A	0.052	0.88
DICEA-B	0.069	0.79
DICEA-C	0.073	0.71

Table 9.22. Summary of the statistical characteristics for the *DICEA* data with $0.28 < H_i/d \leq 0.365$.

Considering all the *DICEA* data with $H_i/d \leq 0.365$, and applying the same methodology already discussed, the plot shown in Figure 9.64 has been

obtained, corresponding to a determination index of 0.83 and a standard error of 0.06 (Table 9.23) Summary of the statistical characteristics for the *DICEA* data for $Hi/d \leq 0.365$. The latter is internal to the acceptance bounds.

Moreover, Figure 9.65 and Figure 9.66 shown the comparison between the residuals and the predicted transmission coefficient and the normality plot, respectively.

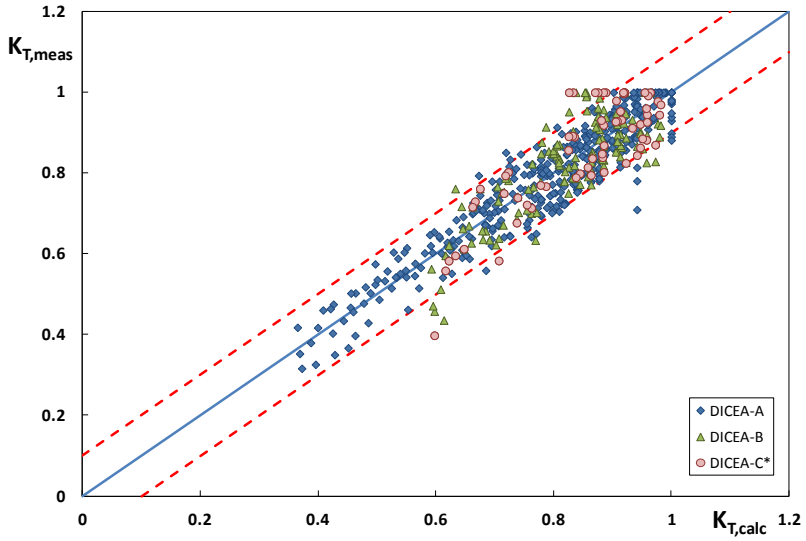

Figure 9.64. Comparison between measured and predicted (Eq. 9.24) transmission coefficients for *DICEA* data with $H_i/d \leq 0.365$.

Configurations	SE	R^2
DICEA	0.060	0.83
DICEA-A	0.052	0.89
DICEA-B	0.070	0.68
DICEA-C	0.072	0.71

Table 9.23. Summary of the statistical characteristics for the *DICEA* data for $H_i/d \leq 0.365$.

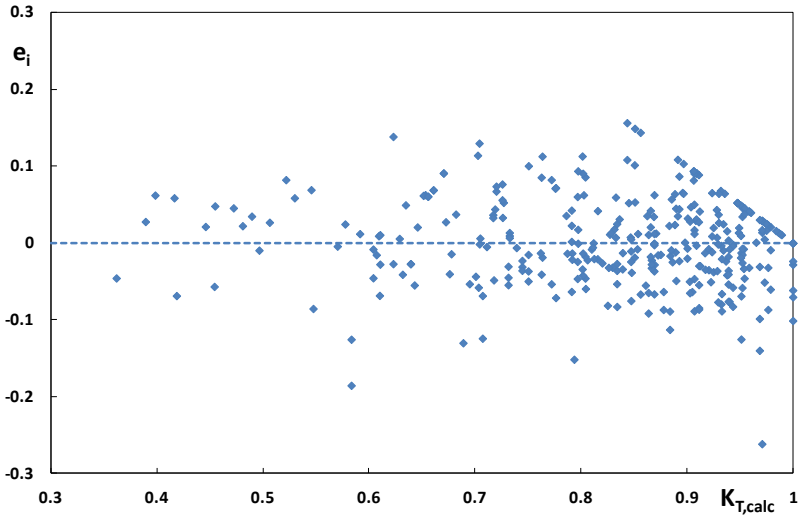

Figure 9.65. Plot of the residuals e_i vs. $K_{T,calc}$ according to Eq. (9.24), for the whole *DICEA* dataset with $H_i/d \leq 0.365$.

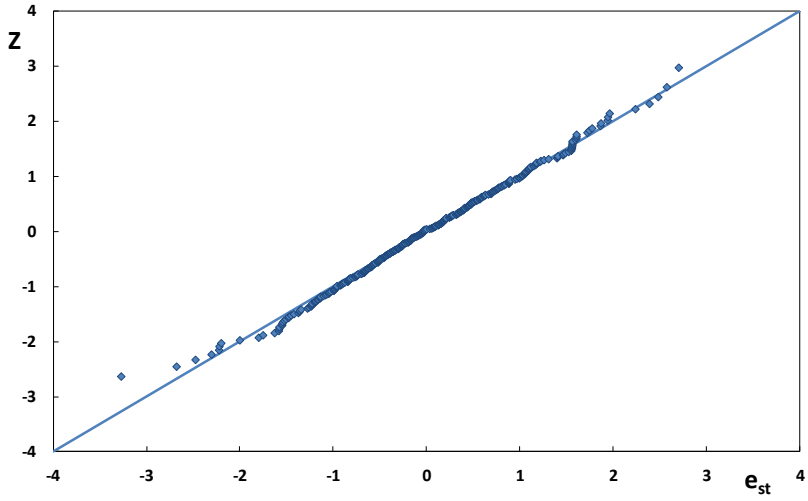

Figure 9.66. Normality plot for $H_i/d \leq 0.365$.

9.4.2.4 *Calibration of the CA friction model for heavily breaking waves*

When applied to heavily breaking waves ($H_i/d > 0.365$), the conceptual approach based on the bottom dissipation produces a surprisingly large scatter. After introducing the corrections reported in Table 9.24, a standard error of 0.071 has been obtained on the configuration *DICEA-A* (Figure 9.67).

h_s/d	ν_{br}
1	0.3
0.88	0.45
0.75	1
0.60	1

Table 9.24.Values of the breaking factor, ν_{br} for H_i/d >0.365.

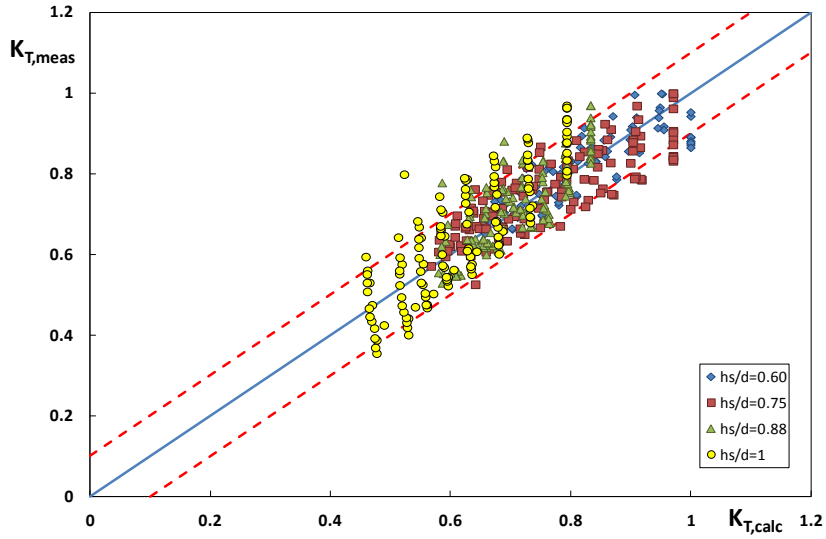

Figure 9.67. Comparison between measured and predicted (Eq. 9.24) transmission coefficients for *DICEA-A* data with H_i/d >0.365.

This deviation could indicate that the damping mechanism is no longer dominated by friction effects, but also by an increase of the strength of breaking.

Two hypotheses have been then formulated: one is that the structure influences the breaking process only if the crest is close to the still water level, the other is that dissipation is entirely dominated by breaking. The models developed according to these assumptions are presented hereinafter.

9.4.3 Development of a conceptual approach based on friction and breaking

Assuming that the dissipation can be governed, depending on the relative submergence, by either friction or breaking, a "mixed" model has been developed. The latter consists in using the asymptotic solution for small submergences (Eq. 9.28) of the model by Buccino et al. (2014) in the range of h_s/d =1÷0.88, whereas the predictive equations based on friction (Eq. 9.24) is assumed to be valid for h_s/d =0.75÷0.60. Thus, the "mixed" model results to be:

$$K_T{}^{1/2} = K_{T,0}{}^{1/2} - G\frac{B_t^*}{\sqrt{H_i L_0}} \qquad \text{for } 0.88 \le h_s/d \le 1 \tag{9.28}$$

$$\frac{1}{K_T} = \frac{1}{K_{T,0}} + 4f'\frac{H_i B}{d^2} \qquad \text{for } 0.60 \le h_s/d \le 0.75 \tag{9.24}$$

As shown in Figure 9.68 and Figure 9.69, the Equation (9.28) can fit the experimental data quite reasonably when a configuration factor v =0.55 is introduced for *DICEA-B* and *-C*. The configuration factor is rather close to the value 0.6 found by Buccino et al. (2014).

As for G and $K_{T,0}{}^{1/2}$, the estimated values are summarized in Table 9.25.

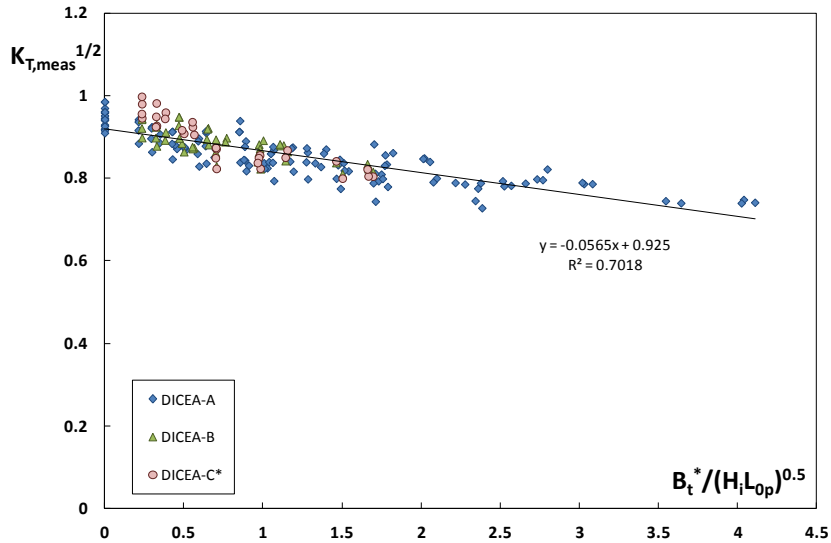

Figure 9.68. Fit of Eq. (9.28) for h_s/d =0.88.

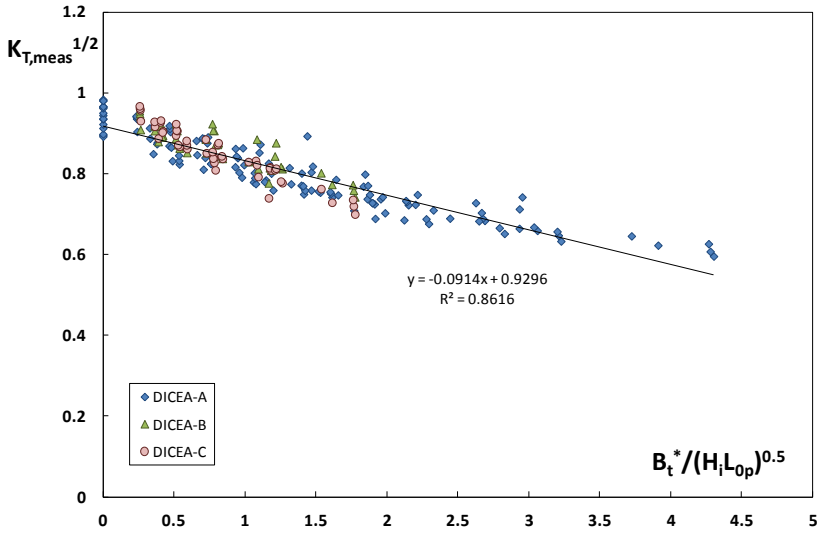

Figure 9.69. Fit of Eq. (9.28) for h_s/d =1.

h_s/d	G	$K_{T,0}^{1/2}$
0.88	0.0565	0.93
1	0.0914	0.93

Table 9.25. Estimated values of the dissipation factor, *G*, and $K_{T,0}^{1/2}$.

The "mixed-predictions" produce a standard error of 0.057 on *DICEA-A* and an overall scatter of 0.061 for all data with H_i/d >0.365. The comparison between predictions and measures are shown in Figure 9.70; the points lie clearly within the acceptance bands, even if a certain funnel structure of residuals is evident. Figure 9.71 and Figure 9.72 display the residuals vs. the predicted transmission coefficient and the normality plot. The statistical characteristic are summarized in the Table below.

Configurations	SE	R^2
DICEA	0.061	0.75
DICEA-A	0.057	0.82
DICEA-B	0.058	0.49
DICEA-C	0.069	0.60

Table 9.26. Summary of the statistical characteristics for the *DICEA* data for H_i/d >0.365.

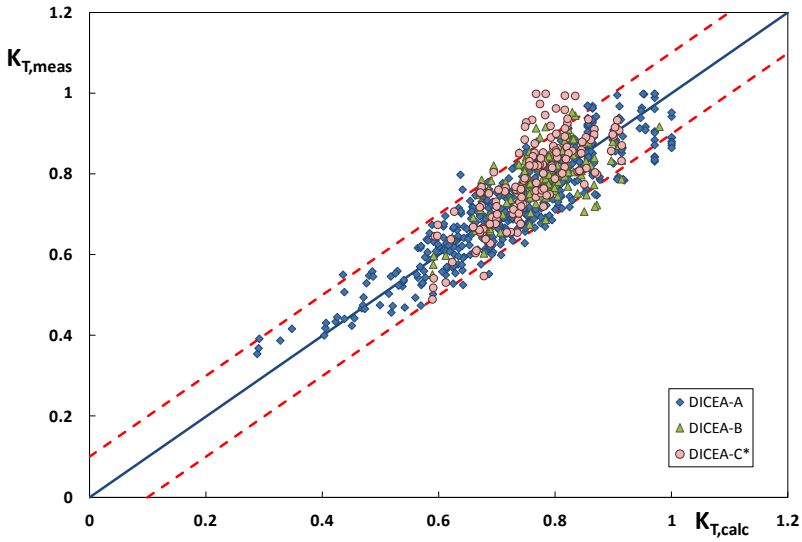

Figure 9.70. Comparison between measured and predicted transmission coefficients via the "mixed" model for *DICEA* data with H_i/d >0.365.

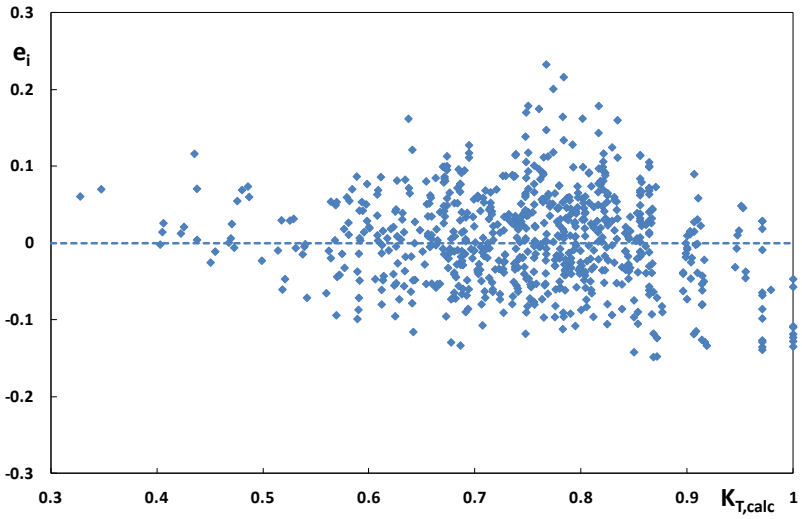

Figure 9.71. Plot of the residuals e_i vs. $K_{T,calc}$ according to the "mixed" model, for the whole *DICEA* dataset with H_i/d >0.365.

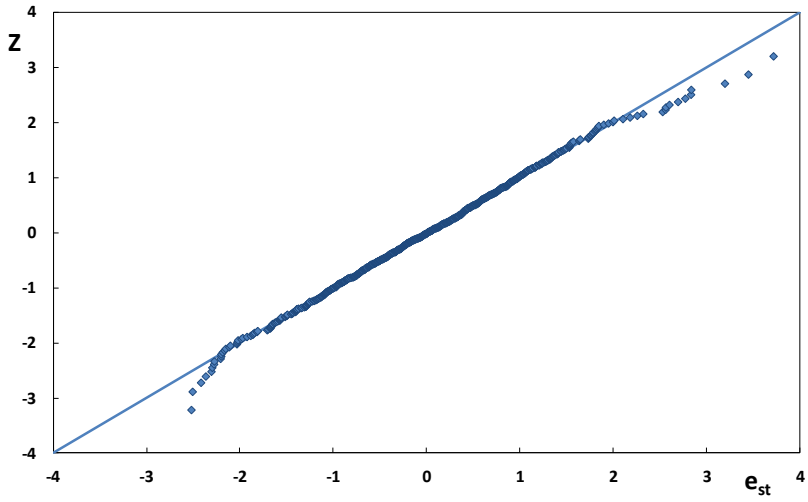

Figure 9.72. Normality plot of the "mixed" models.

9.4.3.1 Comparison with ERCD/CHL data

To have a first idea of the robustness of the previous method, the results provided by their application to *ERDC/CHL* data have been analyzed. Similarly to what already performed, the data characterized by H_i/d =0.83 have been removed.It is evident from Figure 9.73 that *ERDC/CHL* data agree rather well with the "mixed-model", in which both ν_φ and ν_{br} have been set equal to 1 for h_s/d lower than 0.83.

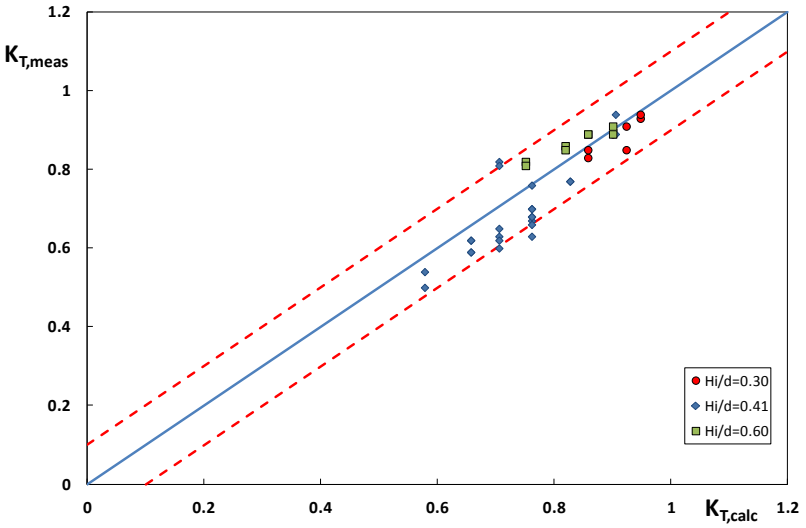

Figure 9.73. Comparison between measured and predicted transmission coefficients via the "mixed-model" for *ERDC/CHL* data.4

9.4.4 Development of a conceptual approach based on breaking

Under the hypothesis that the damping of waves occurs essentially by breaking, the set of Equations suggested by Buccino and Calabrese (2007a) can be used (Sect. 4.2).

First of all, the deeply submerged solution, given in Equation (4.52), has been applied to *DICEA-A*, for increasing values of H_i/R_c. Form Figures 9.74 to 9.76 it can be seen that the theoretical equation fits data rather well till a relative submergence H_i/R_c =1.34.

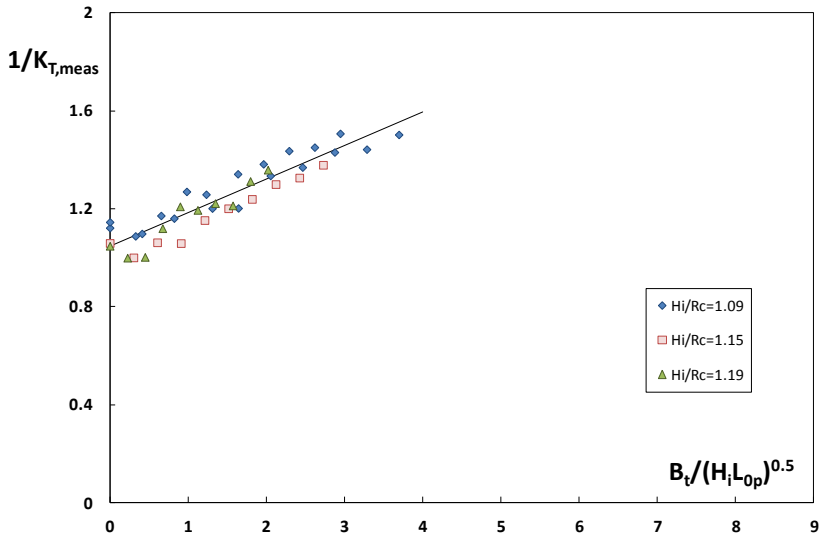

Figure 9.74. Application of Buccino and Calabrese (2007a) model for deeply submerged structures to *DICEA-A* data with $H_i/R_c \leq 1.19$.

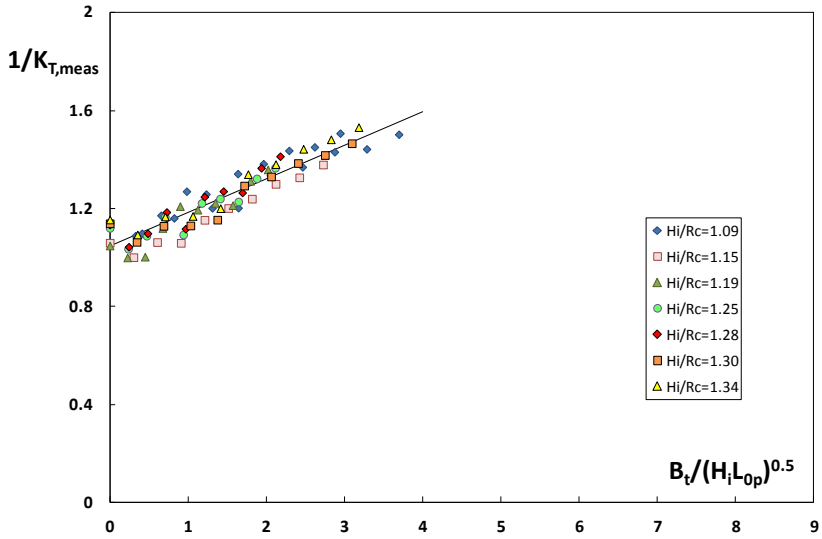

Figure 9.75. Application of Buccino and Calabrese (2007a) model for deeply submerged structures to *DICEA-A* data with $H_i/R_c \leq 1.34$.

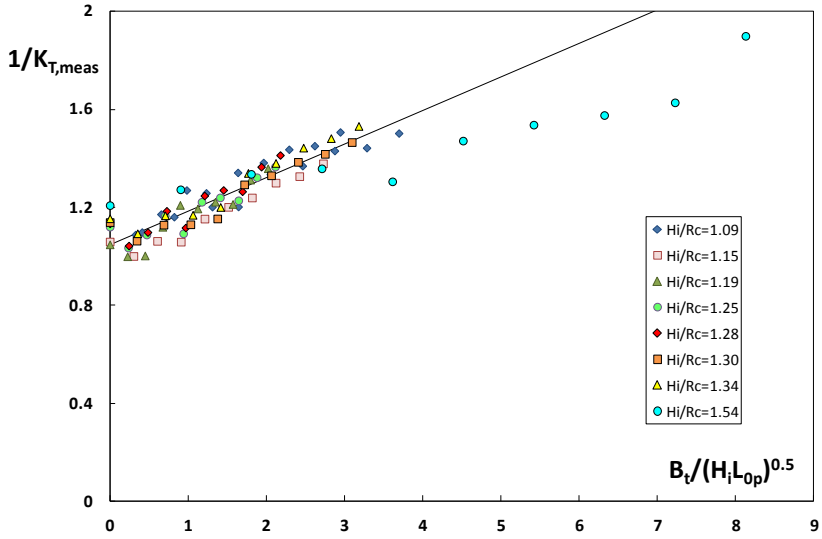

Figure 9.76. Application of Buccino and Calabrese (2007a) model for deeply submerged structures to *DICEA-A* data with $H_i/R_c \leq 1.54$.

Moreover, the Figure 9.77 shows a good agreement between data with $R_c = 0$ and the second asymptotic solution of the Buccino and Calabrese (2007a) model, given in Equation(4.53). This result appears to be consistent with what previously observed in the "mixed" model.

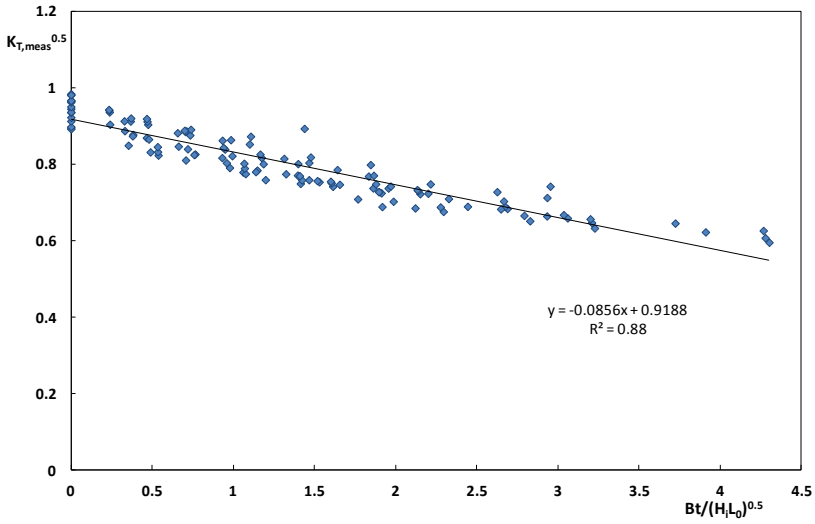

Figure 9.77. Application of Buccino and Calabrese (2007a) model for deeply submerged structures to *DICEA-A* data with *Rc* =0.

Finally, the predictive model expressed by Equation (9.29) has been defined for *DICEA-A*, while a linear interpolation is suggested for $H_i/Rc \geq 1.34$.

$$K_T = \frac{1}{1.048 + 0.137\left(\frac{H_i}{R_C}\right)^{1.5}\frac{B_t^*}{\sqrt{H_i L_0}}} \quad \text{for} \quad \frac{H_i}{R_C} < 1.54$$
$$K_T = \left(0.9188 - 0.0856\frac{B_t^*}{\sqrt{H_i L_0}}\right)^2 \quad \text{for} \quad Rc = 0 \tag{9.29}$$

The model exhibits R^2 =0.83 and *SE* =0.055.

As far as *DICEA-B* and *DICEA-C* are concerned, the model expressed by Equation (9.29) has been used for K_T predictions, and a mean configuration factor, *v*, has been searched for, by minimizing the standard error, *SE*, and imposing a bias included between ±0.01. As a result, an average configuration factor of 0.65 has been found, which leads to a standard error of 0.054 for *DICEA-B* and 0.068 for *DICEA-C*.

Overall, the Figure 9.78 shows the comparison between predictions and measures for all data with H_i/d >0.365 under the hypothesis of breaking

dominated dissipation process. A standard error of 0.061 has been obtained, which is slightly larger than that found with the "mixed-model" discussed before. Figure 9.80 and Figure 9.81 show the plot of the residuals vs. the predicted transmission coefficient and the normality plot.

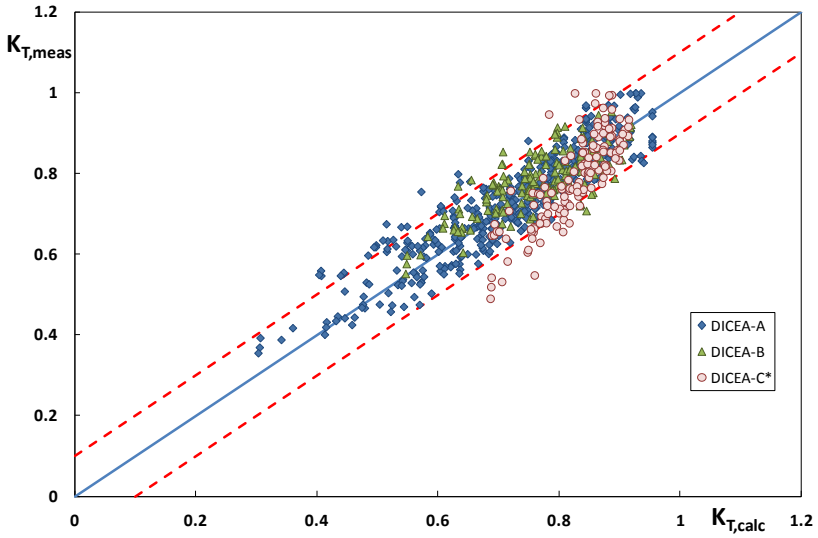

Figure 9.78. Comparison between measured and predicted transmission coefficients via the "purely breaking" model for *DICEA* data with H_i/d >0.365.

Configurations	SE	R^2
All	0.061	0.76
DICEA-A	0.055	0.83
DICEA-B	0.054	0.60
DICEA-C	0.068	0.68

Table 9.27. Summary of the statistical characteristics for the *DICEA* data with H_i/d >0.365, obtained from the application of the "purely breaking" model.

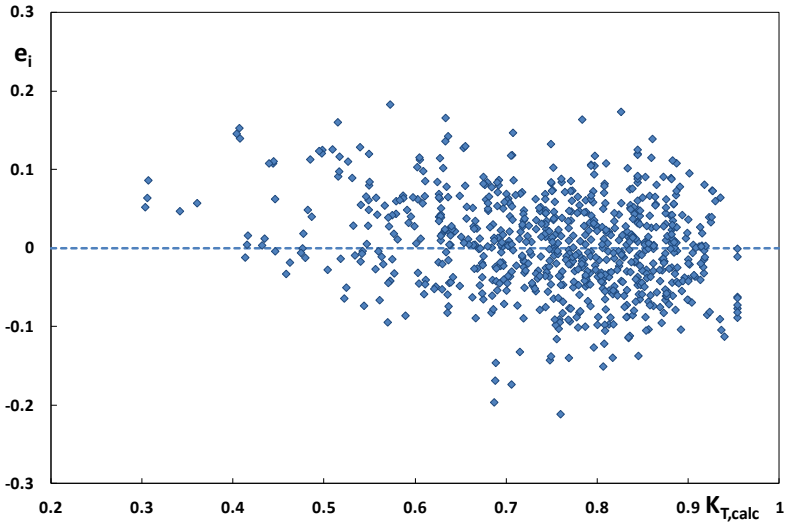

Figure 9.79. Plot of the residuals e_i vs. $K_{T,calc}$ according to the "purely breaking" model, for the whole *DICEA* dataset with H_i/d >0.365.

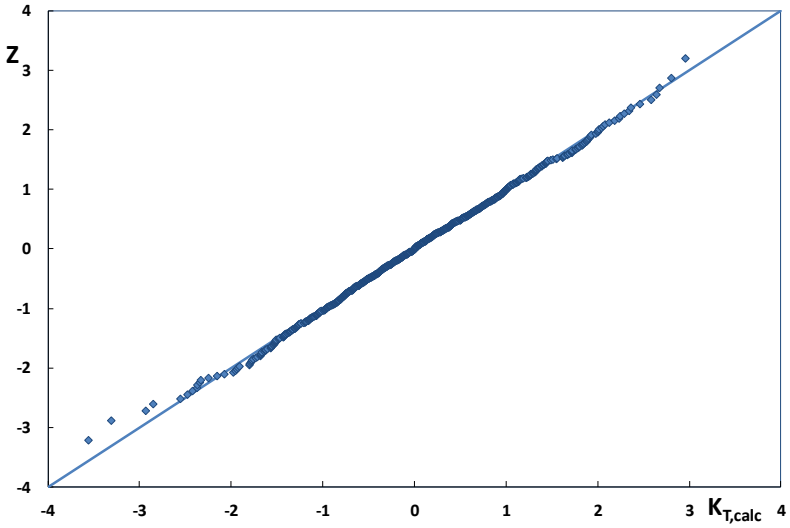

Figure 9.80. Normality plot of the "purely breaking" models.

9.4.4.1 Comparison with ERCD/CHL data

The application of the "breaking" model to the *ERDC/CHL* is shown in (Figure 9.81), where it possible to observe that, points with H_i/d equal to 0.30 and 0.60

can be reasonably predicted by the models while for H_i/d =0.41 a large overestimation con be observed.

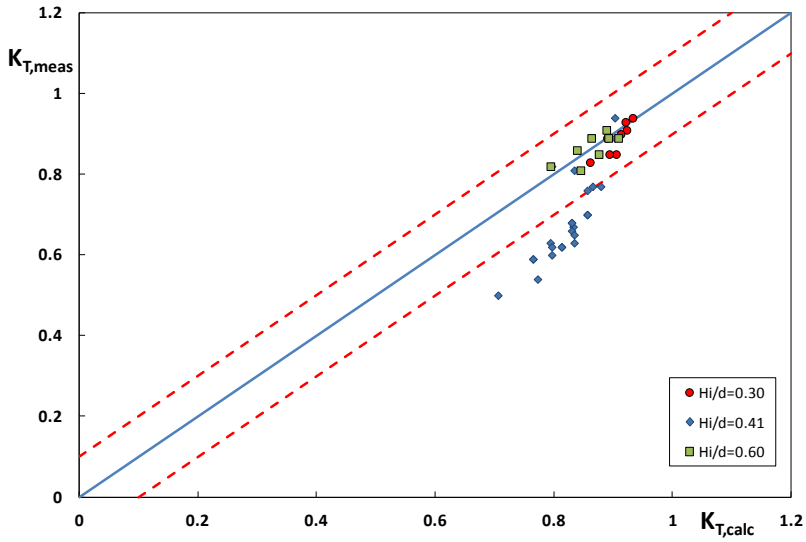

Figure 9.81. Comparison between measured and predicted transmission coefficients via the "purely-breaking" model for *ERDC/CHL* data.

Chapter 10 – ANALYSIS OF THE WAVE SET-UP FOR THE *DICEA* TESTS

As already discussed in Sect. (4.3), submerged breakwaters generally induce an increment of the medium see water level shoreward the structure (wave set-up), that often causes erosive nearshore currents in the protected area. More specifically, the wave set-up phenomenon is related to the reduction of the momentum flux due to the occurrence of the wave breaking on a conventional breakwater. Although the latter represents the main mechanism of energy dissipation for rubble mound breakwaters, it has been observed that, in case of Reef Ball barriers, a reduction of the transmission coefficient may occur even for non-breaking tests ($H_i/d \leq 0.28$), suggesting a different hydraulic behaviour of this type of structures (Chapter 9).

In order to study the effect of Reef Ball barriers on the shadow zone hydrodynamics, the results of the *DICEA* experimental campaign have been employed in this study. This represents the first attempt in literature to investigate wave set-up for this type of barriers.

Following the approach proposed by Diskin et al. (1970) for traditional breakwaters (Sect. 4.3), the ratio between the wave set-up measured in presence of the structure, δ_s, and the energetic wave height, H_{en}, has been plotted vs. R_c/H_{en}.

The results are shown from Figures 10.1 to 10.3, for each investigated configuration. From the observation of these graphs, the following considerations can be drawn:

- non-breaking ($H_i/d < 0.28$) and weakly-breaking ($0.28 < H_i/d < 0.365$) tests are characterized by an almost negligible value of the wave set-up, while slightly higher values are exhibited by heavily-breaking tests ($H_i/d > 0.365$). In the latter case the dimensionless set-up, δ_s/H_{en}, assumes values less than 0.2;

- no significant differences have been observed between *DICEA-A*, *-B* and *-C*;
- the Diskin's model (Eq. 4.62) provides δ_s/H_{en} values which are, for each configuration investigated, larger than the experimental ones, especially at low values of R_c/H_{en}.

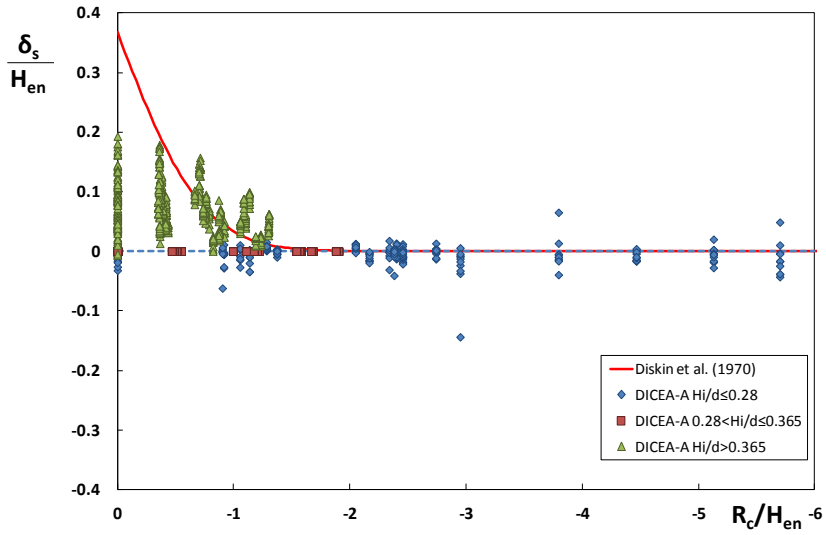

Figure 10.1. Wave set-up computed in the presence of structures for the *DICEA-A* data, grouped by H_i/d.

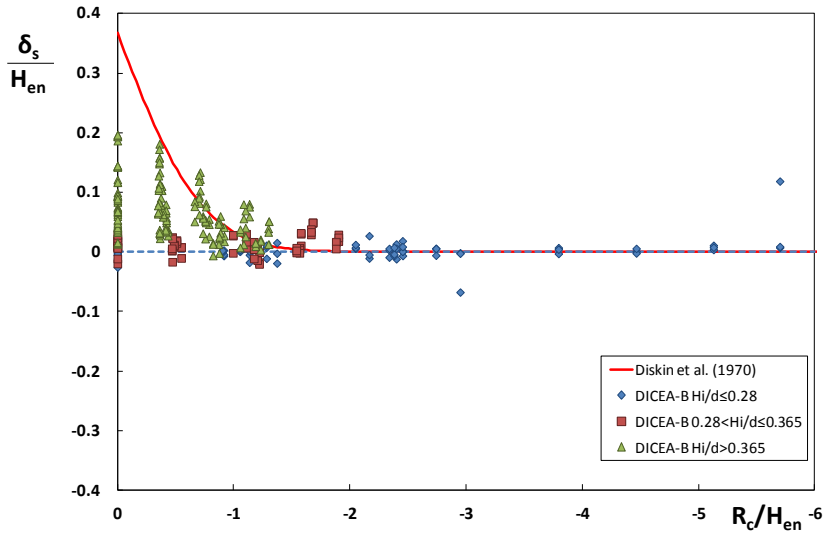

Figure 10.2. Wave set-up computed in the presence of structures for the *DICEA-B* data, grouped by H_i/d.

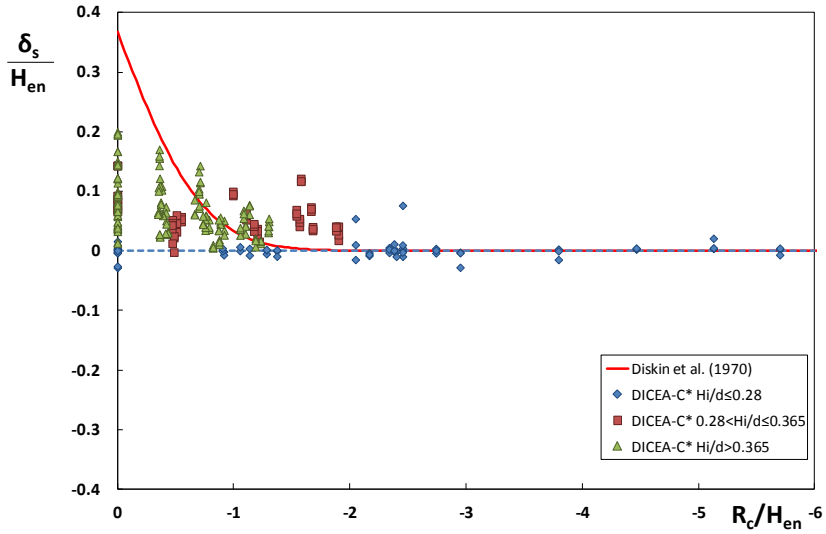

Figure 10.3. Wave set-up computed in the presence of structures for the *DICEA-C** data, grouped by H_i/d.

The graphs shown from Figures 10.4 to 10.6, in which the experimental tests have been simply grouped by h_s/d instead of H_i/d, clearly show that the wave set-up decreases as the submergence increases; accordingly, a reduction in energy dissipation implies lower values of the wave set-up.

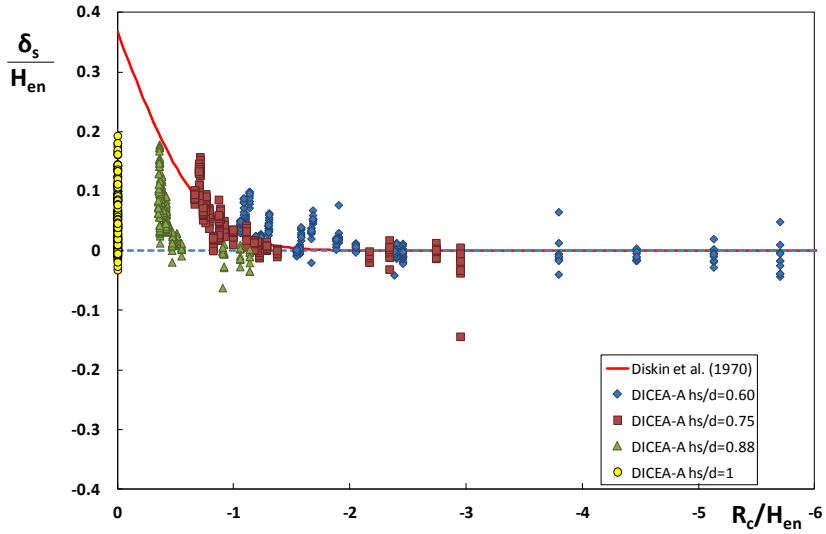

Figure 10.4. Wave set-up computed in the presence of structures for the *DICEA-A* data, grouped by h_s/d.

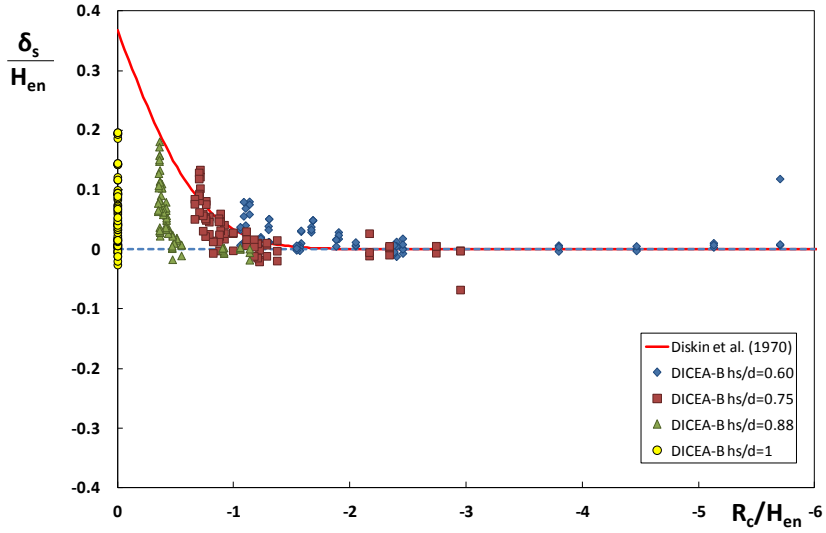

Figure 10.5. Wave set-up computed in the presence of structures for the *DICEA-B* data, grouped by h_s/d.

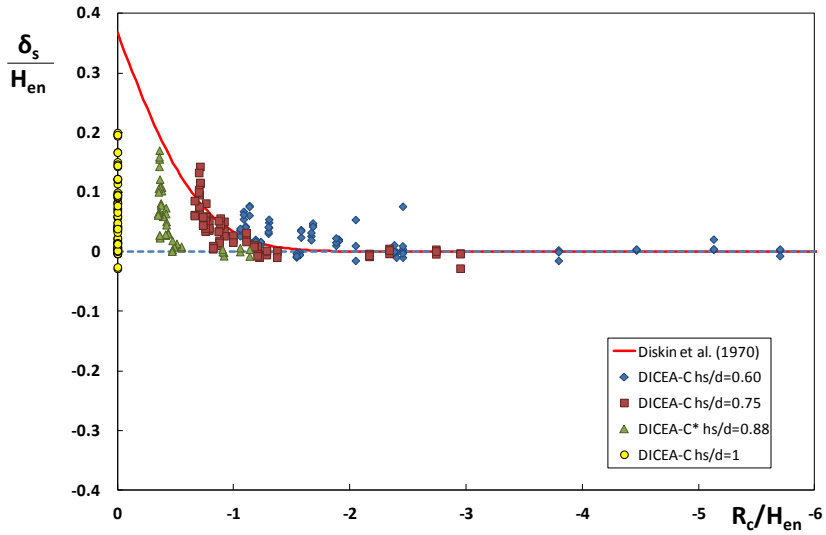

Figure 10.6. Wave set-up computed in the presence of structures for the *DICEA-C* data, grouped by h_s/d.

It is worth noting that the wave set-up measured in presence of structures can be obviously effected by the mean water level variation eventually occurring without the structures, δ_{ns}. Hence, instead of δ_s, the use of the difference between δ_s and δ_{ns}, seems more appropriate to assess the influence of a RB barrier on the littoral current. In fact, δ_s-δ_{ns} represents the hydraulic gradient leading to nearshore currents.

As it possible to observe from Figures 10.7 to 10.9, the presence of RB structures does not produce any significant variation of the mean still water level. Furthermore, for heavily-breaking waves and low submergences, an inversion from positive values of $\frac{\delta_s - \delta_{ns}}{H_{en}}$ to negative ones can be observed, which could indicate an inversion of the direction of nearshore currents, potentially reducing the erosion effect in the protected area.

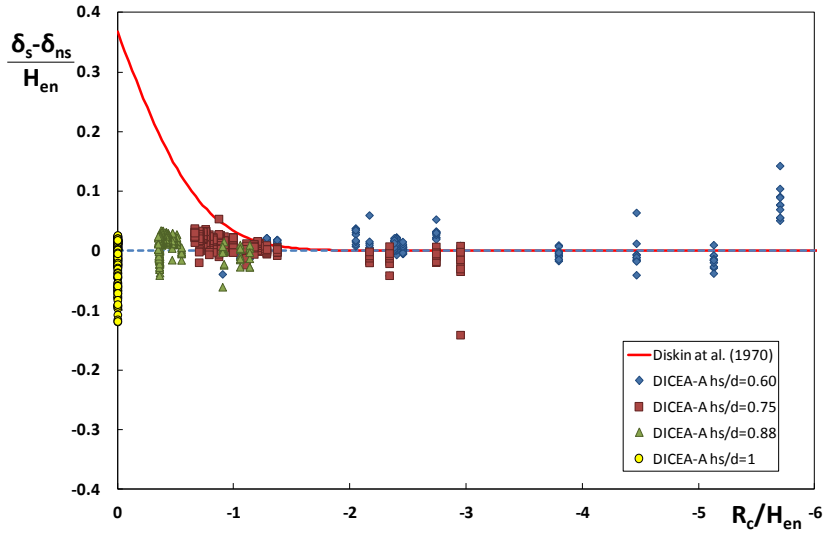

Figure 10.7. Wave set-up computed as difference between δ_s and δ_{ns} for the *DICEA-A* data, grouped by h_s/d.

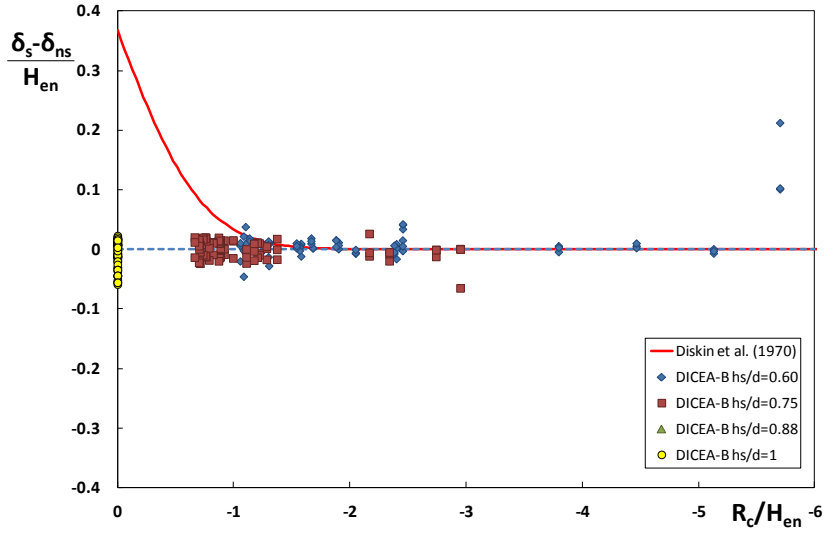

Figure 10.8. Wave set-up computed as difference between δ_s and δ_{ns} for the *DICEA-B* data, grouped by h_s/d.

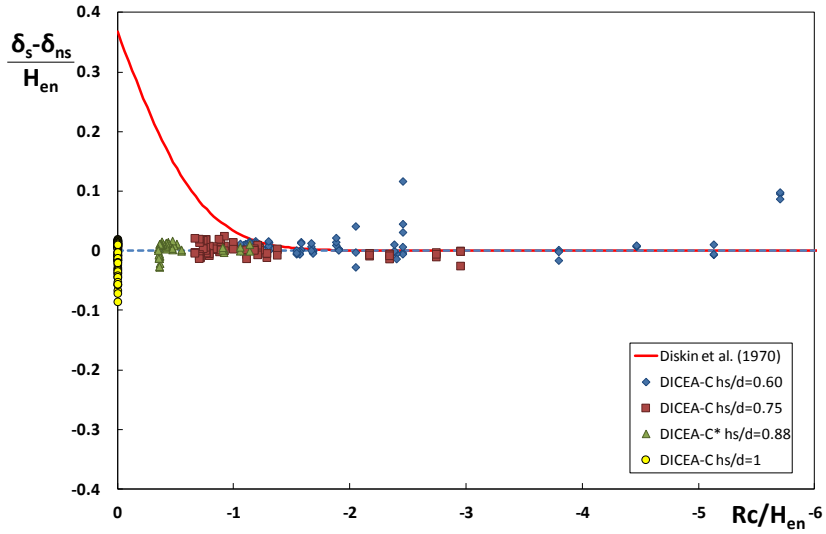

Figure 10.9. Wave set-up computed as difference between δ_s and δ_{ns} for the *DICEA-C* data, grouped by h_s/d.

Chapter 11 – WAVE PERIODS TRANSMISSION

It has long been known that the cross shore beach response to a wave attack strongly depends on wave period.
After a detailed review of literature, Kraus (1992) indicated a set of predictors by which engineers may infer the presence of a berm (beach accretion) or a bar (beach erosion) after a storm of given characteristics. The Author concluded that the most effective parameters are:

- the offshore wave steepness, $s_0 = \frac{2\pi H_0}{gT^2}$;
- the offshore Dean parameter $N_0 = \frac{H_0}{wT}$, where w indicates the fall velocity of sediments.

It was recognized that each of the above quantities must be small for a beach to accrete. The lower wave steepness, the more narrow the surf zone and accordingly the weaker the effects of the undertow current.
Analogously, a small Dean number implies a suspended sand particle to undergo a net movement in the shoreward direction instead of the seaward one.
Hence, the reduction of wave height alone does not lead necessarily to an improvement of the beach response predictors. The final behavior, rather depends on the rate of transmission of wave periods.
In fact, after the interaction with the structure, the wave height reduces from H_I to H_T and the shore is actually loaded by a different storm, which deep water wave height can be estimated as:

$$H_0' = \frac{H_T}{K_{sh}'} \tag{11.1}$$

where K'_{sh} is the shoaling coefficient[5], that also depends on the transmitted wave period.

[5]A simple normal attack is assumed.

From the definition of transmission coefficient, it follows that:

$$H_0' = \frac{K_T H_I}{K_{sh}'} = \frac{K_T K_{sh} H_0}{K_{sh}'} \tag{11.2}$$

where K_{sh} is calculated with reference to the incident storm without the structure. Since at the normal depths of placement of submerged breakwater it can be reasonably assumed $K_{sh} \cong K'_{sh} \cong 1$, it is readily obtained that the transmitted wave attack is equivalent to an ideal offshore wave steepness equal to:

$$s_{0T} = \left(\frac{K_T}{K^2_{T,T}}\right) s_0 \tag{11.3}$$

where $K_{T,T}$ generically indicates a transmission coefficient of the wave period.
The previous relationship suggests that the efficiency of a barrier in transforming an erosion event into an accretion one, actually depends on the quantity: $\left(\frac{K_T}{K^2_{T,T}}\right)$, which mixes the transmission coefficient of the wave height, K_T, with the square of the transmission coefficient of the wave period, $K_{T,T}$.
Following a similar path for the Dean number, it is readily obtained:

$$N_{0T} = \left(\frac{K_T}{K_{T,T}}\right) N_0 \tag{11.4}$$

From the Equations (11.3)-(11.4), it is clear that from the point of view of cross-shore sediment transport, a barrier should minimize K_T and maximize $K_{T,T}$. In particular, it would be convenient that the structure returned $K_{T,T} > 1$ (low pass filter) or at most $K_{T,T} = 1$.
To render the discussion on wave period more specific, it is worth noticing that while for the wave height H_{m0} is universally considered, in the engineering practice three characteristic periods are commonly employed: the peak period, T_p, the mean zero crossing wave period, T_{01}, and the "harmonic" average period, T_{-10}.

T_{01} and T_{-10} are defined in terms of spectral moments as follows:

$$T_{01} = \frac{m_0}{m_1} \tag{11.5}$$

$$T_{-10} = \frac{m_{-1}}{m_0} \tag{11.6}$$

Hence, for the transmission coefficient of T_{01} to be unitary, it is necessary that:

$$(T_{01})_T = (T_{01})_I \Rightarrow \frac{m_{0,T}}{m_{1,T}} = \frac{m_{0,I}}{m_{1,I}} \tag{11.7}$$

and then:

$$\frac{m_{1,T}}{m_{1,I}} = K_{m1} = \frac{m_{0,T}}{m_{0,I}} = K_T^2 \tag{11.8}$$

Analogously, for T_{-10}:

$$(T_{01})_T = (T_{01})_i \Rightarrow K_{m-1} = K_T^2 \tag{11.9}$$

Recalling that also the invariance of the peak period ($T_{p,T} = T_{p,I}$) is desirable it can be concluded that an efficient barrier should generate a transmitted spectrum as similar as possible to the incident one (whenever an increase of the characteristic periods is not possible). Unfortunately, a great deal of literature indicates that conventional breakwaters tends to increase the amount of high frequency power, so that $K_{T,T} < 1$.
As an example, Calabrese and Buccino (2007) found:

$$K_{m1} = 1.20K_T^2 \tag{11.10}$$

which implies a transmission coefficient of T_{01} equal to:

$$\left(K_{T,T}\right)_{01} = \frac{K_T^2}{K_{m,1}} = 0.83 \tag{11.11}$$

Combining the Equations (11.11) and (11.3), it is argued that a conventional breakwater produces a reduction of the equivalent offshore wave steepness only if

$$\frac{K_T}{\left(K_{T,T}\right)_{01}} < 1 \Rightarrow K_T < 0.83^2 = 0.69 \tag{11.12}$$

In other words, as long as the transmission coefficient does not fall below 0.69, the mean steepness of the waves attacking the shore will not reduce. If K_T =0.80, then waves behind the structure would steepen, likely aggravating the erosional response.

A similar reasoning can be repeated for T_{-10}, the transmission coefficient of which has been found to be 0.9 (Del Vecchio, 2006).

Figures from 11.1 to 11.6 plot K_{m1} and K_{m-1} vs. K_T^2 for *DICEA-A*, *-B* and *-C*. In the graph also the straight line found by Calabrese and Buccino (2007) and Del Vecchio (2006) are depicted.

It appears pretty clearly that the great permeability of modules reduces the generation of high frequency components, which is typical of conventional barriers, producing a transmitted wave spectrum more similar to the incident one. The following findings deserve to be highlighted:

- for *DICEA-A*, the transmitted spectrum appears substantially similar to the incident one for non-breaking waves. When the wave height to depth ratio overcomes 0.28 and K_T^2 <0.4, $K_{m,1}$ and $K_{m,-1}$ tend to be close to the curves of Calabrese and Buccino and Del Vecchio respectively;
- the spacing between the modules leads to a lower generation of high frequency components, with the transmitted spectrum which remains in similitude with the incident one.

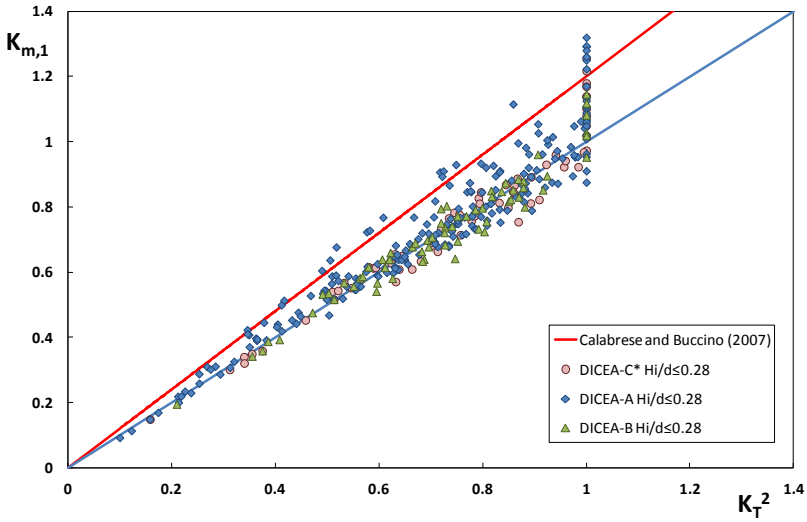

Figure 11.1 Comparison between K_T^2 and $K_{m,1}$ for the *DICEA* configurations with $H_i/d \leq 0.28$.

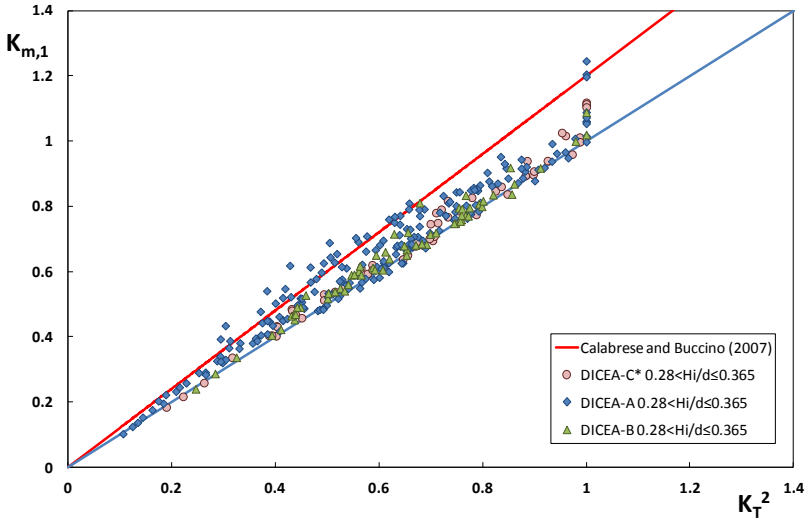

Figure 11.2 Comparison between K_T^2 and $K_{m,1}$ for the *DICEA* configurations with $0.28<H_i/d\leq 0.365$.

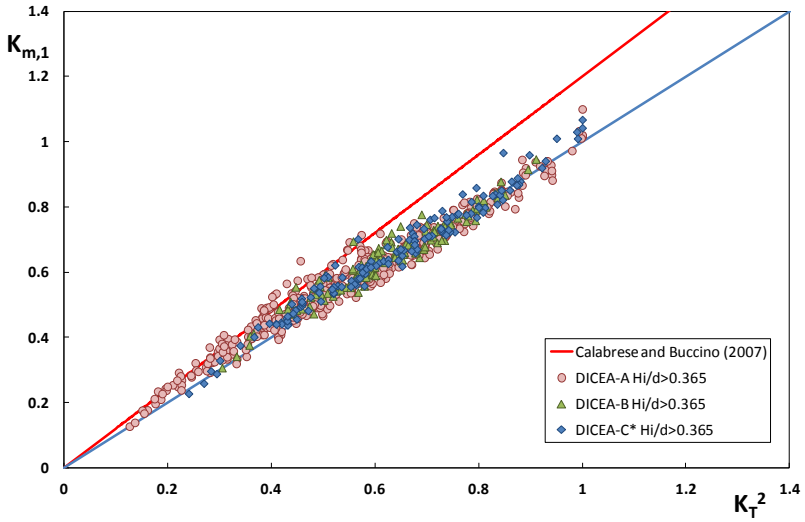

Figure 11.3 Comparison between K_T^2 and $K_{m,1}$ for the *DICEA* configurations with H_i/d >0.365.

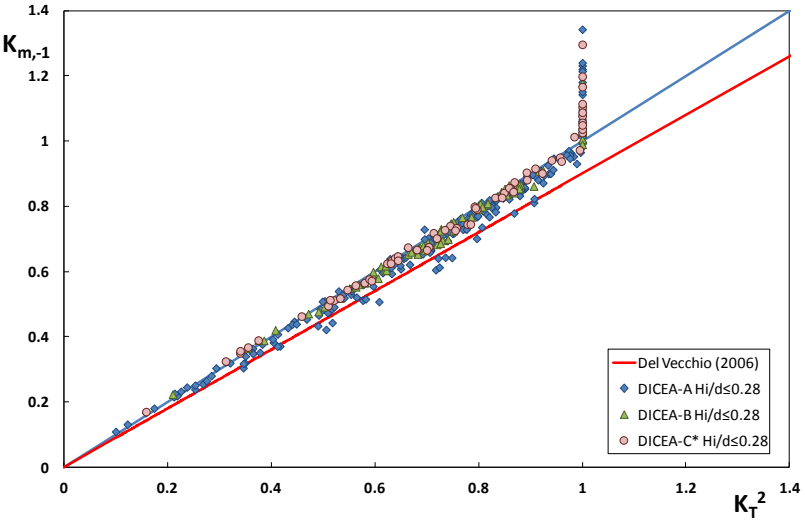

Figure 11.4 Comparison between K_T^2 and $K_{m,-1}$ for the *DICEA* configurations with $H_i/d \leq 0.28$.

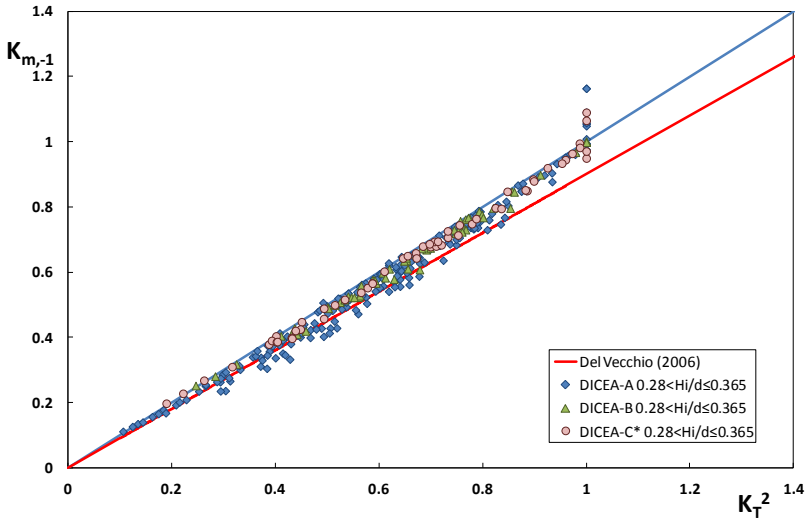

Figure 11.5 Comparison between K_T^2 and $K_{m,-1}$ for the *DICEA* configurations with $0.28< H_i/d \leq 0.365$.

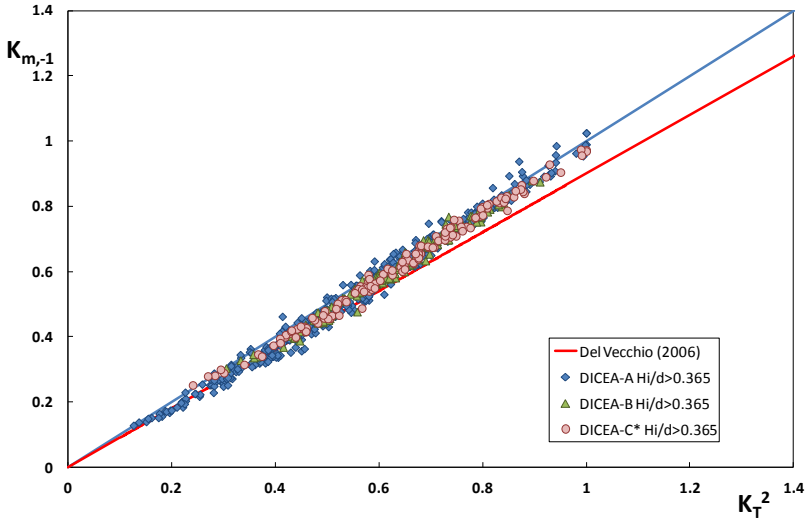

Figure 11.6 Comparison between K_T^2 and $K_{m,-1}$ for the *DICEA* configurations with $H_i/d >0.365$.

Altogether, a power form equation can be proposed for the prediction of K_{m1} and K_{m-1}:

$$K_m = aK_T^{2b} \tag{11.13}$$

The values of a and b are reported in Table 11.1. The cases in which the transmitted spectrum remains almost undistorted are characterized by $a = b = 1$.
In the Figures from 11.7 to 11.9 the incident peak period, T_{pi}, is compared to the transmitted one, T_{pT}.
In all cases no-systematic variation of the dominant frequency has been detected, like observed for traditional breakwaters. However, in a few experiments T_{pT} is lower than T_{pi}; no specific explanation has been found for this result, which might be also due to the technique used for smoothing the spectra.

Data-set	**H_i/d**	**$K_{m,1}$**		**$K_{m,-1}$**	
		a	**b**	**a**	**b**
DICEA-A	≤0.28	1.0	1.0	1.0	1.01
	0.28÷0.365	1.1	1.0	1.0	1.0
	>0.365	1.0	0.9	1	1.1
DICEA-B	≤0.28	1.0	1.0	1.0	1.0
	0.28÷0.365	1.0	1.0	1.0	1.01
	>0.365	1.0	0.9	1	1.1
*DICEA-C**	≤0.28	1.0	1.1	1.0	1.0
	0.28÷0.365	1.1	1.0	1.0	1.0
	>0.365	1.0	1.0	1.0	1.0

Table 11.1. Summary of *a* and *b* coefficients for the *DICEA* configurations.

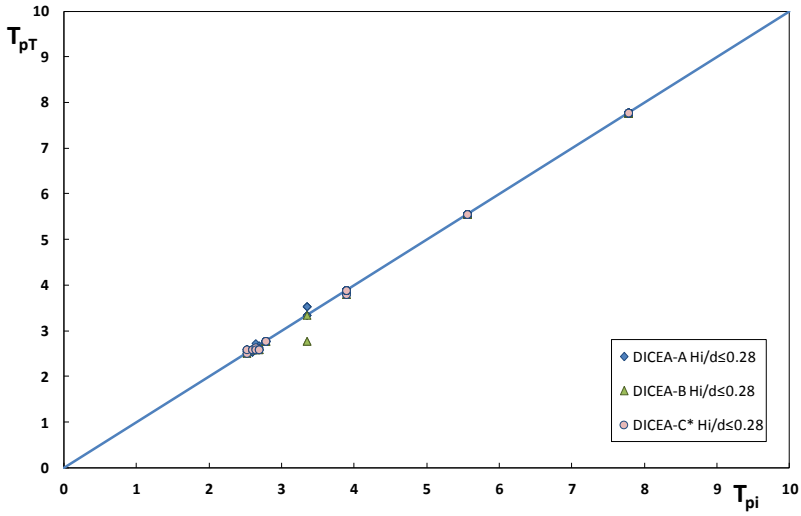

Figure 11.7 Comparison between T_{pT} and T_{pi} for the *DICEA* configurations with $H_i/d \leq 0.28$.

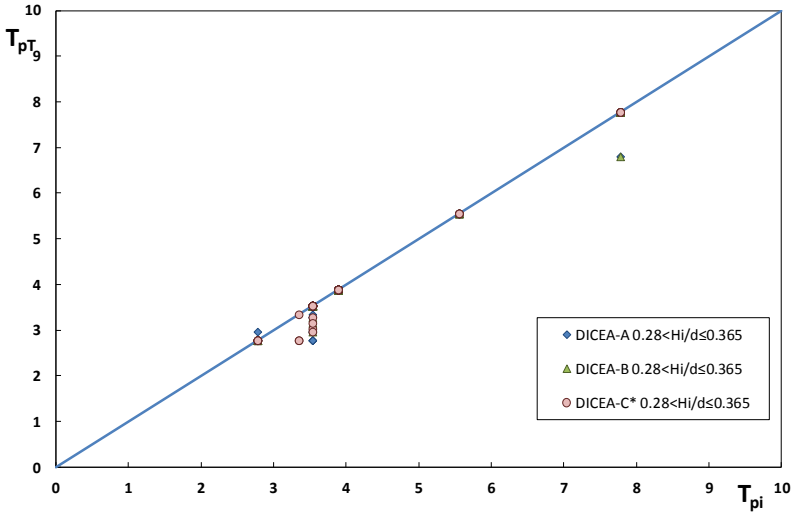

Figure 11.8 Comparison between T_{pT} and T_{pi} for the *DICEA* configurations with $0.28 < H_i/d \leq 0.365$.

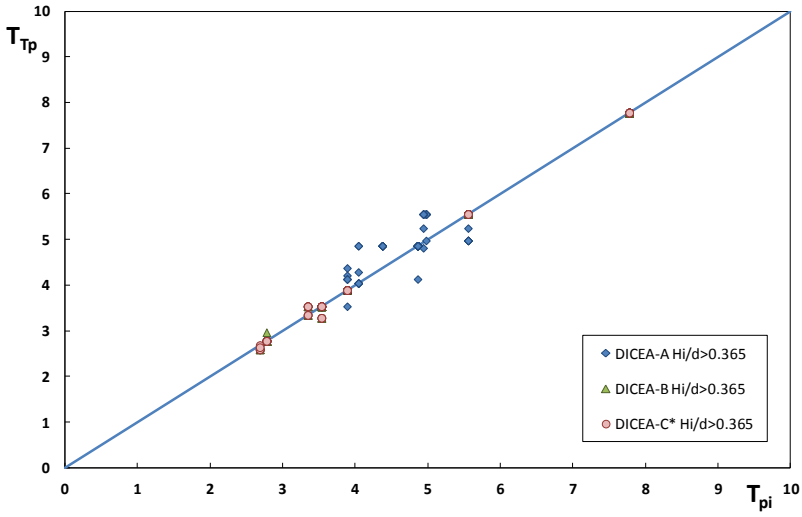

Figure 11.9 Comparison between T_{pT} and T_{pi} for the *DICEA* configurations with H_i/d >0.365.

Chapter 12 – CONCLUSIONS

The Reef Ball modules represent an endearing solution for beach erosion control, due to their capability of interacting with marine ecosystems.
Despite some evidences of successful protection has been provided, no systematic analysis on the hydrodynamic properties of such units has been developed so far.
In this study a great deal of random wave experiments have been conducted at the Department of Civil, Architectural and Environmental Engineering of the University of Naples "Federico II" with the purpose of having a deeper insight on several aspects of engineering significance, such as wave breaking occurrence, wave transmission, barrier induced wave set-up and characteristics of the transmitted spectrum.
Altogether, 1,440 tests have been collected on single layer bottom seated RB arrangements including different spacing among the modules. The results achieved can be summarized as follows.

- Reef Balls have been not observed to cause waves to break. Rather, in some cases they may accelerate the breaking occurrence in nearly unstable sea states. The dominant mode of dissipation is then macro-roughness, although when models are placed in a surf zone the rate of dissipation by breaking may be enhanced.

- Prediction of wave transmission appears more complicate than for traditional breakwaters, mainly because of the complex shape of the units in their large permeability. Generally, the presence of spacing among the modules leads to a less predictability essentially because the structure tends to behave like a series of isolated elements rather than an unique barrier. This produces a considerable scatter of data, even if the expected values of transmission coefficients is nearly the same. The derivation of a predictive equations capable of reducing the scatter up to the values commonly accepted for traditional breakwaters (a standard

error around 0.06) required actually a large number of parameters; this reflects the complexity of the process.

- A simple log-linear model proposed by Armono has been tested, which though did not lead to a reduction of data scatter consistent with our target. In particular a standard error around 0.07 has been obtained.

- The use of a conceptual approach to estimate K_T revealed itself rather fruitful, since allowed calibrating a number of parameters based on a clear physical meaning. In particular, a predictive scheme bearing on a dissipation mechanism dominated by friction has been developed, which provided promising results mainly when the structures are located outside the surf zone or in presence of a low number of breaking waves. Interestingly, a correction for taking into account the distance among the modules was necessary only for barrier with crest close to the still water level. As soon as the barrier becomes submerged the effect of spacing weakens.
  With increasing the number of breaking waves (structures located in the inner surf zone) a predictive method based on wave breaking proved more appropriate, especially for poorly underwater structures. In this case, a mixed model has been proposed in which the main dissipation mechanism is breaking for structure height to depth ratios larger than 0.88, and friction for deeper submerged barriers. Altogether the conceptual approach allowed keeping the standard error within the desired value of 0.06.

- As a counterpart of a larger rate of transmission compare to the traditional breakwaters, RB modules produce a nearly zero wave set-up in the sheltered area. The latter is in fact responsible of a structure generated rip currents which may heavily affect the shoreline response. As a relevant variable in this process the difference between the wave set-up with and without structures have been studied. The latter represents the alongshore hydraulic gradient which activates the feeder of rear rip. Surprisingly, it has been found that when the crest of the

barrier is close to the sea level, the difference above becomes negative, indicating a favorable (accreting) circulation from the heads to the center of the structure. This result appears rather important and deserves to be further verified, also with a direct comparison with conventional breakwaters.

- For the beach response, also the transmission of wave periods must be accounted for. It has been shown that the permeability of RB modules lead to transmitted spectra rather similar to the incident ones, reducing the generation of high frequency components typical of conventional breakwaters. The latter leads waves to steepen and may trigger unwanted erosional mechanisms. A set of predictive formulae for the mean spectral periods T_{01} and T_{-10} have been provided for design purposes.

The effect of this study on the Italian engineering community has been interesting till now. Based on preliminary results on wave transmission a shore protection barrier consisting of three rows of modules has been designed at lido *Onda Azzura* in Duna Verde, Caorle (VE).
At the same time a contract has been stipulated with the City of Riccione (RI) for a desk and experimental study aimed to the placement of a 150 m long structure including five rows of modules. The latter is of interest because it would represent the first structural protection measure in the region of Emilia Romagna (ER) after nearly 10 years. The government of ER accepted to derogate in virtue of the highly environmental compatibility of RBs.

BIBLIOGRAPHY

Ahrens, J.P. (1987). "Characteristics of reef breakwaters". Technical report, CERC, Viksburg, Technical Report CERC-87-17.

Allsop, N.W.H. (1983). "Low-crest breakwaters, studies in random waves". Proceeding of Coastal Structures'83, Arlington, Virginia, 94-107.

Allsop, N. W. H., Durand, N. and Hurdle, D. P. (1998). "Influence of steep seabed slopes on breaking waves for structures design" Proceedings of 26th Int. Conf. Coastal Eng, ASCE, Los Angeles, 906-919 .

Armono, H. D. (2003). "Hemispherical Shaped Artificial Reefs". Dissertation. Queen's University, Kingston, Ontario, Canada.

Armono, H.D. and Hall, K.R. (2003) "Wave transmission on submerged breakwaters made of hallow hemispherical shape artificial reefs". Proceedings of 31st annual conference of the Canadian Society for Civil Engineering Moncton, New Brunswick, Canada.

Arnouil, D. S. (2008). "Shoreline Response for a Reef Ball™ Submerged Breakwater System offshore of Grand Cayman Island". Degree of Master of Science in Ocean Engineering, Melbourne, Florida.

Baine, M. (2001). "Artificial reefs: a review of their design, application, management and performance". Ocean and Coastal Management, ELSEVIER, (44), 241-259.

Bali, J. (2006). "Using Reef Balls to protect critical turtle habitatin Sarawak, Malaysia". (www.ioseaturtles.org/).

Barber, R.T. (2001). "Reef Ball™: An Advanced Technique to Mimic Natural Reef System using Designed Artificial Reef". (www.artificialreefs.org).

Basco, D. (1985). "Qualitative description of wave breakers (motion patterns)". Journal of Waterway, Port, Coastal and Ocean Engineering, ASCE, 111 (2), 171-188.

Battjes, J.A. (1974). "Surf Similarity". Coastal Engineering. 14, 466-480.

Battjes, J.A. and Janssen, J.P.F.M. (1978). "Energy loss and set-up due to breaking of irregular waves". Proceeding of 16th Coastal Engineering Conference, Hamburg, 1, 563-587.

Battjes, J.A. and Stive, M.F. (1985). "Calibration and verification of a dissipation model for random breaking". Journal of Geophysical Research: Oceans (1978-2012) 90(C5), 9159-9167.

Bellotti, G. (2004). "A simplified model of rip currents system around discontinuous submerged barriers". Coastal Engineering 51(4). 185-203.

Bijlsma, L., Ehler, C.N., Klein, R.J.T., Kulshrestha, S.M., McLean, R.F., Mimura, N., Nicholls, R.J., Nurse, L.A., Perez Nieto, H., Stakhiv, E.Z., Turner, R.K. and Warrick, R.A. (1996). "Coastal Zones and Small islands". In Impacts, Adaptations and

Mitigation of Climate Change: Scientific Technical Analyses, Watson, R.T., Zinyowera, M.C. and Moss, R.H. (eds). Cambridge University Press, Cambridge.

Buccino, M. and Calabrese, M. (2007a). "Conceptual Approach for Predicting of Wave Transmission at Low-Crested Breakwater". Journal of Waterway, Port, Coastal and Ocean Engineering. ASCE, 213-224.

Buccino, M. and Calabrese, M. (2007b). "Physically to wave transmission at low-crested breakwater". Proceedings of Coastal Structures. Venice, Italy, July, 2007.

Buccino, M, Del Vita, I. and Calabrese, M. (2014). "Engineering modelling of wave transmission of Reef Ball™". Journal of Waterway, Port, Coastal and Ocean Engineering.

Burcharth H.F., Hawkins T., Zanuttigh B. and Lamberti A., (2007). "Environmental Design Guidelines for Low Crested Coastal Structures".

Burke, L., Kura, Y., Kasem, K., Revenga, C., Spalding, M. and McAllister, D. (2001). "Coastal Ecosystems". Washington DC World Resource Institute.

Calabrese, M., Vicinanza, D. and Buccino, M. (2002). "Large scale experiments on the behaviour of low crested and submerged breakwaters in presence of broken waves". Proceeding of 28th International Conference on Coastal Engineering, ASCE, pp: 1900-1912.

Calabrese, M., Vicinanza, D. and Buccino, M. (2003). "Low-crested and Submerged Breakwaters in Presence of Broken Waves". Proceeding of International Conference Towards a Balance Methodology in European Hydraulic Research, 22-23 May 2003 Budapest, 8/1-8/23.

Calabrese, M., Vicinanza, D. and Buccino, M. (2005). "Verification and re-calibration of an engineering method for predicting 2D wave setup behind submerged structures". Proceeding of the 2nd International Coastal Symposium, Hoepn, Iceland, June 2005.

Calabrese, M, and Buccino, M. (2007). "Estimating power spectral density behind low crested breakwaters". Proceedings of the 5th International Conference on Coastal Structures (1),805-816.

Calabrese, M., Buccino, M. and Pasanisi, F. (2008a). "Wave breaking macrofeatures on a submerged rubble mound breakwater". Journal of Hydro-environment Research, ELSEVIER, 1, 216-225.

Calabrese, M., Vicinanza, D. and Buccino, M. (2008b). "2D wave setup behind submerged breakwaters". Ocean Engineering, ELSEVIER, 35, 1015-1028.

Calabrese, M., Di Pace, M., Buccino, M., Tomasicchio, G.R., and Ciralli, E. (2011). "Nearshore circulation at a coastal defence system in Sicily. Physical and numerical experiments". Journal of Coastal Research ISSUE 64:474-478.

Costanza, R., d'Arge, R., deGroot, R., Farber, S., Grasso, M., Hannon, B., Naeem, S., Limburg, K., Paruelo, J., O'Neill, R.V., Raskin, R., Sutton, P. and ven den Belt, M. (1997). "The value of the world's ecosystem services and natural capital". Nature 387, 253–260.

d'Angremond, K. Van der Meer, J.W. and De Jong, R.J. (1996). “Wave transmission at low-crested structures”. Coastal Engineering, 2418-2426.

Daemen, I.F.R. (1991). “Wave transmission at low-crested structures”. MSc Thesis Delft University of Technology, Facoulty of Civil Engineering, Delft Hydraulics Report H 462.

Daemrich, K. and Kahle, W. (1985). “Schutzwirkung von Unterwasser Wellen brechern unter dem Einfluss unregelmässiger Seegangswellen. Eigenverslag des Franzius-Instituts fur Wasserbau und Küsteningenieurswesen”. Technical Report Helf 61. (In German).

Dalrymple, R.A., and Dean, R.G. (1971). “Piling-up behind low and submerged permeable breakwaters”. Discussion note on Diskin et al. (1970). Journal of Waterways and Harbor Division WW2, 97(2), 423-427.

Danel, P. (1952). “On the limiting clapotis”. Gravity waves, US Department of Commerce, National Bureau of Standards, Circular no. 521, 35-38.

Dar I.A., Dar, M.A., (2009). “Prediction of shoreline recession using geospatial technology; a case study of Chennai Coast, Tamil Nadu, India”. Journal of Coastal Research, Vol. 25(6), 1276-1286.

Dattatri, J., Raman, H., ShanKar, N.J. (1978). “Performance Characteristics of submerged breakwaters”. Proceeding of 16th Conference on Coastal Engineering, Hamburg, Germany No.16, 2153- 2171.

de Jong, R. J. (1996). “Stability of tetrapods, crest and rear of a low crested breakwater”. MS thesis, Delft University of Technology, Delft, The Netherlands.

Dean, R.G., Chen, R. and Brower, A.E. (1997). “Full scale monitoring study of a submerged breakwater, Palm Beach, Florida, USA”. Coastal Engineering, Elsevier, 29, (3-4), 291-315.

Del Vecchio, G. (2006). “Analisi teorico sperimentale sulle trasformazioni indotte da una barriera a cresta bassa allo spettro di potenza di onda regolari”. M. Sc Thesis. (In italian).

Del Vita, I. (2012). “Trasmissione ondosa a tergo di barriere sommerse in elementi Reef Ball”. M. Sc Thesis. (In italian).

Di Pace, P. (2006). “Riflessione di onde regolari in presenza di opera a gettata”. Ph.D Thesis, University of Naples “Federico II, Italy. (In italian).

Dick, T.M, (1968). “On solid and permeable submerged breakwater”. CE Research Report No. 59. Queens University, Ontario.

Diskin, M.H., Vajada, M.L. and Amir, I. (1970). “Piling-up behind low and submerged permeable breakwaters”. Journal of Waterways and Harbor Division WW2, 96(2), 359-372.

Douglas, B.C. and Peltier, W.R. (2002). “The puzzle of global sea-level rise”. In Physics Today 55:35–41

Draper, N.R. and Smith, H. (1998). “Applied regression analysis” (third edition). Wiley Series in Probability and Statistics.

Friebel, H. and Harris, L. (2004). "A new wave transmission coefficient model for submerged breakwaters". Proceedings 29th International Conference on Coastal Engineering, Lisbon, Portugal.

Galvin, C. J. (1968). "Breaker type classification on three laboratory beaches.". Journal Geophysical Research, AGU, 73 (12), 3651-3659.

Galvin, C. J. (1969). "Breaker traveller and choice of design wave height". Journal Waterways Harbour Division, ASCE, 9 (2), 175-200.

Garcia, N., Lara, J. L. and Losada, J. L. (2004). "2D numerical analysis of near-field flow at low crested permeable breakwaters". Coastal Engineering 51(10), 991–1020.

Gironella, X., Sànchez-Arcilla, A., Briganti, R., Sierra, J.P. and Moreno, L. (2002). "Submerged detached breakwaters: towards a functional design". Proceeding of International Conference of Coastal Engineering, ASCE. Reston, Va.,1768–1776.

Goda, Y. (1964). "Wave forces on a vertical circular cylinder: Experiments and a proposed method of wave force computation". Report of the Port and Harbour Research Institute. Ministry of Transportation, 8, 74.

Goda, Y., Takeda, H. and Moriya, Y. (1967). "Laboratory Investigation on Wave Transmission over Breakwaters". Port and Harbour Technical Research Institute.

Goda, Y. (1970). "A synthesis of breaker indices". Trans, JSCE, 2, 227-230.

Goda, Y. (1974). "New wave pressure formula for composite breakwater". Proceeding 14th Coastal Engineering Conference, ASCE, 1702-1720.

Gómez Pina, G. and Valdéz Fernández de Alarcón, J.M.V.Z (1990). "Experiments on Coastal Protection Submerged Breakwaters: a Way to Look at the Results". Proceeding of 22nd Conference on Coastal Engineering, Delft, Netherlands, 1592-1604.

Haller, M., Dalrymple, R.A. and Svendsen, I. . (1997). "Rip-channels and nearshore circulation: experiments". Proceeding of Coastal Dynamic, ASCE, Reston, VA, 594-603.

Haller, M., Dalrymple, R.A. and Svendsen, I.A. (2000). "Experiments on rip currents and nearshore circulation". Research Report No. CACR-00-04, Center for Applied Coastal Research, Ocean Engineering Laboratory, University of Delaware, Newark, Del.

Hara, M., Yasuda, T., and Sakakibara, Y. (1992). "Characteristics of a solitary wave breaking caused by submerged obstacle". Proceedings of the 23rd International Conference on Coastal Engineering, ASCE, 253-266.

Harris, L.E. (2001). "Appendix: survey data and beach profile graphs for the Reef Ball™ artificial reef submerged breakwaters at Gran Dominicus Beach Resort, near Bayahibe, Dominican Republic". (www.artificialreefs.org)

Harris, L.E. (2002). "Submerged Artificial Reef for Beach Erosion Control". (http://www.artificialreefs.org/ScientificReports/Oasis%20RB%20BW2.pdf).

Harris, L.E. (2003). "Status report for the submerged Reef Ball artificial reef

submerged breakwater beach stabilization project for the Grand Cayman Marriott Hotel" (www.reefball.org).

Harris, L.E. (2007a). "Designed Reefs Coastal Stabilization and Reef Restoration". (www.artificialreefs.org).

Harris, L.E. (2007b). "Investigations and Recommendations for Solutions to Beach Erosion Problems in the City of Herzylia, Israel". (http://www.reefball.org).

Harris, L. E. (2009). "Artificial Reefs for Ecosystem Restoration and Coastal Erosion Protection with Aquaculture and Recreational Amenities". Reef Journal 1(1) pp: 235-246.

Hattori, M. and Sakai, H. (1994). "Wave breaking over permeable submerged breakwaters". Proceeding of the 24th International Conference on Coastal Engineering, ASCE, 1101-1114.

Hirose, N., Watunuki, A. and Saito, M. (2002). "New Type Units for Artificial Reef Development of Ecofriendly Artiifcial Reefs and Effectiveness Thereof". Proceeding of 30th International Navigation Congress, PIANC.

Homma, M. and Sokou, T. (1959). "An experimental study on the submerged breakwaters". Coastal Engineering in Japan 2, 103-109.

Homma, M. and Hoikawa, K. (1961). "A study on submerged breakwaters". Coastal Engineering in Japan 4, 85-102.

Hur, D.S., Kawashima, N. and Iwata, K. (2003). "Experimental study of the breaking limit of multidirectional random waves passing over an impermeable submerged breakwater". Ocean Engineering 30, 1923-1940.

IPCC (2007). "Climate change 2007: the physical science basis. contribution of working group I to the fourth assessment report of the intergovernmental panel on climate change". In: Solomon, S., Qin, D., Manning, M., Chen, Z., Marquis, M., Averyt, K.B., Tignor, M., Miller, H.L. (Eds.). Cambridge University Press,Cambridge, United Kingdom.

Iribarren, C.R. and Nogales, C. (1949). Protection des Ports, II, Comm. 4, 17*th* Int. Nav. Congress, Lisbon, 31-80.

Iversen, H.W. (1951). "Laboratory study of breakers". Proc. Symposium on Gravity Waves, U.S. National Bureau of Standard, Circular 521, pp. 9-32.

Iwata, K. and Kiyono, H. (1985). "Breaking of standing two component composite and irregular waves". Coastal Engineering in Japan 28, 71-87.

Jensen, A. (1998). "European Artificial Reef Research Network". Final Report and Recommendations. Published by the University of Southampton.

Jonson, J.W., Fuchs, R.A and Morison, J.B. (1951). "The Damping Action of Submerged Breakwaters". Trans, American Geophysical Union, 32(5), 704-718.

Kamphuis, J.W. (1991). "Incipient wave breaking". Coastal Engineering 15, 185-203.

Kawasaki, K. and Iwata, K. (1996). Numerical analysis of wave breaking submerged structure, Proc. 6th Int. Onshore Polar Eng. Conf., 168-175.

Kawasaki, K., and Iwata, K. (2001). "Wave breaking-induced dynamic pressure due to submerged breakwater". Proceeding of the 11th International Offshore and Polar Engineering Conference, ISOPE, 488-494.

Kramer, M., Zanuttigh, B., van der Meer, J., Vidal, C. and Girondella, F. (2005). "Laboratory experiments on low-crested breakwaters". Coastal Engineering 52(10-11), 867-885.

Kraus, N.C. (1992). "Engineering approach to cross-shore sediment transport process". Proceedings of the 23th International Conference of Coastal Engineering, Short Course on Design and Reliability of Coastal Structures, Venice, 175-209.

Lamberti A. (2005). "Editorial Paper on *DELOS* project". Coastal Engineering 52, 815-818.

Lamberti, A., Martinelli, L., Zanuttigh, B. (2007). "Prediction of wave induced water flow over and through the structure of set-up and rip-currents". Environmental Design Guidelines for Low Crested Coastal Structures, Section13.5, Elsevier, Amsterdam.

Le Méhauté, B. (1962). "On unsaturated breakers and the wave run-up". Proceeding of the 8th International Conference on Coastal Engineering, American Society of Civil Engineers, New York, (8)77-92.

Longuet-Higgins, M.S. and Steward, R.W. (1962). "Radiation stress and mass transport in gravity waves, with application to surf beats". Journal of Fluid Mechanics 13, 481-504.

Longuet-Higgins, M.S. (1967). "On the wave induced difference in mean sea level between two side of a submerged breakwater". Journal of Marine Research 25(2), 148-153.

Lorenzoni, C., Soldini, L., Macinelli, A., Piattella, A. and Brocchini, M. (2004). "La circolazione dinamica a tergo di barriere sommerse: un'analisi sperimentale". Proceeding of 29th Convegno di Idraulica e Costrizioni Idrauliche. Vol.3, BIOS, Cosenza, Italy, 573-580. (In Italian).

Loveless, J.H. and Debski, D. (1997). "The design and the performance of submerged breakwaters". Report completed for UK Ministry of Agriculture, Fisheries and Food. Contract no. CSA 2606, University of Bristol, UK, 137.

Loveless, J.H., Debski, D. and McLeod, A.B. (1998). "Sea level set-up behind detached breakwaters". Proceedings of the 26th International Conference on Coastal Engineering, Vol. 2, ASCE, Reston, Va., 1715-1725.

MacMahan, J.H., Thornton, E.B. and Reniers, A.J.H.M. (2006). "Rip current review". Coastal Engineering, 53,ELSEVIER, 191-208.

Martínez, M.L., Intralawan, A., Vázquez, G., Pérez-Maqueo, O., Sutton, P. and Landgrave, R. (2007). "The coasts of our world: ecological, economic and social importance". Ecological Economics, ELSEVIER, (63),254-272.

McCowan, J. (1894). "On the highest waves of permanent type". Philosophical Magazine, Edinburgh, 38 (5), 351-358.

Melito, I. and Melby, J.A. (2002). "Wave runup, transmission, and reflection for structures armoured with CORE-LOC". Journal of Coastal Engineering 45, Elsevier, 33-52.

Miche, R. (1944). "Mouvements ondulatoires des mere en profounder constant on decroissante". Ann. Des Ponts et Chaussees, Chap 114, 131-164, 270-292, and 369-406.

Mitsuyasu, H., (1962). "Experimental study on wave force against a wall". Report of the Transportation Technical Research Institute, No. 47, p. 39 (in Japanese).

Moore, B.D. (1982). "Beach profile evolution in response to changes in water level and wave height". Master's Thesis. Department of Civil Engineering of the University of Delaware.

Nakamura, M., Shirashi, H. and Sasaki, Y., 1966. "Wave damping effect of submerged dike". Proceedings of the 10th International Conference on Coastal Engineering. ASCE, 254-267.

Nelson, R.C. (1996). "Hydraulic roughtness of coral reef platform". Applied Ocean Research 18, 265-274.

Nicholls, R.J., Wong, P.P., Burkett, V.R., Codignotto, S.L., Hay, J.E., Mclean, R.F., Ragoonaden, S. and Woodroffe, C.D., (2007). "Coastal systems and low-lying areas". In: Parry, M.L., Canziani, O.F., Palutikof, J.P., Van der Linden, P.J., Hanson, C.E. (eds) Climate Change 2007: Impacts, adaptation and vulnerability. Contribution of the Working Group II to the Fourth Assessment report of the Intergovernmental Panel on Climate Change, Cambridge University Press, Cambridge, pp315-356.

NOAA (2013). Global Self-consistent Hierarchical High-resolution Geography (GSHHG). National Oceanic and Atmospheric Administration. Version 2.2.2, January 2013,<http://www.ngdc.noaa.gov/mgg/shorelines/data/gshhg/latest/>.

Okayasu, A. (1989). "Characteristics of turbulence structures and undertow in the surf zone". Ph.D Thesis, University of Tokyo.

Ostendorf, D. W. and Madsen, O. S. (1979). "Analysis of longshore current and associated sediment transport in the surf zone", Report No. 241, Department of Civil Engineering, MIT.

Pasanisi, F., Buccino, M. and Calabrese, M. (2006). "Observation of breaker types at submerged breakwaters". Proceeding of the 2nd Short Course on Coastal and Port Engineering, Cosenza, Italy, May 2006.

Pilarczyk, K. W. (2003). "Design of low-crested submerged structures-an overview". Proceeding of 6th International. Conference on Coastal and Port. Engineering in Developing Countries, Pianc-Copedec, Colombo, Sri-Lanka, 1–16.

Powell, K.A., and Allsop, J.P. (1985). "Low-crested breakwaters, hydraulic performance and stability". Hydraulics research, Wallingford, Technical Report SR 57.

Putnam, J. A. and Johnson, W. (1949). "The dissipation of wave energy by bottom friction". Eos. Trans. AGU, 30, 67-74.

Ranasinghe, R. and Turner, I.L., (2006). “Shoreline response to submerged structure: a review”. Coastal Engineering, Elsevier, 53, 65-79.

Rangel-Butrago, N. and Anfuso, G., (2009). “Assessment of coastal vulnerability in La Guajra Peninsula, Columbian Carribean Sea”. Journal of Coastal Research, SI56, 792-796.

Reef Ball Foundation (2006-2008). “A step-by-step guide for grassroots and efforts to Reef Rehabilitation”. (www.reefball.org).

Reef Ball Foundation (2010). “Reef Ball as Built Survey for Experimental Reef Ball Marsh Erosion Control Project, Venice, Italy”. (www.reefballitalia.it).

Ruol, P., Faedo, A. and Paris, A. (2003). “Prove sperimentali sul comportamento di una scogliera a cresta bassa e sul fenomeno del piling-up a tergo di essa”. Studi Costieri 7, 41-59 (In Italian).

Sawaragi, T. (1995). “Coastal Engineering Waves, Beaches, Wave- Structure Interaction”. ed. T. Sawaragi, ELSEVIER, Amsterdam.

Seabrook, S.R. and Hall, K.R. (1998). “Wave transmission at Submerged Rubblemound breakwaters”. Coastal Engineering, 2000-2013.

Seeling, W. N. (1980). “Two dimensional tests of wave transmission and reflection characteristics of laboratory breakwaters”. WES, CERC, Fort Belvoir, Technical Report No. 80-1.

Sherman, R. L., Gilliam, D. S., and Spieler, R. E. (2002). “Artificial Reef Design: void space, complexity and attractants”. ICES Journal of Marine Science n. 59 pp.196-200.

Smith, E.R. and Krouse, N. (1991). “Laboratory study of wave breaking over bars and artificial reefs”. Journal of Waterway, Port, Coastal and Ocean Engineering, 117(4),307-325.

Soldini, L., Lorenzoni, C., Brocchini, M., Macinelli, A. and Cappietti, L. (2009). “Modeling of the Wave Setup Inshore of an Array of Submerged Breakwaters”. Journal of Waterway, Port, Coastal and Ocean Engineering, ASCE, 132(2), 38-51.

Southgate, H. N. (1995). “Prediction of wave breaking process at the coastline”. Advances in Fluid Mechanism, Ed. Rahaman M., Computation Mechanism Publications.

Srisuwan, C. and Rattanamenee, P. (2015). “Modeling of Seadom as artificial reefs for coastal wave attenuation”. Ocean Engineering (103), 198-210.

Svendsen, I.A. (1984). “Mass flux and undertow in the surf zone”. Coastal Engineering 8, 347-365.

Svendsen, I.A. and Bhur Hansen, J. (1986). “Cross-share currents in surf-zone modelling”. Coastal Engineering 12.

Svendsen, I.A. and Petrevu, U. (1993). “Surf zone wave parameters from experimental data”. Coastal engineering, ELSEVIER, 19(3), 283-310.

Stokes, G. G. (1847). “On the theory of oscillatory waves”. Trans. Cambridge Phil. Soc. 8, 441-455.

Stokes, G. G. (1880). “Consideration relative to the greatest height of oscillation waves, which can be propagate without change of form. Mathematical and Physical Papers.

Tanaka, N. (1976). “Effect of submerged rubble-mound breakwaters on wave attenuation and shoreline stabilization”. Proceeding of Japanese Coastal Engineering Conference, 152-157. (In Japanese).

Thornton, E. B. and Guza, R.T. (1983). “Transformation of wave height distribution”. Journal of Geophysical Research, 88(C10), 5925-5938.

UNEP (2005). “GEO Year Book 2004/5. An Overview of Our Changing Environment”. United Nations Environment Programme, Nairobi.

Van der Meer, J.W. (1988). “Rock slopes and gravel beaches under wave attack”. PhD thesis Delft University of Technology, Delft Hydraulics Report 396.

Van der Meer, J.W. (1990). “Data on wave transmission due to overtopping”. Technical report, Delft Hydraulic, Technical Report No. H 986.

Van der Meer, J.W. and d’Angremond, K. (1991). “Wave transmission at low-crested structures”. Coastal Structures and Breakwaters, ICE, London, 25-42.

Van der Meer. K.W (1992). “Conceptual design of rubble mound breakwaters”. Proceeding .of 23rd International Conference of Engineering, ASCE, Reston, Va, 447-509.

Van der Meer, K.W, Briganti, R., Zanuttigh, B. and Boaxing, W. (2005). “Wave transmission and reflection at low-crested structures: design formulae, oblique wave attack and spectral change”. Coastal Engineering 52, ELSEVIER, 915-929.

Van der Meulen, F., Bakker, T.W.M. and Houston, J.A. (2004). “The costs of our coasts: examples of dynamic dune management from Western Europe”. In: Martínez, M.L., Psuty, N. (Eds.), Coastal Dunes: Ecology and Conservation. Springer-Verlag, Berlin, pp. 259–278.

Van Rijn, L.C. (2011). “Coastal erosion and control”. Ocean & Coastal Management, Vol. 54(12) (December 2011), 867-887

Wamsley, T.V. and Ahrens, J.P. (2003). “Computation of wave transmission coefficient at detached breakwaters for shoreline response modeling”. Proceedings of Coastal Structures, ASCE, 593-605.

Ward, D.L. (2011). “Phisical Model Study of an Experimental Reef Ball(TM) Breakwater for Miami Beach, Florida”. Contract Report submitted to U.S. Army Engineer Research and Development Center, Coastal and Hydraulics Laboratory, Vicksburg, MS. (Personal communication).

Weggel, J. R. (1972). “Maximum breaker height for design”. Coastal Engineering Research Center, Washington D.C. 20016, 21, 419-432.

Withford, G. (2001). “Striving to revive the Underwater Rainforest”. CRA magazine.